

Investigations into the Reactivity and Structure of Phosphinophosponium Cations
and Related Species

by

Yuen-ying S. Carpenter

Submitted in partial fulfillment of the requirements
for the degree of Doctor of Philosophy

at

Dalhousie University
Halifax, Nova Scotia
December 2010

© Copyright by Yuen-ying S. Carpenter, 2010

DALHOUSIE UNIVERSITY

DEPARTMENT OF CHEMISTRY

The undersigned hereby certify that they have read and recommend to the Faculty of Graduate Studies for acceptance a thesis entitled "Investigations into the Reactivity and Structure of Phosphinophosphonium Cations and Related Species" by Yuen-ying S. Carpenter in partial fulfillment of the requirements for the degree of Doctor of Philosophy.

Dated: December 7, 2010

External Examiner: _____

Research Supervisor: _____

Examining Committee: _____

Departmental Representative: _____

DALHOUSIE UNIVERSITY

DATE: December 7, 2010

AUTHOR: Yuen-ying S. Carpenter

TITLE: Investigations into the Reactivity and Structure of Phosphinophosponium
Cations and Related Species

DEPARTMENT OR SCHOOL: Department of Chemistry

DEGREE: PhD CONVOCATION: May YEAR: 2011

Permission is herewith granted to Dalhousie University to circulate and to have copied for non-commercial purposes, at its discretion, the above title upon the request of individuals or institutions. I understand that my thesis will be electronically available to the public.

The author reserves other publication rights, and neither the thesis nor extensive extracts from it may be printed or otherwise reproduced without the author's written permission.

The author attests that permission has been obtained for the use of any copyrighted material appearing in the thesis (other than the brief excerpts requiring only proper acknowledgement in scholarly writing), and that all such use is clearly acknowledged.

Signature of Author

Table of Contents

List of Tables	x
List of Figures	xiii
List of Schemes	xix
List of Charts	xxii
Abstract	xxiii
List of Abbreviations and Symbols Used	xxiv
Acknowledgements	xxix
Chapter 1. Introduction	1
1.1 Catenation and Logical Evolution in Chemical Synthesis.....	1
1.2 <i>Catena</i> -phosphorus Chemistry.....	4
1.2.1 <i>Catena</i> -phosphorus Anions.....	6
1.2.2 Neutral <i>Catena</i> -phosphines.....	10
1.2.3 <i>Catena</i> -phosphorus Cations.....	16
1.3 Phosphinophosponium Cations as Building Blocks	22
1.3.1 Phosphorus as an Acceptor	24
1.3.2 Phosphenium Cations, $[\text{PR}_2]^+$	27
1.4 Summary	31
Chapter 2. 2,3-Diphosphino-1,4-diphosponium Ions	33
2.1 Introduction.....	33
2.2 Synthesis and Behaviour of Chlorophosphinophosponium Cations	33
2.2.1 Reactivity of Chlorophosphinophosponium Cations.....	36

2.3	Reductive Coupling of Chlorophosphinophosphonium Cations	38
2.4	2,3-Diphosphino-1,4-diphosphonium Cations	41
2.4.1	³¹ P NMR Features of 2,3-Diphosphino-1,4-diphosphonium Cations	41
2.4.2	Solid-state Structures	43
2.4.3	Reactivity of 2,3-Diphosphino-1,4-diphosphonium Dications	47
2.4.4	Computational Studies and Diastereoselectivity	55
2.5	Summary	58
Chapter 3.	Reductive Coupling of Polychlorophosphinophosphonium Cations	60
3.1	Introduction	60
3.2	Phosphinochlorophosphonium Cations	61
3.3	Reductive Coupling of 1-Phosphino-2-chloro-2-phosphonium or 1-Chloro-1-phosphino-2-chloro-2-phosphonium Cations	63
3.4	Structure and Solution Behaviour of the <i>Cyclo</i> -triphosphino-1,3-diphosphonium cation 3.9 (ⁱ Pr)	71
3.5	Cyclotetraphosphinochlorophosphonium Cations, 3.8'	82
3.6	Summary	88
Chapter 4.	Acyclic 2-Phosphino-1,3-diphosphonium Cations	90
4.1	Introduction	90
4.2	Synthesis and ³¹ P NMR Spectroscopy	91
4.3	Solid-state Structures	97
4.4	Competitive 2,3-Diphosphino-1,4-diphosphonium Synthesis	102
4.5	Summary	105
Chapter 5.	Electrochemistry of Phosphinophosphonium Cations	106

5.1	Introduction.....	106
5.2	Electrochemistry of $[\text{Ph}_3\text{P-PPhCl}][\text{OTf}]$, $[\mathbf{2.1(Ph)}][\text{OTf}]$	110
5.2.1	Selection of the Working Electrode.....	111
5.2.2	Sweep Rate Studies.....	113
5.2.3	Proposed Mechanism for Electroreduction.....	116
5.3	Dissociation of $[\text{Ph}_3\text{P-PPhCl}][\text{OTf}]$, $[\mathbf{2.1(Ph)}][\text{OTf}]$	119
5.3.1	Effect of TBAPF_6 as a Supporting Electrolyte	122
5.4	Electrochemistry of Other <i>Catena</i> -phosphorus Cations	127
5.5	Summary	128
Chapter 6.	Stibinophosponium Cations.....	130
6.1	Background	130
6.1.1	<i>Catena</i> -antimony Compounds	132
6.1.2	<i>Catena</i> -antimony Coordination Complexes	134
6.1.3	Stibenium Cations, $[\text{SbR}_2]^+$	136
6.1.4	Background Summary	140
6.2	Synthesis of Functionalized Stibinophosponium Cations	140
6.3	Redistribution and Reductive Coupling: <i>Cyclo</i> - $\{(\text{Me}_3\text{P})\text{Sb}\}_4^{4+}$	150
6.4	Summary	156
Chapter 7.	Conclusions.....	157
7.1	Summary	157
7.2	Future Work.....	158
Chapter 8.	Experimental	163
8.1	General.....	163

8.2	NMR Spectroscopy.....	164
8.2.1.1	Dynamic NMR Analysis of 3.9(iPr)	166
8.3	Miscellaneous Instrumental Analyses.....	168
8.4	X-ray Crystallography	169
8.4.1	Synthesis and Characterization of Compounds in Chapter 2.....	170
8.4.1.1	[Ph ₃ P-PPh(Cl)][GaCl ₄], [2.1(Ph)][GaCl ₄].....	170
8.4.1.2	[Me ₃ P-PPh(Cl)][OTf], [2.1'(Ph)][OTf].....	170
8.4.1.3	General procedure for [Ph ₃ P-PR'(Cl)][OTf], 2.1 [OTf].....	170
8.4.1.4	[Me ₃ P-PCy(Cl)][OTf], [2.1'(Cy)][OTf]	172
8.4.1.5	[Ph ₃ P-P ^t Bu(Cl)][OTf], [2.1(^tBu)][OTf].....	172
8.4.1.6	[Ph ₃ P-P ^t BuCl][GaCl ₄], [2.1(^tBu)][GaCl ₄]	172
8.4.1.7	[Me ₃ P-P ^t Bu(Cl)][OTf], [2.1'(^tBu)][OTf].....	173
8.4.1.8	[Me ₃ P-P ^t Bu(Cl)][GaCl ₄], [2.1'(^tBu)][GaCl ₄]:	173
8.4.1.9	Phosphenium exchange studies	173
8.4.1.10	[Ph ₃ P-PEt-PEt-PPh ₃][OTf] ₂ , [2.2(Et)][OTf] ₂	174
8.4.1.11	[Ph ₃ P-P ⁱ Pr-P ⁱ Pr-PPh ₃][OTf] ₂ , [2.2(ⁱPr)][OTf] ₂	175
8.4.1.12	[Ph ₃ P-PCy-PCy-PPh ₃][OTf] ₂ , [2.2(Cy)][OTf] ₂	177
8.4.1.13	General Ligand Exchange on [Ph ₃ P-PPh-PPh-PPh ₃][OTf] ₂ , [2.2(Ph)][OTf] ₂	177
8.4.2	Computational Methods Used in Chapter 2.....	178
8.5	Synthetic Methods Used in Chapter 3	179
8.5.1	Sample Preparation for Derivatives of [R ₂ (Cl)P-PR'Cl][GaCl ₄], 3.1 [GaCl ₄]	179
8.5.2	Sample Preparation for Derivatives of [R(Cl) ₂ P-PRCl][GaCl ₄], 3.2 [GaCl ₄]	179

8.5.3	Generalized Procedure for Reductive Coupling Reactions	179
8.5.3.1	NMR Observation of [Et ₂ (Cl)P _X -P _A Et-P _A Et-P _X (Cl)Et ₂][GaCl ₄] ₂ , [3.4'(Et)][GaCl ₄] ₂ and <i>Cyclo</i> -[Et ₇ P ₅][GaCl ₄] ₂ , [3.9(Et)][GaCl ₄] ₂	180
8.5.3.2	NMR Observation of <i>Cyclo</i> -[(MeP) ₃ (PPh ₂) ₂][GaCl ₄] ₂ , [3.9(Ph₂/Me)][GaCl ₄] ₂	181
8.5.3.3	Synthesis of <i>Cyclo</i> -[ⁱ Pr ₇ P ₅][GaCl ₄] ₂ , [3.9(ⁱPr)][GaCl ₄] ₂	181
8.5.3.4	Synthesis of [ⁱ Pr ₂ (Cl)P-P ⁱ Pr-P ⁱ PrCl][GaCl ₄], [3.5(ⁱPr)][GaCl ₄].....	182
8.6	Synthetic Methods Used in Chapter 4	183
8.6.1	Synthesis and Isolation of [Me ₃ P-P ^t Bu-PMe ₃][OTf] ₂ , [4.1(^tBu)][OTf] ₂	183
8.6.2	Synthesis and Isolation of [Me ₃ P-PR-PMe ₃][OTf] ₂ , 4.1 [OTf] ₂ , R = N ⁱ Pr ₂ , Cy.....	184
8.6.2.1	[Me ₃ P-P(N ⁱ Pr ₂)-PMe ₃][OTf] ₂ , [4.1(NⁱPr₂)][OTf] ₂	184
8.6.2.2	[Me ₃ P-PCy-PMe ₃][OTf] ₂ , [4.1(Cy)][OTf] ₂	185
8.6.3	Reaction Mixtures and ³¹ P NMR Observation of Other Derivatives	186
8.6.3.1	[Me ₃ P-PR-PMe ₃][OTf] ₂ , 4.1 [OTf] ₂ , R = Me, ⁱ Pr.....	186
8.6.3.2	[Me ₃ P-PR-PMe ₃][OTf] ₂ , 4.1 [OTf] ₂ , R = Ph, and Attempted Syntheses of [Et ₃ P-PR-PEt ₃][OTf] ₂ , 4.2 [OTf] ₂ ,	187
8.7	Electrochemical Methods.....	187
8.7.1	Reagents and Preparation of Analytes for Electrochemistry	187
8.7.2	Solution Preparation.....	187
8.7.2.1	Solutions for the Calibration of Ph ₃ P Concentration.....	188
8.7.2.2	Solutions Related to the Effects of Varied TBAPF ₆ Concentration.....	189
8.7.2.3	Solutions Related to the Effect of Me ₃ SiCl	190

8.7.3	Cyclic Voltammetry.....	191
8.7.4	Uncertainty Calculations.....	193
8.7.4.1	Random Errors.....	193
8.7.4.2	Linear Regression and Calibration Errors	194
8.8	Synthesis and Characterization of Compounds in Chapter 6.....	194
8.8.1	[ⁱ Pr ₃ P-SbPhCl][OTf], [6.23(ⁱ Pr)][OTf],	194
8.8.2	[Bn ₃ P-SbPhCl][OTf], [6.23(Bn)][OTf]	195
8.8.3	[Me ₃ P-SbCl ₂][OTf], 6.24[OTf].....	197
8.8.4	[(Ph ₃ P) ₂ SbCl ₂][OTf], 6.26[OTf]	198
8.8.5	Observation of <i>cyclo</i> -[(Me ₃ P)Sb] ₄ [OTf] ₄ , 6.28[OTf] ₄	199
8.9	Crystallographic Experimental Details	200
Appendix A1. Statistical Treatment of Data		205
A1.2.	Dynamic NMR Lineshape Analysis and Regression (Section 3.4).....	205
Appendix A2. Cremer-Pople Puckering Coordinates		209
References	212

List of Tables

Table 1.1.	Comparison of selected fundamental parameters of carbon and phosphorus. References from Emsley ⁹ unless otherwise noted.	4
Table 1.2.	Lewis depictions and nomenclature of the available bonding environments for phosphorus with single bonds only.	6
Table 1.3.	Reported isolated yields and structural features of readily synthesized homoleptic cyclopolyphosphines, from Baudler ²² unless otherwise noted.	13
Table 2.1.	³¹ P{ ¹ H} NMR parameters for phosphinophosphonium salts. Data are reported for spectra obtained at 298 K unless otherwise indicated. Chemical shifts (δ) are reported in units of ppm and coupling constants (¹ J _{PP}) in units of Hz.	35
Table 2.2.	³¹ P{ ¹ H} NMR parameters at 101.3 MHz for 2,3-diphosphino-1,4-diphosphonium triflate salts. All spectra are AA'BB' spin systems, with parameters derived by iterative fitting of experimental data at 298 K. Minor diastereomer shifts could not be simulated, so are approximate if given. Chemical shifts (δ) are reported in ppm and coupling constants (J) in Hz.	42
Table 2.3.	Selected solid-state structural parameters of 2,3-diphosphino-1,4-diphosphonium triflate salts, [R ₃ P-PR'-PR'-PR ₃][OTf] ₂	44
Table 2.4.	³¹ P{ ¹ H} NMR parameters at 101.3 MHz for cyclic 2,3-diphenyldiphosphino-1,4-diphosphonium triflate salts in CH ₂ Cl ₂ . All spectra are AA'BB' spin systems, with parameters derived by iterative fitting of experimental data at 298 K. Chemical shifts (δ) are reported in ppm and coupling constants (J) in Hz.	49
Table 2.5.	Selected solid-state structural parameters for the cation in 2.7 [OTf] ₂	53
Table 2.6.	Calculated structural parameters for 2,3-diphosphino-1,4-diphosphonium cations.	56
Table 3.1.	³¹ P{ ¹ H} NMR parameters for selected phosphinophosphonium gallate salts. Data are reported for spectra obtained in CH ₂ Cl ₂ at 101.3 MHz.	64

Table 3.2.	Products observed for reductive coupling reactions ^a of [R ₂ (Cl)P-PR'Cl][GaCl ₄] including (a) 3.1(Ph) , (b) 3.1(Me) , and (c) 3.1(Et) . Relative yield of the products versus the most predominant species (based on the area of the ³¹ P{ ¹ H} NMR signals) is indicated by shading according to the following ranges:	65
Table 3.3.	Selected homoatomic distances (Å) and bond angles (°) ^a in the solid-state structure of [3.9(ⁱPr)][GaCl ₄]·CH ₂ Cl ₂ and comparative values for 3.9' and 3.9''. ⁵⁵ Also indicated are the calculated Cremer-Pople ^{120,121} puckering angle (φ, °), puckering parameter (Q, Å), and conformation.....	72
Table 3.4.	³¹ P{ ¹ H} NMR parameters ^a for [3.9(Et)][GaCl ₄] ₂ , [3.9(ⁱPr)][GaCl ₄] ₂ and [3.9(Ph₂/Me)][GaCl ₄] ₂ in comparison with previously reported heteroleptic derivatives of 3.9 [OTf]. Substituents at P4 and P5 are <i>trans</i> -oriented in all cases.....	78
Table 3.5.	³¹ P{ ¹ H} NMR parameters ^a for [3.8'(Ph)][GaCl ₄] in comparison to those for [3.8(Ph)][OTf] ⁵³ and [3.7'(Cy)][OTf] ⁵⁶	84
Table 4.1.	³¹ P{ ¹ H} NMR parameters at 101.3 MHz for derivatives of the 2-phosphino-1,3-diphosphonium framework. Coupling constants are derived by iterative fitting of spectra at 298 K and 101.3 MHz.	93
Table 4.2.	Selected relevant bond lengths and angles in the solid-state structures of the dications in characterized acyclic 2-phosphino-1,3-phosphonium triflates 4.1 [OTf] ₂	99
Table 4.3.	³¹ P{ ¹ H} NMR parameters at 101.3 MHz for previously unreported 2,3-diphosphino-1,4-diphosphonium triflate salts observed in MeCN during the attempted synthesis of 2-phosphino-1,3-diphosphonium species. Chemical shifts (δ) are reported in ppm and coupling constants (J) in Hz.....	103
Table 6.1.	Comparison of selected properties of phosphorus vs. antimony. References are from Emsley ⁹ unless otherwise indicated.....	130
Table 6.2.	Selected structural parameters for stibinophosphonium cations.....	143
Table 6.3.	Comparison of selected structural parameters in <i>cyclo</i> -[{(Me ₃ P)Sb} ₄] ⁴⁺ (6.28) vs. <i>cyclo</i> -(^t BuSb) ₄ . Single value parameters indicate the average.	153
Table 8.1.	Rate constants determined by lineshape analysis of ³¹ P{ ¹ H} NMR spectra of [3.9(ⁱPr)][GaCl ₄] ₂ in EtCN.....	168

Table 8.2.	Selected crystallographic data and collection parameters for compounds in Chapter 2. Data collected and refined at the University of New Brunswick.	200
Table 8.3.	Selected crystallographic data and collection parameters for [3.9(ⁱ Pr)][OTf] ₂ , <i>cyclo</i> -[ⁱ Pr ₇ P ₅][GaCl ₄] ₂ (Chapter 3). Data collected and refined at the University of Alberta.	201
Table 8.4.	Selected crystallographic data and collection parameters for derivatives of [4.1(R)][OTf] ₂ , [Me ₃ P-PR-PMe ₃][OTf] ₂ (Chapter 4). Data collected and refined at the University of Alberta.	202
Table 8.5.	Selected crystallographic data and collection parameters for stibinophosphonium cations in Chapter 6. Data collected and refined at the University of Alberta.	203
Table 8.6.	Selected crystallographic data and collection parameters for miscellaneous phosphine-stabilized stibenium cations (Chapter 6).	204
Table A1.1.	Comparative results of simple and weighted linear regression analysis of Eyring plot data for [3.9(ⁱ Pr)][GaCl ₄] ₂ in EtCN. Error limits indicated for ΔH [‡] and ΔS [‡] are standard deviations, while error in ΔG [‡] is reported at the 95% confidence level. Standard error in the simple regression was calculated based on the sum of the squared residuals.	208

List of Figures

Figure 1.1.	Graphical representation of the development of increasing structural complexity in synthetic organic chemistry, proceeding from fundamental chemical reactions (a-b) to intricate single molecules (c) to stereoregular polymers (d) and self-assembled supramolecular structures (e). Structure e has been adapted from reference 5.....	2
Figure 1.2.	Structure of Hittorf's (violet) phosphorus (1.1) and a representative phosphorus nanorod (1.2) with a P ₁₂ repeat unit. Note the structurally similar P ₈ cage unit found in both allotropes.....	4
Figure 1.3.	Two structural representations of the P ₇ ³⁻ anion, which can be used to rationalize the observation of only one signal in ³¹ P NMR spectra of M ₃ P ₇ at room temperature. Colouration of the atoms serves to highlight the interconversion between phosphorus sites, e.g. the blue phosphorus atom is apical at the left, but basal at the right.....	7
Figure 1.4.	Simplified skeletal drawings of selected polycyclic polyphosphorus polyanions, P ₁₆ ²⁻ (1.3) and P ₂₁ ³⁻ (1.4). Vertices represent phosphorus atoms.....	7
Figure 1.5.	Selected examples of neutral polycyclic frameworks. ^{22,35,53,54}	16
Figure 1.6.	Lewis (1.35) and coordinate (1.35') bonding descriptions for the anion [PBr ₄] ⁻	24
Figure 1.7.	Solid-state structure of the anion in [ⁿ Pr ₄ N][PBr ₄]. Note the P··Br distance between monomer units is 3.460(4) Å (cf. P-Br _{eq} = 2.2-2.3 Å; P-Br _{ax} = 2.5-2.6 Å) ⁹⁰	25
Figure 1.8.	Orbital depiction of a phosphenium cation.....	27
Figure 2.1.	Comparison of simulated and experimental ³¹ P{ ¹ H} NMR spectra of [2.2(Et)][OTf] ₂	42
Figure 2.2.	Comparison of simulated and experimental ³¹ P{ ¹ H} NMR spectra of [2.2(Pr)][OTf] ₂	43

Figure 2.3.	ORTEP representations of the solid-state structure of (a) the centrosymmetric <i>meso</i> -dication in [2.2(Ph)][OTf] ₂ and the (<i>S,S</i>)-enantiomer of the dication in (b) [2.2(Me)][OTf] ₂ and (c) [2.2(Et)][OTf] ₂ . Thermal ellipsoids are shown at the 50% probability level and hydrogen atoms omitted for clarity. τ_R^c indicates the C-P-P-C torsion angle between the central substituents, while τ_{PR3} indicates the P-P-P-P torsion angle of the phosphorus backbone.....	45
Figure 2.4.	ORTEP representations of the solid-state structure of (a) the centrosymmetric <i>meso</i> -dication in [2.2'(Ph)][OTf] ₂ and (b) the (<i>S,S</i>)-enantiomer of the dication in [2.2'(Me)][OTf] ₂ . Thermal ellipsoids are shown at the 50% probability level and hydrogen atoms omitted for clarity. τ_R^c indicates the C-P-P-C torsion angle between the central substituents, while τ_{PR3} indicates the P-P-P-P torsion angle of the phosphorus backbone.....	46
Figure 2.5.	Experimental (upright) and simulated (inverted) expansions of the ³¹ P{ ¹ H} NMR spectrum at 101.3 MHz of the 1:1 mixture of the five-membered dication 2.6 (blue, AA'BB') and the six-membered dication 2.7 (red, ABB'CC'), from the redissolved crystalline material isolated from dpmm ligand exchange on 2.2(Ph)	51
Figure 2.6.	Top (<i>left</i>) and side-on (<i>right</i>) views of the ORTEP representation of the dication in 2.7 [OTf] ₂ , indicating a half-twisted boat conformation in the solid state. Thermal ellipsoids are shown at the 50% probability level and hydrogen atoms are omitted for clarity. Unlabelled atoms at left indicate carbon atoms, while only ipso carbons are shown at right. Disorder of the C14-C19 phenyl moiety on P2 has been modelled.	52
Figure 2.7.	Skeletal depiction of the unit cell in crystalline 2.7 [OTf] ₂ showing the alignment of adjacent rings. Triflate counterions are indicated in red.	54
Figure 2.8.	Representative conformations of the <i>meso</i> - and (<i>S,S</i>)-diastereomers. Idealized torsion angles between the central R-substituents are indicated (\square_R), and the preferred conformation in the gas phase is highlighted.	58
Figure 3.1.	Experimental (upright) and simulated (inverted) expansions of the ³¹ P{ ¹ H} NMR spectra of [3.4'(Et)][GaCl ₄] ₂ in the reaction mixture of [3.1(Et)][GaCl ₄] with 2 SbPh ₃ and GaCl ₃ . Minor impurities in the reaction mixture are marked with asterisks.....	68

Figure 3.2.	Experimental (upright) and simulated (inverted) expansions of the $^{31}\text{P}\{^1\text{H}\}$ NMR spectrum at 202.6 MHz of the 2:1 mixture of <i>trans</i> (blue) and <i>cis</i> (red) isomers of 3.9 (Ph ₂ /Me), with characteristic AGHMX and ABB'XX' spin systems, respectively. Broad peaks at 0.5 and 72 ppm (not simulated) correspond to the phosphinophosphonium cation 1.34 (Ph).....	70
Figure 3.3.	ORTEP views of the cation in [3.9 (ⁱ Pr)][GaCl ₄] ₂ ·CH ₂ Cl ₂ . Thermal ellipsoids are shown at the 50% probability level, carbon atoms are unlabelled and hydrogen atoms are omitted for clarity. Right view shows only the phosphorus framework and associated α-carbons, indicating a ⁴ E conformation.	71
Figure 3.4.	Possible pseudorotational conformations of 3.9 described according to the Cremer-Pople puckering angle, φ. Conformations observed in the solid state are highlighted in boxes. Figure adapted from Dyker <i>et al.</i> ⁵⁹	74
Figure 3.5.	Experimental (upright) and simulated (inverted) expansions of the $^{31}\text{P}\{^1\text{H}\}$ NMR spectrum of [3.9 (ⁱ Pr)][GaCl ₄] ₂ in EtCN at 101.3 MHz and 188 K. Parameters for the AGHMX spin system are listed in Table 3.4.....	74
Figure 3.6.	Variable-temperature $^{31}\text{P}\{^1\text{H}\}$ NMR spectra of [3.9 (ⁱ Pr)][GaCl ₄] ₂ in EtCN at 101.3 MHz.	76
Figure 3.7.	Skeletal representations of the time-averaged planar structure of symmetrically substituted 3.8 (left), geminal asymmetrically-substituted 3.8' (center, R ≠ R'), and 3.9 , to rationalize the $^{31}\text{P}\{^1\text{H}\}$ NMR spin systems.	77
Figure 3.8.	Experimental (left) and simulated (right) $^{31}\text{P}\{^1\text{H}\}$ NMR spectra used in lineshape analysis of [3.9 (ⁱ Pr)][GaCl ₄] ₂ . Resulting rate constants are listed in Table 8.1.....	79
Figure 3.9.	Eyring plot for the dynamic behaviour of [3.9 (ⁱ Pr)][GaCl ₄] ₂ in EtCN based on rate constants (<i>k</i>) from line shape analysis of $^{31}\text{P}\{^1\text{H}\}$ NMR spectra between 246-292 K (simulated and experimental spectra available in the supporting information). Error bars are plotted based on error estimates in dNMR lineshape fitting, and the 95% confidence interval about the regression line is indicated with dashed lines.	80
Figure 3.10.	Experimental (upright) and simulated (inverted) expansions of the $^{31}\text{P}\{^1\text{H}\}$ NMR spectrum of [3.8' (Ph)][GaCl ₄], <i>cyclo</i> -[(Ph ₅ P ₅)Cl][GaCl ₄] at 280 K and 202.6 MHz, displaying an AGHMX spin system with a downfield resonance (δ _X = 89 ppm) characteristic of a Cl-substituted phosphonium centre.	83

Figure 3.11.	$^{31}\text{P}\{^1\text{H}\}$ NMR solution spectrum of the reaction of [3.2(Ph)][GaCl₄] with SbPh ₃ after 30 h (top) and 7 days (bottom) at 101.3 MHz, indicating the decomposition of [3.8'(Ph)][GaCl₄] to [3.8(Ph)][GaCl₄] . $t_{1/2}$ was estimated by integration of the well-separated phosphonium resonances in [3.8(Ph)][GaCl₄] (<i>shaded</i>) vs. [3.8'(Ph)][GaCl₄] . PhPCl ₂ (162 ppm, not shown) was also present in solution.	86
Figure 3.12.	$^{31}\text{P}\{^1\text{H}\}$ COSY NMR spectrum of the MeCN-soluble product(s) resulting from the reductive coupling of [Me(Cl)₂P-PMeCl] , [3.2(Me)][GaCl₄]	88
Figure 4.1.	$^{31}\text{P}\{^1\text{H}\}$ NMR spectra for selected derivatives of 4.1 , showing the variations in spin system: (a) 4.1(NⁱPr₂) , A ₂ B, (b) 4.1(^tBu) , AB ₂ (asterisk indicates a minor impurity), and (c) 4.1(Me) , AXX'.	94
Figure 4.2.	Lewis (left) and coordinate (middle) bonding model depictions of 4.1(NⁱPr₂) showing possible resonance contribution of the π -donating amido-substituent.	95
Figure 4.3.	ORTEP representations of the solid-state structure of the cation in (a) 4.1(^tBu)[OTf]₂ (b) 4.1(Cy)[OTf]₂ and (c) 4.1(NⁱPr₂)[OTf]₂ , from a front and side perspective. Hydrogen atoms are omitted for clarity and thermal ellipsoids shown at the 50% probability level. Unlabelled atoms in the front view are carbon atoms. Relevant parameters are listed in Table 4.2.	100
Figure 4.4.	ORTEP representation of the solid-state structure of the asymmetric unit in 4.1(^tBu)[OTf]₂ , indicating weak interactions between hydrogen atoms of the cation and the triflate counterions. Non-hydrogen atoms are represented with Gaussian ellipsoids at the 50% probability level, while hydrogen atoms are shown with arbitrarily small thermal parameters.	101
Figure 5.1.	Cyclic voltammogram of a 2.00 mM solution of [Ph₃P-PPhCl][OTf] , [2.1(Ph)][OTf] , in 0.1 M TBAPF ₆ /MeCN ($v = 100$ mV/s). Potentials are reported relative to the ferrocene redox couple Fc/Fc^+ , marked with an asterisk.	111
Figure 5.2.	Behaviour of platinum disc (Pt, $r = 0.8$ mm) vs. glassy carbon disc (GC, $r = 1.6$ mm) working electrodes. Solutions tested were 1.00 mM Fc on (a) Pt and (b) GC, and 2.00 mM [2.1(Ph)][OTf] /1.00 mM Fc on (c) Pt and (d) GC. Dotted lines on (a) and (c) indicate the upper and lower redox limits for the glassy-carbon working electrode for comparison.	113

Figure 5.3.	Cyclic voltammograms of a 5 mM solution of [2.1(Ph)] [OTf] in 0.1 M TBAPF ₆ /MeCN at varying sweep rates (v). Peaks corresponding to the internal standard (1 mM F _c) are marked with asterisks.....	114
Figure 5.4.	Peak potentials ($vs. F_c/F_c^+$) and normalized current of the partially-reversible voltammetric peaks IIIc/IIIa over a range of sweep rates (v) for a 5.00 mM solution of [2.1(Ph)] [OTf] in 0.1 M TBAPF ₆ /MeCN.....	115
Figure 5.5.	Calibration curves for (a) current and (b) charge vs. Ph ₃ P concentration for a series of Ph ₃ P standard solutions. Error bars are too small to be plotted in (b).....	121
Figure 5.6.	Anodic peak current $vs.$ TBAPF ₆ concentration for various concentrations of [2.1(Ph)] [OTf].....	123
Figure 5.7.	Scaled current function ($i_{pa} \cdot C^{-1}$) $vs.$ the molar ratio of supporting electrolyte to analyte for [2.1(Ph)] [OTf]. Regression lines are plotted for all data and excluding data at 25 mM TBAPF ₆ , to compare the possible effect of solution resistance.....	124
Figure 5.8.	Calculated concentration of Ph ₃ P $vs.$ reaction based on anodic peak currents observed in cyclic voltammograms of reaction mixtures of Ph ₃ P, PhPCl ₂ and Me ₃ SiOTf in 0.1 M TBAPF ₆ /MeCN. Ph ₃ P concentrations calculated based on calibration curve H3.....	125
Figure 5.9.	Cyclic voltammograms of a 2.00 mM solution of [2.1(Ph)] [OTf] in 0.1 M TBAOTf/MeCN, with potentials referenced to 1 mM F _c /F _c ⁺ (*). Arrows indicate the direction of the initial sweep.....	126
Figure 5.10.	Cyclic voltammogram of a 2 mM solution of [Ph₃P-PPh₂] [OTf], 1.24 [OTf] at 100 mV/s in 0.1 M TBAPF ₆ /MeCN, with an initial potential sweep in the anodic direction.....	127
Figure 6.1.	ORTEP representation of the crystal structure of [(Me₃P-SbPh₂)₄Cl]³⁺, 6.18[PF₆]₃. Thermal ellipsoids are shown at 30% probability, and hydrogen atoms have been omitted for clarity (adapted from published CIF).²³⁷.....	138
Figure 6.2.	ORTEP representations of the solid-state structure of (a) 6.24(Me) [OTf], (b) 6.23(ⁱPr) [OTf], and (c) 6.23(Bn) [OTf]. Thermal ellipsoids are shown at 50% probability, and hydrogen atoms have been omitted for clarity. The triflate counterion is shown in (b) as an example to indicate the geometry about Sb when the weak cation-anion contact is considered.....	142
Figure 6.3.	Possible bonding models to describe the bonding in 6.26 [OTf].....	146

Figure 6.4.	ORTEP representation of the solid-state structure of 6.26 . Thermal ellipsoids are shown at 50% probability. Carbon atoms have been left unlabelled and hydrogen atoms omitted for clarity. Relevant angles are as follows: C11-Sb-P: 81.519(18)° / 82.142(18)°; C12-Sb-P: 84.404(19)° / 88.230(19)°.....	146
Figure 6.5.	Alternative view of 6.26 [OTf] showing the close cation-anion contact (Sb-O: 2.6793(17) Å). Only the ipso carbons of the phenyl substituents are shown (unlabelled atoms). Thermal ellipsoids are shown at 50% probability, and hydrogen atoms have been omitted for clarity. Other relevant bond angles are as follows: C11-Sb-O: 88.45(4)°; C12-Sb-O: 170.49(5)°; P1-Sb-O: 103.33(4)°; P2-Sb-O: 86.02(4)°.....	147
Figure 6.6.	ORTEP representations of the solid-state structure of the cation in 6.28 [OTf] ₄ ·MeCN from above and alongside the Sb ₄ -ring. Thermal ellipsoids are shown at 50% probability, and hydrogen atoms have been omitted for clarity. Unlabelled ellipsoids represent carbon atoms.	152
Figure A1.1.	Comparison between the results of simple (unweighted) linear regression (left) and weighted regression (right) for the Eyring plot of the solution dynamics of [3.9 (¹ Pr)][GaCl ₄] ₂ in EtCN. Note that the weighted regression line falls within the 95% confidence interval for the simple regression (dotted lines on both plots).....	208
Figure A2.1.	Cremer-Pople puckering angles (θ, φ) of six-membered rings.....	210

List of Schemes

Scheme 1.1.	Alkali metal ($M^I = \text{Li, Na, K}$) reduction of cyclopolyphosphines to acyclic polyphosphides.	9
Scheme 1.2.	Synthesis of monocyclic catena-phosphorus anions ($R = \text{}^t\text{Bu, }^i\text{Pr, Ph}$).	9
Scheme 1.3.	Disproportionation of acyclic polyphosphorus hydrides to a monocyclophosphine and diphosphine.	11
Scheme 1.4.	Generalizable routes to neutral monocyclic polyphosphines.	12
Scheme 1.5.	Methylation products in CH_2Cl_2 solution or in the absence of solvent.	17
Scheme 1.6.	Alkylation and protonation reactions of cyclo-polyphosphines resulting in net ring-size retention (<i>a-c</i>) or ring-size expansion (<i>d-f</i>).	18
Scheme 1.7.	Successive chloronium addition to <i>cyclo</i> -(PCy) ₄ to produce functionalized derivatives of framework x (1.29) and xii (1.30).	20
Scheme 1.8.	Alternative alkylation (a) or direct synthesis (b) routes to framework vii (1.32).	20
Scheme 1.9.	Phosphenium insertion reactions leading to monocationic polyphosphorus species. Reactions involving cyclic species have been known to proceed with either ring size expansion or ring size retention. ⁵⁹	22
Scheme 1.10.	Synthesis of a generic phosphinophosponium cation by halide abstraction from a chlorophosphine.	23
Scheme 1.11.	Ligand exchange behaviour in phosphinophosponium cations	23
Scheme 1.12.	Phosphine (Lewis base) stabilization of a diamidophosphenium cation.	30
Scheme 1.13.	Formation of GaCl_3 -adducts with alkylphosphines in the presence of excess GaCl_3	30
Scheme 1.14.	An NHC-stabilized phosphenium centre ($R = \text{Ph, }^i\text{Pr, Cy}$) acting as a strongly π -accepting ligand, as indicated by high ν_{CO} ($2075\text{-}2082\text{ cm}^{-1}$)	31
Scheme 2.1.	Synthesis of chlorophosphinophosponium cations 2.1 or 2.1' as triflate or tetrachlorogallate salts.	34

Scheme 2.2.	Phosphenium (acceptor) exchange reaction yielding [1.24(Ph)][OTf] from [2.1(Ph)][OTf]	36
Scheme 2.3.	Reductive coupling reaction of [2.1][OTf] to give [2.2][OTf] ₂	38
Scheme 2.4.	Proposed reaction pathway for the reductive coupling of [2.1][OTf] to [2.2][OTf] ₂ . Intermediate [2.3][OTf] ₂ has been observed using ³¹ P{ ¹ H} NMR spectroscopy for sterically encumbered derivatives (R' = ¹ Pr, Cy, ^t Bu).....	40
Scheme 2.5.	Phosphine exchange reactions on phosphinophosphonium and 2,3-diphosphino-1,4-diphosphonium cations.....	47
Scheme 2.6.	Stereochemical considerations in associative ligand substitution reactions of the two possible diastereomers of 2.2[OTf] ₂	50
Scheme 3.1.	Proposed mechanism for a reductive coupling chain extension of 1.34, as observed in Equation [6].....	64
Scheme 3.2.	Addition of excess GaCl ₃ to suppress dissociation of [GaCl ₄] ⁻	68
Scheme 3.3.	Conversion of [3.4'(Et)][GaCl ₄] ₂ to [3.9(Et)][GaCl ₄] ₂	70
Scheme 3.4.	Possible inversion pathways for 3.9(ⁱ Pr) which effect time-averaged C ₂ symmetry.	76
Scheme 3.5.	Ring-opening and ring-closing products observed by ³¹ P{ ¹ H} NMR spectroscopy during the thermal-decomposition and ESI-MS analysis of [3.9(ⁱ Pr)][GaCl ₄] ₂ in EtCN.....	82
Scheme 3.6.	Reductive coupling of [3.2][GaCl ₄] to yield [3.8'] ₂ [GaCl ₄], for R = Ph, Et.....	85
Scheme 4.1.	Possible synthetic routes to acyclic 2-phosphino-1,3-diphosphonium dications	90
Scheme 4.2.	Direct reaction of a trialkylphosphine (R = Me, Et) with a variety of dichlorophosphines and Me ₃ SiOTf to generate 2-phosphino-1,3-diphosphonium triflate salts. Substituents at R' are indicated in brackets in the text.....	91
Scheme 4.3.	Possible reaction pathways resulting in the generation of either a three- or four-phosphorus dication.....	104
Scheme 5.1.	Proposed mechanism for the reductive coupling of [2.1][OTf] to [2.2][OTf] ₂ . Intermediate [2.3][OTf] ₂ has been observed by ³¹ P{ ¹ H} NMR spectroscopy for sterically encumbered derivatives (R' = ⁱ Pr, Cy, ^t Bu). See also, Chapter 2.....	110

Scheme 5.2.	Dissociative equilibrium proposed for [2.1(Ph)] [OTf] resulting in low concentrations of free Ph ₃ P in solution.....	120
Scheme 6.1.	Reaction of Sb or Bi trihalides with phosphine or N-heterocyclic carbene donor ligands to yield 2:1 adducts.....	131
Scheme 6.2.	Synthesis of stibinophosponium cations by halide abstraction.....	140
Scheme 6.3.	Proposed halide abstraction from dimeric (Ph ₃ P) ₂ SbCl ₃ complexes.	145
Scheme 6.4.	The differing reactivity of P and Sb with 1-2 equivalents of phosphine.	149
Scheme 6.5.	Attempted reductive coupling of PhSbCl ₂ yielding the tetracation 6.28 [OTf] ₄	151
Scheme 6.6.	Possible reaction pathways for the formation of 6.28 [OTf] ₄ , both of which involve substituent redistribution and reductive coupling.	154
Scheme 7.1.	Synthesis of branched <i>cyclo</i> -polyphosphorus cations from chloro-functionalized cations.	158
Scheme 7.2.	Systematic generation of polycyclic polycations from chloro-functionalized cationic phosphorus rings.....	159
Scheme 7.3.	Proposed synthesis and potential reactions of bridged bis(phosphinophosponium) dications.	161
Scheme 7.4.	Ring-opening of cationic <i>catena</i> -phosphorus rings by attack of strong nucleophiles.	162

List of Charts

Chart 1.1.	The isolobal nature of four-coordinate carbon and phosphorus (phosphonium) fragments.	17
Chart 1.2.	Skeletal representations of all known cationic catena-phosphorus frameworks (updated from reference 64), categorized into acyclic monocations (i-v) and dications (vi-viii), monocyclic monocations (ix-xi) and dications (xii-xv) and polycyclic cations (xvi-xviii). Vertices represent phosphorus atoms, while terminal positions represent organic substituents. Frameworks in dotted boxes have been observed ^{65,66} but are not yet reported in the literature.	19
Chart 3.1.	Known poly-halide functionalized catena-phosphorus cations.	60
Chart 3.2.	Representative phosphinophosphonium cation frameworks, accompanied by the numbering scheme used throughout this chapter for clarity. Any previous numbering schemes are also listed in italics for reference. Substituents are indicated in brackets following the compound number in the text – where there are mixed substituents, substituents at the phosphonium are indicated with a subscript numeral two, e.g. 3.1(X₂/Y) represents [X ₂ (Cl)P-PY(Cl)] ⁺	61
Chart 3.3.	Framework drawings of halide-functionalized <i>catena</i> -phosphinophosphonium cations. Vertices represent phosphorus atoms. The first derivatives of frameworks in boxes are reported here as products of the reductive coupling of the phosphinophosphonium cations in the dotted box.	89

Abstract

Carbon and phosphorus have often been compared owing to their diagonal relationship on the periodic table. However, relative to carbon, there remains an enormous breadth of polyphosphorus chemistry that is unexplored, particularly in the area of cationic phosphorus. A key step in the systematic and rational development of larger catenated organo-polyphosphorus cations is a fundamental understanding of the reactivity of small cationic building blocks. The smallest catenated framework in this context is the phosphinophosponium monocation $[\text{R}_3\text{P-PR}_2]^+$ (or phosphine-stabilized phosphenium cation), which can be prepared with a variety of functional groups at either phosphorus centre. This dissertation explores the diverse reactivity of chloro-substituted phosphinophosponium cations, with a particular focus on reductive coupling as a synthetic route to novel *catena*-phosphorus systems. The resulting cationic frameworks are comprehensively described in terms of their diastereoisomerism, solution dynamics, and solid-state structural features. Additionally, fundamental electrochemical investigations of these diphosphorus cations are outlined as a tool for understanding and quantifying the reactivity of phosphenium cations. Finally, extension of reductive coupling methodology to the first chlorostibinophosponium cations presents a promising outlook towards the catenation of the heavier pnictogen cations.

List of Abbreviations and Symbols Used

(θ , φ)	Cremer-Pople phase angles for 6-membered rings	C_x	concentration of x
		Cy	cyclohexyl
$^{\circ}\text{C}$	degrees Celsius	d	days
A	amperes	d	doublet (<i>in NMR</i>)
Å	angstrom	d.p.	decomposition point
Abs	halide abstractor	DFT	density functional theory
Ar	generic aryl substituent	Dmp	2,6-dimethylphenyl
avg.	average	dmpm	bis(dimethylphosphino) methane
b	broad (<i>in NMR and IR</i>)	dppe	bis(diphenylphosphino) ethane
biphep	2,2'-bis(diphenylphosphino)-1,1'-biphenyl	dppm	bis(diphenylphosphino) methane
Bn	benzyl	E	electron transfer step (in an <i>electrochemical mechanism</i>)
C	coulomb	E	generic element/atom
C	chemical reaction step (in an <i>electrochemical mechanism</i>)	<i>e.g.</i>	for example
<i>cf.</i>	compared to	E°	standard reduction potential (at 298 K, 1 atm, 1 M)
C.I.	confidence interval	$E^{\circ'}$	formal reduction potential (under experimental conditions)
<i>ca.</i>	approximately (<i>circa</i>)	$E_{1/2}$	polarographic half-wave potential
CIF	crystallographic information file	E_n	envelope conformation, with atom <i>n</i> below the plane of the ring
CN	coordination number		
COSY	(homonuclear) correlation spectroscopy (<i>NMR</i>)		
C_p	cyclopentadienyl ligand		
CV	cyclic voltammogram		

E_p	peak potential	i_{pa}	anodic peak current
E_{pa}	anodic peak potential	i_{pc}	cathodic peak current
E_{pc}	cathodic peak potential	i_{Pr}	isopropyl
EPR	electron paramagnetic resonance	i_{PrF}	perfluoro-isopropyl
ESI-MS	electrospray ionization mass spectrometry	K	kelvin
<i>et al.</i>	and others	k	rate constant
Et	ethyl	k_b	Boltzmann constant
Et_2O	diethyl ether	K_{eq}	equilibrium constant
EtCN	propionitrile	L	generic neutral 2-electron donor ligand
F	Faraday's constant	LUMO	lowest unoccupied molecular orbital
F_c or $FeCp_2$	ferrocene	m	medium intensity (<i>in IR</i>)
FT-IR	fourier-transform infrared spectroscopy	<i>m-</i>	meta (for aryl substituents)
g	grams	M	moles per litre
GC	glassy carbon/vitreous carbon	m	multiplet (<i>in NMR</i>)
h	hour	m.p.	melting point
h	Planck constant	<i>m/z</i>	mass-to-charge ratio
HOMO	highest occupied molecular orbital	mA	milliamperes
HSQC	heteronuclear single quantum correlation spectroscopy (<i>NMR</i>)	Me	methyl
Hz	hertz	MeCN	acetonitrile
<i>i.e.</i>	that is	Mes	mesityl / 2,4,6-trimethylphenyl
i_p	peak current	mg	milligrams
		MHz	megahertz
		min	minute

mL	millilitres	Ph	phenyl
mT_n	twist conformation, with atom <i>m</i> below and atom <i>n</i> above the plane of the ring	Pn	generic pnictogen atom
		ppm	parts per million
mV	millivolt	<i>p</i> -Tol	<i>para</i> -tolyl / 4-methylphenyl
n.r.	not reported	Q	Cremer-Pople puckering parameter
n/a	not applicable	q	quartet (<i>in NMR</i>)
${}^n\text{Bu}$	<i>n</i> -butyl	q_{pa}	charge under an anodic peak
${}^n\text{E}$	envelope conformation, with atom <i>n</i> above the plane of the ring	q_{pc}	charge under a cathodic peak
NHC	N-heterocyclic carbene	quin	quintet (<i>in NMR</i>)
NHE	normal hydrogen electrode	r	radius
${}^nJ_{XY}$	<i>n</i> -bond coupling constant between X and Y	R	universal gas constant
NMR	nuclear magnetic resonance	r	radius
NO ₃	nitrate	r_{cov}	covalent radius
NPA	natural population analysis	rpm	revolutions per minute
${}^n\text{Pr}$	<i>n</i> -propyl	R _s	solution resistance
<i>o</i> -	ortho (for aryl substituents)	r_{vdw}	van der Waals radius
ORTEP	Oakridge thermal ellipsoid plot	s	second
OTf	triflate (trifluoromethanesulfonate)	s	singlet (<i>in NMR</i>)
<i>p</i> -	<i>para</i> (for aryl substituents)	SCE	saturated calomel electrode
		sept	septet (<i>in NMR</i>)
		SHE	standard hydrogen electrode

T	temperature	\bar{x}	statistical mean (average); also applicable to other variables, e.g. ${}^1\bar{J}_{PP}$ is the average 1-bond coupling constant between phosphorus nuclei
t	triplet (<i>in NMR</i>)		
t _{1/2}	half-life		
TBA	tetra- <i>n</i> -butylammonium		
TBAOTf	tetra- <i>n</i> -butylammonium triflate	Z _{eff}	effective nuclear charge
TBAPF ₆	tetra- <i>n</i> -butylammonium hexafluorophosphate	δ	chemical shift (ppm)
Tbt	2,6-([(Me ₃ Si) ₂ CH]C ₆ H ₃)	Δ	difference <i>or</i> change in
^t Bu	<i>tert</i> -butyl	ΔE	change in electronic energy of the reaction (<i>in DFT</i>)
T _c	coalescence temperature (<i>in NMR</i>)	ΔG	Gibbs free energy of the reaction
Tol	toluene	ΔG [‡]	Gibbs free energy of the transition state
Trip	2,4,6-triisopropylphenyl	ΔH	reaction enthalpy
V	volt	ΔH [‡]	enthalpy of the transition state
<i>vide infra</i>	see below	ΔS	reaction entropy
<i>vide supra</i>	see above	ΔS [‡]	entropy of the transition state
<i>vs.</i>	versus		
VSEPR	valence shell electron pair repulsion	η ^m	<i>m</i> contiguous atom coordination of a ligand to a single acceptor atom
VT-NMR	variable temperature NMR	κ ⁿ	<i>n</i> two-electron-donor atom coordination mode of a multidentate ligand
w	weak intensity (<i>in IR</i>)		
X	generic halogen atom	μA	microamperes
xs.	excess	μC	microcoulomb
		μL	microlitres
		v	sweep rate

σ	uncertainty	τ	torsional angle <i>or</i> dihedral angle
Σ	sum		
σ^*	Taft polar substituent constant	ϕ	Cremer-Pople phase angle for 5-membered rings
σ^*	sigma symmetry anti- bonding orbital	ϕ_{LP}	“dihedral angle” between the lone pairs on adjacent P atoms
σ^+	Hammett substituent parameters	χ^P	electronegativity (Pauling scale)
σ^ϕ	Kabachnik substituent constants		

Acknowledgements

I would like to recognize my family and friends for their support through the years of my Ph.D., especially through the writing of this thesis. My thanks especially to all those whose direct contributions made this thesis possible, including: my supervisor, Prof. Neil Burford, for allowing me the freedom to explore new areas of chemistry; the members of the Burford research group whom I've met and worked with over the years I have been here; Prof. Laura Turculet, for support on my research endeavours and use of electrochemical equipment; Prof. Heather Andreas, for an infinite amount of knowledge, teaching and discussion on the subject of all things electrochemical; Drs. Mike Lumsden and Kathy Robertson at NMR-3 for their assistance with variable-temperature NMR spectroscopy and helpful discussions of complex NMR spin systems; Drs. Bob McDonald and Mike Ferguson at the University of Alberta, and Dr. Andreas Decken at the University of New Brunswick for crystal structure solutions; Dr. Peter Wentzell, for teaching me how to properly analyze data and do my own linear regressions; the students I've had the pleasure to supervise over the years, particularly Ryan Tilley and Lauren Doyle, whose contributions inform this thesis; Xiao Feng, for assistance with ESI-MS measurements; Sarah Whittleton and Prof. Russell Boyd, for helpful discussions on computational chemistry; and, the organizations that fund our lab and my thesis work: Natural Sciences and Engineering Research Council of Canada, Killam Trusts, Eliza Ritchie Scholarship Foundation, Walter C. Sumner Fellowship, Canada Research Chairs program, Canada Foundation for Innovation, and Nova Scotia Research and Innovation Trust Fund.

Chapter 1. Introduction

1.1 Catenation and Logical Evolution in Chemical Synthesis

Modern applications of homogeneous or solution-state synthetic chemistry have a diverse scope, ranging from pharmaceutical compounds to novel plastics and materials. The majority of these compounds reflect structures based on a catenated, or homoatomically bonded, carbon backbone, such as is found in polypropylene or complex drug molecules. The predominance of carbon frameworks in synthetic chemistry derives not only from the natural abundance of carbon-backbone molecules in nature, but also from the substantial fundamental research in organic, or *catena*-carbon, chemistry over the past century.

To appreciate the extent of the development in organic synthetic methodology, it is useful to consider the hypothetical evolution of increasing complexity in chemical synthesis as represented in Figure 1.1. To approach the total synthesis of complex organic frameworks possessing numerous functional groups and precise stereochemical relationships between framework atoms [*e.g.* (-)-muraymycin-D2, an antibacterial natural product¹ (Figure 1.1c)], the synthetic chemist must possess detailed knowledge of a diverse set of bond-forming reactions. In the realm of organic synthesis, extensive detail is presently understood about numerous fundamental C-C bond forming reactions, such as a Diels-Alder (Figure 1.1a) or Grignard reaction (Figure 1.1b). To utilize these simple single-bond forming reactions in the precise synthesis of a more complex framework, however, a strong understanding of the reaction mechanism is needed. Knowledge of the stereoselectivity of the reaction (*e.g.* preference of the endocyclic transition state in [a]), effects of judicious selection of substituents (*e.g.* electron-withdrawing or donating

substituents in [a]), and the limitations of the reaction scope (e.g. functional group tolerance in [b]) in organic synthetic methodology allow for the application of these methods to the synthesis of comparatively large and precisely controlled structures.² This understanding can further extend to the synthesis of complex macromolecular architectures, including polymers and materials with precise tacticity and low polydispersity (e.g. poly(lactic acid), PLA, a biodegradable polymer. Figure 1.1d)^{3,4} and self-assembling macromolecular structures for electronic and optical applications (e.g. oligoether structures assembled into a honeycomb architecture, Figure 1.1e).⁵

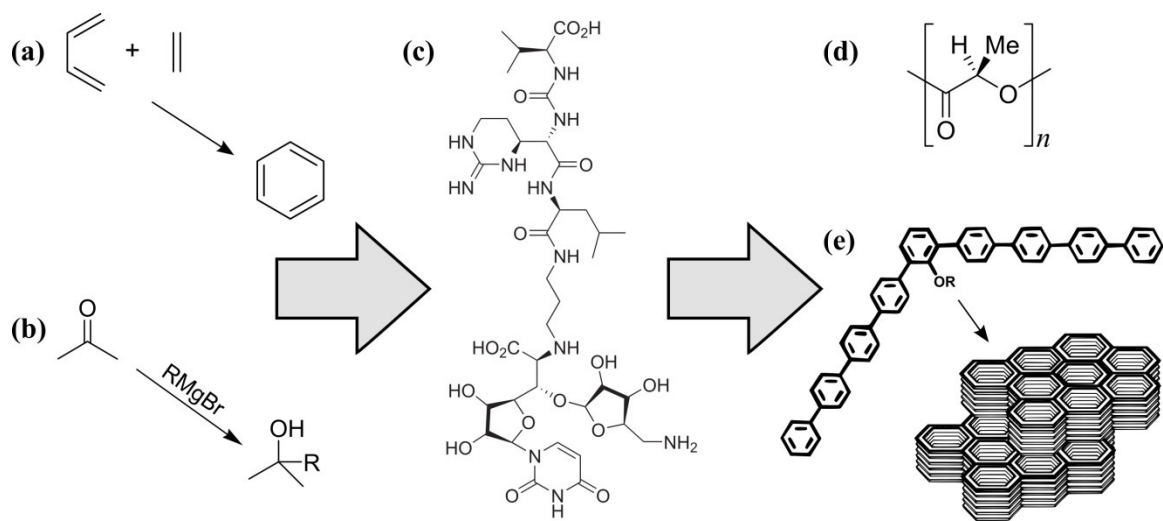


Figure 1.1. Graphical representation of the development of increasing structural complexity in synthetic organic chemistry, proceeding from fundamental chemical reactions (a-b) to intricate single molecules (c) to stereoregular polymers (d) and self-assembled supramolecular structures (e). Structure e has been adapted from reference 5.

In all cases, the logical extension of organic reactions to increasingly complex structures with specific real-world applications relies heavily on the well-developed understanding of simple carbon catenation reactions such as [a] and [b]. The development in this area has been in part assisted by the tendency of carbon to catenate, which is evident in the

numerous naturally occurring allotropes of carbon, *e.g.* graphite, diamond, and amorphous coal. This catenation chemistry, however, is not limited to carbon, and can be seen for other main group elements. The closest analogue is phosphorus, which has often been referred to in the literature as a “carbon copy.”⁶ Indeed, as phosphorus is situated diagonally adjacent to carbon on the periodic table, the two elements display similar electronegativities and correspondingly similar chemistry.⁶ The development of phosphoorganic chemistry, *i.e.* of compounds with mixed carbon-phosphorus frameworks, although newer than organic chemistry, is nonetheless becoming rapidly ubiquitous, particularly with applications in phosphoalkene polymerization and phosphoorganic π -conjugated materials for electronics.^{7,8} However, the catenation chemistry of strictly phosphorus frameworks is notably hampered by its larger atomic radius and lower effective nuclear charge, resulting in both weaker homoatomic bonds and greater kinetic lability (Table 1.1). Although the P-P homoatomic bond is weaker than its organic analogue, it is nonetheless thermodynamically favourable, and the availability of *d*-orbitals of compatible energies presents opportunities for structural diversity not available in a strictly carbon frame.

Catena-phosphorus chemistry has been well-developed for both neutral and anionic phosphorus frameworks (*vide infra*). Systematic methods for the synthesis of cationic *catena*-phosphorus derivatives from small molecule building blocks, however, remain comparatively unexplored.

Table 1.1. Comparison of selected fundamental parameters of carbon and phosphorus. References from Emsley⁹ unless otherwise noted.

	C	P
Electronegativity (Pauling, χ^P)	2.55	2.19
Single-bond covalent radius, r_{cov} (Å)	0.75 ¹⁰	1.11 ¹⁰
van der Waals radius, r_{vdw} (Å)	1.85	1.90
E-E bond length (Å)	1.54	2.21
E-E bond strength (kJ/mol)	346	201
E-C bond strength (kJ/mol)	<i>as above</i>	264

1.2 Catena-phosphorus Chemistry

Like carbon, phosphorus exists in a number of naturally occurring allotropes, including tetrahedral white phosphorus,^{11,12} amorphous red phosphorus,¹³ and graphitic sheet black phosphorus.^{14,15} Of these, black phosphorus is the most stable under ambient temperature and pressure conditions.¹⁶ In addition, a variety of other phases are known (Figure 1.2), including violet Hittorf's phosphorus (**1.1**)¹⁷ and phosphorus nanorods (*e.g.* **1.2**),^{18,19} which have been isolated and characterized, as well as diphosphorus, P₂, which has been identified in the gas phase.²⁰

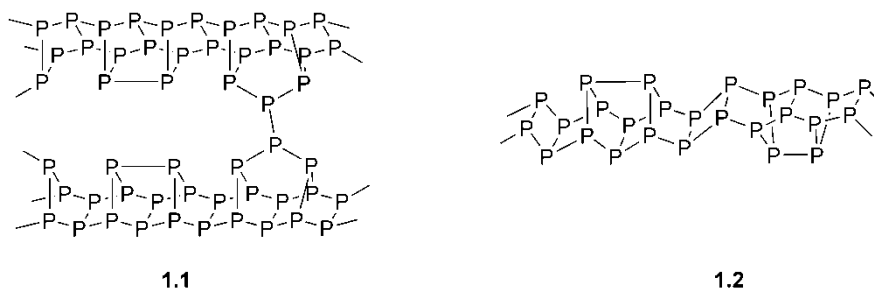


Figure 1.2. Structure of Hittorf's (violet) phosphorus (**1.1**) and a representative phosphorus nanorod (**1.2**) with a P₁₂ repeat unit. Note the structurally similar P₈ cage unit found in both allotropes.

Evident in the allotropes is the tendency for neutral 3-coordinate phosphorus to adopt significantly different geometries than those predicted by VSEPR theory. Whereas amines (NR_3) adopt pyramidal geometries with angles close to those of the tetrahedral carbon analogue (109.5°), phosphines (PR_3), including the atoms in elemental phosphorus, display bond angles between 90 - 100° .¹⁶ These consistently smaller bond angles emphasize that the traditional hybridization model used for chemistry of the second period ($n = 2$) is inconsistent with the properties of the heavier elements such as phosphorus ($n = 3$), where the diffuse np orbitals disfavour s - p mixing.²¹ The lone pair therefore retains predominantly s -character, and the bond angles around the phosphorus centre reflect primarily p -orbital contribution to the P-R bond. Notably, P(V) centres, such as those typified by phosphonium (tetrahedral) and phosphorane (trigonal bipyramidal) topologies (Table 1.2), are observed to adopt predicted VSEPR model geometries in the absence of the phosphorus lone pair. Regardless of these geometric considerations, however, the ready catenation of elemental phosphorus suggests that the synthesis of smaller molecular polyphosphorus frameworks should be likewise attainable.

Before proceeding with a discussion of the synthetic methods and known frameworks, a short discussion of phosphorus nomenclature is valuable. It should be noted that there are substantial inconsistencies in the literature in this regard, the most common being the substitution of the terms phosphine and phosphane when referring to three-coordinate neutral environments in North American and European contexts. For the purposes of this dissertation, the terminology for singly-bonded phosphorus frameworks listed in Table 1.2 will be used.

Table 1.2. Lewis depictions and nomenclature of the available bonding environments for phosphorus with single bonds only.

CN	cationic	neutral	anionic
1	$\text{:P}^{\oplus\oplus}\text{—}$ <i>phosphinidinium</i>	$\text{:P}\text{—}$ <i>phosphinidene</i>	
2	$\begin{array}{c} \ddot{\text{P}} \\ \oplus \\ \diagup \quad \diagdown \end{array}$ <i>phosphenium</i>		$\begin{array}{c} \ddot{\text{P}} \\ \ominus \\ \diagup \quad \diagdown \end{array}$ <i>phosphide</i>
3		$\begin{array}{c} \ddot{\text{P}} \\ \diagup \quad \diagdown \\ \text{ } \end{array}$ <i>phosphine</i>	
4	$\begin{array}{c} \\ \oplus \\ \text{P} \\ \diagup \quad \diagdown \\ \text{ } \end{array}$ <i>phosphonium</i>		$\begin{array}{c} \\ \ominus \\ \text{P} \\ \diagup \quad \diagdown \\ \text{ } \end{array}$ <i>phosphoramide</i>
5			$\begin{array}{c} \\ \text{P} \\ \diagup \quad \diagdown \\ \text{ } \end{array}$ <i>phosphorane</i>
6			$\begin{array}{c} \\ \ominus \\ \text{P} \\ \diagup \quad \diagdown \\ \text{ } \end{array}$ <i>phosphate</i>

1.2.1 Catena-phosphorus Anions

The closest synthetic analogs of elemental phosphorus are the unsubstituted polycyclic *catena*-phosphorus anions, which are readily derived via nucleophilic attack of LiPH_2 or Na on white phosphorus.²² The smallest and most stable compound synthesized by this route is the lithium salt of the P_7^{3-} cage. This heptaphosphorus trianion gives rise to a

single ^{31}P NMR resonance at room temperature, but three distinct resonances at low temperature, suggesting a dynamic equilibrium between the relevant phosphine and phosphide moieties.²³

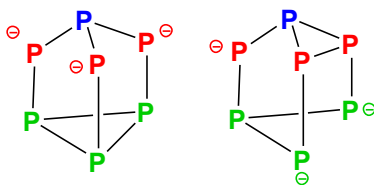


Figure 1.3. Two structural representations of the P_7^{3-} anion, which can be used to rationalize the observation of only one signal in ^{31}P NMR spectra of M_3P_7 at room temperature. Colouration of the atoms serves to highlight the interconversion between phosphorus sites, *e.g.* the blue phosphorus atom is apical at the left, but basal at the right.

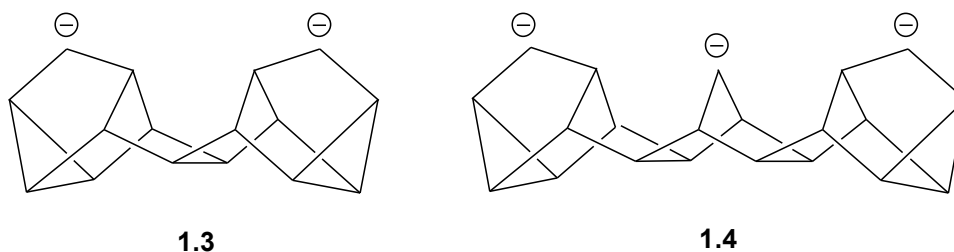
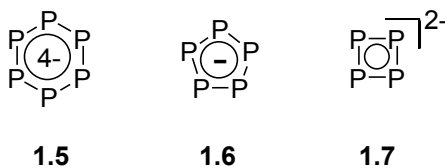


Figure 1.4. Simplified skeletal drawings of selected polycyclic polyphosphorus polyanions, P_{16}^{2-} (**1.3**) and P_{21}^{3-} (**1.4**). Vertices represent phosphorus atoms.

Larger polycyclic polyphosphides are also well-known, and examples **1.3**²⁴ and **1.4**²⁵ (Figure 1.4) serve to highlight the recurrent structural elements of these species, as both can be envisioned as P_7 units bridged by either P_2 or norbornene-like structures. Other structurally dissimilar anions are also known, although each nonetheless highlights the P_8 structure of Hittorf's phosphorus as a recurring motif (*vide supra*, Figure 1.2).^{22,23}

Additionally, transition metal complexes of extended unsubstituted polyphosphorus frameworks of this type are also known,²⁶⁻²⁸ but fall outside of the scope of this thesis.

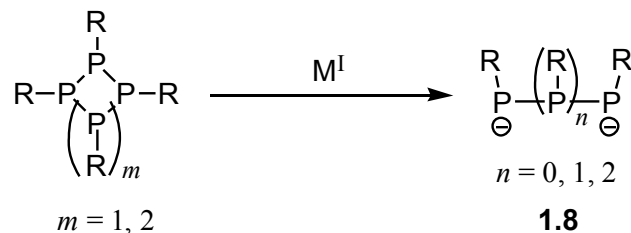
Sodium reduction of white phosphorus in coordinating solvents have been known to yield monocyclic polyphosphines as minor products, which were described as aromatic systems, based on their strongly downfield shifted ^{31}P NMR resonances.²² With the use of heavier alkali metals ($M = \text{K}, \text{Rb}, \text{Cs}$), solid state characterization was possible for M_4P_6 (**1.5**). The anion was found to be planar, with substantially shortened P-P bond lengths, (2.15 Å vs. 2.20 Å for a typical P-P single bond),²⁹⁻³¹ although later calculations by Korber and coworkers call into question the aromatic nature of this anion.³² Solution ^{31}P NMR studies indicated, however, that these six-membered anions undergo rapid redistribution once dissolved, yielding the more stable monoanionic five-membered cyclopentadiene analog **1.6** (^{31}P NMR: 475 ppm).³³ The dianionic four-membered ring **1.7** has also been synthesized separately and exhibits a solution ^{31}P NMR chemical shift (328-345 ppm) characteristic of an aromatic polyphosphine.³⁴



Alkali metal reduction of organocyclophosphines, or RPCl_2 and PCl_3 , rather than elemental phosphorus, provide routes to acyclic and cyclic organopolyphosphides, respectively. In the case of linear polyphosphides (Scheme 1.1), the stoichiometry of the reduction was found to determine the length of the resulting chain **1.8** regardless of the substituents chosen.^{23,35} More recently, several groups have investigated the reductive coupling of RPCl_2 ($\text{R} = \text{tBu}, \text{Ph}, \text{Mes}$) as a more direct route to the four-membered dianions **1.8**_{n=2}, thus eliminating the need to synthesize the neutral ring (Section 1.2.2).³⁶⁻

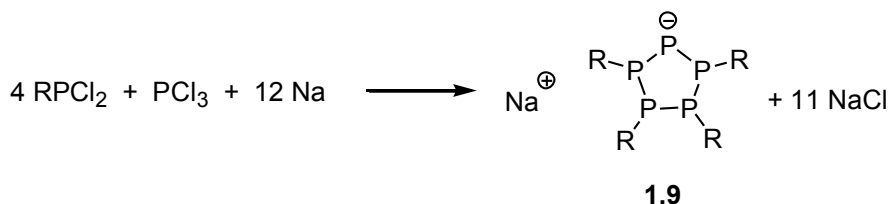
³⁹ The assignment of these linear anions was supported through ^{31}P NMR studies, as well

as cyclic voltammetry and other electrochemical studies, which will be described in greater depth in Chapter 5.



Scheme 1.1. Alkali metal ($\text{M}^{\text{I}} = \text{Li}, \text{Na}, \text{K}$) reduction of cyclopolyposphines to acyclic polyphosphides.

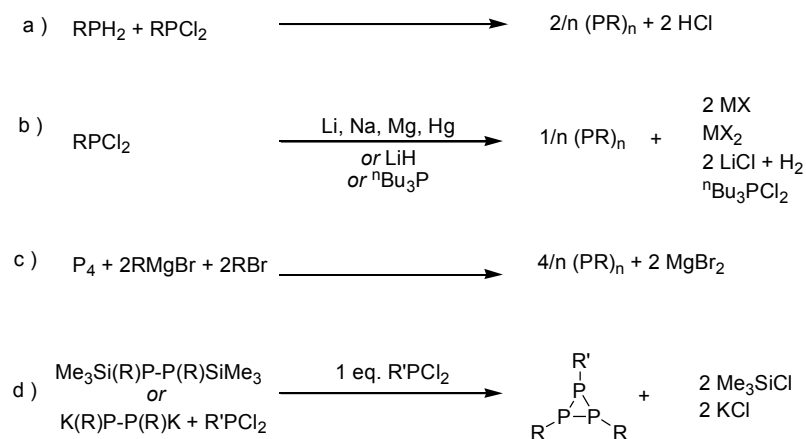
Observation of $\mathbf{1.8}_{n=2}$ from the sodium reduction of RPCl_2 led additionally to the development of routes to cyclic monoanions, as the linear fragments were observed to coordinate M^+ cations in the solid state in a fashion structurally reminiscent of a five-membered ring. Introduction of PCl_3 into the reduction provided the source of “naked” phosphide en route to $\mathbf{1.9}$ (Scheme 1.2).⁴⁰⁻⁴²



Scheme 1.2. Synthesis of monocyclic catena-phosphorus anions ($\text{R} = \text{}^t\text{Bu}, \text{}^i\text{Pr}, \text{Ph}$).

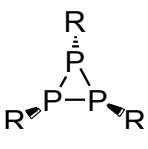
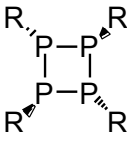
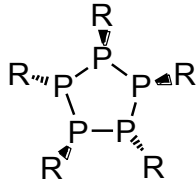
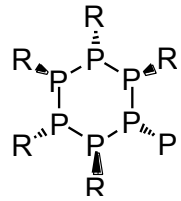
Although comparatively rare, the synthesis of linear organopolyphosphorus anions has been accomplished via the *in situ* silylation of naked phosphorus atoms from P_4 . The reaction of silanides, $\text{M}[\text{Si}^t\text{Bu}_3]$ ($\text{M} = \text{Li}, \text{Na}, \text{K}$), with white phosphorus led to the formation of the monoanion $\mathbf{1.10}$, while the heavier alkali silanides ($\text{M} = \text{Rb}, \text{Cs}$) permitted the isolation of the dianionic supersilyl derivative $\mathbf{1.11}$.

The addition of organic substituents allows for the isolation of remarkably similar acyclic frameworks, as well as a series of well-characterized cyclic polyphosphines. Several general methods for the synthesis of neutral cyclic frameworks are known, namely (a) dehydrohalogenation, (b) reduction, (c) activation of P₄ by Grignard reagents, and (d) metathesis (Scheme 1.4). Notably, reductive coupling (b) has also been accomplished using electrochemical means.²² A variety of alternative methods for the synthesis of specific cyclic polyphosphines are also known,²² but these are not relevant to the present discussion of methodology as they have extremely limited applicability.



Scheme 1.4. Generalizable routes to neutral monocyclic polyphosphines.

Table 1.3. Reported isolated yields and structural features of readily synthesized homoleptic cyclopolyposphines, from Baudler²² unless otherwise noted.

				
	1.15	1.16	1.17	1.18
Endocyclic bond angles	60-61°	80-87°	94-108° (\bar{x} =100°)	95-96°
Conformation	planar	folded (τ = 25-46°)	twisted envelope	chair
Substituent (R)	% Yield of (RP) _n isolated			
Ph	--	82 ^a	93 ^b	n.r. ^b
Me	--	--	67	--
Et	--	--	81	--
ⁿPr	--	--	92	--
ⁿBu	--	--	82	--
ⁱPr	38	80	--	--
Cy	18	79 ^b	7	--
NⁱPr₂	--	57	--	--
^tBu	60 ^b	63 ^b	--	--
ⁱPr_F	100	--	--	--

n.r. Not reported. ⁱPr_F = perfluoro-isopropyl. ^a From Stephan and coworkers.⁴⁹

^b Crystallographically characterized.

With the exception of the reaction depicted in Scheme 1.4d, which proceeds via a [2+1] or [3+1]-cyclocondensation mechanism, the remaining reactions are non-specific with regards to ring size. That is, regardless of the reaction stoichiometry, the cyclic products

that result are those with the thermodynamically most-favourable ring size with respect to the steric constraints imposed by the substituents. This feature is highlighted in Table 1.3, which demonstrates the tendency of bulky substituents to enforce smaller ring sizes. Even when other ring sizes are initially synthesized, the weak P-P bond (vs. C-C) allows for ready oligomerization. For example, (PPh)₃ oligomerizes at room temperature to yield first (PPh)₄ and then (PPh)₅, while (PPh)₆ decomposes back to (PPh)₅ upon heating.²²

The stability of the five-membered ring in the absence of sterically demanding substituents highlights the geometric features of phosphorus (Section 1.2) in comparison to carbon, which is most stable as a six-membered cyclohexane derivative. Where cyclohexanes allow for the minimum torsional strain in carbon-centric systems, trans-annular repulsion between phosphine lone pairs is virtually non-existent. Further, the wider angles in cyclopentaphosphines (~100°) are the least strained, mimicking those of unrestricted PR₃ phosphines, and the commonly observed envelope conformation (featuring four coplanar phosphorus atoms) allows for delocalization of the lone pair on the out-of-plane atom into the σ^* -orbitals of the P-P bonds in the ring.⁵⁰ This additional stability, described as pentagonal stabilization, provides strong rationale for the recurrence of this 5-membered ring motif in all areas of *catena*-phosphorus synthesis.

A limited number of branched ring systems have been reported in the literature, typically with kinetically stabilizing ^tBu substituents. Although the majority of the branched *cyclo*-polyphosphines have been prepared via the thermolysis of acyclic species, two other routes to these species are relevant in the context of methodology development in phosphorus chemistry. Extension of the metathesis reaction described earlier permits the isolation of branched three-membered rings by the reaction of *cyclo*-triphosphines

bearing an SnMe₃ functionality with PCl₃ or ^tBuPX₂ (X = Cl, I), highlighting the utility of functionalized polyphosphines in the development of new frameworks.⁵¹ Similarly, metathesis and Me₃SiCl elimination from a mixed Me₃Si- and Cl-substituted acyclic triphosphine generates an unstable intermediate phosphino-diphosphene (^tBu₂P-P=PR), which subsequently dimerizes to generate a four-membered branched ring.⁵²

A diverse array of polycyclic polyphosphines have also been reported in the literature, generally synthesized via the reductive coupling of PCl₃ and RPCl₂ (or the already reduced cyclopolyphosphines [RP]_n) with Mg, thereby generating apical (unsubstituted) P-centres from PCl₃ and achieving kinetic stabilization via phosphinidene (RP) fragments. The substitution of P₄ for PCl₃ as a source of unsubstituted phosphorus is also known.²² The vast array of different polycyclic structures,^{22,23} ranging from bicyclic to octacyclic systems, is too extensive for review herein, but a selection of different architectures is highlighted in Figure 1.5. Of note is the familiar structural motif in framework **1.19**, seen previously in discussion of allotropic Hittorf's phosphorus (Section 1.2), as well as the apparent thermodynamic preference for phosphorus skeletons with repeated five-membered ring elements. Furthermore, the formation of [*m.n.1*] (**1.20**) or [*x.y.0*](**1.21**) bicyclic motifs predominate the structural chemistry of these polycyclic species except in the case of the sterically demanding *tert*-butyl substituent. The additional steric shielding offered by the bulky *tert*-butyl groups has allowed for the isolation of skeletal frameworks such as **1.22** and **1.23** with relatively linear linkages between rings. In general, however, the synthesis of polycyclic species results in mixtures of different frameworks, so the majority have been characterized solely *in situ* via analysis of their complex ³¹P NMR spectra.

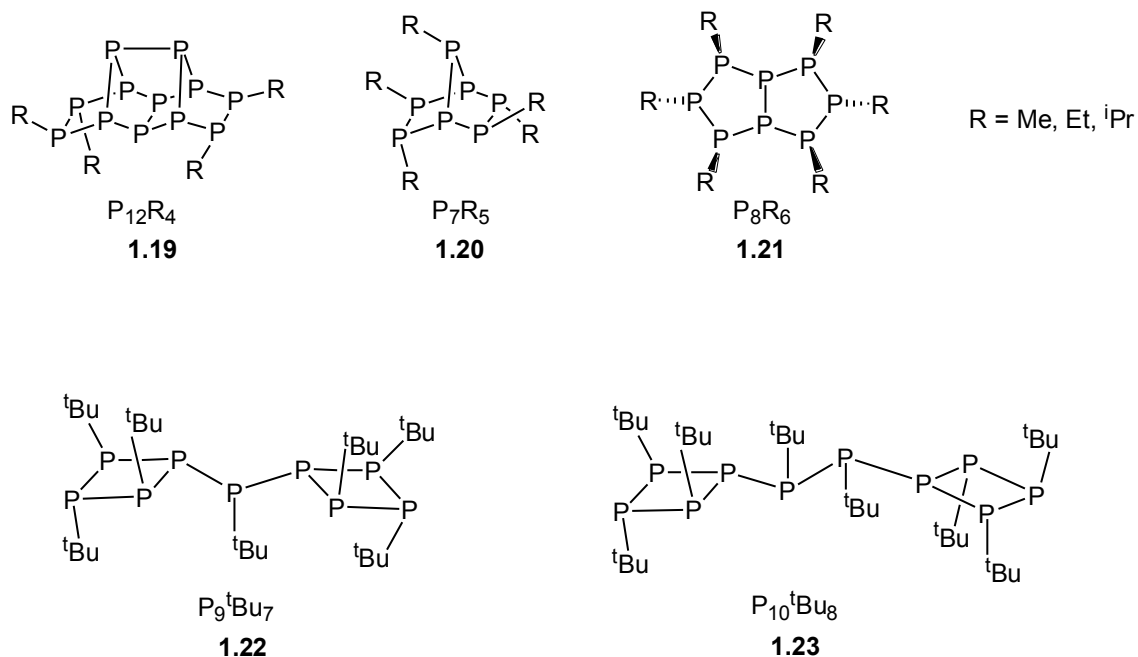


Figure 1.5. Selected examples of neutral polycyclic frameworks.^{22,35,53,54}

1.2.3 Catena-phosphorus Cations

The most commonly occurring motif in carbon backbone frameworks is the four-coordinate, tetrahedral carbon centre, it being the most unreactive carbon environment owing to the inherent strength of the C-C σ -bond (σ : 346 kJ·mol⁻¹ vs. π : 256 ± 21 kJ·mol⁻¹).^{55,56} Extension of the carbon-phosphorus analogy (see Section 1.1) therefore suggests that the isolobal four-coordinate phosphonium moiety (Chart 1.1), and by extension, cationic polyphosphorus chemistry, merits significant consideration. Indeed, while geometric parameters of neutral and anionic phosphorus nuclei remain at odds with traditional carbon bonding models which invoke hybridization, phosphonium centres display nearly tetrahedral angles (*vide supra*), and therefore more closely mimic the geometric environment about the ubiquitous carbon frame.

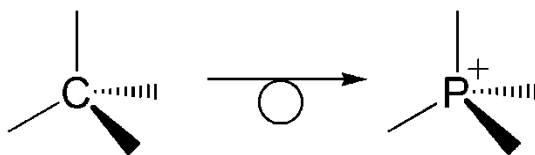
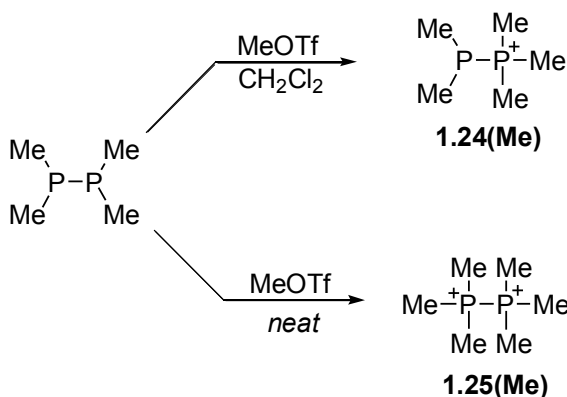


Chart 1.1. The isobal nature of four-coordinate carbon and phosphorus (phosponium) fragments.

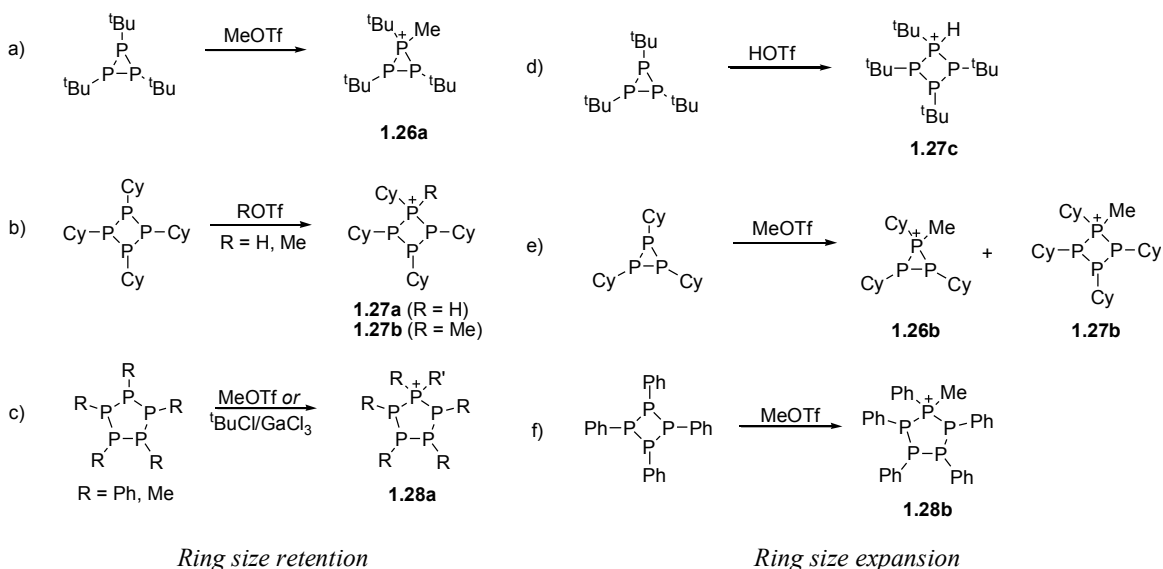
Despite this comparison, the chemistry of cationic polyphosphorus systems remains underdeveloped relative to the anionic and neutral analogues. Chart 1.2 depicts all known *catena*-phosphorus frameworks possessing an overall positive charge. Reactions directed toward the synthesis of such molecules are often high yielding owing this positive charge, which provides for a distinct low energy reaction pathway. These reactions, rather than the frameworks themselves, will be the focus of this section, as it is methodology development and reactivity that form the primary motivation for this thesis.



Scheme 1.5. Methylation products in CH_2Cl_2 solution or in the absence of solvent.

At present, the majority of synthetic approaches to cationic polyphosphorus systems rely on the use of neutral polyphosphines as starting materials. Solution alkylation or protonation reactions of diphosphines (Scheme 1.5, top) and cyclo- $(\text{PR})_n$ species (Scheme 1.6) yield the acyclic monocationic phosphinophosponium cations (**i**) and the cyclic monocations (**ix-xi**).⁵⁷⁻⁵⁹ Binary reaction mixtures or solvent-free reactions of

MeOTf with the same polyphosphines (*e.g.* Scheme 1.5, bottom) has allowed for the high yielding synthesis of the corresponding dications (**vi**, **xii** and **xiv**).^{58,60,61} Recent work has also demonstrated that analogous solution halonium addition (Scheme 1.7) allows for the isolation of chloro-substituted versions of the frameworks **x** and **xii**.⁶² Alkylation or protonation of the monocationic triphosphonium framework (**ii**) offers one route towards the acyclic dication **vii**, although these derivatives can also be directly synthesized (Scheme 1.8).⁶³



Scheme 1.6. Alkylation and protonation reactions of cyclo-polyphosphines resulting in net ring-size retention (*a-c*) or ring-size expansion (*d-f*).

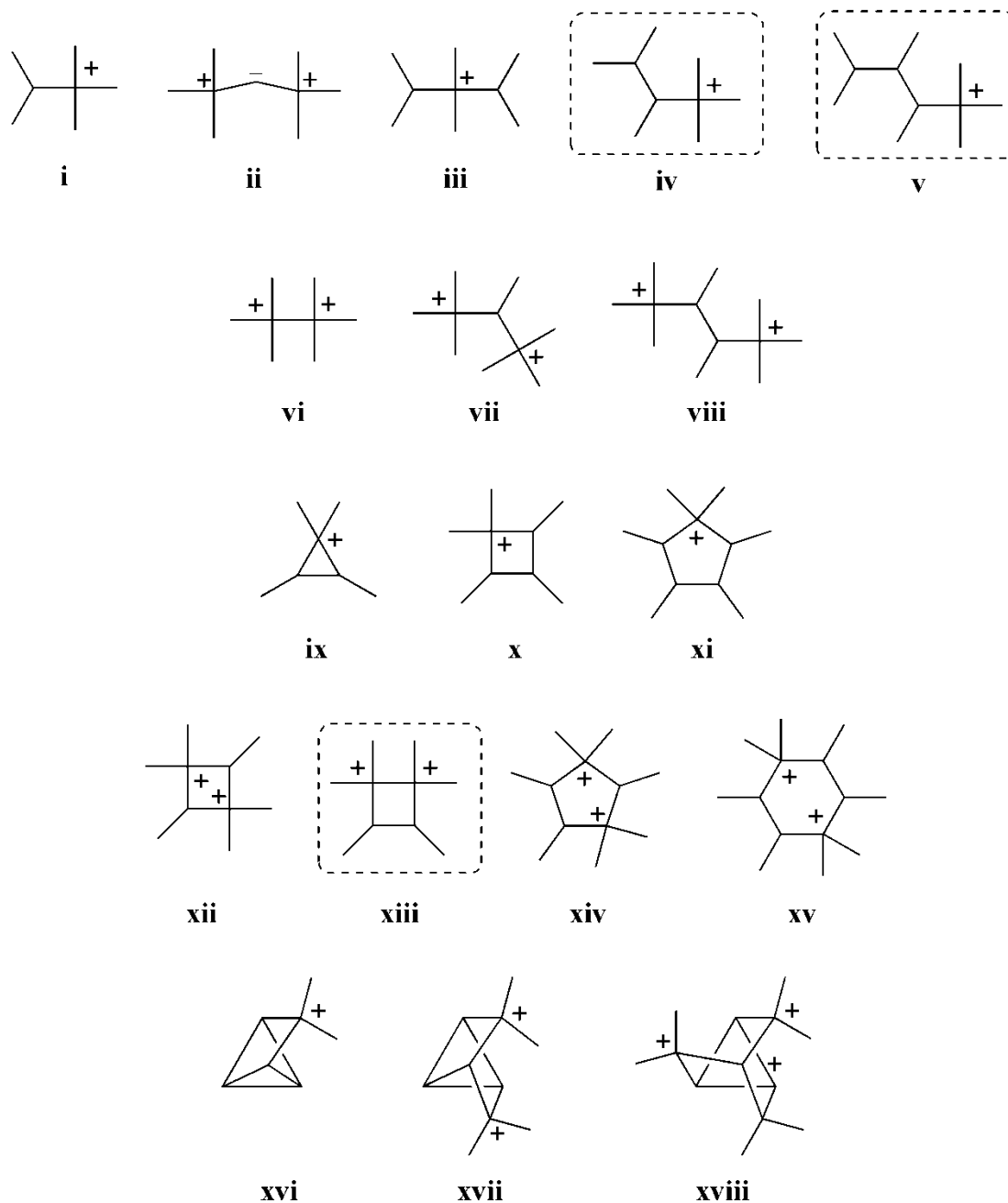
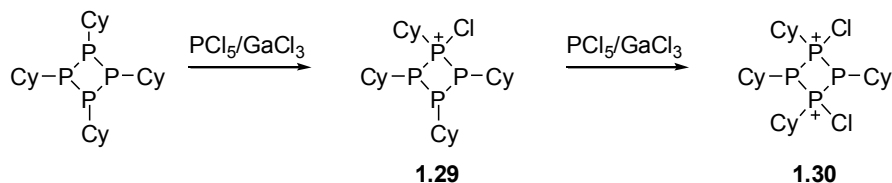
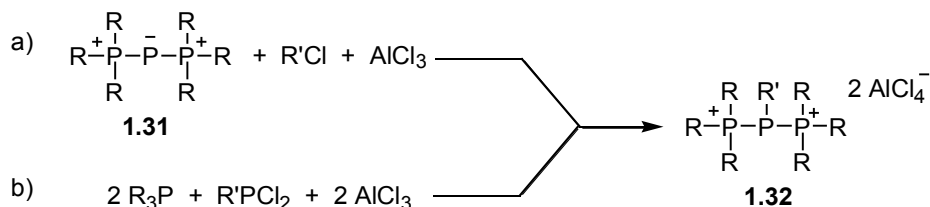


Chart 1.2. Skeletal representations of all known cationic catena-phosphorus frameworks (updated from reference 64), categorized into acyclic monocations (**i-v**) and dications (**vi-viii**), monocyclic monocations (**ix-xi**) and dications (**xii-xv**) and polycyclic cations (**xvi-xviii**). Vertices represent phosphorus atoms, while terminal positions represent organic substituents. Frameworks in dotted boxes have been observed^{65,66} but are not yet reported in the literature.



Scheme 1.7. Successive chloronium addition to *cyclo*-(PCy)₄ to produce functionalized derivatives of framework **x** (**1.29**) and **xii** (**1.30**).



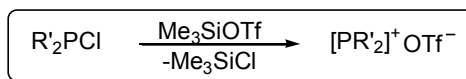
Scheme 1.8. Alternative alkylation (a) or direct synthesis (b) routes to framework **vii** (**1.32**).

A second route to polyphosphorus cations arises from the insertion of *in situ* generated phosphonium cations $[\text{PR}_2]^+$ into the P-P bonds of diphosphines⁶⁷ and *cyclo*-polyphosphines^{59,68} (Scheme 1.9). The chemistry of phosphonium cations will be discussed in greater detail in Section 1.3.2, but in the context of these insertion reactions, $[\text{PR}_2]^+$ is generated by halide abstraction from a chlorophosphine. Reactions of $[\text{PR}_2]^+$ with diphosphines $\text{R}'_4\text{P}_2$ ($\text{R}' = \text{Ph}, \text{Me}$) yielded the first examples of the framework (**iii**), resulting from either insertion $[\text{R}'_2\text{P}-\text{PR}_2-\text{PR}'_2]^+$ or coordination $[\text{R}'_2\text{P}-\text{PR}'_2-\text{PR}_2]^+$ of the phosphonium moiety depending on the steric constraints of the substituents.⁶⁷

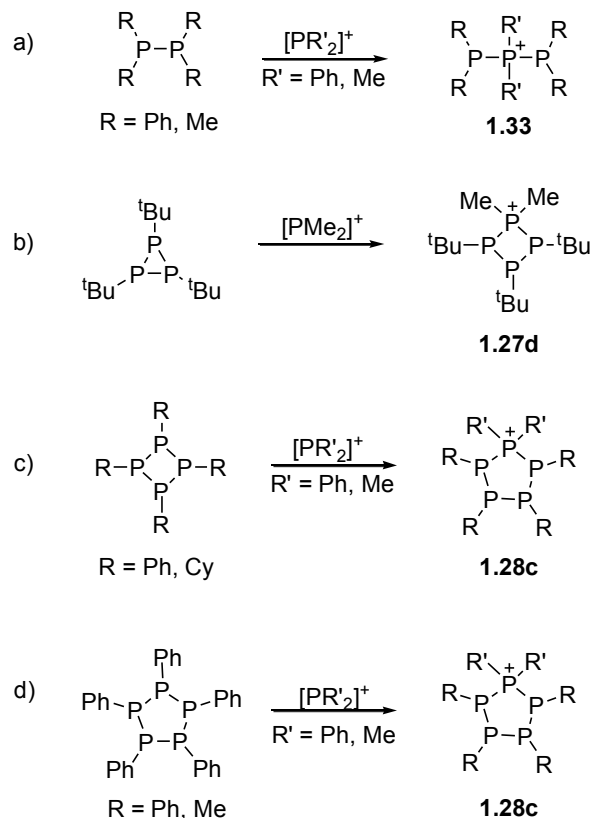
Phosphonium insertion into cyclopolyphosphines in solution yielded the monocationic

derivatives **x** and **xi** via ring-size expansion (Scheme 1.9[b] and [c]) or ring-size retention pathways (Scheme 1.9[d]), presumably resulting from rapid solution redistribution reactions proceeding to the thermodynamically preferred ring-size (*cf.* neutral ring size redistribution reactions, Section 1.2.2).^{59,67,68} In contrast, the melt reaction of polyphosphines (PhP)₅, (MeP)₅, or white phosphorus, P₄, with Ph₂PCl and GaCl₃ allows for the insertion of multiple [Ph₂P]⁺ units, resulting in the frameworks **xv-xviii**.^{69,70}

The third general method to polyphosphorus cations does not rely on the use of neutral polyphosphines, but rather involves the reductive coupling of chlorophosphines in the presence of a donor phosphine R₃P and a halide abstractor. This method was originally developed by Schmidpeter and coworkers to generate the triphosphenium monocations **ii**⁷¹⁻⁷³, and this methodology has since been extended to numerous cyclic and acyclic derivatives of this framework.^{74,75} Variations of this reaction, including the use of cyclohexene⁷⁶ or SnCl₂⁷⁷ as reducing agents, demonstrate that reductive coupling to yield cationic frameworks necessitates the use of relatively weak reductants compared to the reduction to neutral polyphosphines (*cf.* Section 1.2.2). This framework has also been prepared from the reaction of chelating diphosphines with PI₃, which is proposed to act as an *in situ* source of P(I), owing to its equilibrium disproportionation first to P₂I₄ and I₂ and subsequently to (PI)_n.^{78,79} Reductive coupling has also been utilized in the preparation of the framework **viii**,⁸⁰⁻⁸² as will be detailed in Chapter 2.



in situ generation of phosphonium cations



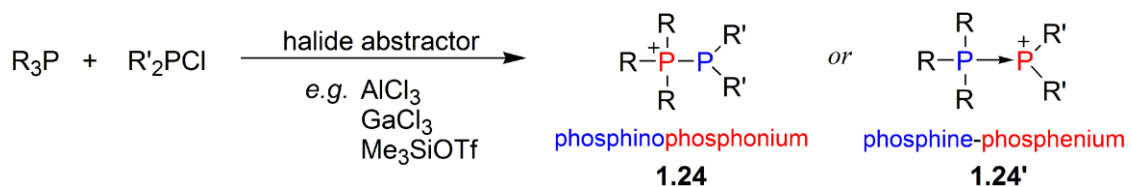
Scheme 1.9. Phosphenium insertion reactions leading to monocationic polyphosphorus species. Reactions involving cyclic species have been known to proceed with either ring size expansion or ring size retention.⁵⁹

Of all the known cationic frameworks, then, the simplest is the phosphinophosponium monocation **i**, and its potential utility as a synthon for larger cationic frameworks without reliance on neutral polyphosphorus starting materials forms the basis for this thesis.

1.3 Phosphinophosponium Cations as Building Blocks

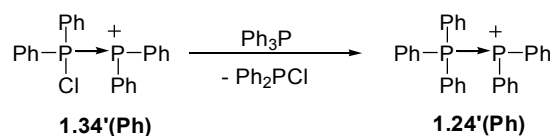
The smallest cationic *catena*-phosphorus building blocks are the phosphinophosponium cation **1.24**. These can be synthesized by halide abstraction (*e.g.* with Me₃SiOTf, GaCl₃

or AlCl₃) from a chlorophosphine in the presence of another equivalent of a donor phosphine (Scheme 1.10).⁸³⁻⁸⁵ To approach the use of these compounds as building blocks toward larger catenated cationic frameworks, one must first understand the bonding and reactivity of these deceptively simple monocation salts. The phosphorus-phosphorus bond in phosphinophosponium cations can be readily described by one of two models: a covalent interaction depicted by a standard Lewis structure (**1.24**) or a coordinate or dative bond (**1.24'**)



Scheme 1.10. Synthesis of a generic phosphinophosponium cation by halide abstraction from a chlorophosphine.

Although recent computational studies⁸⁶ have suggested that a covalent model of the P-P bond is better suited when R = alkyl, the coordinate bonding model (**1.24'**) of these complexes is supported by their demonstrated capacity to undergo ligand exchange. This includes the dynamic behaviour observed in the solution state ³¹P NMR spectra of the amido-derivatives (e.g. [(Me₂N)₃P-P(NMe₂)₂][AlCl₄]),⁸⁷ as well as the quantitative displacement of the phosphonium moiety by stronger phosphine donors^{84,88} (Scheme 1.11). It follows, then, that the acceptor chemistry of phosphorus may offer some insight into the chemistry of these ions.



Scheme 1.11. Ligand exchange behaviour in phosphinophosponium cations

1.3.1 Phosphorus as an Acceptor

The traditional view of coordination complexes characterizes the coordinate bond as strictly formed by the donation of electrons from an electron-rich non-metal ligand to an electron-poor metal centre.⁸⁹ In this context, pnictogen, or group 15, centres (Pn) bearing an available lone pair for donation must be classified as Lewis bases. However, such Pn(III) species possess a demonstrated capacity to function as Lewis acidic acceptors. The simplest example of this behaviour exists in the phosphoranide anion $[\text{PBr}_4]^-$, which can be described by a traditional Lewis/VSEPR bonding model as a disphenoidal anion with four substituents (**1.35**), or, alternately, as a donor-acceptor complex of Br^- and PBr_3 (**1.35'**).⁹⁰

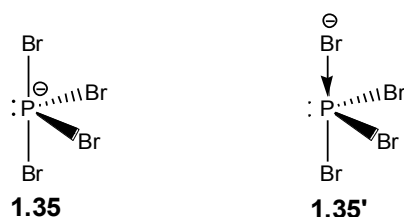


Figure 1.6. Lewis (**1.35**) and coordinate (**1.35'**) bonding descriptions for the anion $[\text{PBr}_4]^-$

In general, phosphoranides are hypervalent anionic phosphorus(III) species featuring a distorted disphenoidal geometry in the solid state, with typically longer axial bonds and an angle of only $160\text{-}170^\circ$ between axial substituents, purportedly due to repulsion by the lone pair of electrons in the formally equatorial position.⁹⁰ Halophosphoranides, such as **1.35**, that have been structurally characterized in the solid state are either weakly dimeric as in the anions of $[\text{Pr}_4\text{N}][\text{PBr}_4]$ (Figure 1.7),⁹¹ or monomeric as in the anions of $[\text{Et}_4\text{N}][\text{PBr}_4]$, in which one axial P-Br bond is significantly longer than the other.⁹² This supports a coordination model (**1.35'**) for the bonding in these species, where three halide

substituents are covalently bonded to the P(III) centre, while the remaining axial substituent is bonded via a weaker coordinate interaction.

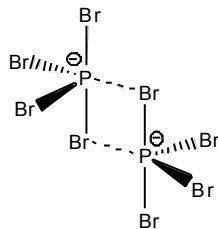
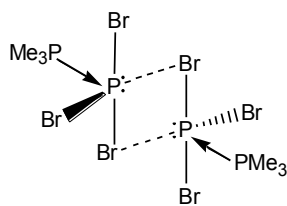
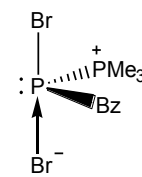


Figure 1.7. Solid-state structure of the anion in $[\text{nPr}_4\text{N}][\text{PBr}_4]$. Note the P...Br distance between monomer units is 3.460(4) Å (*cf.* P-Br_{eq} = 2.2-2.3 Å; P-Br_{ax} = 2.5-2.6 Å)⁹⁰

What is more interesting, however, is the debate as to whether such adducts are best described by a covalent or ionic formulation, particularly as neutral adducts of this type are also known. For example, the solid-state structure of the dimeric $\text{Me}_3\text{P} \rightarrow \text{PBr}_3$ adduct (**1.36**)⁹³ displays the expected distorted disphenoidal geometry (axial Br-P-Br: 170°) which characterizes the previously discussed phosphoranides. The donor phosphine lies in the equatorial plane and demonstrates a normal P-P single bond length (2.26 Å). In addition to much longer P-Br distances (3.33 Å) between monomer units, one axial P-Br bond in each unit is significantly elongated [2.677(2) Å vs. 2.424(2) Å]. Müller and coworkers therefore describe each monomer in this complex as intermediate between a coordinate covalent and an ionic interaction (*i.e.* $[\text{Me}_3\text{P-PBr}_2]^+\text{Br}^-$).⁹³



1.36



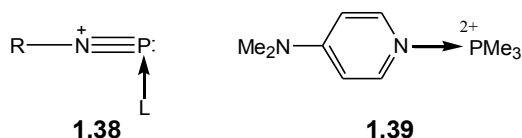
1.37

In contrast, $\text{Me}_3\text{P} \rightarrow \text{PBnBr}_2$ (**1.37**)⁹³ is monomeric, but nonetheless possesses one significantly lengthened axial P-Br bond (2.96 Å) in the solid state. This suggests that the weaker acceptor capability of PBnBr_2 results in dissociation of the Br^- anion instead of expected weakening of the P-P bond (2.24 Å). The authors thus describe this system as primarily ionic in nature (i.e. $[\text{Me}_3\text{P-PBrBn}]^+\text{Br}^-$), consisting of a pyramidal phosphorus centre with a weak interaction with the associated anion, and they remark that the distortion from the theoretical disphenoidal structure is too large to be justified by solely lone pair repulsion (equatorial P-P-C: $100.8^\circ \ll 120^\circ$).

Regardless of whether these Lewis donor-acceptor adducts are regarded as covalent or ionic species, the primary thermodynamic factors affecting their formation remain essentially constant – a delicate balance between the energy of the newly formed adduct bond and the required geometric or structural adjustments about the donor and acceptor centres.⁸⁹ As the geometry changes are comparatively minimal in neutral species where the phosphorus centre remains essentially pyramidal, the bond energy in the resulting adduct depends principally on the stabilization that results from the HOMO/LUMO interaction. Thus, the heavier pnictogens are comparatively poor acceptors, since their higher energy valence orbitals result in a higher energy LUMO.

On the other hand, cationic systems possess a lower energy LUMO, which provides increased stabilization of the adduct relative to the neutral derivatives. In addition,

coordinative unsaturation at cationic centres improves the favourability of adduct formation by reducing the steric congestion about the pnictogen centre. Finally, the resultant ionic complex further benefits from stabilizing electrostatic interactions and crystal lattice energy. These factors thus favour the isolation of ligand-stabilized cationic pnictogen centres, such as phosphadiazonium derivatives (**1.38**[OTf])⁹⁴⁻⁹⁶ or even the dicationic P(V) species [PMe₃]²⁺ (**1.39**[OTf]₂).⁹⁷



1.3.2 Phosphenium Cations, [PR₂]⁺

In contrast to the phosphoranides and their heavier congeners, where *d*- or σ^* -orbital involvement is typically invoked to rationalize the hypervalent Lewis bonding description, phosphenium cations [PR₂]⁺ possess only two substituents in addition to the lone pair, thus leaving an empty p-orbital available for coordination (Figure 1.8).

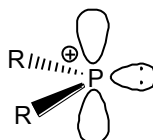
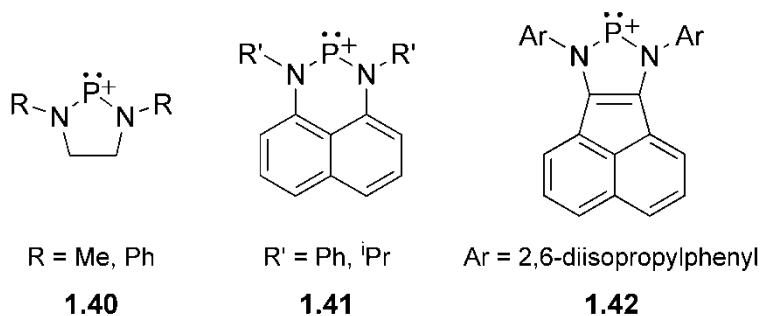


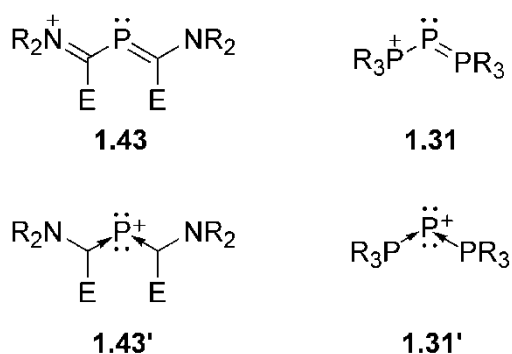
Figure 1.8. Orbital depiction of a phosphenium cation

The majority of isolable uncomplexed phosphenium salts demonstrate some degree of substituent stabilization by π -delocalization.⁹⁸ Indeed, the first reported example of a stabilized phosphenium centre, [**1.40**(Me)][PF₆], possesses a chelating diamido framework.⁹⁹ Like the analogous neutral compound, the well-studied isolobal N heterocyclic carbene (NHC),¹⁰⁰ **1.40**(Me) and other N-heterocyclic phosphenium

cations^{98,101} are stabilized by $p\pi$ -donation from two amido-substituents, regardless of the structural diversity in the carbon backbone evidenced in more recently synthesized extended N-heterocyclic phosphonium cations **1.41**^{102,103} and **1.42**,¹⁰⁴ which possess extended π -aromatic structures.

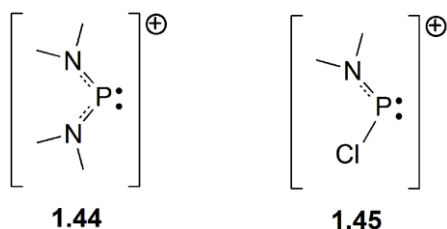


The phosphonium bonding environment should be regarded as distinct from other two-coordinate phosphorus monocations such as phosphamethine cyanines **1.43** ($E = \text{CR}_3$, NR_2 , or SR) and triphosphonium cations **1.31**, where the reactivity (*vide infra*) and ³¹P NMR chemical shift of the dicoordinate phosphorus atom (**1.43**: -129 to +156 ppm; **1.31**: -290 to -173 ppm)¹⁰⁵ indicate a higher degree of π -delocalization of the positive charge onto the substituents.

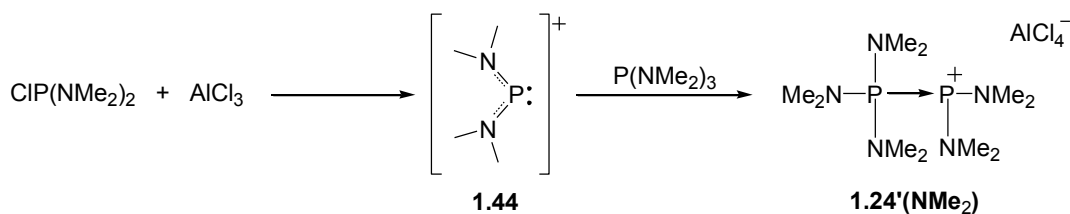


In spite of the substantial π -stabilization provided by the amido-donors, N-heterocyclic phosphonium salts, such as **1.40-1.42**, display the strongly downfield ³¹P NMR signals

(222 to 366 ppm) expected of a P(III) phosphonium centre (200 to 500 ppm).⁹⁸ Moreover, while compounds of type **1.43** or **1.31** act as weak Lewis bases and are subject to protonation,¹⁰⁵ N-heterocyclic phosphonium centres are relatively poor σ -donors and strong Lewis acidic π -acceptors.¹⁰⁶

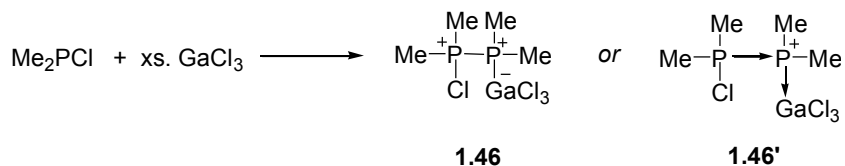


The earliest isolated acyclic phosphonium cations (**1.44**[AlCl₄] and **1.45**[AlCl₄]) were similarly stabilized by donation from N-substituents, although they lack additional delocalization into the aromatic backbone found in many of the aforementioned N-heterocyclic derivatives. Nonetheless, these salts possess the expected downfield ³¹P NMR chemical shift parameters associated with the cationic phosphorus centre (from 250-510 ppm, although most commonly found between 250-350 ppm).^{98,107} However, without adequate stabilization from substituents, the synthesis of isolated phosphonium centres seemed impossible; indeed, typical strategies for halide abstraction have been observed to fail in the absence of adequately bulky π -donating substituents. Instead, neutral adduct formation was observed between chlorophosphines and Lewis acidic halide abstractors such as AlCl₃ in the absence of at least one π -donating substituent such as an amido or ferrocenyl moiety.^{108,109} This therefore suggests that thermodynamic stabilization from π -donating substituents is more crucial than the steric protection offered by bulky substituents.⁹⁸



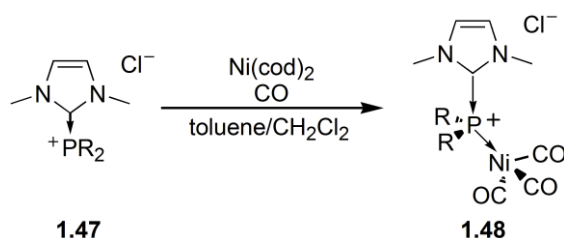
Scheme 1.12. Phosphine (Lewis base) stabilization of a diamidophosphenium cation

The observation of adduct-formation suggests an alternative route to phosphonium cations, namely via ligand stabilization of the empty p-orbital at the phosphonium centre. Parry and coworkers^{87,110} established, using ³¹P NMR spectroscopy, that the addition of a second equivalent of phosphine resulted in phosphine-stabilized phosphonium cations (Scheme 1.12), an assertion which was supported by the much later isolation and crystallographic characterization of **1.24(Ph)** [Ph₃P-PPh₂][OTf].⁸⁸ These phosphine-stabilized phosphonium centres will be discussed in greater depth in terms of their role in *catena*-phosphorus chemistry in later chapters. It is significant to note, however, that in the absence of π -donating substituents at phosphorus, an excess of the halide abstractor GaCl₃ results only in the formation of a GaCl₃-adduct (**1.46**) of the phosphine-stabilized phosphonium unit (Scheme 1.13), whereas quantitative conversion to the phosphonium cation **1.44** occurs with (Me₂N)₂PCl.¹¹¹ Again, this indicates the comparative stabilization provided by π -donating substituents.



Scheme 1.13. Formation of GaCl₃-adducts with alkylphosphines in the presence of excess GaCl₃

Furthermore, theoretical studies have shown that phosphonium and arsenium cations with π -donating substituents form weaker interactions with donor ligands, characterizing them as primarily coordination complexes (e.g. **1.24**), while analogous cations with methyl substituents form covalent bonds to incoming donors.⁸⁶ Finally, the isolation of the GaCl₃-adduct **1.46** re-emphasizes the Lewis amphoteric nature of these phosphonium cations, clearly indicated in the coordinate bonding description **1.46'**. This property can be exploited in traditional coordination chemistry as well, as demonstrated by the recent use of the N-heterocyclic carbene stabilized phosphonium cation **1.47** as a strongly π -accepting ancillary ligand on a Ni-carbonyl complex, **1.48** (Scheme 1.14).¹¹²



Scheme 1.14. An NHC-stabilized phosphonium centre (R = Ph, ⁱPr, Cy) acting as a strongly π -accepting ligand, as indicated by high ν_{CO} (2075-2082 cm⁻¹)

1.4 Summary

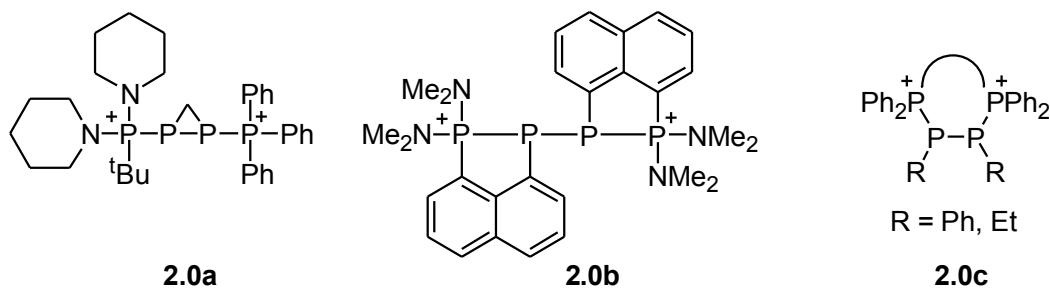
The logical development of *catena*-phosphorus chemistry requires the investigation of generalizable synthetic methods which can be applied to diverse functionalized small molecule building blocks. While methodologies for the synthesis of diverse anionic and neutral frameworks have been extensively explored, the field of cationic *catena*-phosphorus chemistry remains comparatively limited. One of the most significant shortcomings of existing methods in cationic polyphosphorus synthesis is the heavy reliance on neutral polyphosphorus starting materials. However, this reliance is

unsurprising given the scarcity of known functionalized cationic frameworks which might be utilized as reagents in the synthesis of larger polycationic architectures. The focus, therefore, of this dissertation is to explore the chemical and electrochemical reactivity of chloro-functionalized phosphinophosphonium cations and related antimony analogues as starting points for the rational assembly of complex cationic molecules.

Chapter 2. 2,3-Diphosphino-1,4-diphosphonium Ions

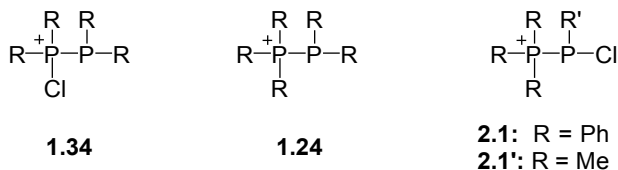
2.1 Introduction

The first published derivative¹¹³ of the 2,3-diphosphino-1,4-diphosphonium framework (**2.0a**) was reported more than two decades ago, and further syntheses of cyclized species **2.0b**¹¹⁴ and **2.0c**⁸² have since been reported. Nevertheless, reports of truly acyclic derivatives of this type are rare,^{80,115} and generalizable syntheses essentially unknown. New derivatives of the chlorophosphinophosphonium cation are described here along with their demonstrated capacity to be reductively coupled in a general fashion to yield diverse acyclic 2,3-diphosphino-1,4-diphosphonium dicationic species.



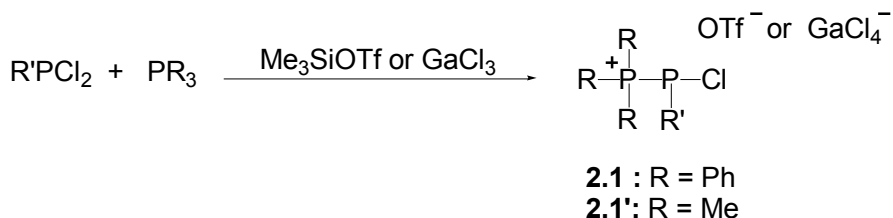
2.2 Synthesis and Behaviour of Chlorophosphinophosphonium

Cations



In line with the known synthesis of homoleptic phosphinophosphonium cations **1.24** (Section 1.3), the reaction of a tertiary phosphine, a dichlorophosphine and a chloride ion abstracting agent (Scheme 2.1) yields salts containing the chlorophosphinophosphonium

cations **2.1** or **2.1'**, which represent isomers of the previously described phosphinochlorophosphonium cations **1.34**.⁸⁴



Scheme 2.1. Synthesis of chlorophosphinophosphonium cations **2.1** or **2.1'** as triflate or tetrachlorogallate salts.

The solid-state structures of [**2.1(Ph)**][OTf]⁸⁰ and [**2.1(Me)**][OTf] have been determined by X-ray crystallography.⁸⁴ As the phosphonium centre and triflate ion are highly disordered in the crystal structure of [**2.1(Me)**][OTf], bond lengths have been restrained using [$\text{Ph}_3\text{P-PMe}_2$]⁺ as a model compound. As such, any quantifiable comparison of these parameters would be meaningless; however, the overall geometry about both phosphorus atoms in [**2.1(Me)**][OTf] is in good agreement with other known derivatives **1.24** and **1.34**. In contrast to the derivatives [**1.24**][GaCl₄], [**1.34(Ph)**][GaCl₄], and [**1.34(Me or Cy)**][OTf] and [**2.1**][GaCl₄], which exhibit two doublets at room temperature in the ³¹P{¹H} NMR spectra (Table 2.1), the P-P coupling is unresolved for [**2.1**][OTf]; indeed, the ³¹P{¹H} NMR spectra of [**2.1**][OTf] exhibit two sharp singlets.

The ³¹P{¹H} NMR spectra of solutions containing [**2.1(ⁱPr)**][OTf] or [**2.1(Cy)**][OTf] at room temperature showed significant broadening of the upfield signal as well as the presence of unreacted dichlorophosphine implicating the establishment of a dissociation equilibrium. Presumably, the enhanced steric bulk at the acceptor phosphonium site favours the dissociation of the P-P bond. In addition, reaction mixtures of Ph₃P and

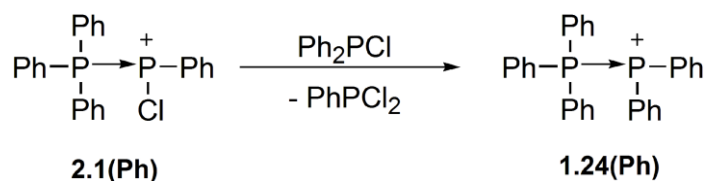
^tBuPCl₂ with Me₃SiOTf or GaCl₃ give ³¹P{¹H} NMR spectra at 213 K showing only 64% formation of **2.1**(^tBu). Nevertheless, the stronger donor Me₃P enables the quantitative formation of [**2.1'**(^tBu)][OTf]. Unlike [**2.1**][OTf], for which P-P coupling is not resolved in ³¹P{¹H} NMR spectra at room temperature, the ³¹P{¹H} NMR spectrum of reaction solutions containing [**2.1'**][OTf] showed doublets for both phosphorus centers, indicative of a stronger P-P interaction.

Table 2.1. ³¹P{¹H} NMR parameters for phosphinophosponium salts. Data are reported for spectra obtained at 298 K unless otherwise indicated. Chemical shifts (δ) are reported in units of ppm and coupling constants (¹J_{PP}) in units of Hz.

Cation	Donor	Acceptor	Anion	Spin System	δ _{PR3}	δ _{PR2}	¹ J _{PP} (T)
1.24(Ph)	Ph ₃ P	PPh ₂	[OTf] ⁸⁴	---	15	-10	---
			[GaCl ₄] ⁸⁴	AB	13	-12	-340
1.24(Me)	Me ₃ P	PMe ₂	[OTf] ⁶⁷	AX	18	-60	-275
1.24(Cy)	Cy ₃ P	PCy ₂	[OTf] ⁸⁴	AX	25	-21	-361
1.34(Ph)	Ph ₂ (Cl)P	PPh ₂	[GaCl ₄] ¹¹⁶	AX	73	0	-393
1.34(Me)	Me ₂ (Cl)P	PMe ₂	[GaCl ₄] ¹¹⁶	AX	99	-33	-340
2.1(Ph)	Ph ₃ P	PPh(Cl)	[OTf] ⁸⁰	AB	22	55	-333 (213 K)
			[GaCl ₄]	AB	22	55	-338
2.1'(Ph)	Me ₃ P	PPh(Cl)	[OTf]	AB	26	46	-305
2.1(Me)	Ph ₃ P	PMe(Cl)	[OTf]	AX	24	61	-313 (202 K)
2.1(Et)	Ph ₃ P	PEt(Cl)	[OTf]	---	18	76	--- (203 K)
2.1(ⁱ Pr)	Ph ₃ P	P ⁱ Pr(Cl)	[OTf]	AX	22	72	-344 (213 K)
2.1(Cy)	Ph ₃ P	PCy(Cl)	[OTf]	AX	23	65	-343 (202 K)
2.1'(Cy)	Me ₃ P	PCy(Cl)	[OTf]	AX	23	76	-326
2.1(^t Bu)	Ph ₃ P	P ^t Bu(Cl)	[OTf]	AX	16	90	-390 (213 K)
			[GaCl ₄]	AX	17	98	-398
2.1'(^t Bu)	Me ₃ P	P ^t Bu(Cl)	[OTf]	AX	23	95	-350
			[GaCl ₄]	AX	20	94	-356

2.2.1 Reactivity of Chlorophosphinophosponium Cations

The chloro-functionalization and increased lability of the P-P bond in **2.1** implies a wealth of reactivity, so a series of preliminary $^{31}\text{P}\{^1\text{H}\}$ NMR studies were conducted to assess the potential reaction pathways. In this context, phosphonium exchange behaviour for derivatives of **2.1**[OTf] has been observed. Solutions containing equimolar amounts of [**2.1(Ph)**][OTf] and Ph_2PCl give [**1.24(Ph)**][OTf] and PhPCl_2 (Scheme 2.2), indicating that $[\text{PPh}_2]^+$ exhibits a greater Lewis acidity towards Ph_3P than $[\text{PPh}(\text{Cl})]^+$, presumably due to π -interaction of non-bonding pairs on chlorine with phosphorus in $[\text{PPh}(\text{Cl})]^+$. Indeed, recent work¹¹⁷ with diamino-phosphonium cations suggests that weakly Lewis acidic phosphonium species preferentially form Cl-bridged adducts rather than phosphinophosponium cations in the presence of a chlorophosphine. Given the expected equilibrium dissociation of [**2.1(Ph)**][OTf] to yield $[\text{PPh}(\text{Cl})]^+$ in solution, the transfer of chloride via a $[\text{Ph}_2\text{P}\cdots\text{Cl}\cdots\text{PPh}(\text{Cl})]^+$ transition state therefore yields the phosphinophosponium cation involving the more Lewis acidic $[\text{PPh}_2]^+$ acceptor. While phosphonium exchange was also observed between $[\text{PPh}_2]^+$ and $[\text{PMe}_2]^+$, extremely broad ^{31}P NMR resonances suggest that the difference in Lewis acidity between these two species is not as substantial, and preference for either phosphinophosponium cation could be observed.



Scheme 2.2. Phosphonium (acceptor) exchange reaction yielding [**1.24(Ph)**][OTf] from [**2.1(Ph)**][OTf]

Reactions of [**2.1(Ph)**][OTf] with the diphosphine Ph₄P₂ were targeted as potential routes to chloro-functionalized 1,3-diphosphino-2-phosphonium cations [R₂P-PR₂-PRCl]⁺. However, ³¹P{¹H} NMR spectra of the 1:1 reaction indicated that [Ph₃P-PPh₂][OTf], **1.24(Ph)**[OTf] was the major product of this reaction, along with a several smaller unidentifiable resonances and trace amounts of *cyclo*-[Ph₆P₅][OTf]. The generation of **1.24** can be rationalized as originating from the formal Ph₃P-abstraction of diphenylphosphenium [Ph₂P]⁺ by from the intermediate 1-chloro-1,3-diphosphino-2-phosphonium cation [Ph₂P-PPh₂-PPhCl]⁺ produced by initial ligand exchange.

In an effort to target the elusive 2,3-diphosphino-1-phosphonium cations, reactivity of **2.1'** with silylphosphines or mono- and di-organo phosphines (RPH₂ and R₂PH) was studied. Reactions of **2.1** were not investigated since the low basicity of Ph₃P was expected to result in ligand exchange behaviour (Section 1.3.2) rather than the desired chloro-centric reaction.

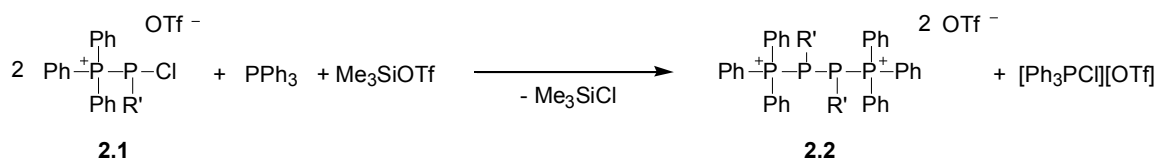
Attempted dehydrohalocoupling reactions of RPH₂ (R = Cy, Ph) and [**2.1'(Me)**][OTf] in the presence of NEt₃ showed no reaction according to ³¹P NMR analysis of the crude reaction mixture, while analogous addition of Ph₂PH to sterically hindered derivatives of **2.1'** (R = ⁱPr, ^tBu) showed displacement of Me₃P and subsequent decomposition to unidentified products. In contrast, analysis of ³¹P{¹H} NMR spectra from the 1:1 reaction of [**2.1'(^tBu)**][OTf] with Ph₂PH in the presence of NEt₃ indicated the production of the desired three-membered monocation [Me₃P-PMe-PPh₂][OTf] (³¹P{¹H} NMR: AMX spin system, δ_A = -70.9 ppm, δ_M = -28.5 ppm, δ_X = 20.3 ppm; ¹J_{AX} = 285 Hz, ¹J_{AM} = 158 Hz, ²J_{MX} = 61 Hz). However, several unassignable broad ³¹P NMR resonances were also

observed, and attempted isolation of the desired monocationic product proved unsuccessful.

In contrast to the reactions described in this section, the reductive coupling of **[2.1][OTf]** proceeded in high yield and was generalizable to a variety of organo-substituents on the phosphine. This reaction will be described in more detail in the following section.

2.3 Reductive Coupling of Chlorophosphinophosphonium Cations

As illustrated in Scheme 2.3, the addition of Ph_3P and Me_3SiOTf to derivatives of **[2.1][OTf]** ($\text{R}' = \text{Ph, Me, Et, } ^i\text{Pr}$) result in the formation of the corresponding 2,3-diphosphino-1,4-diphosphonium salts **[2.2][OTf]₂**. The $^{31}\text{P}\{^1\text{H}\}$ NMR spectra of these reaction mixtures show AA'BB' spin systems (Figures 2.2-2.3, Table 2.2) assigned to **2.2** and a singlet corresponding to $[\text{Ph}_3\text{PCl}][\text{OTf}]^{71}$ ($\delta = 66$ ppm).



Scheme 2.3. Reductive coupling reaction of **[2.1][OTf]** to give **[2.2][OTf]₂**

The AA'BB' spin system is not observed for mixtures of **[2.1][OTf]** with Ph_3P in the absence of Me_3SiOTf , suggesting that the formation of $[\text{Ph}_3\text{PCl}][\text{OTf}]$ is a key thermodynamic driving force in the P-P coupling process, rather than formation of Ph_3PCl_2 . Mixtures of Ph_3P , GaCl_3 and **[2.1(Ph)][GaCl₄]** likewise show no evidence for the generation of **2.2**, and ^{31}P NMR analyses of these solutions indicate only substantially broadened resonances for **2.1(Ph)**. Furthermore, reactions of **[2.1(Ph)][OTf]** with comparatively strong reducing agents such as Na or Mg give complex mixtures

containing *cyclo*-Ph₅P₅^{118,119} as the only product identifiable using ³¹P{¹H} NMR spectroscopy, thereby emphasizing the contrasting reduction chemistry of the cationic vs. neutral phosphorus systems. The ³¹P{¹H} NMR spectra of reaction mixtures containing weaker reducing agents, such as Zn, SnCl₂, or cyclohexene, indicated the presence of **2.1(Ph)** together with a number of unidentified phosphorus containing products. Formation of derivatives of **2.2** contrast the previously reported reaction of PhPCl₂, Ph₃P and AlCl₃ to give [Ph₃P-PPh-PPh₃][AlCl₄]₂ (**[1.31(Ph)]**)[AlCl₄]₂,⁶³ however, the formation of **[2.2(Ph)]**[AlCl₄]₂ and its solid-state structure has been described.¹¹⁵

The ³¹P{¹H} NMR spectra of solutions containing Ph₃P, Me₃SiOTf and **[2.1(Cy)]**[OTf] (prepared *in situ*) show partial formation of **[2.2(Cy)]**[OTf]₂ after two days, while solutions of Ph₃P, Me₃SiOTf and **[2.1(^tBu)]**[OTf] show no evidence of **[2.2(^tBu)]**[OTf]₂. These observations are indicative of steric restrictions at the phosphonium site. Both of these solutions exhibit an AMX spin system, which is tentatively assigned to [Ph₃P_M-P_AR'-P_XR'Cl][OTf], **[2.3]**[OTf]. A similar pattern was observed as a component in dilute solutions of Ph₃P and Me₃SiOTf with **[2.1(ⁱPr)]**[OTf]. In contrast to the analogue of **2.3** proposed by Dillon and coworkers,⁸² the terminal P_X signal in this new AMX spin system (e.g. **[2.3(ⁱPr)]**[OTf]: δA = -35.7 ppm, δM = 23.0 ppm, δX = 96.5 ppm, ¹J_{AM} = -309 Hz, ¹J_{AX} = -305 Hz, ²J_{MX} = 59 Hz) is shifted significantly downfield relative to the P_M terminus (Δδ ≥ 70 ppm). Nonetheless, while smaller magnitude ¹J_{PP} coupling constants (< 300 Hz) are typically observed between P(III)-P(III) spin pairs, the introduction of an electronegative substituent such as chlorine is expected to increase the magnitude of ¹J_{AX}, justifying the similar ¹J_{AX} and ¹J_{AM} in **2.3**. Finally, ¹H NMR spectra of reaction mixtures containing both **[2.1(ⁱPr)]**[OTf] and **[2.3(ⁱPr)]**[OTf]

2.4 2,3-Diphosphino-1,4-diphosphonium Cations

2.4.1 ^{31}P NMR Features of 2,3-Diphosphino-1,4-diphosphonium Cations

Derivatives of **[2.2][OTf]₂** exhibit second-order AA'BB' spin systems observed in solution phase $^{31}\text{P}\{^1\text{H}\}$ NMR spectra for all derivatives of **2.2** are characteristic and the patterns have been simulated for most derivatives by iterative fitting with the chemical shift and coupling constant parameters listed in Table 2.2. Comparison of the simulated and experimental patterns is shown for **[2.2(Et)][OTf]₂** (Figure 2.1) and **[2.2(ⁱPr)][OTf]₂** (Figure 2.2). Chemical shift parameters for the terminal phosphonium centers (δ_{B}) occur in a typical narrow range (20-32 ppm), while the phosphine centers (δ_{A}) exhibit more varied shifts ($\Delta\delta > 40$ ppm). This is consistent with the dependence of the chemical shielding on the geometry of the phosphorus center,¹²¹ as the tetracoordinate phosphonium centers have less geometric flexibility than tricoordinate phosphine centers. This geometric and conformational flexibility at the phosphine site is further supported by the substantially increased line broadening for δ_{A} observed at 202.6 MHz. The $^1\text{J}_{\text{AB}}$ coupling constants for derivatives of **2.2** (Table 2.2) are consistent with the established range of $^1\text{J}_{\text{PP}}$ values for phosphinophosphonium cations.⁸⁴ However, the $^1\text{J}_{\text{AA'}}$ values are significantly smaller (*ca.* 100 Hz) for derivatives with phenyl substituents at the phosphine centers [*i.e.* **2.2(Ph)** and **2.2'(Ph)**].

Table 2.2. $^{31}\text{P}\{^1\text{H}\}$ NMR parameters at 101.3 MHz for 2,3-diphosphino-1,4-diphosphonium triflate salts. All spectra are AA'BB' spin systems, with parameters derived by iterative fitting of experimental data at 298 K. Minor diastereomer shifts could not be simulated, so are approximate if given. Chemical shifts (δ) are reported in ppm and coupling constants (J) in Hz.



	R'	R	solvent	δ_A	δ_B	$^1\text{J}_{\text{AA}'}$	$^1\text{J}_{\text{AB}} = ^1\text{J}_{\text{A}'\text{B}'}$	$^2\text{J}_{\text{A}'\text{B}} = ^2\text{J}_{\text{AB}'}$	$^3\text{J}_{\text{BB}'}$
2.2(Ph)	Ph	Ph ⁸⁰	CH ₂ Cl ₂	-33	24	-124	-343	69	51
			<i>minor diastereomer</i>	CH ₂ Cl ₂	-42	22	<i>not simulated</i>		
2.2'(Ph)	Me	Ph ⁸⁰	MeCN	-52	25	-105	-305	66	56
			<i>minor diastereomer</i>	MeCN	-56	23	<i>not simulated</i>		
2.2(Me)	Ph	Me ⁸¹	CH ₂ Cl ₂	-71	26	-278	-282	78	62
				MeCN	-67	32	<i>not simulated</i>		
2.2'(Me)	Me	Me ⁸¹	MeCN	-73	26	-238	-269	80	58
2.2(Et)	Ph	Et	MeCN	-53.6	24.1	-276	-297	82	59
2.2(ⁱPr)	Ph	ⁱ Pr	MeCN	-25.5	22.2	-318	-348	98	63
2.2(Cy)	Ph	Cy	CH ₂ Cl ₂	-34	20	<i>not simulated</i>			

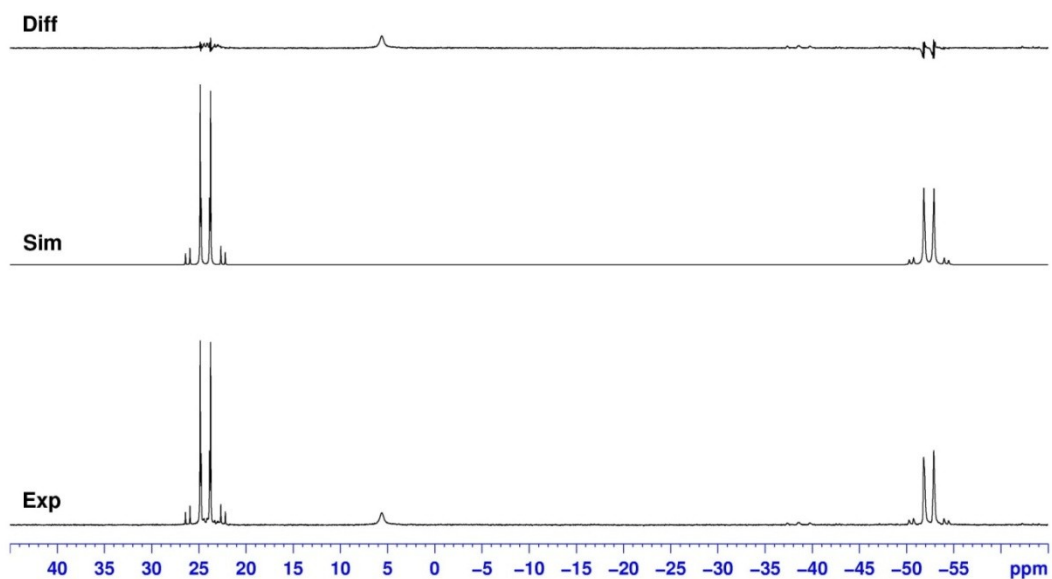


Figure 2.1. Comparison of simulated and experimental $^{31}\text{P}\{^1\text{H}\}$ NMR spectra of $[\mathbf{2.2}(\text{Et})][\text{OTf}]_2$.

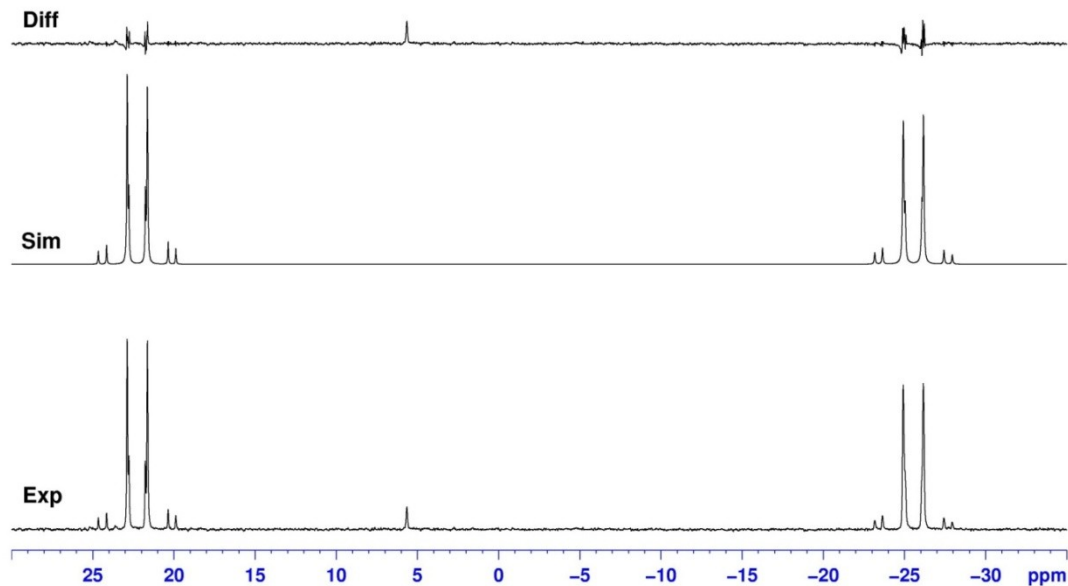


Figure 2.2. Comparison of simulated and experimental $^{31}\text{P}\{^1\text{H}\}$ NMR spectra of $[\mathbf{2.2}(\text{Pr})][\text{OTf}]_2$

2.4.2 Solid-state Structures

Selected structural parameters from the solid-state structures of the dication in the triflate salts of **2.2** (R = Ph, Me, Et, Figure 2.3) are presented in Table 2.3, where τ_{R} indicates the C-P-P-C torsion angle between the central substituents and τ_{PR_3} indicates the P-P-P-P torsion angle of the phosphorus backbone. Crystals of $[\mathbf{2.2}(\text{Ph})][\text{OTf}]_2$ contain the *R,S meso*-isomer of the dication, which is centrosymmetric with central torsion angles (τ_{PR_3} and τ_{R}) of 180° . Solid state ^{31}P CP/MAS NMR data for $[\mathbf{2.2}(\text{Ph})][\text{OTf}]_2$ further implies that both the *R,S meso* isomer and the (*R,R*)/(*S,S*) diastereomeric pair are present in the bulk solid sample as well as in solution,⁸¹ rather than proposing a solution inversion pathway as observed for neutral acyclic tetra- and pentaphosphines (Section 1.2.2).^{23,35,46}

Table 2.3. Selected solid-state structural parameters of 2,3-diphosphino-1,4-diphosphonium triflate salts, $[R_3P-PR'-PR'-PR_3][OTf]_2$.

	R_3P	PR'	P-P (Å) [†]	$C_{R'}-P-P$ (°) [†]	$\tau_{R'}$ (°)	τ_{PR_3} (°)	Ref.
2.2(Ph)	Ph	Ph	2.258(1) [mid] 2.221(1)	101.65(8)	180	180	80,81
2.2'(Ph)	Me	Ph	2.2041(9) [mid] 2.2318(12)	101.02(8)	180	180	80,81
2.2(Me)	Ph	Me	2.2061(13) [mid] 2.2284(12) 2.2125(13)	109.3(1) 107.9(1)	0.95(14)	-159.98(4)	65,81
2.2'(Me)	Me	Me	2.192(2) [mid] 2.243(2) 2.191(2)	101.1(2) 102.8(2)	31.25(11)	-126.72(3)	65,81
2.2(Et)	Ph	Me	2.2048(8) [mid] 2.2153(11)	109.52(9)	3.49(13)	-142.35(3)	<i>this work</i>

[†] [mid] indicates the central P-P bond, while the indicated $C_{R'}-P-P$ values describe the angle subtended by the central substituent (Me, Et, Ph) and this bond. $\tau_{R'}$ indicates the C-P-P-C torsion angle between the central substituents, while τ_{PR_3} indicates the P-P-P-P torsion angle of the phosphorus backbone.

Crystals of **[2.2(Me)][OTf]₂** contain a racemic mixture of the (*R,R*)/(*S,S*) enantiomeric pair. As shown in Figure 2.3, the cation adopts an essentially eclipsed conformation of the methyl substituents with a central C-P-P-C torsion angle ($\tau_{R'}$) of 0.95(14)°. Unlike for **[2.2(Ph)][OTf]**, NMR analysis of either the redissolved crystals or the reaction mixtures showed only one diastereomer, indicating that the (*R,R*)/(*S,S*) racemic mixture of **[2.2(Me)][OTf]₂** is formed exclusively in the reductive coupling of the racemic **[2.1(Me)][OTf]**. Likewise, crystals of **[2.2(Et)][OTf]₂** contain an (*R,R*)/(*S,S*) racemic mixture of configurational isomers of the cation (Figure 2.3, Table 2.3), adopting an eclipsed conformation of the central substituents [$\tau_{R'} = 3.49(13)^\circ$] in spite of the slightly greater steric presence of the ethyl vs. methyl moieties. Correspondingly, both **2.2(Me)** and **2.2(Et)** adopt larger central $C_{R'}-P-P$ angles [107.9(1)-109.52(9)°] relative to **2.2(Ph)** [101.65(8)°], presumably in order to minimize steric congestion.

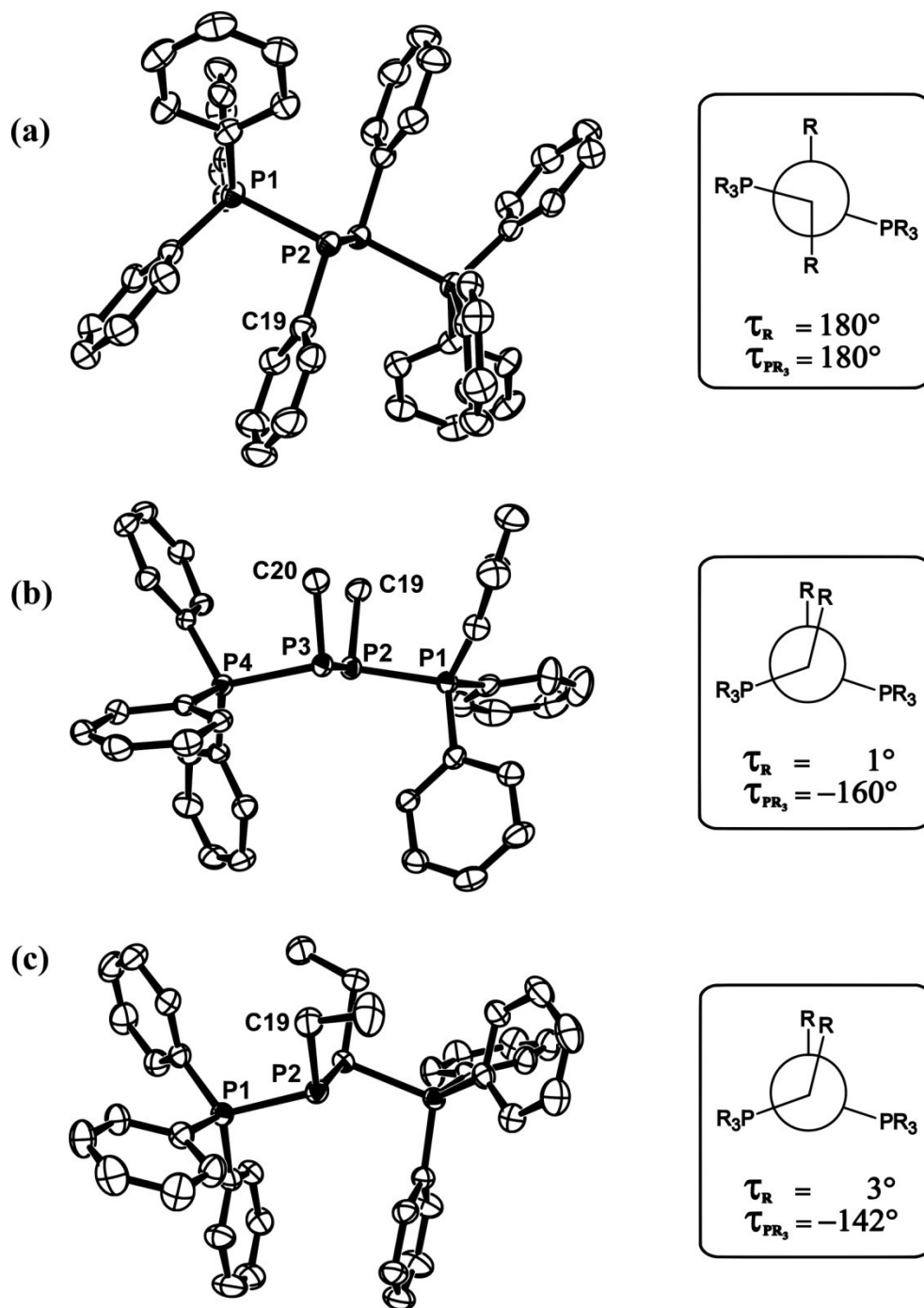


Figure 2.3. ORTEP representations of the solid-state structure of (a) the centrosymmetric *meso*-dication in [2.2(Ph)][OTf]₂ and the (*S,S*)-enantiomer of the dication in (b) [2.2(Me)][OTf]₂ and (c) [2.2(Et)][OTf]₂. Thermal ellipsoids are shown at the 50% probability level and hydrogen atoms omitted for clarity. τ_R° indicates the C-P-P-C torsion angle between the central substituents, while τ_{PR_3} indicates the P-P-P-P torsion angle of the phosphorus backbone.

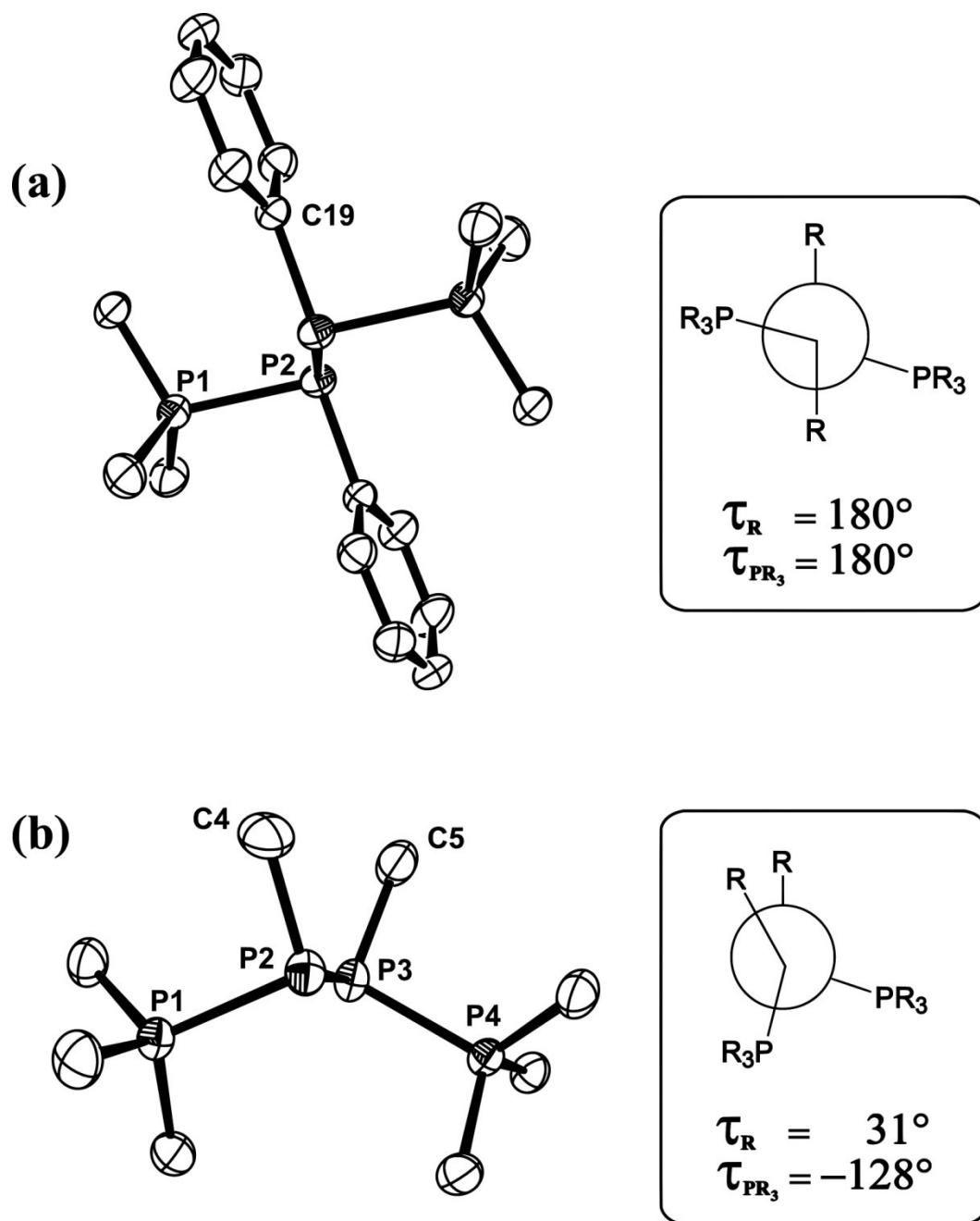
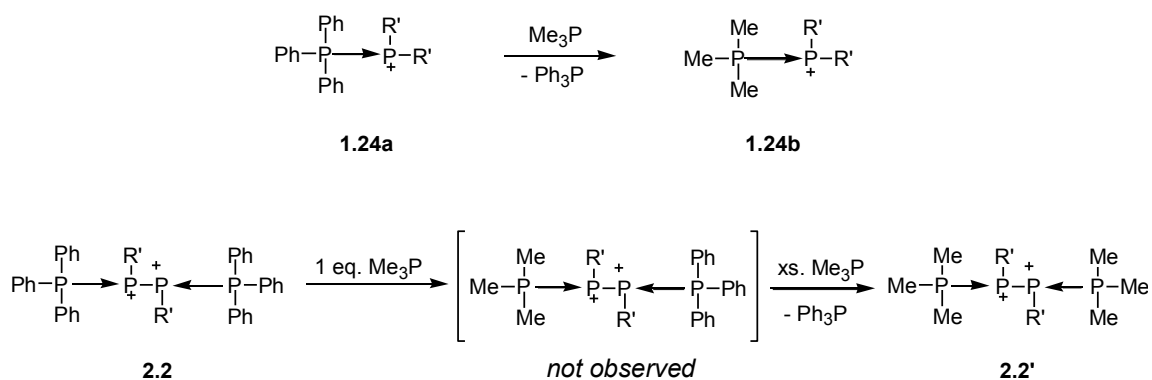


Figure 2.4. ORTEP representations of the solid-state structure of (a) the centrosymmetric *meso*-dication in $[2.2'(\text{Ph})][\text{OTf}]_2$ and (b) the (*S,S*)-enantiomer of the dication in $[2.2'(\text{Me})][\text{OTf}]_2$. Thermal ellipsoids are shown at the 50% probability level and hydrogen atoms omitted for clarity. τ_{R} indicates the C-P-P-C torsion angle between the central substituents, while τ_{PR_3} indicates the P-P-P-P torsion angle of the phosphorus backbone.

2.4.3 Reactivity of 2,3-Diphosphino-1,4-diphosponium Dications

The previously reported ligand exchange reaction of **[2.2(Ph)][OTf]₂** or **[2.2(Me)][OTf]₂** with excess Me₃P was observed to quantitatively form the corresponding derivatives **2.2'**[OTf]₂ (Scheme 2.5), with no evidence for the monosubstitution product.^{80,81}



Scheme 2.5. Phosphine exchange reactions on phosphinophosponium and 2,3-diphosphino-1,4-diphosponium cations

It was therefore of interest to investigate the potential scope of this ligand exchange behaviour to assess the viability of **2.2**[OTf]₂ as a stabilized source of the diphosphenium dication [RP-PR]²⁺, analogous to stabilized phosphinidene^{122,123} or diphosphorus⁴³ fragments known for neutral phosphorus centres.

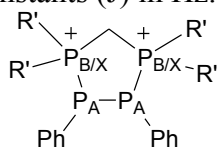
Reactions of **2.2**[OTf]₂ with diphosphines R₂P-PR₂ (R = Ph, Me) yielded [Ph₃P-PR₂]⁺ as the only identifiable ³¹P NMR resonances, presumably proceeding via an identical mechanism to that described for exchange reactions on **2.1**[OTf] (Section 2.2.1, page 36). No reaction was observed between the potential *cyclo*-polyphosphine donor (PCy)₄, which likely reflects steric constraints of the bulky cyclohexyl substituents.

The addition of potentially chelating donor phosphines bis(diphenylphosphino)methane [dppm] and bis(dimethylphosphino)methane [dmpm] proved more successful, and 1:1

reactions of **2.2(Ph)**[OTf]₂ with dmpm showed nearly quantitative conversion to the five-membered ring species **2.4**[OTf]₂ according to ³¹P NMR analyses of the reaction solutions (AA'XX' spin system, Table 2.4). Reactions of the weaker donor, dppm, yielded a more complex product distribution, and initial ³¹P NMR spectra of the reaction solution after 1 h at room temperature showed only three broad peaks (which were unresolved even at low temperature) in addition to the expected AA'BB' spin system of the cyclized product (Table 2.4, compound **2.5**). Vapour diffusion of Et₂O into the reaction solution yielded a white crystalline material, crystals of which were identified using X-ray crystallography as the unexpected six-membered cyclic dication **2.7**. Redissolution of the bulk material in CH₂Cl₂ gave ³¹P NMR spectroscopic features that were attributed to an approximately 1:1 mixture of the five- and six- membered rings **2.6** and **2.7**. Notably, the AA'BB' spin system attributed to the redissolved five-membered ring **2.6** did not display the same chemical shifts and coupling constants as the originally observed tetraphosphorus species **2.5**. Comparing the ¹J_{PP} coupling constants between the central phosphines (P_A) provides insight into the nature of the two five-membered derivatives, ¹J_{AA} in **2.5** was observed to be substantially larger than in **2.6** (ΔJ = 65 Hz). Empirically and theoretically, ¹J_{PP} values for adjacent phosphorus nuclei with *cis*-oriented substituents in neutral *cyclo*-polyphosphines have been shown to be substantially more negative than their *trans*-oriented counterparts.¹²⁴⁻¹²⁸ This concept will be revisited again in later chapters, but, in this example, this rationale is sufficient to suggest the assignment of **2.5** and **2.6** as the *cis*- and *trans*- isomers of the five-membered dicationic framework, respectively. The stereochemistry of the dmpm derivative **2.4** cannot be conclusively determined, as ¹J_{AA} is intermediate between the *cis*- and *trans*- configured dppm

frameworks, and differences of up to 40 Hz were observed upon Me₃P substitution in the acyclic derivatives (Table 2.2). Comparison to the only previously known derivative of this five-membered framework **2.8**,⁸² which features dmpm and Et substituents and was observed to be *trans*-oriented in the solid state, might lend additional support to the hypothesis that **2.4** is *trans*-oriented as well, but this is in no way definitive.

Table 2.4. ³¹P{¹H} NMR parameters at 101.3 MHz for cyclic 2,3-diphenyldiphosphino-1,4-diphosphonium triflate salts in CH₂Cl₂. All spectra are AA'BB' spin systems, with parameters derived by iterative fitting of experimental data at 298 K. Chemical shifts (δ) are reported in ppm and coupling constants (J) in Hz.

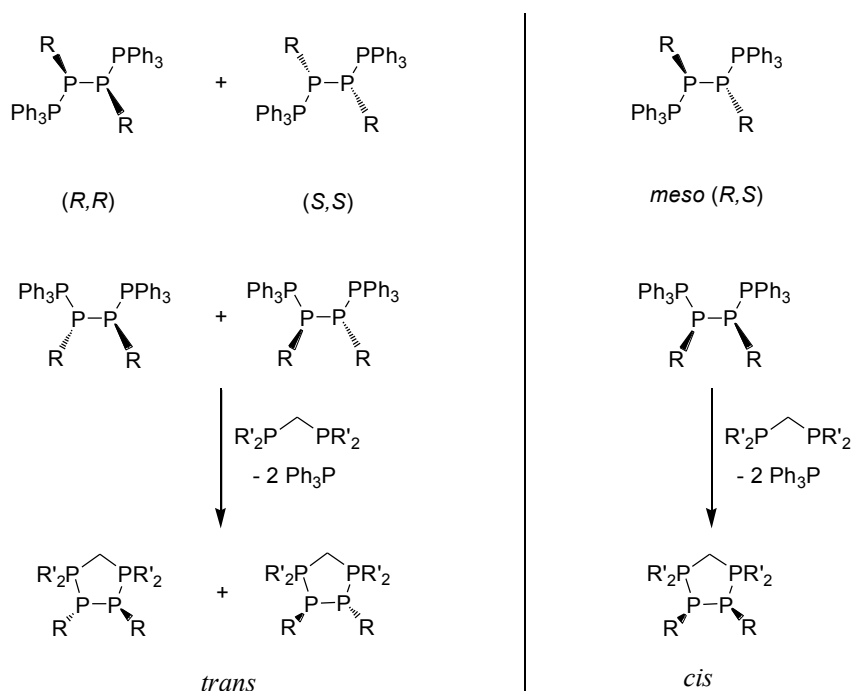


	R'	δ _A	δ _B	¹ J _{AA'}	¹ J _{AB} = ¹ J _{A'B'}	² J _{A'B} = ² J _{AB'}	³ J _{BB'}	Spin system
2.4	Me	-40.6	41.9	-183	-293	4	18	AA'XX'
2.5	Ph	-36.9	41.4	-228	-248	5	83	AA'BB'
2.6	Ph	-43.9	27.2	-163	-306	5	17	AA'BB'
2.8 ⁸²	Me ^a	-40.8	57.5	-175 ^b	-357 ^b	30 ^b	-74 ^b	AA'XX'

^a Central substituents in this comparable derivative from Boyall *et al.* are Et, not Ph. ^b ¹J_{PP} was reported as positive in this reference, but all the signs herein are switched to follow the convention respected in this thesis.

Notably, the seemingly kinetically favoured initial formation of the *cis*-substituted derivative **2.5** lends some mechanistic insight to the substitution reaction and the nature of the major diastereomer of **2.2(Ph)** in solution. Given that mono-substitution was not observed for reactions of **2.2** with Me₃P, it seems reasonable to propose that mono-substitution is likewise disfavoured for dppm and dmpm, despite the additional unassigned broad resonances observed using ³¹P NMR spectroscopy of dppm reaction solutions. If an associative mechanism for ligand substitution is considered, as suggested by Slattery *et al.* for alkyl-substituted phosphonium cations,¹²⁹ there should be no

opportunity for free rotation about the RP-PR bond after Ph_3P dissociation and before coordination of the second phosphorus centre of the diphosphine. Thus, the initial species produced by ligand substitution should reflect the orientation of the central substituents in the major diastereomer of **2.2(Ph)** in solution.



Scheme 2.6. Stereochemical considerations in associative ligand substitution reactions of the two possible diastereomers of **2.2**[OTf]₂.

With this consideration in mind, the $(R,R)/(S,S)$ enantiomeric pair should yield the *trans*-substituted ring upon reaction with dppm, while the *meso (R,S)* diastereomer would yield the corresponding *cis*-isomer (Scheme 2.6). The observed immediate generation of the *cis*-product **2.5** would suggest, therefore, that the major isomer of **2.2(Ph)** in solution is the *meso-(R,S)* diastereomer. Notably, however, a dissociative mechanism generates a transient planar phosphonium centre, and therefore implies nothing of the stereochemistry of **2.2(Ph)**.

The *trans*-product **2.6** would be expected to be thermodynamically more favourable, and conversion to **2.6** from the kinetic product **2.5** might be envisioned to proceed via dissociation of one arm of the diphosphine, and transient planarity of the phosphonium cation prior to re-coordination. This type of dissociative equilibrium has been previously proposed for the Ph₃P derivatives of phosphinophosponium cations **2.1** (Section 2.2).

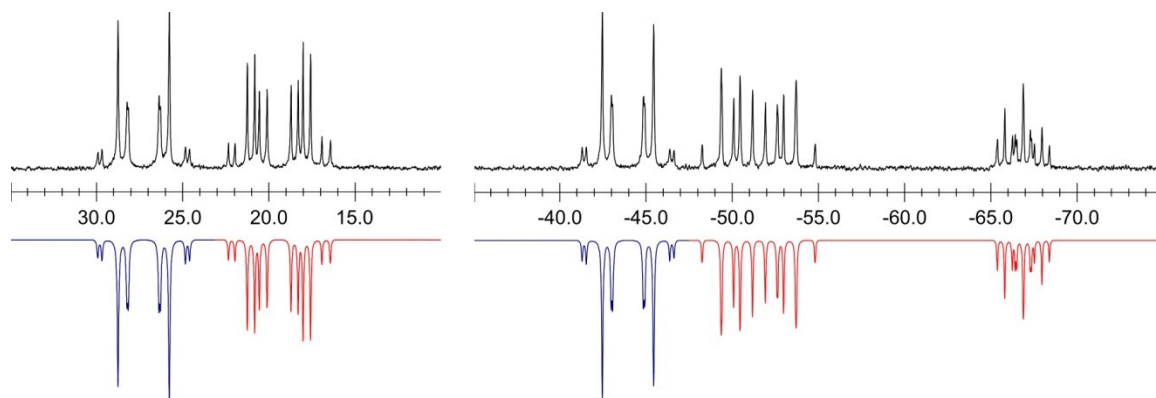


Figure 2.5. Experimental (upright) and simulated (inverted) expansions of the ³¹P{¹H} NMR spectrum at 101.3 MHz of the 1:1 mixture of the five-membered dication **2.6**(blue, AA'BB') and the six-membered dication **2.7**(red, ABB'CC'), from the redissolved crystalline material isolated from dppm ligand exchange on **2.2(Ph)**.

The adventitious observation of the six-membered dication **2.7** from one reaction of **2.2** with dppm further supports the proposition that dppm allows for short-lived κ^1 -coordination *in situ*, which would be required for insertion of an additional phosphinidene (:P̄R) unit into the ring. The ³¹P NMR features of **2.7** are comparable to those of the five-membered rings and have been simulated as an AMM'XX' spin system, wherein the phosphonium centres have the most downfield chemical shift ($\delta_A = -66.9$, $\delta_M = -51.5$, $\delta_X = 19.4$ ppm; $^1J_{AM} = -108$, $^1J_{MX} = -324$, $^1J_{AM'} = -110$, $^2J_{AX} = 44$, $^2J_{AX'} = 45$, $^2J_{MM'} = 185$, $^3J_{MX'} = -4$, $^2J_{XX'} = -1$ Hz). The small coupling constants between adjacent

phosphine centres is suggestive of *trans*-oriented Ph-substituents, a feature supported by the X-ray analysis of the isolated crystals.

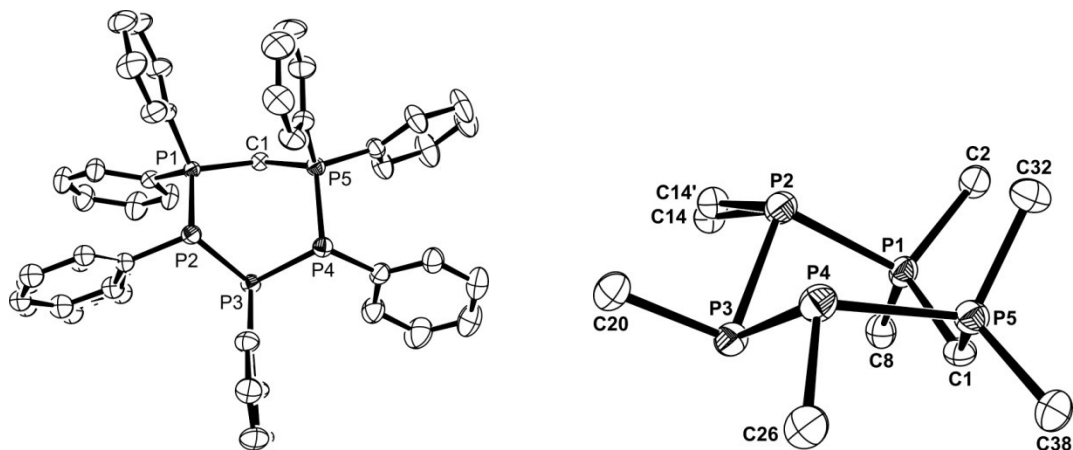


Figure 2.6. Top (*left*) and side-on (*right*) views of the ORTEP representation of the dication in **2.7**[OTf]₂, indicating a half-twisted boat conformation in the solid state. Thermal ellipsoids are shown at the 50% probability level and hydrogen atoms are omitted for clarity. Unlabelled atoms at left indicate carbon atoms, while only ipso carbons are shown at right. Disorder of the C14-C19 phenyl moiety on P2 has been modelled.

Overall, the solid-state structural features of **2.7**[OTf]₂ (Figure 2.6) are typical of phosphinophosphonium species, and relevant parameters are tabulated in Table 2.5.

Disorder in the crystal at one backbone phenyl group (at P2) was modelled. Average P-P bond lengths are typical of P-P single bonds and are not significantly different regardless of whether a phosphonium centre is involved. Endocyclic bond angles are substantially smaller (91-99°) about the phosphine centres compared to the phosphonium centres (109-112°), but they do not differ substantially from the endocyclic angles (97-98° about the phosphines and 107-110° about the phosphonium) in the related previously reported five-membered dication **2.8**[SnCl₆].⁸² The Cremer-Pople puckering parameters¹³⁰ of the ring (Table 2.5), calculated using the PLATON software package,¹³¹ indicated that the dication adopts a slightly twisted boat conformation in the solid state, with the ring

carbon (C1) and opposing phosphine (P3) atoms the most substantially out of plane.[†] Effectively, this renders the five phosphorus atoms as an envelope conformation, with the lone pair in P3 able to delocalize into the σ^* orbitals of the P-P ring framework as previously described for five-membered phosphorus rings (Section 1.2.2). Since the ring strain in five-membered and six-membered rings is comparably low, the ability of the six-membered framework to adopt this P-envelope conformer may render it more stable in this case.

Table 2.5. Selected solid-state structural parameters for the cation in **2.7**[OTf]₂.

Bond lengths (Å)			
<i>Involving tetrahedral atoms</i>		<i>Involving only neutral phosphines</i>	
P1-P2	2.2294(14)	P2-P3 P3-P4	2.2338(14) 2.2454(16)
P4-P5	2.2284(16)		
P1-C1	1.824(4)		
P5-C1	1.815(4)		
avg. P-C _{Ph}	1.795(4)	avg. P-C _{Ph}	1.847(10)
Endocyclic Bond Angles (°)			
<i>Subtending tetrahedral atoms</i>		<i>Subtending neutral phosphines</i>	
C1-P1-P2	108.69(13)	P1-P2-P3	95.34(5)
C1-P5-P4	112.17(14)	P2-P3-P4	91.56(5)
P1-C1-P5	117.14(19)	P3-P4-P5	99.44(5)
Σ(angles) (°)			
P1	657	P2 ^a	296
P5	657	P3	283
		P4	304
Puckering parameters ¹³⁰	Q	θ	φ
	1.3834(19)	106.84(8)	343.57(6)

^a Averaged between disordered atoms C14 and C14'

[†] For a more detailed treatise of the conformational description designated by Cremer-Pople puckering parameters in six-membered rings, see Appendix A2.

Although the cations in **2.7**[OTf] stack in well-aligned columns (Figure 2.7), there are no close contacts ($< 5\text{\AA}$) between the rings or phenyl substituents to offer favourable π -stacking interactions.

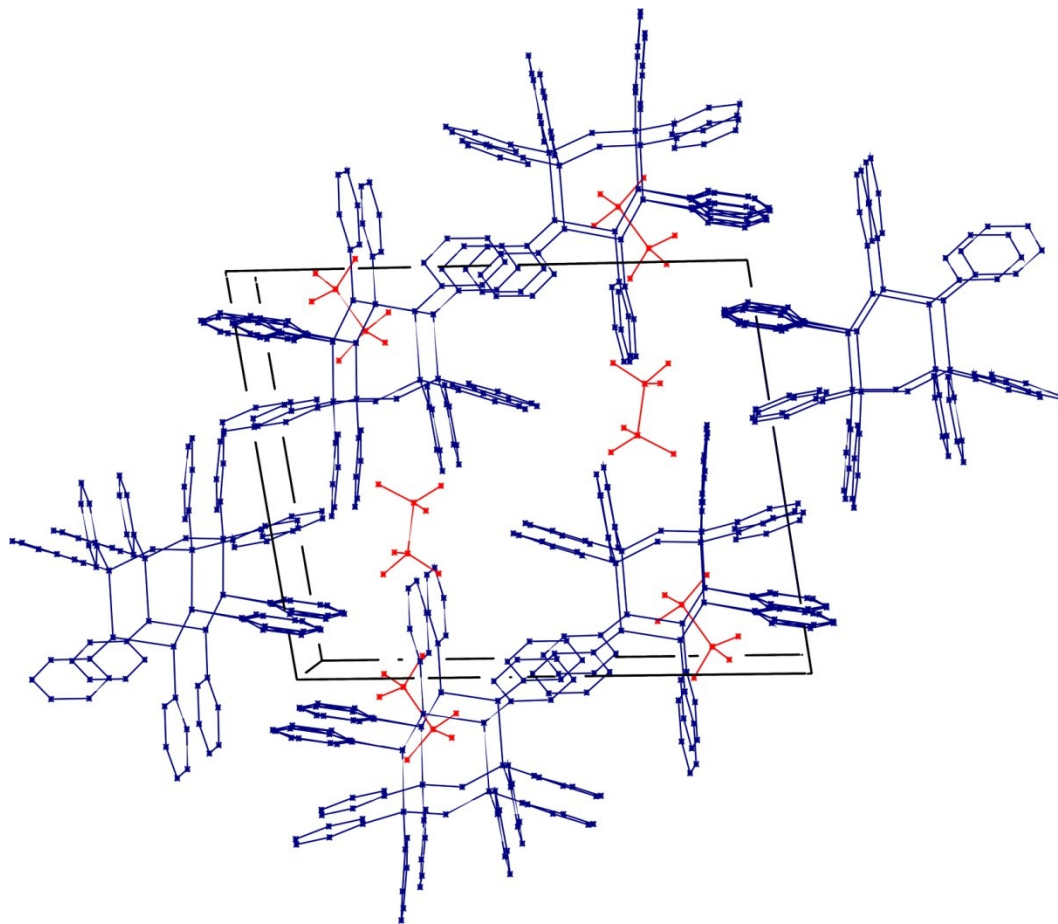


Figure 2.7. Skeletal depiction of the unit cell in crystalline **2.7**[OTf]₂ showing the alignment of adjacent rings. Triflate counterions are indicated in red.

In spite of the apparent stabilizing features of the six-membered structure, attempts to favour the production of the larger ring by addition of PhPCl₂ and additional Ph₃P (as a reducing agent) to the ligand exchange reaction were unsuccessful.

2.4.4 Computational Studies and Diastereoselectivity

Both **[2.2(Ph)][OTf]₂** and **[2.2'(Ph)][OTf]₂** have been observed to form as unequal mixtures of the *meso* (*R,S*) and (*R,R*)/(*S,S*) diastereomers in solution, but crystallize solely as the *meso* diastereomer in a *trans* conformation.^{65,81} In contrast, only one diastereomer was observed in solution for each of **[2.2(Me)][OTf]₂**,^{65,81} **[2.2'(Me)][OTf]₂**,^{65,81} and **[2.2(Et)][OTf]₂** and all three were found to crystallize solely as the (*R,R*)/(*S,S*) enantiomeric pair in comparatively eclipsed conformations ($\tau_R = 1-31^\circ$).

The favoured diastereomer in solution could not be definitively identified for these species, so to assess the factors responsible for defining the conformational preferences and diastereoselectivity observed in the solid-state structures, comparative ground state energy calculations were performed using DFT methods in Gaussian 03¹³² [B3LYP/6-31+G(d)] for staggered, eclipsed and gauche conformations of the *meso*- and (*S,S*)-diastereomers for the dications **2.2'(Ph)** and **2.2'(Me)** in the gas phase. Calculated structural parameters for the lowest energy structures are presented in Table 2.6. In all cases, the results are in agreement with the experimental solid-state structures: the (*R,S*)-*meso*-isomer is favoured for **2.2'(Ph)**, ($R' = \text{Ph}$, $|\Delta E| = 6.3 \text{ kJ/mol}$) while the (*R,R*)/(*S,S*) diastereomer is favoured for **2.2'(Me)** ($R' = \text{Me}$, $|\Delta E| = 15.3 \text{ kJ/mol}$). It is noteworthy that the energy difference between the two diastereomers of **2.2'(Ph)** is small, providing a rationale for the observation of a mixture of diastereomers in the solution state ³¹P NMR spectra.

Table 2.6. Calculated structural parameters for 2,3-diphosphino-1,4-diphosphonium cations

[Me ₃ P-PPh-PPh-PMe ₃], 2.2'(Ph) <i>(R,S) meso</i> -diastereomer favoured ($\Delta E = 6.3$ kJ/mol) <i>anti conformer favoured</i>				
	P-P (Å)[†]	C_{R'}-P-P (°)[†]	τ_{R'} (°)	τ_{PR3} (°)
Experimental	2.2041(9) [mid] 2.2318(12)	101.02(8)	180	180
<i>Calculated</i>	<i>2.259</i> <i>[mid] 2.286</i>	<i>102.2</i>	<i>180.0</i>	<i>180.0</i>

[Me ₃ P-PMe-PMe-PMe ₃], 2.2'(Me) <i>(R,R)/(S,S)</i> -diastereomer favoured ($\Delta E = 15.3$ kJ/mol) <i>eclipsed conformer favoured</i>				
	P-P (Å)[†]	C_{R'}-P-P (°)[†]	τ_{R'} (°)	τ_{PR3} (°)
Experimental	2.192(2) [mid] 2.243(2) 2.191(2)	101.1(2) 102.8(2)	31.25(11)	-126.72(3)
<i>Calculated</i>	<i>2.242</i> <i>[mid] 2.265</i>	<i>107.2</i>	<i>-1.9</i>	<i>-152.3</i>

[†] [mid] indicates the central P-P bond, while the indicated C_{R'}-P-P values describe the angle subtended by the central substituent (Me, Et, Ph) and this bond. τ_{R'} indicates the C-P-P-C torsion angle between the central substituents, while τ_{PR3} indicates the P-P-P-P torsion angle of the phosphorus backbone.

The thermodynamically favoured staggered conformation for the (*R,S*) *meso*-diastereomer is explained (Figure 2.8) in terms of the minimization of steric interactions between both the Me₃P termini and the central substituents [τ_{R'} = τ_{PR3} = 180°] in this rotamer. Indeed, computational studies that begin with an eclipsed initial geometry for the (*R,S*) *meso*-diastereomer undergo geometry optimization to give the

staggered conformation. The thermodynamic preference of the (*R,R*)/(*S,S*) diastereomer for the eclipsed conformation seems counterintuitive, but suggests that steric interactions between the terminal phosphonium substituents play a dominant role in determining the lowest energy conformer (Figure 2.8). Even for smaller terminal ligands (PH₃) or larger central alkyl substituents at the internal phosphine sites, computational models indicate that the eclipsed conformation of the (*S,S*) diastereomer is favoured over the gauche or staggered conformers. In addition, calculations on the theoretical structure of **2.2'**(^{*i*}Pr) demonstrate that the (*R,R*)/(*S,S*) racemic mixture is thermodynamically favoured over the *meso*-diastereomer even for more sterically hindered alkyl derivatives ($|\Delta E| = 19.5$ kJ/mol), suggesting that the single diastereomer observed for both **2.2**(Et) and **2.2'**(^{*i*}Pr) in solution is the (*R,R*)/(*S,S*) racemic mixture. This prediction has since been further supported by the isolation and crystallographic characterization of [**2.2'**(Cy)][GaCl₄]₂ by Weigand *et al.*, which also demonstrates a preference in the solid state for the (*R,R*)/(*S,S*) diastereomer in an eclipsed conformer [$\tau_{\text{Cy}} = -8^\circ$].⁶² Extension of this general principle to the heavier pnictogens seems viable as well, in light of recently observed solid-state structures of [R₃Pn-PR'-PR'-PnR₃][AlCl₄]₂ (Pn = As, Sb).¹³³ For these interpnictogen dications, derivatives with central aryl substituents (R' = Ph; Pn = As, Sb) are observed as the centrosymmetric (*R,S*) *meso* diastereomer in a *trans* conformation [$\tau_{\text{R}'} = 180^\circ$], while derivatives with alkyl substituents (R = ^{*i*}Pr; Pn = Sb) present as the (*R,R*)/(*S,S*) enantiomeric pair in an eclipsed conformation [$\tau_{\text{R}'} = -5^\circ$].

The calculated structural parameters for **2.2'**(Ph) closely parallel those experimentally determined in the solid state (Table 2.6). In contrast, the calculated parameters for **2.2'**(Me) more closely resemble those of the conformer for **2.2**(Me) that is observed in

the solid state, possessing a nearly idealized eclipsed conformation [$\tau_{R'} = 1.9^\circ$], and a correspondingly larger P-P-P-P torsion angle [$\tau_{PR_3} = 152.3^\circ$] and C_R-P-P angle [107.2°]. Crystal packing effects and lattice energy in the solid state may be a significant contributor to the deviation from calculated gas-phase parameters of **2.2'(Me)**.

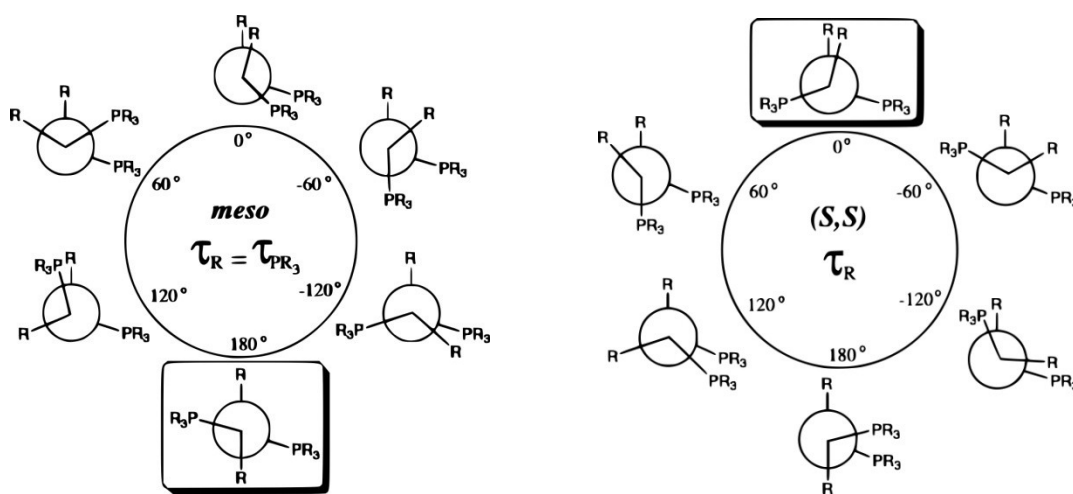


Figure 2.8. Representative conformations of the *meso*- and (*S,S*)-diastereomers. Idealized torsion angles between the central R-substituents are indicated (τ_R), and the preferred conformation in the gas phase is highlighted.

2.5 Summary

New chlorophosphinophosphonium ions have been prepared and characterized, and their reductive coupling under mild conditions with Ph₃P yields the first acyclic *catena*-2,3-diphosphino-1,4-diphosphonium ions. These new dications are also formed in a one-pot combination of a dichlorophosphine, a tertiary phosphine and Me₃SiOTf. The diastereoselectivity of the reactions and counterintuitive conformational preferences observed in the solid-state structures have been interpreted in the context of computational models, which extend well to other interpnictogen frameworks of this type. Ligand exchange reactions with chelating diphosphines further enhance the

understanding of solution diastereoisomerism in these cations and led to the first example of a 2,3,4-triphosphino-1,5-diphosphonium architecture.

Chapter 3. Reductive Coupling of Polychlorophosphinophosphonium Cations

3.1 Introduction

Reductive coupling is well-established in the literature as a synthetic method for the isolation of neutral polyphosphines from chlorophosphines (Section 1.2.2), particularly with respect to monocyclic and polycyclic polyphosphines.²² Although cyclic derivatives of the 2,3-diphosphino-1,4-diphosphonium framework were recently reported by Dillon and coworkers,⁸² these cyclized species are mixed carbon-phosphorus rings, where cyclization is imparted by bridging diphosphines. Application of reductive coupling to the synthesis of purely polyphosphorus cations has been limited by the scarcity of polyhalide-functionalized cationic building blocks (Chart 3.1).^{62,134-140} Towards this end, this chapter outlines investigations into the reduction of several newly reported bifunctional chlorophosphinophosphonium and chlorophosphinodichlorophosphonium cations. The frameworks of interest are highlighted in Chart 3.2.

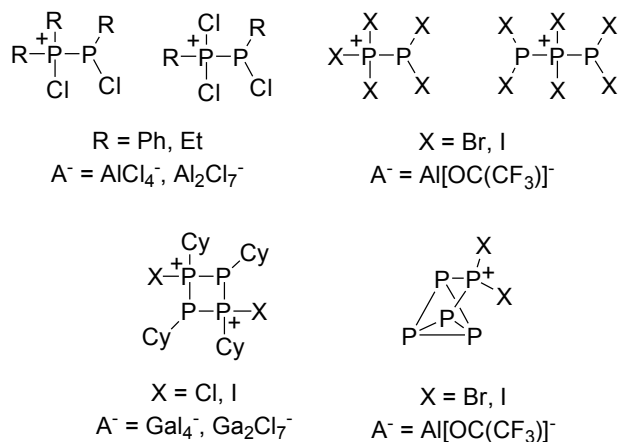
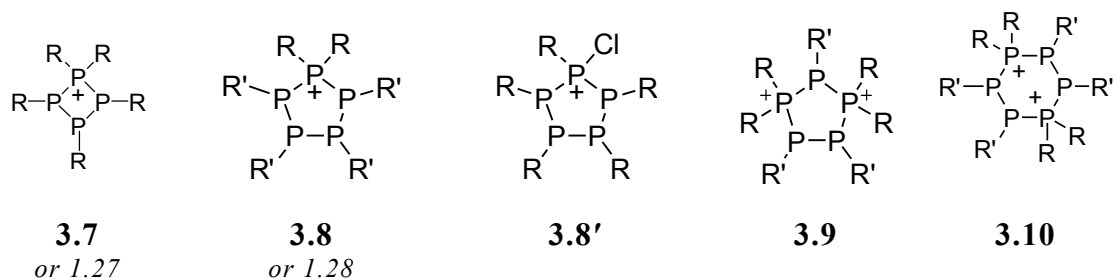
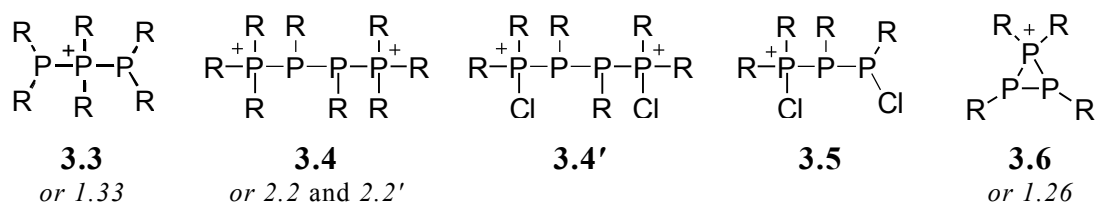
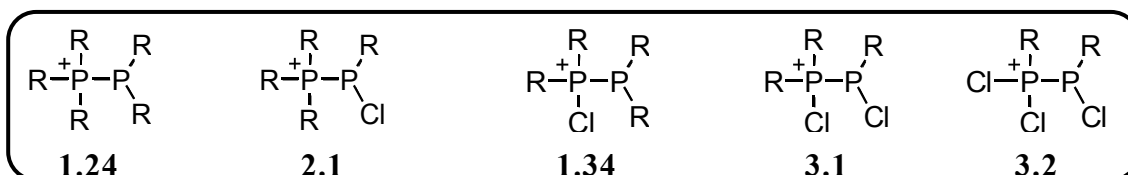


Chart 3.1. Known poly-halide functionalized catena-phosphorus cations.

Chart 3.2. Representative phosphinophosphonium cation frameworks, accompanied by the numbering scheme used throughout this chapter for clarity. Any previous numbering schemes are also listed in italics for reference. Substituents are indicated in brackets following the compound number in the text – where there are mixed substituents, substituents at the phosphonium are indicated with a subscript numeral two, *e.g.* **3.1**(X₂/Y) represents [X₂(Cl)P-PY(Cl)]⁺.



3.2 Phosfinochlorophosphonium Cations

Reaction mixtures of a chlorophosphine (R₂PCl) with a halide abstracting agent

(Abs = AlCl₃, GaCl₃ for any R = aryl, alkyl; Me₃SiOTf also for R = Me) quantitatively

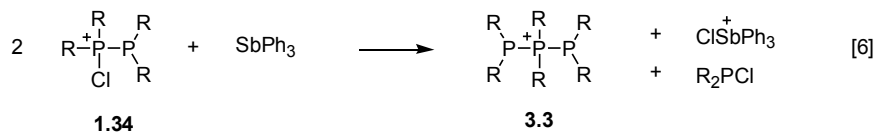
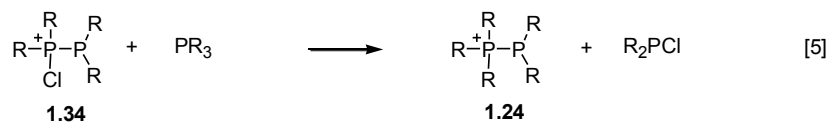
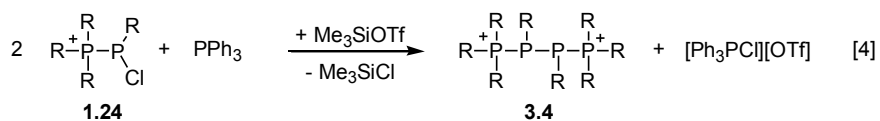
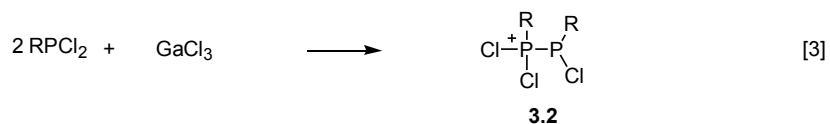
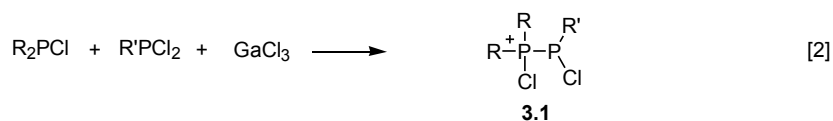
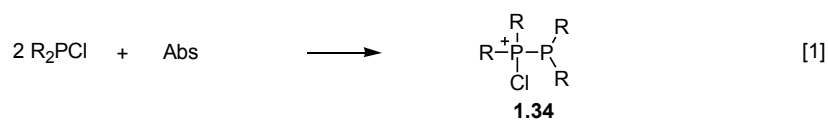
form phosfinochlorophosphonium cations **1.34**, as shown in Equation [1].¹¹⁶ The

process can be envisaged to involve formation of a Lewis acidic phosphonium cation

[PR₂]⁺ and subsequent coordination of the chlorophosphine ligand. This procedure has

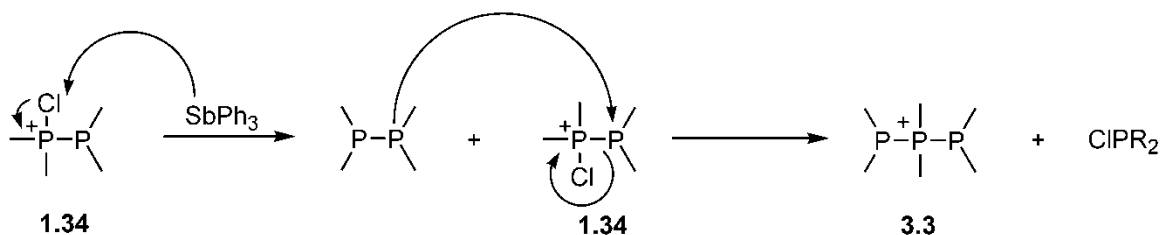
here been extrapolated to the reaction of dichlorophosphines (Equations [2] and [3]),

where $^{31}\text{P}\{^1\text{H}\}$ NMR spectra of reaction mixtures show quantitative formation of **3.1**[GaCl₄] and **3.2**[GaCl₄], respectively. Chemical shifts and coupling constants for all derivatives are summarized in Table 3.1. While $^{31}\text{P}\{^1\text{H}\}$ NMR spectra for derivatives of **3.1** are sufficiently resolved at room temperature to distinguish $^1J_{\text{PP}}$, spectra for derivatives of **3.2** contain broad peaks, perhaps indicating dynamic dissociation of the coordinate P-P bond due to the comparatively weak donation from the dichlorophosphine. Attempts to prepare dichlorophosphinophosphonium salts [Ph₃P-PCl₂][A] (A = GaCl₄ or OTf) by these methods were not successful, yielding only starting materials or triphosphenium cations⁷² **1.31** [Ph₃P-P-PPh₃]⁺ as products.



3.3 Reductive Coupling of 1-Phosphino-2-chloro-2-phosphonium or 1-Chloro-1-phosphino-2-chloro-2-phosphonium Cations

Chlorophosphinophosphonium cations **2** react with PPh_3 to give 2,3-diphosphino-1,4-diphosphonium dications via a redox reaction according to Equation [4].^{80,81} In contrast, the isomeric 1-phosphino-2-chloro-2-phosphonium cations **1.34** react with PPh_3 or trialkylphosphines via ligand exchange^{84,88} to produce the prototypical phosphinophosphonium cations **1**, illustrated in Equation [5]. Interestingly, reaction of derivatives of **1.34**[GaCl₄] with the less nucleophilic reductant SbPh_3 yields the 1,3-diphosphino-2-phosphonium tetrachlorogallate **3.3**[GaCl₄], representing a chain extension, as illustrated in Equation [6]. This reaction may be envisaged to proceed via formal chloronium abstraction from **1.34** by SbPh_3 to give tetraphenyldiphosphine and a chlorostibonium cation. The diphosphine competes with R_2PCl as a ligand, effecting ligand exchange on **1.34** to give **3.3**, as proposed in Scheme 3.1. $^{31}\text{P}\{^1\text{H}\}$ NMR spectra of reaction mixtures indicate that **1.34** is not completely consumed in the reaction with SbPh_3 , whereas reduction with SbBu_3 effects quantitative formation of the extended framework **3.3**. Reaction with one equivalent of SbBu_3 effects not only reduction of **1.34** to **3.3**, but also reduction of the *in situ* generated R_2PCl to the diphosphine, resulting in exchange-broadened ^{31}P NMR spectra. Addition of GaCl_3 to the reaction mixture with either reductant instead regenerates **1.34** from the eliminated chlorophosphine, as in Equation [1].



Scheme 3.1. Proposed mechanism for a reductive coupling chain extension of **1.34**, as observed in Equation [6].

Table 3.1. $^{31}\text{P}\{^1\text{H}\}$ NMR parameters for selected phosphinophosphonium gallate salts. Data are reported for spectra obtained in CH_2Cl_2 at 101.3 MHz.

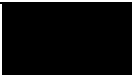
Cation	Donor	Acceptor	Spin System	$\delta_{\text{B or X}}$ [ppm] (phosphonium)	δ_{A} [ppm] (phosphine)	$^1J_{\text{PP}}$ [Hz] (T) ^a
1.34(Ph) ¹¹⁶	Ph ₂ (Cl)P	PPh ₂	AX	73	0	-393
3.1(Ph)		PPh(Cl)	AB	72	57	-395
3.2(Ph)	Ph(Cl) ₂ P	PPh(Cl)	---	131	81-85	<i>broad</i> (213 K)
1.34(Me) ¹¹⁶	Me ₂ (Cl)P	PMe ₂	AX	99	-33	-340
3.1(Me)		PMe(Cl)	AB	93	74	-365
3.2(Me)		PMe(Cl)	AX	154	97	-400 (213 K)
1.34(Et) ^b	Et ₂ (Cl)P	PEt ₂	AX	109	-19	-378
3.1(Et)		PEt(Cl)	AB	107	79	-391
3.2(Et)	Et(Cl) ₂ P	PEt(Cl)	--	148	79	<i>sharp singlets</i>
			AX	137	92	-446 (193 K)
3.1(ⁱPr)	¹ Pr ₂ (Cl)P	P ¹ Pr(Cl)	AB	110	93	-431
3.1(Cy)	Cy ₂ (Cl)P	PCy(Cl)	AB	101	88	-437
3.1(Ph₂/Me)	Ph ₂ (Cl)P	PMe(Cl)	AB	76	72	-378

^a Spectra recorded at 298 K unless otherwise indicated ^b Correction to previously reported ^{31}P NMR data for this compound.¹¹⁶

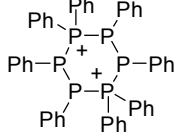
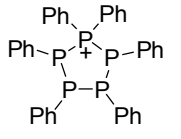
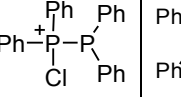
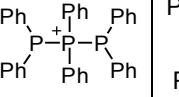
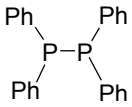
Reaction mixtures of chlorophosphinochlorophosphonium cations **3.1** with either SbPh₃ or SbBu₃ show a number of products by $^{31}\text{P}\{^1\text{H}\}$ NMR spectroscopy depending on the

reaction stoichiometry. Addition of one equivalent of SbPh₃ to **3.1(Ph)**[GaCl₄] in CH₂Cl₂ results in a mixture of **3.8(Ph)**[GaCl₄],⁵⁹ **3.10(Ph)**[GaCl₄]₂,⁶⁹ and **1.34(Ph)**[GaCl₄] as the major products after 12 h (summarized in Table 3.2a). Addition of two equivalents of SbPh₃ gives a similar product distribution, with **3.3(Ph)**[GaCl₄] appearing as an additional minor product. In contrast, addition of two equivalents of the stronger reductant SbBu₃ gives more reduced (less charged) species, **3.8(Ph)**[GaCl₄] and Ph₂P-PPh₂. Addition of 1.5 equivalents of SbBu₃ yielded **3.8(Ph)**[GaCl₄] as the sole cyclic product; however, the remaining Ph₂PCl was incorporated into both Ph₂P-PPh₂ and **3.3(Ph)**[GaCl₄]. Both of these products appear as broad resonances in the ³¹P NMR spectra, indicating dynamic exchange of [Ph₂P]⁺ units between molecules. Addition of less than one equivalent of either reducing agent results in incomplete consumption of **3.1**.

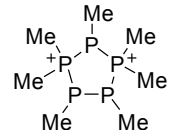
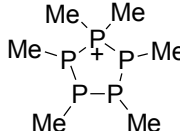
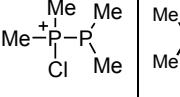
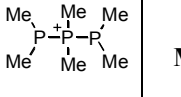
Table 3.2. Products observed for reductive coupling reactions^a of [R₂(Cl)P-PR'Cl][GaCl₄] including (a) **3.1(Ph)**, (b) **3.1(Me)**, and (c) **3.1(Et)**. Relative conversion (based on the area of the ³¹P{¹H} NMR signals) to each of the products vs. the most predominant species (assigned as 100%) is indicated by shading according to the following ranges:

High	> 70%	
Medium	41-70%	
Low	10-40%	
Negligible	< 10 %	

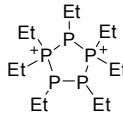
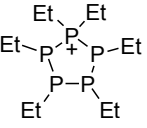
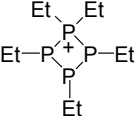
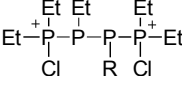
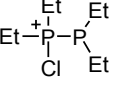
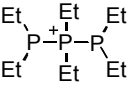
(a)

<i>Products</i> \ <i>Reagents</i>	 3.10(Ph)	 3.8(Ph)	 1.34(Ph)	 3.3(Ph)	
2 SbPh ₃ 1 GaCl ₃					
1-2 SbPh ₃ or 1 SbBu ₃					
1.5 SbBu ₃					
2 SbBu ₃					

(b)

<i>Products</i> \ <i>Reagents</i>	 3.9(Me)^b	 3.8(Me)	 1.34(Me)	 3.3(Me)	MePCl₂
1 SbPh ₃					
1 SbBu ₃					
1 SbBu ₃ (solvent: MeCN)					
2 SbBu ₃					

(c)

<i>Products</i>						
<i>Reagents</i>	3.9(Et)	3.8(Et)^c	3.7(Et)^d	3.4'(Et)	1.34(Et)	3.3(Et)
2 SbPh ₃ 1 GaCl ₃						
1 SbBu ₃						
1 SbBu ₃ 1 GaCl ₃ ^e						
2 SbBu ₃						

^a All reactions conducted in CH₂Cl₂ unless otherwise noted. ^b **[3.9(Me)][GaCl₄]₂** was isolated as a precipitate from CH₂Cl₂-reactions, and re-dissolved in MeCN to be identified using ³¹P{¹H} NMR spectroscopy. Relative abundance could not be assessed by NMR, so shading indicates only the presence or absence of this product in these reactions. ^c ³¹P{¹H} NMR parameters could not be simulated due to overlap with other products (approximate chemical shifts: $\delta = 91 \pm 1$, 12 ± 3 , and -3 ± 4 ppm). ^d ³¹P{¹H} NMR parameters, A₂BX system: $\delta_A = -62.3$, $\delta_B = -54.4$, $\delta_X = 12.5$ ppm; $^1J_{AB} = -225$, $^1J_{BX} = -112$, $^2J_{AX} = 21$. ^e Also contains Et₂P-PEt₂ ($\delta_{31P} = -25$ ppm, broad singlet) as a major product.

In contrast, addition of two equivalents of SbPh₃ and one equivalent of GaCl₃ to **4(Ph)** resulted in nearly quantitative conversion to the dication **3.10(Ph)**. Notably, the previously observed decomposition⁶⁹ of **[3.10(Ph)][GaCl₄]₂** to the five-membered monocation **[3.8(Ph)][GaCl₄]** ($t_{1/2} = 24$ h) in solution is negligible here. This preference for the more charged species is effected by the comparatively weak reducing agent (SbPh₃ vs. SbBu₃), as well as the *in situ* formation of the [Ga₂Cl₇]⁻ anion from [GaCl₄]⁻. The addition of excess GaCl₃ suppresses the equilibrium formation of the chloride anion (Scheme 3.2), which is proposed to undergo nucleophilic attack on the dication **3.10**.



Scheme 3.2. Addition of excess GaCl₃ to suppress dissociation of [GaCl₄][−]

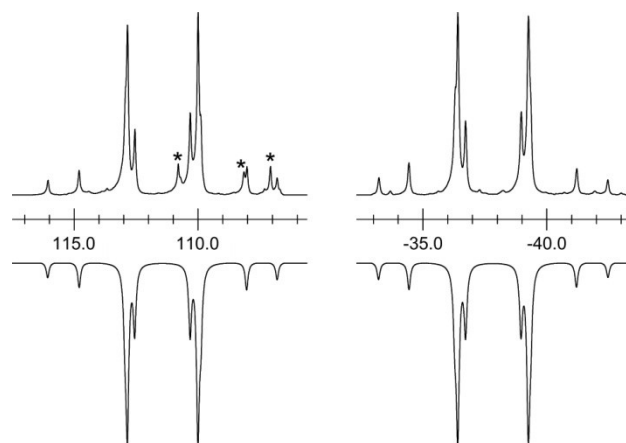


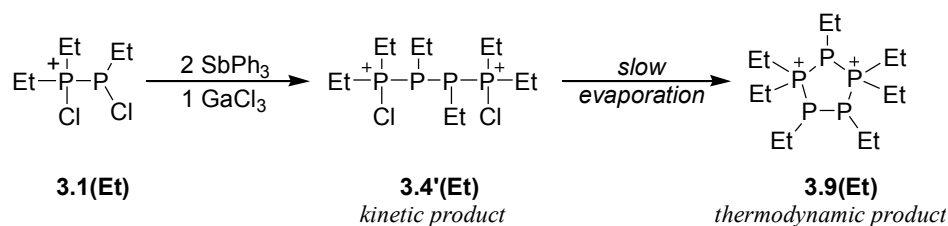
Figure 3.1. Experimental (upright) and simulated (inverted) expansions of the ³¹P{¹H} NMR spectra of [3.4'(Et)][GaCl₄]₂ in the reaction mixture of [3.1(Et)][GaCl₄] with 2 SbPh₃ and GaCl₃. Minor impurities in the reaction mixture are marked with asterisks.

The reductive coupling of [3.1(Me)][GaCl₄] (summarized in Table 3.2b) demonstrates a thermodynamic preference for the five-membered dicationic ring [3.9(Me)][GaCl₄]₂⁶¹ over the six-membered alternative. Likewise, reaction of [3.1(Et)][GaCl₄] with 1 eq. SbBu₃ yields a mixture of [1.34(Et)][GaCl₄] with 3.8(Et) and [3.9(Et)][GaCl₄]₂ (summarized in Table 3.2c). In contrast, the ³¹P NMR spectrum of the reaction mixture of SbPh₃ with GaCl₃ and [3.1(Et)][GaCl₄] indicates nearly quantitative formation of an acyclic 2,3-diphosphino-1,4-diphosphonium cation, identified by the characteristic AA'XX' spin system shown in Figure 3.1 assigned here to [Et₂(Cl)P-PEt-PEt-P(Cl)Et₂][GaCl₄]₂, [3.4'(Et)][GaCl₄]₂. Attempted crystallization of [3.4'(Et)][GaCl₄]₂ by slow evaporation over a period of weeks resulted in precipitation of

a yellow solid identified as **[3.9(Et)][GaCl₄]₂** (³¹P{¹H} NMR parameters: Table 3.4), suggesting that **3.4'** is a kinetically stabilized intermediate en route to **3.9** (Scheme 3.3). In the analogous reduction reaction of [Ph₂(Cl)P-PMeCl][GaCl₄], **3.1(Ph₂/Me)**, the kinetic product **3.4'(Ph₂/Me)** was observed in the reaction solution by ³¹P{¹H} NMR spectroscopy for less than 22 h prior to its complete conversion to the thermodynamically-favoured dicationic ring **3.9(Ph₂/Me)**. Notably, while all other known derivatives of **3.9** adopt a *trans*-orientation of substituents at the adjacent phosphine sites, **3.9(Ph₂/Me)** was consistently produced as a 2:1 mixture of the *trans*- and *cis*-isomers (Figure 3.2). The higher (C_s) symmetry of the *cis*-isomer readily distinguishes it as an ABB'XX' spin system in ³¹P{¹H} NMR spectra. The one-bond coupling constant between the phosphine sites (P4/P5) was observed to be substantially larger in the *cis*-isomer (¹J_{PP(*cis*)} = -323 Hz; ¹J_{PP(*trans*)} = -260 Hz). This is in agreement with previous experimental¹²⁴⁻¹²⁶ and theoretical^{127,128} studies indicating the substantial stereochemical dependence of ³¹P-³¹P coupling constants – specifically, that coupled phosphorus nuclei with *cis*-oriented lone pairs exhibit one-bond coupling constants that are substantially greater than their *trans*-oriented analogues, *i.e.* |¹J_{PP(*cis*)}| > |¹J_{PP(*trans*)}|^{22,126,128}. As the lone pair orientation is not itself observable, configurations can instead be described by the dihedral angle (φ_{LP}) between the bisectors of the R-P-R angle at each phosphorus atom – the maximum magnitude for ¹J_{PP} is expected for φ_{LP} between 60-90°.

In addition, the ³¹P NMR chemical shifts of all three phosphine sites in the *cis*-isomer are considerably upfield shifted relative to the *trans*-isomer (Δδ = 25-35 Hz). Although rare among *cis-trans* isomers of neutral cyclopolyphosphines, such a large magnitude

difference in chemical shift has been previously observed in the case of *cyclo*- $(^t\text{BuP})_2\text{P}^i\text{Pr}$.²² **[3.9(Ph₂/Me)]**[GaCl₄]₂ represents, however, the first observation of adjacent *cis*-substituents in a cationic *catena*-phosphorus ring system.



Scheme 3.3. Conversion of **[3.4'(Et)]**[GaCl₄]₂ to **[3.9(Et)]**[GaCl₄]₂.

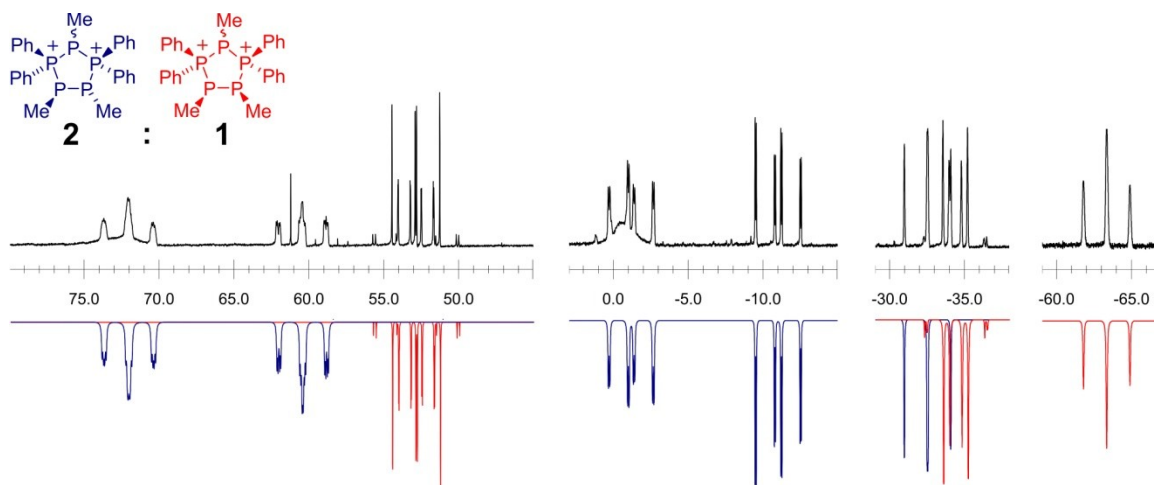


Figure 3.2. Experimental (upright) and simulated (inverted) expansions of the $^{31}\text{P}\{^1\text{H}\}$ NMR spectrum at 202.6 MHz of the 2:1 mixture of *trans* (blue) and *cis* (red) isomers of **3.9(Ph₂/Me)**, with characteristic AGHMX and ABB'XX' spin systems, respectively. Broad peaks at 0.5 and 72 ppm (not simulated) correspond to the phosphinophosphonium cation **1.34(Ph)**.

3.4 Structure and Solution Behaviour of the Cyclo-triphosphino-1,3-diphosphonium cation **3.9**(ⁱPr)

Crystals of [**3.9**(ⁱPr)][GaCl₄]₂ have been isolated from the reaction of [**3.1**(ⁱPr)][GaCl₄] with SbBu₃. Views of the cation are shown in Figure 3.3. Using the PLATON software package,¹³¹ the solid-state structure of [**3.9**(ⁱPr)][GaCl₄]₂ was determined to approximate a ⁴E envelope conformation with a Cremer-Pople¹³⁰ phase angle (φ) of 286.80(5)° and puckering amplitude (Q) of 0.9040(7) Å (Figure 3.4). Bond lengths and angles within the ring are generally comparable to those observed for the two previously reported⁶¹ cyclo-triphosphino-1,3-diphosphonium cations (Table 3.3), although the angle about one phosphonium centre (P3) is significantly smaller in **3.9**(ⁱPr), presumably as a result of substituent steric strain. The closest cation-anion contact is a Cl-H interaction at 2.68 Å (Σr_{vdw} 2.84 Å) between a tetrachlorogallate anion and a methyl proton of one isopropyl group in the adjacent asymmetric unit.

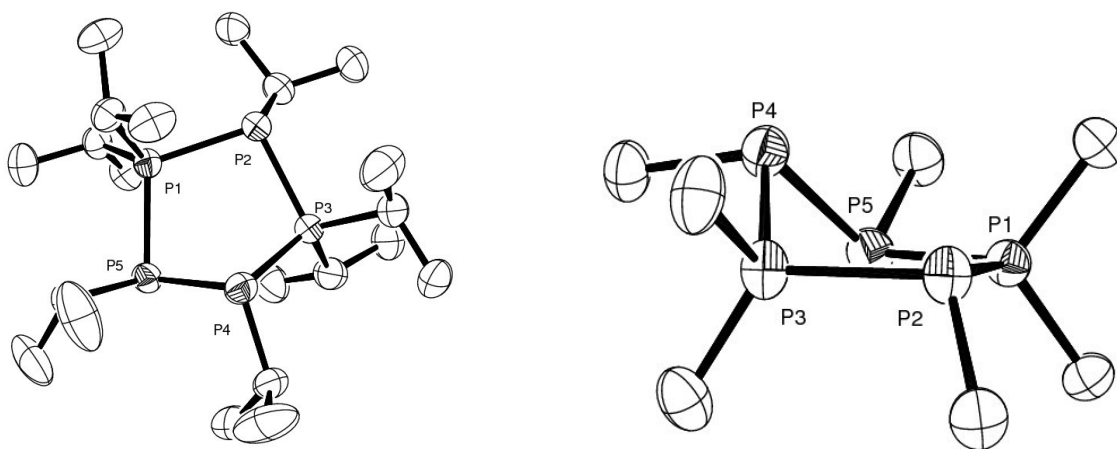
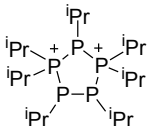
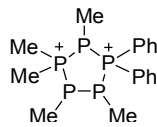
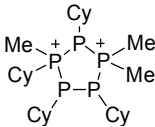


Figure 3.3. ORTEP views of the cation in [**3.9**(ⁱPr)][GaCl₄]₂·CH₂Cl₂. Thermal ellipsoids are shown at the 50% probability level, carbon atoms are unlabelled and hydrogen atoms are omitted for clarity. Right view shows only the phosphorus framework and associated α -carbons, indicating a ⁴E conformation.

Table 3.3. Selected homoatomic distances (Å) and bond angles (°)^a in the solid-state structure of [3.9(ⁱPr)][GaCl₄]·CH₂Cl₂ and comparative values for 3.9' and 3.9''.⁶¹ Also indicated are the calculated Cremer-Pople^{130,131} puckering angle (φ, °), puckering parameter (Q, Å), and conformation.

			
	[3.9(ⁱPr)] [GaCl ₄] ₂ ·CH ₂ Cl ₂	3.9' [OTf] ₂	3.9'' [OTf] ₂
P-P Range	2.2022(9)-2.2341(10)	2.199-2.238	2.193(2)-2.234(2)
P-P Average	2.214	2.228	2.213
P-P1-P	109.07(4)	107.17(9)	109.58(8)
P-P2-P	98.43(4)	95.84(10)	95.05(8)
P-P3-P	101.24(4)	109.25(10)	106.26(8)
P-P4-P	94.63(4)	93.99(10)	105.23(7)
P-P5-P	95.56(4)	93.96(9)	101.79(7)
C-P4-P5-C	92.99(14)	100.74(35)	143.23(26)
φ	286.80(5)	312.08(12)	218.14(12)
Q	0.9040(7)	0.8922(19)	0.6614(14)
Pseudorotational Conformation	⁴ E	⁴ T ₅	² E

^a Angles indicated in bold centre on the phosphonium centres (P1, P3)

Simulation of the AGHMX spin system apparent in $^{31}\text{P}\{^1\text{H}\}$ NMR spectra of solutions of **3.9**(^iPr) at 188 K (Figure 3.5, Table 3.4) yields chemical shift and coupling constant parameters that are comparable to known derivatives⁶¹ of **3.9**. However, $^1J_{\text{PP}}$ between the backbone phosphorus atoms P4-P5 was observed to be significantly smaller in magnitude (-149 Hz) for **3.9**(^iPr) relative to other derivatives of **3.9** with *trans*-oriented substituents (-260 to -315 Hz). Although all derivatives in Table 3.4 are *trans*-substituted, the magnitude of $^nJ_{\text{PP}}$ is expected to depend more specifically on the relative lone pair orientation (ϕ_{LP}) of the phosphorus atoms in question.¹²⁸ Since ϕ_{LP} may be formally defined by the dihedral angle between the bisectors of the R-P-R angle at each phosphorus atom (*vide supra*), it is inversely proportional to the dihedral angle between the substituents. Among the three crystallographically characterized derivatives of **3.9**, there is substantial variation in the C-P4-P5-C dihedral angle between the *trans*-oriented substituents in the solid state (Table 3.3). The observed C-P4-P5-C dihedral angle in **3.9**(^iPr) (93°) implies a large ϕ_{LP} angle and a correspondingly small magnitude $^1J_{\text{P4P5}}$ relative to **3.9**'' (C-P4-P5-C 143°).

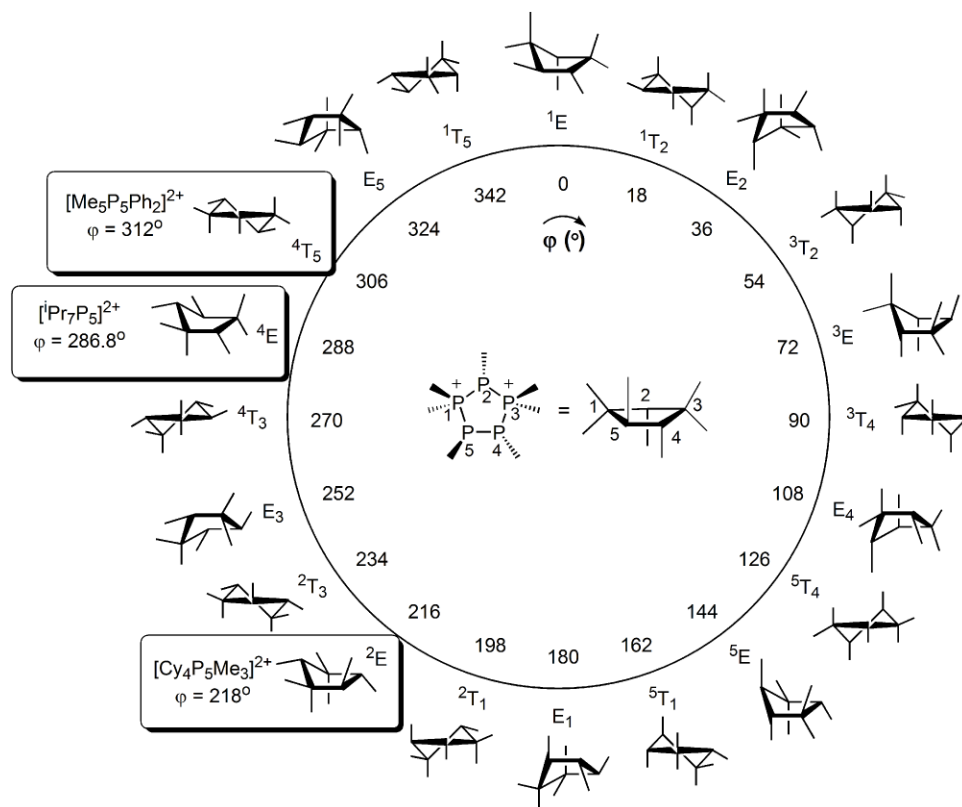


Figure 3.4. Possible pseudorotational conformations of **3.9** described according to the Cremer-Pople puckering angle, ϕ . Conformations observed in the solid state are highlighted in boxes. Figure adapted from Dyker *et al.*⁵⁹

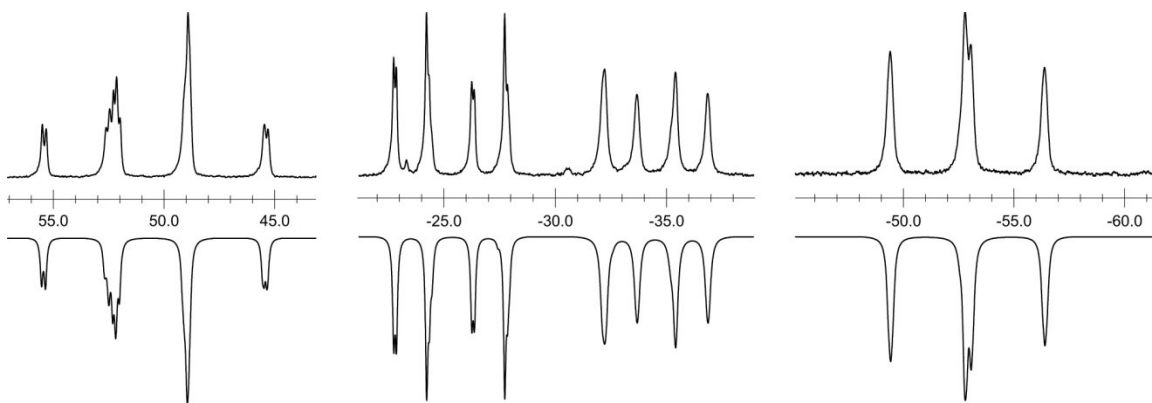
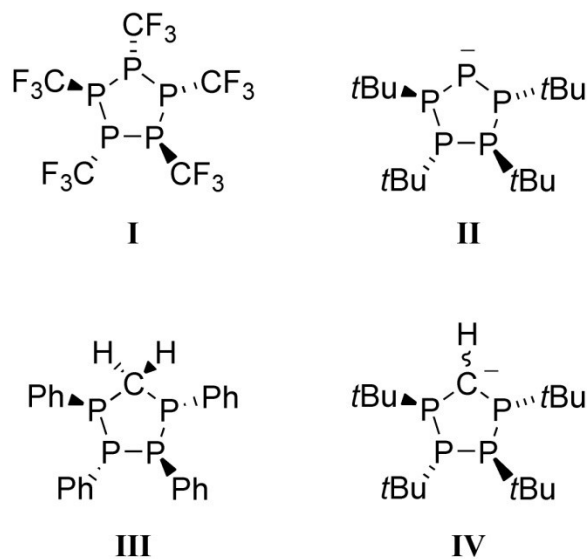
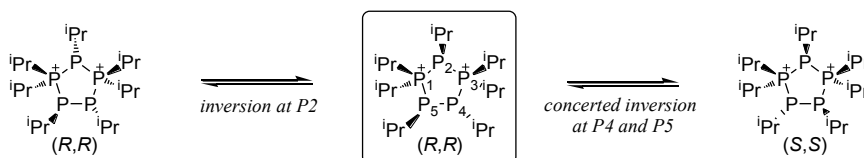


Figure 3.5. Experimental (upright) and simulated (inverted) expansions of the $^{31}\text{P}\{^1\text{H}\}$ NMR spectrum of $[\mathbf{3.9}(\text{iPr})][\text{GaCl}_4]_2$ in EtCN at 101.3 MHz and 188 K. Parameters for the AGHMX spin system are listed in Table 3.4.



$^{31}\text{P}\{^1\text{H}\}$ NMR analysis of EtCN solutions of crystalline $[\mathbf{3.9}(\text{iPr})][\text{GaCl}_4]_2$ at a variety of temperatures revealed substantial peak broadening near room temperature (Figure 3.6), indicative of dynamic behaviour in solution. It is particularly noteworthy that the resonance attributed to P2 (-44 ppm [291 K] to -53 ppm [188 K]) appeared sharp, with a lineshape that was relatively invariant as a function of temperature, implying that the net solution exchange process(es) do not affect the environment of this atom. Further, low temperature ^{31}P NMR data for $\mathbf{3.9}(\text{iPr})$ suggests a molecule with C_1 symmetry, whereas, at high temperature, the observed AMM'XX' spin system suggests effectively time-averaged C_2 or C_s symmetry. A survey of existing five-membered ring systems (I,^{126,141,142} II,⁴⁰ III,¹⁴³ IV¹⁴⁴ and $\mathbf{3.8}$ ⁵⁹) with a predominantly *catena*-phosphorus frame indicate a preference for low symmetry (C_1) solid-state structures, with varied symmetry in solution (C_1 symmetry (ABCDX) for two derivatives of $\mathbf{3.8}$,⁵⁹ $[(\text{PhP})_4\text{PPhMe}][\text{OTf}]$ and $[(\text{PhP})_4\text{PPh}^t\text{Bu}][\text{GaCl}_4]$, and higher symmetry for I¹²⁶ (AA'BB'C), II⁴⁰ (ABB'CC'), III¹¹⁸ (AA'BB'), IV¹⁴⁴ (ABCD at -100°C; AA'BB' at 60°C), and other derivatives of $\mathbf{3.8}$ (AA'BB'X),⁵⁹ $[\mathbf{3.8}(\text{Me})][\text{OTf}]$, $[\mathbf{3.8}(\text{Me}_2/\text{Cy})][\text{OTf}]$, $[\mathbf{3.8}(\text{Ph})][\text{OTf}]$ and $[\mathbf{3.8}(\text{Me}_2/\text{Ph})][\text{OTf}]$). These observations have been previously rationalized by invoking

inversion at phosphorus, static solution C_2 or C_s conformations, or pseudorotation (ring-puckering) processes. To understand the fluxional process occurring in solution for **3.9**(ⁱPr), it is instructive to compare it directly with the analogous monocation **3.8**.



Scheme 3.4. Possible inversion pathways for **3.9**(ⁱPr) which effect time-averaged C_2 symmetry.

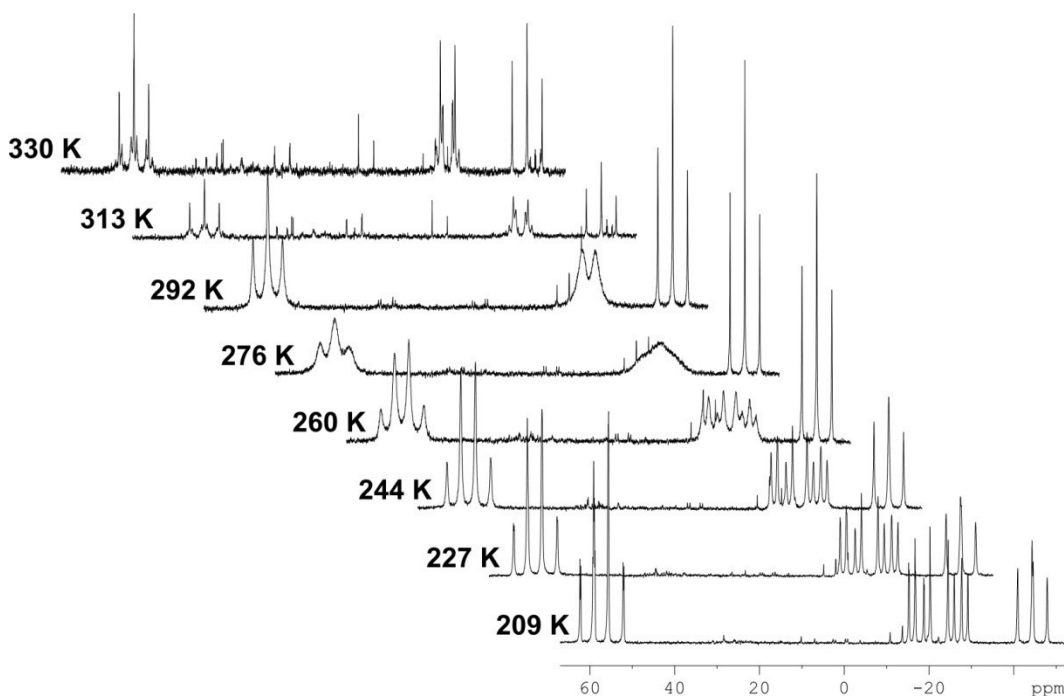


Figure 3.6. Variable-temperature $^{31}\text{P}\{^1\text{H}\}$ NMR spectra of **[3.9**(ⁱPr)**][GaCl₄]₂** in EtCN at 101.3 MHz.

For the monocations **3.8**, pseudorotation provides sufficient rationale for the observation ($^{31}\text{P}\{^1\text{H}\}$ NMR) of effective C_2 symmetry in derivatives with symmetric substituents at the phosphonium centre and effective C_1 symmetry in asymmetrically-substituted derivatives. Pseudorotation is, however, insufficient to explain the symmetry observed in

high temperature NMR spectra of **3.9(iPr)**, as even a time-averaged planar structure presents only C_1 symmetry (Figure 3.7). Inversion at phosphorus may be additionally invoked to rationalize the observed $AMM'XX'$ spin system at high temperature.

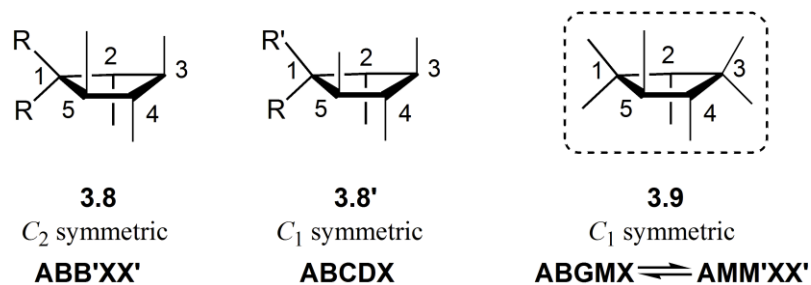
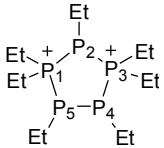
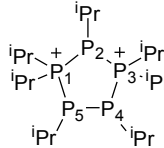
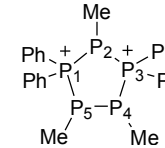
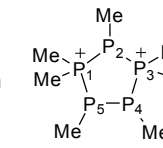
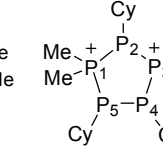


Figure 3.7. Skeletal representations of the time-averaged planar structure of symmetrically substituted **3.8** (left), geminal asymmetrically-substituted **3.8'** (center, $R \neq R'$), and **3.9**, to rationalize the $^{31}\text{P}\{^1\text{H}\}$ NMR spin systems.

Table 3.4. $^{31}\text{P}\{^1\text{H}\}$ NMR parameters^a for **[3.9(Et)][GaCl₄]₂**, **[3.9(ⁱPr)][GaCl₄]₂** and **[3.9(Ph₂/Me)][GaCl₄]₂** in comparison with previously reported heteroleptic derivatives of **3.9[OTf]**. Substituents at P4 and P5 are *trans*-oriented in all cases.

Cation						
	3.9(Et)	3.9(ⁱPr)	3.9(Ph₂/Me)	3.9(Me)⁶¹	3.9'^{61,b}	
δ (ppm)	P1	87.3	52.1	72.5	72.6	52.6 [X]
	P2	-30.9	-52.9	-32.5	-20.9	-29.3 [G]
	P3	82.0	48.9	60.7	67.0	42.8 [M]
	P4	-9.6	-25.3	-0.7	-0.2	-23.6 [B]
	P5	-17.0	-34.5	-11.0	-7	-35.4 [A]
$^1J_{\text{PP}}$ (Hz)	P1P2	-332	-340	-320	-314	-327
	P1P5	-354	-326	-349	-327	-379
	P2P3	-317	-367	-307	-302	-338
	P3P4	-345	-360	-339	-320	-335
	P4P5	-306	-149	-260	-274	-313
$^2J_{\text{PP}}$ (Hz)	P1P3	54	-17	36	36	37
	P1P4	6	< 10^c	21	12	1
	P2P4	64	-12	6	5	-13
	P2P5	-18	< 10 ^c	3	9	-12
	P3P5	21	< 10^c	-14	15	2
Spin system	AGHMX			ABGMX ^d		
T (K)	298	188	298	298	298	
Solvent	CH ₂ Cl ₂	EtCN	CH ₂ Cl ₂	MeCN	MeCN	

^a Bold values indicate parameters involving the phosphonium centre(s). All parameters were derived by iterative fitting of experimental data at 101.3 MHz. ^b Chemical shift assignments for P1 and P3 were not specified in the original reference; the assignments here are assumed and based on similarities the magnitude of the chemical shifts, but should not be taken as definitive. ^c Line-broadening remains significant at 188 K, so $|^2J_{\text{PP}}|$ values < 10 Hz could only be approximated. ^d Designation of this spin system according to convention would erroneously imply a first order relationship between P4 and P5. For clarity, an ABGMX designation, as labeled, is used instead.

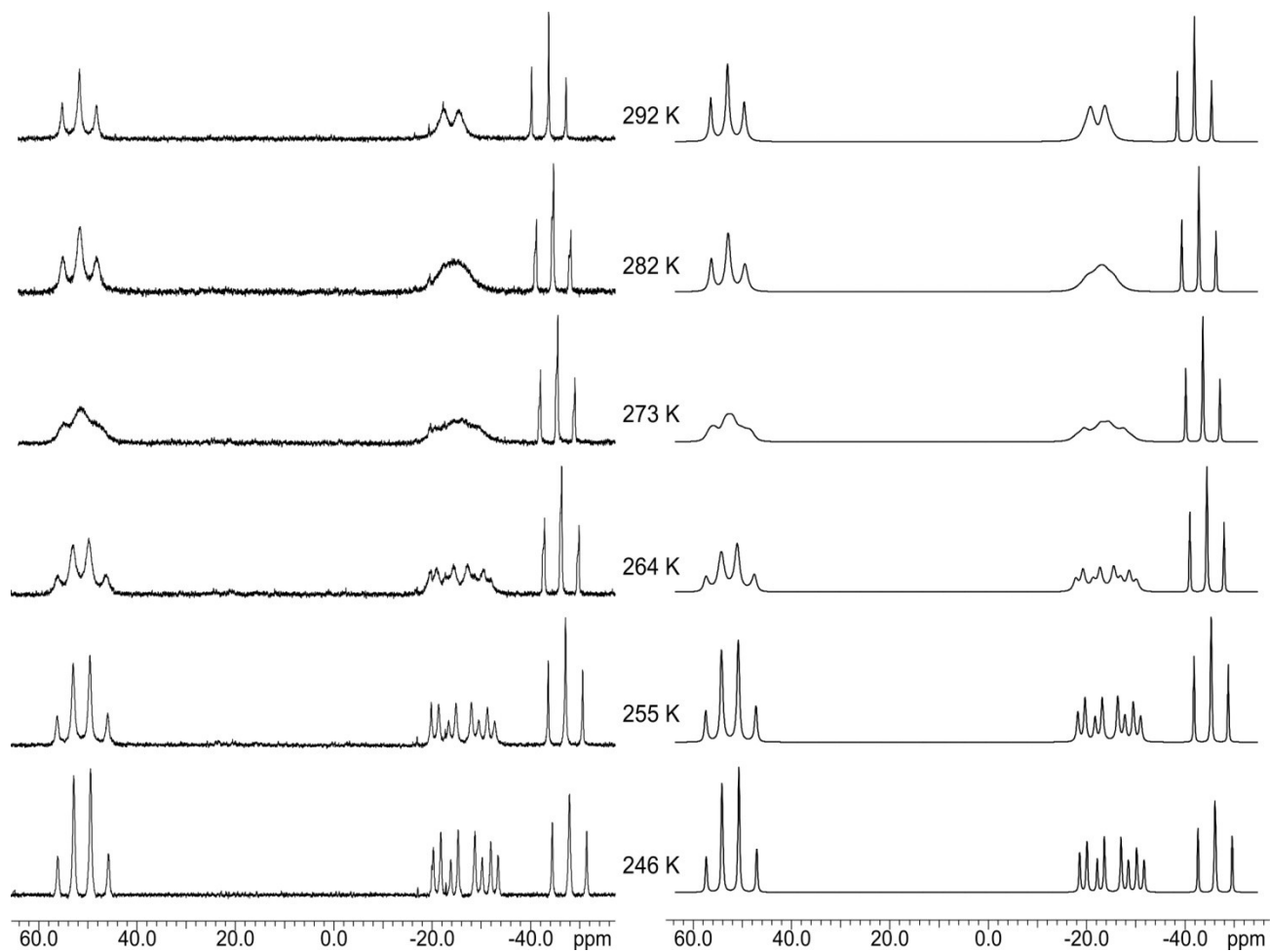


Figure 3.8. Experimental (left) and simulated (right) $^{31}\text{P}\{^1\text{H}\}$ NMR spectra used in lineshape analysis of $[\mathbf{3.9}(\text{iPr})][\text{GaCl}_4]_2$. Resulting rate constants are listed in Table 8.1.

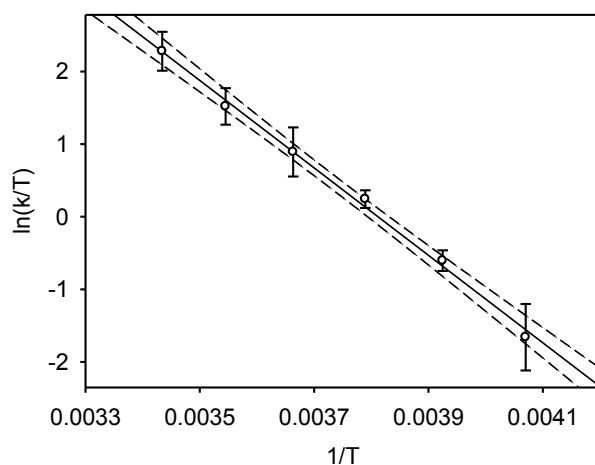
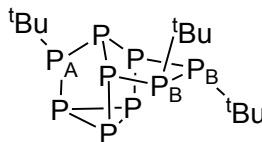


Figure 3.9. Eyring plot for the dynamic behaviour of **[3.9(ⁱPr)]**[GaCl₄]₂ in EtCN based on rate constants (k) from line shape analysis of ³¹P{¹H} NMR spectra between 246-292 K (simulated and experimental spectra available in the supporting information). Error bars are plotted based on error estimates in dNMR lineshape fitting, and the 95% confidence interval about the regression line is indicated with dashed lines.

The significant steric strain imposed by the multiple isopropyl substituents in **3.9(ⁱPr)** promotes comparatively rapid inversion at P2 or P4/P5 as shown in Scheme 3.4.

Assuming a first-order mechanism, the activation parameters for this process, which effectively exchanges the resonances of P1/P3 and P4/P5, were calculated by line-shape analysis of ³¹P{¹H} NMR spectra between 246-292 K (Figure 3.9). In EtCN at 298K, the Gibbs free energy of activation ΔG^\ddagger was determined to be $52 \pm 1.5 \text{ kJ}\cdot\text{mol}^{-1}$ (95% C.I. by weighted linear regression). This is in good agreement with a barrier of $50 \text{ kJ}\cdot\text{mol}^{-1}$ estimated¹⁴⁵ using an approximate coalescence temperature (T_c) of 277 K. This is significantly lower than the previously determined barrier for the inversion of substituted diphosphines⁴⁷ ($94\text{-}100 \text{ kJ}\cdot\text{mol}^{-1}$) or the ^tBu-substituted cage **V** (see next page: $77\pm 8 \text{ kJ}\cdot\text{mol}^{-1}$ at P_A or $126\pm 8 \text{ kJ}\cdot\text{mol}^{-1}$ at P_B),²² and nearly on par with the inversion barrier determined for **IV** ($39\text{-}48 \text{ kJ}\cdot\text{mol}^{-1}$ depending on solvent),¹⁴⁴ which was proposed

to invert via the carbanion centre. Alternately, the lower inversion barrier in **3.9**(^{*i*}Pr) can be rationalized by invoking partial double bond character along P1-P2-P3.

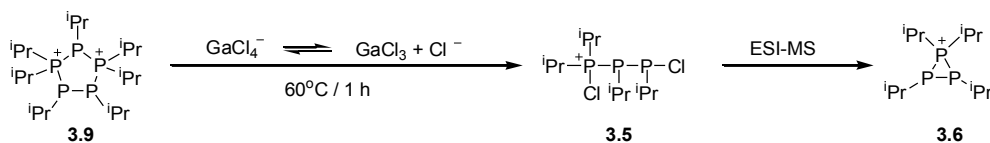


V

Less sterically-encumbered derivatives [**3.9**(Me)][OTf]₂⁶¹ and [**3.9**(Et)][GaCl₄]₂ display characteristic C₁ symmetry in room temperature solutions (ABGMX ³¹P{¹H} NMR spin systems), suggesting slow interconversion for these derivatives on an NMR timescale. As pseudorotation or ring-puckering depends on the barrier to rotation about each P-P single bond, the barrier to interconversion should be directly proportional to the steric requirement of the substituents, rather than inversely proportional as observed here. In contrast, the barrier to inversion, already expected to be lowered for catenated phosphorus systems due to dπ-pπ overlap,^{35,47,48,146} is expected to decrease with increasing steric demand.¹⁴⁷

Heating solutions of [**3.9**(^{*i*}Pr)][GaCl₄]₂ in EtCN resulted in decomposition predominantly to a single product, [**3.5**(^{*i*}Pr)][GaCl₄], which could be isolated as an oil. This product can be envisioned as resulting from the ring-opening of **3.9**(^{*i*}Pr) by the nucleophilic attack of chloride ions (Scheme 3.5) from the equilibrium dissociation of the tetrachlorogallate anion (Scheme 3.2). ESI-MS analysis of MeCN solutions of [**3.5**(^{*i*}Pr)][GaCl₄] support the identification of a monocationic species with a tetrachlorogallate counteranion. However, the base peak (m/z 265.1) was assigned to a molecular ion with the formula [^{*i*}Pr₄P₃]⁺, which is assigned to the three-membered cyclic monocation **3.6**(^{*i*}Pr). The small

magnitude of the ^{31}P - ^{31}P coupling constant J_{MX} (29 Hz) clearly indicates a linear structure in solution, suggesting that the conditions of ESI-MS analysis effect formal loss of Cl_2 from **3.5**(ⁱPr) in the gas-phase and concerted ring-closure to form **3.6**(ⁱPr). Significantly, the addition of donor phosphines such as PPh_3 or PMe_3 did not effect ligand exchange on **3.5**, suggesting a more covalent, rather than coordinative, bonding interaction. No reaction was observed upon heating **3.5**(ⁱPr) to 90°C in EtCN nor upon addition of SbBu_3 as a potential reducing agent, further indicating the substantial kinetic stabilization provided by the bulky isopropyl substituents. Nonetheless, this series of ring assembly and disassembly reactions provides a promising new route to chloro-functionalized *catena*-phosphorus cations which are themselves key building blocks in the development of larger catenated frameworks.



Scheme 3.5. Ring-opening and ring-closing products observed by $^{31}\text{P}\{^1\text{H}\}$ NMR spectroscopy during the thermal-decomposition and ESI-MS analysis of **[3.9**(ⁱPr)**][GaCl₄]₂** in EtCN.

3.5 Cyclotetraphosphinochlorophosphonium Cations, **3.8'**

While the reductive coupling reactions of chlorophosphinochlorophosphonium salts (**3.1**[GaCl_4]) provided an efficient approach to the assembly of aryl and alkyl cyclophosphinophosphonium cations, analogous reactions of the chlorophosphinodichlorophosphonium [**3.2**(Ph)][GaCl_4] with 1-2 equivalents of SbR_3 yielded PhPCl_2 and a new chloro-substituted cyclophosphinophosphonium system

assigned as **[3.8'(Ph)][GaCl₄]**, identified using ³¹P NMR spectroscopy. (Scheme 3.6 and Figure 3.10).

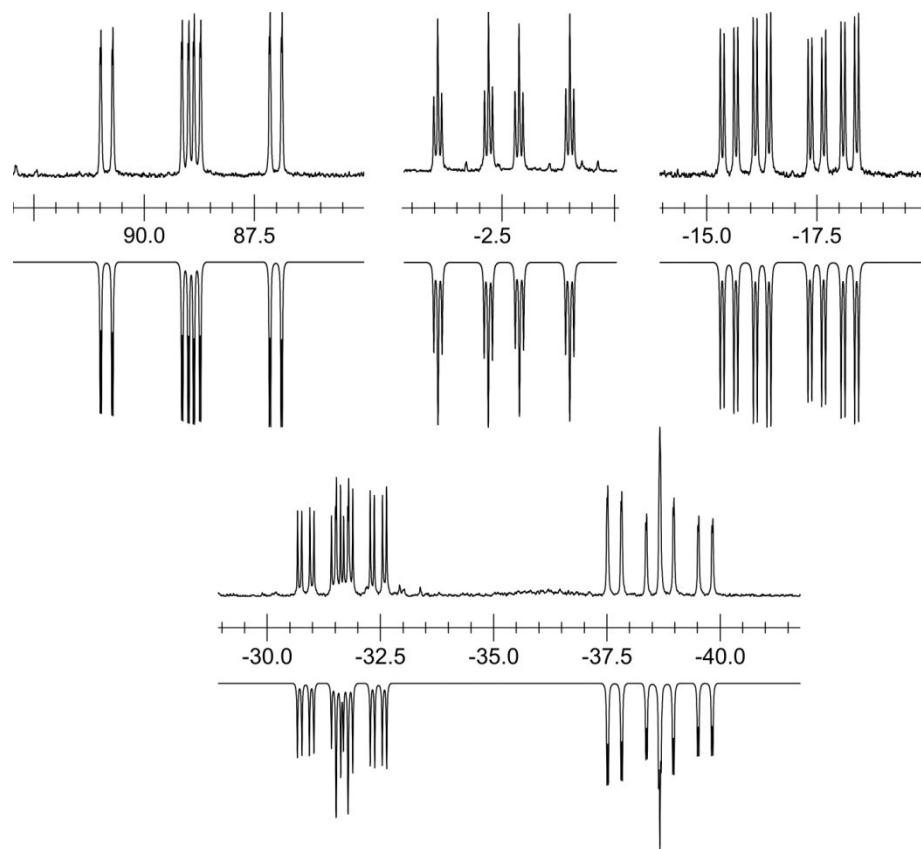
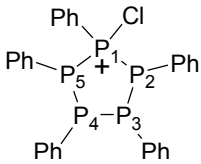
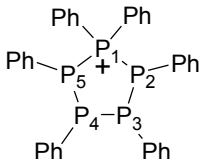
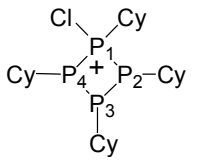
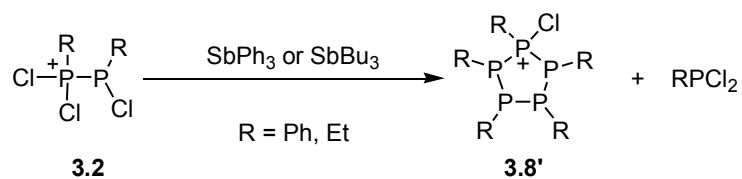


Figure 3.10. Experimental (upright) and simulated (inverted) expansions of the ³¹P{¹H} NMR spectrum of **[3.8'(Ph)][GaCl₄]**, *cyclo*-[(Ph₅P₅)Cl][GaCl₄] at 280 K and 202.6 MHz, displaying an AGHMX spin system with a downfield resonance ($\delta_X = 89$ ppm) characteristic of a Cl-substituted phosphonium centre.

Table 3.5. $^{31}\text{P}\{^1\text{H}\}$ NMR parameters^a for **[3.8'(Ph)][GaCl₄]** in comparison to those for **[3.8(Ph)][OTf]⁵⁹** and **[3.7'(Cy)][OTf]⁶²**.

Cation			
	3.8'(Ph)	3.8(Ph)⁵⁹	3.7'(Cy)⁶²
δ (ppm)	89.3 [1] -15.7 [2] -30.9 [3] -37.5 [4] -1.2 [5]	22 [1] -36 [2/5] -42 [3/4]	95.1 [1] -40.7 [2/4] -54.4 [3]
$^1J_{\text{PP}}$ (Hz)	-403 [1,2] -374 [1,5] -153 [2,3] -232 [4,5] -174 [3,4]	-325 [1,2; 1,5] -142 [2,3; 4,5] -160 [3,4]	-285 [1,2; 1,4] -126 [2,3; 3,4]
$^2J_{\text{PP}}$ (Hz)	54 [1,3] 6 [1,4] 64 [2,4] -18 [2,5] 21 [3,5]	28 [1,3; 1,4] 79 [2,4; 3,5] -24 [2,5]	18 [1,3]
Spin system	AGHMX	AA'BB'X	AM ₂ X
T (K)	298	298	300
Solvent	CH ₂ Cl ₂	CHCl ₃	CH ₂ Cl ₂

^a Numbers in square brackets indicate the phosphorus atoms, as labeled above. Bold values indicate parameters involving the phosphonium centre. All parameters were derived by iterative fitting of experimental data at 101.3 MHz.



Scheme 3.6. Reductive coupling of [**3.2**][GaCl₄] to yield [**3.8'**][GaCl₄], for R = Ph, Et.

Reaction mixtures of **3.2(Ph)** with SbPh₃ initially yield only PhPCl₂ and **3.8'(Ph)**, as observed using ³¹P{¹H} NMR spectroscopy. NMR observation of the gradual generation of **3.8(Ph)** the reaction solution (Figure 3.11) suggest conversion between **3.8'(Ph)** and **3.8(Ph)** by slow Ph/Cl substituent exchange (*t*_{1/2} ≅ 6-7 days) between phosphorus and antimony. Substituent exchange behaviour, although uncommon for phosphorus, is well-known for antimony.^{148,149} In this instance, exchange appeared to be facilitated by GaCl₃, as substantiated by the immediate observation (³¹P NMR) of a 1:1 mixture of [**3.8'(Ph)**][GaCl₄] and [**3.8(Ph)**][GaCl₄] when PhPCl₂ was added to a 1:1 mixture of SbPh₃/GaCl₃, as well as the generation of **3.1(Ph)** from **3.2(Ph)** under the same conditions.

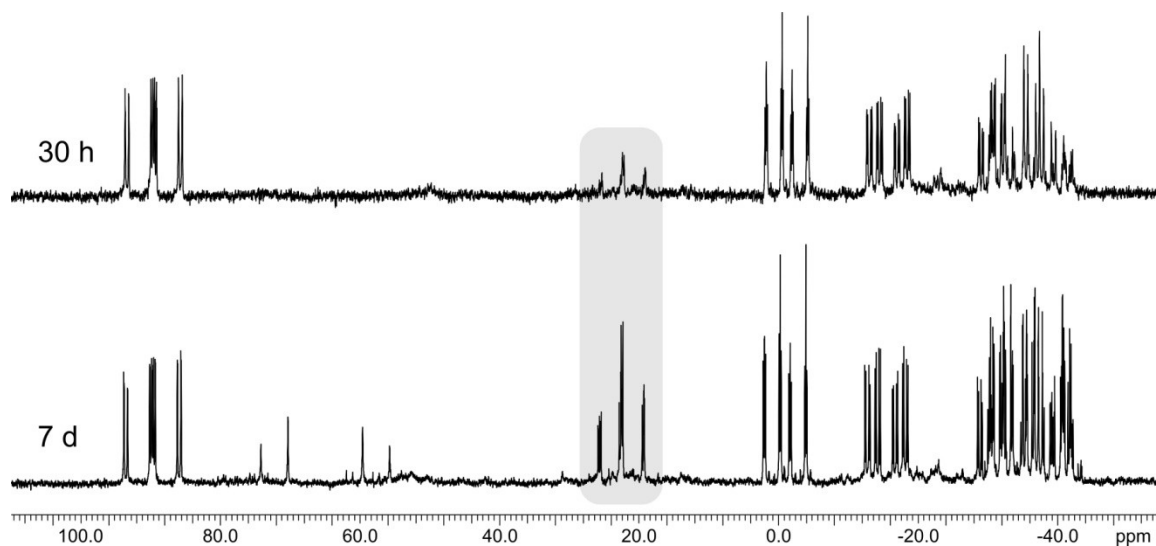
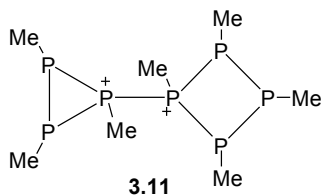


Figure 3.11. $^{31}\text{P}\{^1\text{H}\}$ NMR solution spectrum of the reaction of $[\mathbf{3.2}(\text{Ph})][\text{GaCl}_4]$ with SbPh_3 after 30 h (top) and 7 days (bottom) at 101.3 MHz, indicating the decomposition of $[\mathbf{3.8}'(\text{Ph})][\text{GaCl}_4]$ to $[\mathbf{3.8}(\text{Ph})][\text{GaCl}_4]$. $t_{1/2}$ was estimated by integration of the well-separated phosphonium resonances in $[\mathbf{3.8}(\text{Ph})][\text{GaCl}_4]$ (*shaded*) vs. $[\mathbf{3.8}'(\text{Ph})][\text{GaCl}_4]$. PhPCl_2 (162 ppm, not shown) was also present in solution.

While reduction of $[\mathbf{3.2}(\text{Ph})][\text{GaCl}_4]$ or $[\mathbf{3.2}(\text{Et})][\text{GaCl}_4]$ initially produced the *cyclo*-tetraphosphinochlorophosphonium cation $\mathbf{3.8}'$ as the sole catenated product, the product immediately resulting from the identical reaction of the methyl derivative $[\mathbf{3.2}(\text{Me})][\text{GaCl}_4]$ remains to be conclusively identified. In addition to the production of MePCl_2 , a white powder was generated upon addition of SbR_3 . Redissolution of this solid in MeCN yields the $^{31}\text{P}\{^1\text{H}\}$ NMR COSY spectrum indicated in Figure 3.12, indicating at least six distinct phosphorus environments. This data also supports the proposal that the product is no longer chloro-substituted, as more downfield shifted resonances would be expected for the phosphonium site.

$^1\text{H}\{^{31}\text{P}\}$ NMR data indicates seven distinct signals of equal integration, corresponding to seven distinct methyl environments and suggesting either a single product or a 1:1 mixture of a three-membered and four-membered monocationic rings which display

overlapping signals in the ^{31}P NMR in the region at 45 ppm. In addition, a broad resonance at 2.09 ppm in $^1\text{H}\{^{31}\text{P}\}$ NMR spectrum suggests dynamic behaviour in solution. $^{31}\text{P}\{^1\text{H}\}$ NMR spectra at 202.6 MHz were too substantially line-broadened at 298 K to readily distinguish between these two proposed compositions, but spectra at 101.3 MHz clearly indicate additional small J_{PP} coupling parameters that would not exist in separated three- and four-membered systems. Although this complex spin system has not yet been successfully simulated, the structure is tentatively proposed as the polycyclic dication **3.11**.



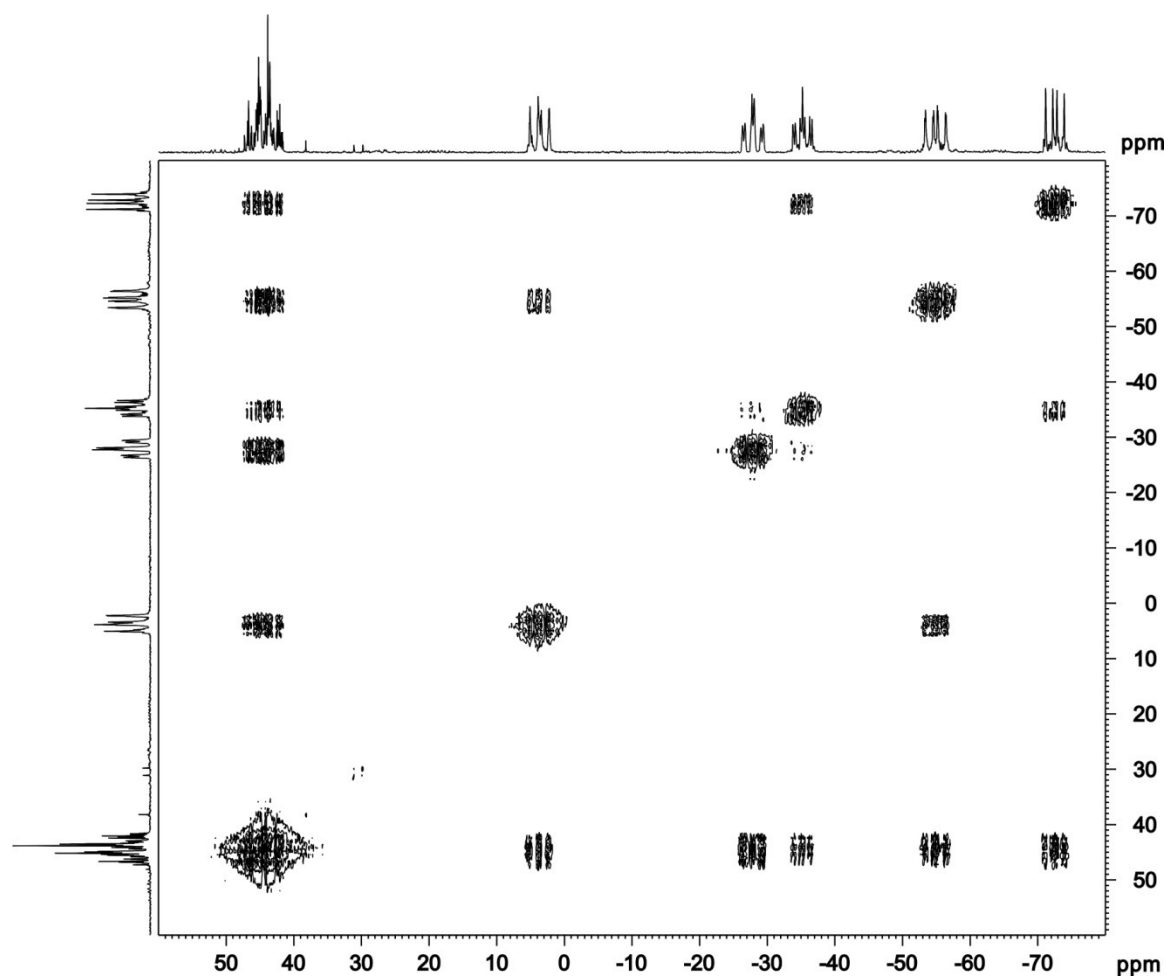


Figure 3.12. $^{31}\text{P}\{^1\text{H}\}$ COSY NMR spectrum of the MeCN-soluble product(s) resulting from the reductive coupling of $[\text{Me}(\text{Cl})_2\text{P}-\text{PMeCl}]$, $[\mathbf{3.2}(\text{Me})][\text{GaCl}_4]$.

3.6 Summary

The synthesis and characterization of the first chlorophosphinochlorophosphonium **3.1** and chlorophosphinodichlorophosphonium **3.2** cations has been shown to provide new synthons for the assembly of larger cationic polyphosphorus frameworks via reductive coupling. ^{31}P NMR studies of reactions with stibine reducing agents have been used to elucidate the dependence of product distribution on stoichiometry and reductant strength. These reactions were shown to readily produce a variety of new and known acyclic and cyclic frameworks, including three new chloro-functionalized cations, highlighted in

Chart 3.2. The first *cis*-substituted derivative of the cyclo-triphosphino-1,3-diphosponium framework [3.9(Ph₂/Me)][GaCl₄]₂ has been observed by ³¹P NMR spectroscopy, and the solution dynamics of this class of class have been analyzed in the context of the variable temperature solution spectra and the solid state crystallographic data for [3.9(ⁱPr)][GaCl₄]₂.

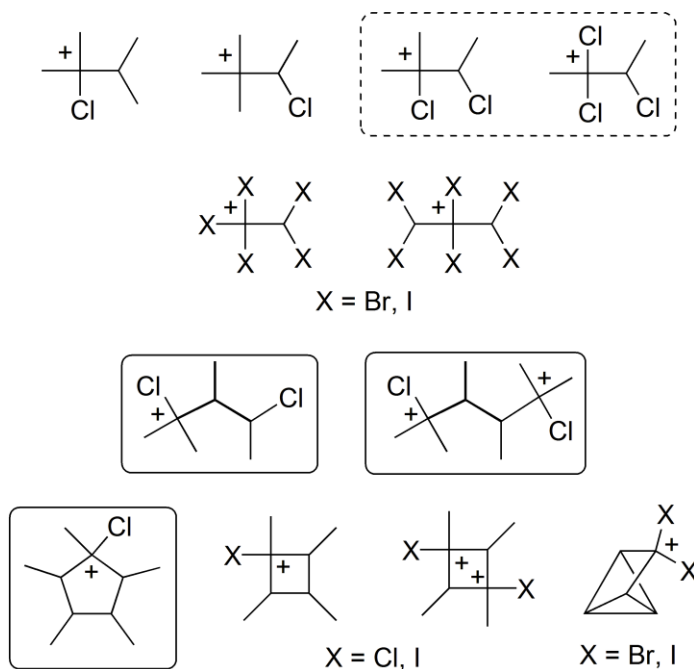
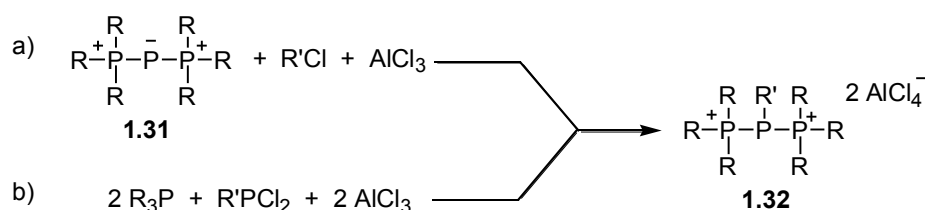


Chart 3.3. Framework drawings of halide-functionalized *catena*-phosphinophosponium cations. Vertices represent phosphorus atoms. The first derivatives of frameworks in boxes are reported here as products of the reductive coupling of the phosphinophosponium cations in the dotted box.

Chapter 4. Acyclic 2-Phosphino-1,3-diphosphonium Cations

4.1 Introduction

Two synthetic pathways to 2-phosphino-1,3-diphosphonium frameworks **1.32** are known in the literature – alkylation of a triphosphenium monocation, or direct synthesis from the component phosphine, dichlorophosphine and halide abstractor (Scheme 4.1). Developed initially in 1985 by Schmidpeter and coworkers,⁶³ both routes have found substantial use in the preparation of derivatives of this framework with a diverse selection of substituents. Surprisingly, however, the number of acyclic derivatives remains limited to those originally reported by Schmidpeter, and only one of these has been structurally characterized.



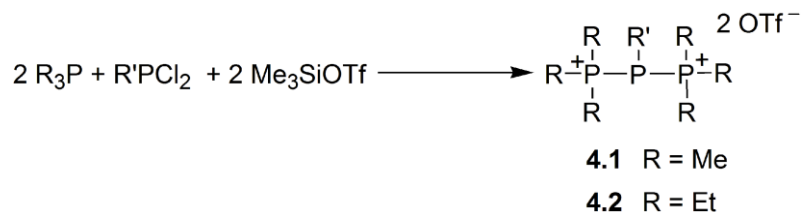
Scheme 4.1. Possible synthetic routes to acyclic 2-phosphino-1,3-diphosphonium dications

Of the two known synthetic pathways, direct synthesis (Scheme 4.1b) has proven to be the more versatile, allowing a greater variety of substituents at the central phosphine, and avoiding the unnecessary additional step of synthesizing the required triphosphenium precursor salt. Furthermore, a one-pot synthesis eliminates the challenge of selecting matched reagents for both the reductive coupling and alkylation, thereby avoiding mixed anion systems which are challenging to crystallize. In the context of this thesis, the route outlined in Scheme 4.1b can be considered to occur in two mechanistic steps – initial

formation of a chlorophosphinophosphonium cation $[\text{Me}_3\text{P-PRCl}]^+$ **2.1'(R)**, followed by a second halide abstraction and donor phosphine coordination. The question therefore arises as to why reductive coupling to a P_4 dication occurs in the situations outlined in Chapter 2, when both P_4 (**2.2**) and P_3 (**1.32**) dicationic products originate from the same reagents. To investigate the factors involved in these two reaction pathways, a series of new 2-phosphino-1,3-diphosphonium triflate salts are reported here, and the stoichiometric and substituent effects on the reaction are assessed.

4.2 Synthesis and ^{31}P NMR Spectroscopy

Given the successful synthesis and solid-state structural characterization of numerous 2,3-diphosphino-1,4-diphosphonium triflates and the nearly exclusive[‡] use of AlCl_3 as a halide abstractor amongst known direct syntheses of the title compound, it was of interest to explore instead the use of Me_3SiOTf as an alternative halide abstractor.



Scheme 4.2. Direct reaction of a trialkylphosphine (R = Me, Et) with a variety of dichlorophosphines and Me_3SiOTf to generate 2-phosphino-1,3-diphosphonium triflate salts. Substituents at R' are indicated in brackets in the text.

[‡] Five cyclic 2-phosphino-1,3-diphosphonium cations have been synthesized directly using SnCl_2 as a halide abstractor, and one of these has been crystallographically characterized.¹⁵⁰ To put this quantity into context, 26 cyclic derivatives directly prepared using AlCl_3 were published in the same manuscript by Dillon and coworkers, in addition to the previously known 12 tetrachloroaluminate salts.⁶³

Addition of two equivalents of a trialkylphosphine (R = Me, Et) with a variety of dichlorophosphines and Me₃SiOTf in CH₂Cl₂ resulted in the immediate formation of a white precipitate, identified in most cases as the corresponding 2-phosphino-1,3-diphosphonium triflate salt (**4.1** or **4.2**). If the reaction was instead conducted in MeCN, all products of the reaction remained in solution, thus allowing the progress of the reaction to be monitored *in situ*. For most derivatives of **4.1**[OTf], the reaction proceeded to completion (defined as the consumption of both starting phosphines as observed by ³¹P NMR spectroscopy) within 1 h at room temperature. Nearly quantitative conversion to the desired product was observed for **4.1**(ⁱPr), **4.1**(Cy), **4.1**(^tBu), **4.1**(NⁱPr₂), and **4.2**(ⁱPr), while the remaining reactions resulted in a mixture of products including the desired dication. The product distributions in these reactions are discussed in more detail in Section 4.4, and the ³¹P{¹H} NMR parameters for all derivatives are listed in Table 4.1.

The reaction of MePCl₂ was noteworthy as ³¹P{¹H} NMR spectra of the reaction solution displayed only broad, unresolved resonances, suggesting a dynamic equilibrium between either multiple species or conformers in solution. However, the solid isolated from this reaction by either removal of MeCN *in vacuo* or vapour diffusion of Et₂O was determined to be exclusively **4.1**(Me), which displayed sharp ³¹P{¹H} NMR resonances when redissolved in EtCN. This suggests that the line broadening observed NMR spectra of the reaction solution was primarily caused by slow equilibrium redistribution between multiple initially produced species, rather than to solution dynamics of the desired product.

Table 4.1. $^{31}\text{P}\{^1\text{H}\}$ NMR parameters at 101.3 MHz for derivatives of the 2-phosphino-1,3-diphosphonium framework. Coupling constants are derived by iterative fitting of spectra at 298 K and 101.3 MHz.

#	Compound [R ₃ P-PR'-PR ₃][A] ₂			Chemical Shift (ppm)		¹ J _{PP} (Hz)	Spin system	Ref.
	R	R'	A	δ _{PR3}	δ _{PR}			
4.1	Me	OTf	Me	25.0	-62.6	-285 -295	AXX'	
			ⁱ Pr	23.0	-27.3	-305 -325	AXX'	
			Cy	22.7	-30.8	-307 -326	AXX'	<i>a</i>
			^t Bu	22.3	-9.5	-333	AB ₂	
			Ph	24.7	-46.3	-286 -298	AXX'	<i>a</i>
			N ⁱ Pr ₂	19.3	31.2	-350	A ₂ B	<i>a</i>
4.2	Et	OTf	Me	41.7	-74.4	-300 -308	AXX'	<i>a</i>
			ⁱ Pr	42.5	-42.9	-324 -337	AXX'	
			Cy	42.4	-47.1	-326 -338	AXX'	
			Ph	42	-60	--- ^b	AXX'	
			N ⁱ Pr ₂	39.6	22.0	-364	AB ₂	
4.3	Ph	AlCl ₄	H	23	-120	-286 ^c	AX ₂	63
			Me	23	-48	-330 ^c		
			ⁱ Pr	21	-23	-354 ^c		

^a In collaboration with Ryan Tilley and Dane Knackstedt. ^b ¹J_{PP} could not be assessed due to overlap with the ³¹P chemical shifts of the diphosphinodiphosphonium product ^c ¹J_{PP} values were reported as positive by Schmidpeter⁶³ and coworkers. Negative values are reported here solely in accordance with the convention¹⁵¹ used in this thesis as most values in the literature have not been definitively assigned. It should be noted, however, that definitive positive values of ¹J_{PP} are experimentally and theoretically known for anions of the type [XO₂P-PO₂X]^{m-} (X = H, O, F).^{128,151}

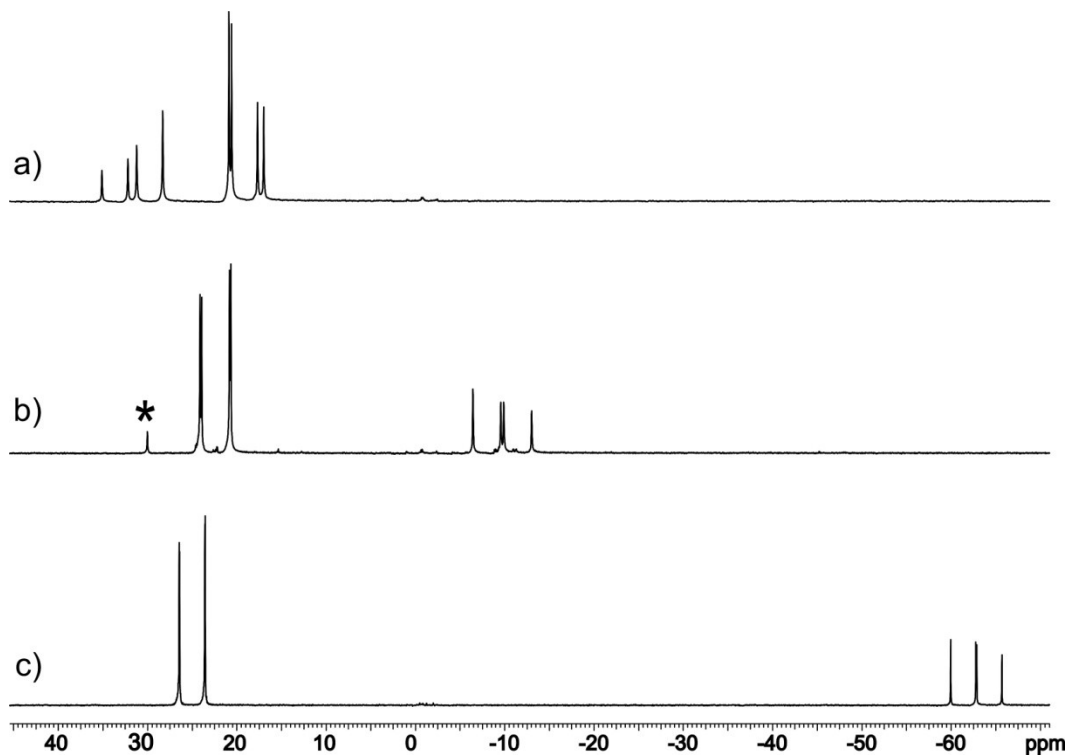


Figure 4.1. $^{31}\text{P}\{^1\text{H}\}$ NMR spectra for selected derivatives of **4.1**, showing the variations in spin system: (a) **4.1**(N^iPr_2), A_2B , (b) **4.1**(^tBu), AB_2 (asterisk indicates a minor impurity), and (c) **4.1**(Me), AXX' .

Comparing the ^{31}P NMR features of the various derivatives, chemical shifts corresponding to the central phosphine span a relatively broad range ($\delta_{\text{PR}} = -63$ to 31 ppm), owing to the geometric flexibility of the three-coordinate phosphorus site, as previously described for 2,3-phosphino-1,4-diphosphonium dications **2.2** (Section 2.4.1). Although the phosphonium chemical shifts (δ_{PR_3}) were observed to be largely independent of the substituent at the central phosphine site, **4.1**(N^iPr_2) was a notable exception, being significantly further upfield relative to the other derivatives of **4.1**. This drastic change can be best rationalized by envisioning these 2-phosphino-1,3-diphosphonium cations according to a dative bonding model, as described for phosphinophosphonium and diphosphinophosphonium cations in Section 1.3. As these cations can be regarded as a dicationic phosphinidinium $[\text{PR}]^{2+}$ fragment, stabilized by

two ligated phosphine donors (Figure 4.2), the strength of the donor-acceptor interaction can be thought to depend on the acceptor strength or Lewis acidity of the phosphinidinium dication. When $R = N^iPr_2$, the amido-substituent stabilizes the cation by π -donation from the lone pair at nitrogen, thereby resulting in lower Lewis acidity. As a result, stabilizing donation of electron density from the adjacent PMe_3 ligands is reduced, and the PMe_3 centres retain greater electronic shielding and a correspondingly upfield-shifted ^{31}P NMR signal. While stabilizing the cation by π -electron donation, the amido-substituent is also expected to be strongly σ -electron withdrawing, as evidenced by the substantial downfield shift of the ^{31}P NMR resonance of the central phosphorus atom in **4.1**(N^iPr_2) relative to the other derivatives of **4.1**. This significant downfield shift, combined with the upfield shift of the phosphonium sites, results in a reversal of the relative peak positions of the two phosphorus environments, and the assignment of this $^{31}P\{^1H\}$ NMR spectrum as the sole A_2B spin system in this series.

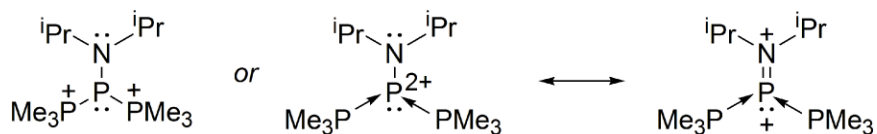


Figure 4.2. Lewis (left) and coordinate (middle) bonding model depictions of **4.1**(N^iPr_2) showing possible resonance contribution of the π -donating amido-substituent.

Coupling constants ($^1J_{PP}$) for all derivatives of **4.1** and **4.2** fall within the range typical for phosphinophosphonium cations and other P(III)-P(V) interactions, and compare well to previously known acyclic⁶³ and cyclic¹⁵⁰ derivatives. Notably, for both **4.1** and **4.2**, it is the N^iPr_2 -substituted derivative that displays the largest magnitude ^{31}P - ^{31}P coupling. This observation is readily rationalized by considering the influence of the electronegativity of

directly bound substituents on ${}^1J_{PP}$. Previous experimental and computational studies^{128,151} suggest that an increase in substituent electronegativity results in a linear increase in the corresponding $|{}^1J_{PP}|$ value due to the increased s-character of the P-P bond. In the series of derivatives of both **4.1**[OTf] and **4.2**[OTf], the amido-substituent was, by far, the most electronegative substituent studied, and consequently, effects the largest magnitude ${}^1J_{PP}$. However, electronic effects alone are expected to be small (*ca.* 5 Hz) when comparing methyl [${}^1J_{PP} = -290$ Hz] to *tert*-butyl [${}^1J_{PP} = -333$ Hz].¹⁵² This steric effect has been previously discussed by McFarlane and McFarlane^{152,153} with reference to the successive replacement of methyl by *tert*-butyl substituents in a series of diphosphines. The authors describe the resulting increase in the magnitude of ${}^1J_{PP}$ as predominantly arising from the increase in hybridization at phosphorus, which is experimentally demonstrated by the substantially larger C-P-C angle enforced by the bulky ^tBu substituent. In concert with this rationale, **4.2**(ⁱPr) and **4.2**(Cy) were observed to also have substantially larger $|{}^1J_{PP}|$ values than the corresponding methyl derivative. Unfortunately, the large difference between the ${}^1J_{AX}$ and ${}^1J_{AX'}$ coupling parameters for **4.1**(ⁱPr) and **4.1**(Cy) exclude them from categorization in this analysis. Analysis of derivatives involving non-alkyl substituents such as NⁱPr₂ and Ph is complicated by the difficulty in distinguishing steric and electronic influences. For NⁱPr₂, the substantial steric bulk reinforces the σ -electron withdrawal described earlier, thereby resulting in the largest magnitude ${}^1J_{PP}$ of the series. For Ph, however, the observed smaller magnitude of ${}^1J_{PP}$ suggests that π -electron withdrawal has limited effect in this situation. Indeed, attempted correlation of ${}^1J_{PP}$ values for either **4.1** or **4.2** with electronic substituent effects as represented by Taft constants (σ^* , predominantly inductive)¹⁵⁴ or Kabachnik's

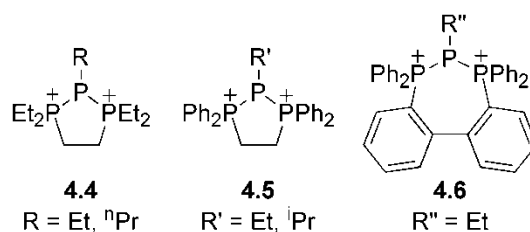
constants (σ^{p} , inductive and mesomeric)¹⁵⁵ was poor, favouring the supposition that geometric constraints imposed by steric effects predominate.

4.3 Solid-state Structures

Three derivatives of the Me₃P donor framework **4.1**[OTf]₂ (R = Cy, ^tBu, NⁱPr₂) have been further characterized by single-crystal X-ray diffraction. Relevant bond lengths and angles are summarized in Table 4.2. As with previously characterized derivatives of this type, the cations in **4.1**(Cy)[OTf]₂, **4.1**(^tBu)[OTf]₂ and **4.1**(NⁱPr₂)[OTf]₂ display significantly longer P-P bonds in the solid state relative to the only structurally characterized¹⁵⁶ parent triphosphenium cation [Ph₃P-P-PPh₃][AlCl₄], **1.31**(Ph) [average: 2.1311(12) Å]. This again supports the single-bond character of the P-P bonds in the dication and the partial double-bond character of the parent monocation.

Besides **4.3**(H)[AlCl₄], the only reported crystallographically characterized derivatives of the 2-phosphino-1,3-diphosphenium framework consist of cyclized derivatives **4.4**[AlCl₄], **4.5**[AlCl₄] and **4.6**[AlCl₄], published by Dillon and coworkers in 2008.¹⁵⁰ However, the geometric parameters of the P-P-P chain in cyclized derivatives are expected to depend primarily on the bite angle enforced by the carbon backbone of the chelating donor ligand. As a consequence, although the P-P-P angles (86-96°) in **4.4-4.6** are significantly smaller than those observed in **4.1**, this comparison is not instructive. Additionally, only limited conclusions may be drawn from these compounds with regards to the influence of the central substituent on the geometry of the resulting compound, owing to the differences in the chelating ligand. The solid-state single crystal characterization of these derivatives of **4.1** presents the first opportunity to assess the

effect of substantial steric bulk at the phosphine on the enforced geometry in the complex.



All three crystallographically characterized derivatives of **4.1**[OTf]₂ (R = ^tBu, Cy, NⁱPr₂) display a smaller P-P-P angle and substantially less pyramidal geometry about the central phosphorus atom (*ca.* 318°) compared with the previously reported acyclic aluminate derivative **4.3(H)** (287°). This is rationalized as a consequence of the substantial steric bulk of the substituents at the central phosphine (P2) in **4.1**, which tends to substantially disfavour the pyramidal structure. If the terminal pseudotetrahedral phosphonium moieties [-PMe₃] can be assumed to approximate the same steric influence as a ^tBu substituent [-CMe₃], comparison to the neutral phosphine ^tBu₃P offers insight. Indeed, the C-P-C angles in ^tBu₃P have been previously estimated at 105.7°,¹⁵⁷ thereby indicating a comparable geometry about the phosphorus centre (Σ_{angles} = 317°). Otherwise, all three newly characterized derivatives of the 2-phosphino-1,3-diphosphonium framework **vii** (Chart 1.2, Section 1.2.3) possess comparable parameters to one another and to **4.3**[AlCl₄]₂, with any deviations being reasonably attributed to steric influence of the central substituent. In all cases, the preferred conformation in the solid state is one with a methyl group of each phosphonium terminus nearly eclipsing the central substituent (Figure 4.3, right). Presumably this rotational conformation minimizes the number of unfavourable steric interactions between these methyl groups and the sterically crowding phosphine-substituent.

Table 4.2. Selected relevant bond lengths and angles in the solid-state structures of the dications in characterized acyclic 2-phosphino-1,3-phosphonium triflates **4.1**[OTf]₂.

	[Me₃P-PR-PMe₃][OTf]₂, 4.1(R)			[Ph₃P-PH-PPh₃][AlCl₄]₂ 4.3(H)⁶³
	4.1(Cy)	4.1(^tBu)	4.1(NⁱPr₂)^a	
P-P (Å)	2.1979(5) 2.1976(6)	2.2391(15) 2.2354(16)	2.2181(9) <i>to</i> 2.2271(9) [σ = 0.004]	2.205(1) 2.224(1)
P-P-P (°)	103.11(2)	100.97(5)	104.26(3) <i>to</i> 105.48(3) [σ = 0.7]	106.39(4)
P2-E (Å) E = H, C, N	1.8589(16)	1.925(3)	1.655(2) <i>to</i> 1.660(2) [σ = 0.003]	1.13(2)
P1/3-C_{avg}	1.7891(17)	1.810 [1.8095]	1.782(3) <i>to</i> 1.799(2) [σ = 0.005]	---
Σ_{angles} (at P2)	318	317	318 <i>to</i> 319 [σ = 0.7]	287
Close contacts (weak interactions)	---	O _{OTf} ··H _{PMe3} : 2.327(6) <i>and</i> 2.426(3)	H _{PMe3} ···F _{OTf} 2.467(4) ^b	---

^a Asymmetric unit contains three crystallographically independent molecules of [**4.1**(NⁱPr₂)]₂[OTf]₂. Range and standard deviation (σ) of the mean value are given.

^b Only one of the three independent cations in the asymmetric unit displays a close contact with an associate triflate anion.

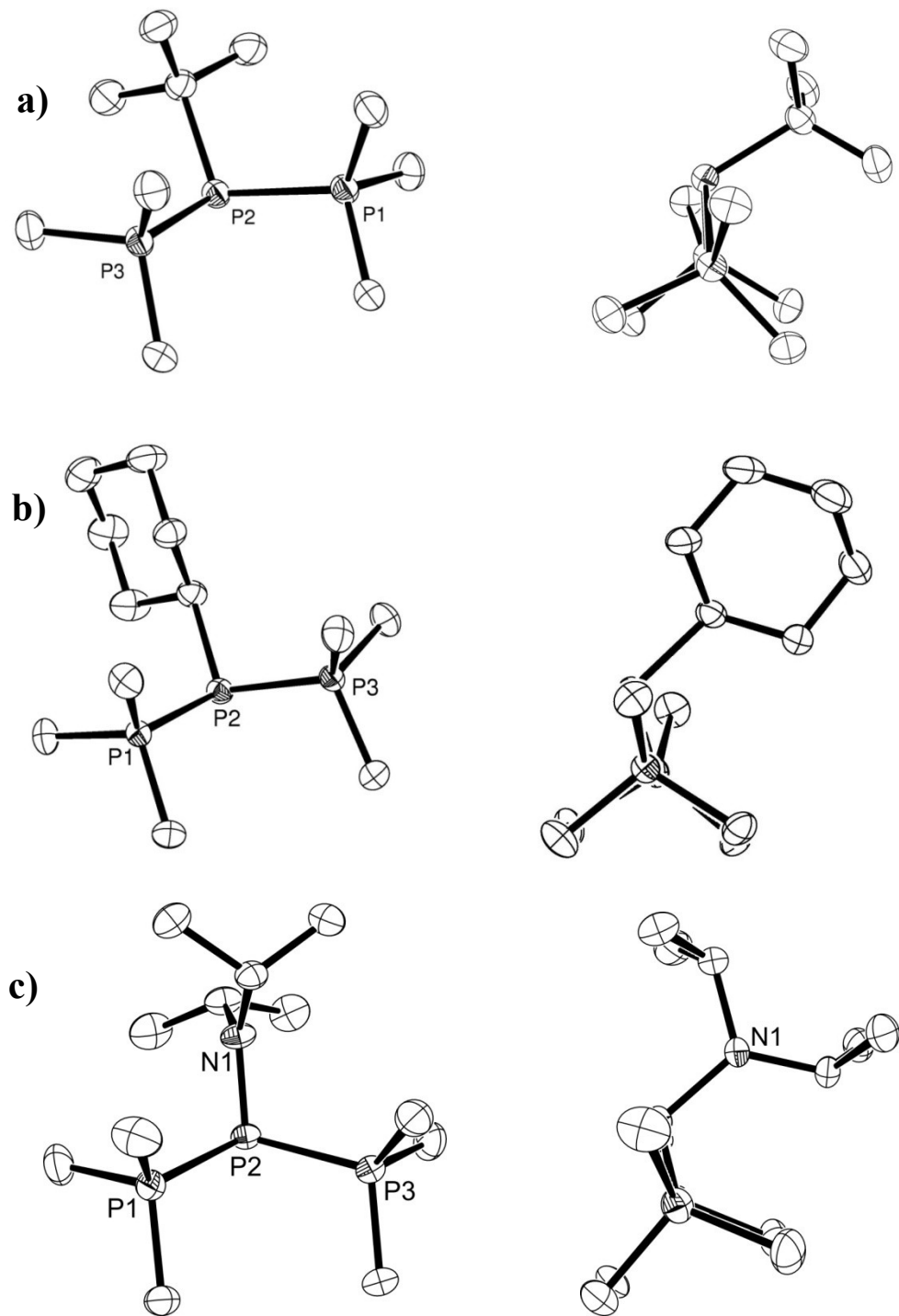


Figure 4.3. ORTEP representations of the solid-state structure of the cation in (a) **4.1(*t*Bu)[OTf]₂** (b) **4.1(Cy)[OTf]₂** and (c) **4.1(*N*ⁱPr₂)[OTf]₂**, from a front and side perspective. Hydrogen atoms are omitted for clarity and thermal ellipsoids shown at the 50% probability level. Unlabelled atoms in the front view are carbon atoms. Relevant parameters are listed in Table 4.2.

The P-N bond length in **4.1(NⁱPr₂)** (average 1.657 Å) is shorter than the idealized N-P σ -only single bond in potassium phosphoramidate, K[H₃N-PO₃] (1.800(4) Å), supporting the previously stated assertion (Section 4.2, Figure 4.2) that this bond exhibits some degree of π -character, although it is still substantially longer than a full double bond (1.54-1.58 Å).¹⁵⁸ Cations **4.1(^tBu)** and **4.1(NⁱPr₂)** possess weak cation-anion contacts in the solid state between the oxygen or fluorine atoms of the triflate counterion and one or more methyl hydrogens of the phosphonium moieties (*e.g.* Figure 4.4), but these distances approach the limiting sum of the van der Waals radii (Σr_{vdw} : OH 2.60 Å; HF 2.55 Å) and should not be considered significant.

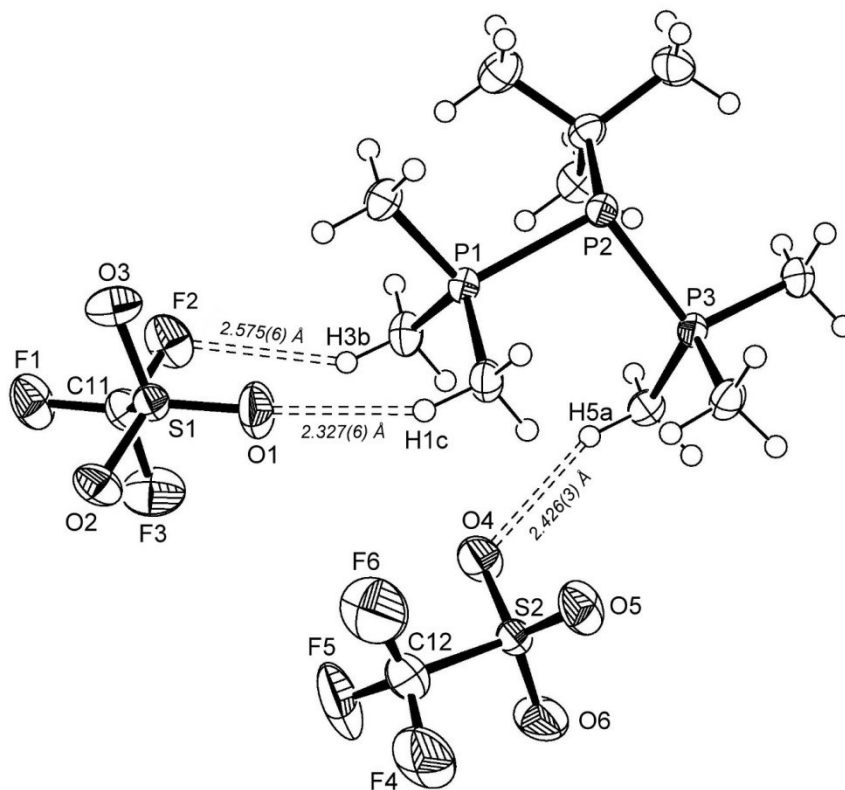


Figure 4.4. ORTEP representation of the solid-state structure of the asymmetric unit in **4.1(^tBu)**[OTf]₂, indicating weak interactions between hydrogen atoms of the cation and the triflate counterions. Non-hydrogen atoms are represented with Gaussian ellipsoids at the 50% probability level, while hydrogen atoms are shown with arbitrarily small thermal parameters.

4.4 Competitive 2,3-Diphosphino-1,4-diphosphonium Synthesis

The synthesis of derivatives of **4.1**[OTf] was generalizable to a variety of central substituents with quantitative conversions observed by ^{31}P NMR spectroscopy except in the case of [**4.1(Ph)**] [OTf] where an inseparable mixture of three-membered (**4.1**) and four-membered dications (**2.2'**, $[\text{Me}_3\text{P-PR-PR-PMe}_3]^{2+}$) was observed. Relative amounts of two dicationic species were concentration dependent, but with the theoretically predicted reaction stoichiometry (Scheme 4.2), dication **2.2'(Ph)** was generally preferred. With only one equivalent of Me_3P present in solution, **2.2'(Ph)** was no longer observed in solution by ^{31}P NMR; however, the scarcity of Me_3P for the generation of **4.1(Ph)** resulted instead in the observation of a mixture of **4.1(Ph)** and the corresponding phosphinophosphonium monocation $[\text{Me}_3\text{P-PPhCl}][\text{OTf}]$, **2.1'(Ph)**.

Reactions of the slightly more sterically hindered trialkylphosphine donor, Et_3P , to generate **4.2**[OTf] also favoured generation of the 4P dication, $[\text{Et}_3\text{P-PPh-PPh-PEt}_3][\text{OTf}]$, **4.7(Ph)**. However, ^{31}P NMR of redissolved precipitates from these reactions indicated that a mixture of **4.2** and **4.4** was generated in all cases except where $\text{R} = \text{N}^i\text{Pr}_2$, for which the reaction remained incomplete. Simulated $^{31}\text{P}\{^1\text{H}\}$ NMR parameters for these previously unreported 2,3-diphosphino-1,4-diphosphonium triflate salts are listed in Table 4.3.

The *in situ* formation of both 3P and 4P dications, regardless of reaction stoichiometry, has been previously noted by Dillon and coworkers⁸² for reactions involving biphep (2,2'-bis(diphenylphosphino)-1,1'-biphenyl) or dppe with EtPCl_2 in the presence of SnCl_2 . No reasons have been previously given for the relative preference for either the 3P

or 4P product in these systems; however, the expanded series of acyclic triflates reported herein may offer some insight.

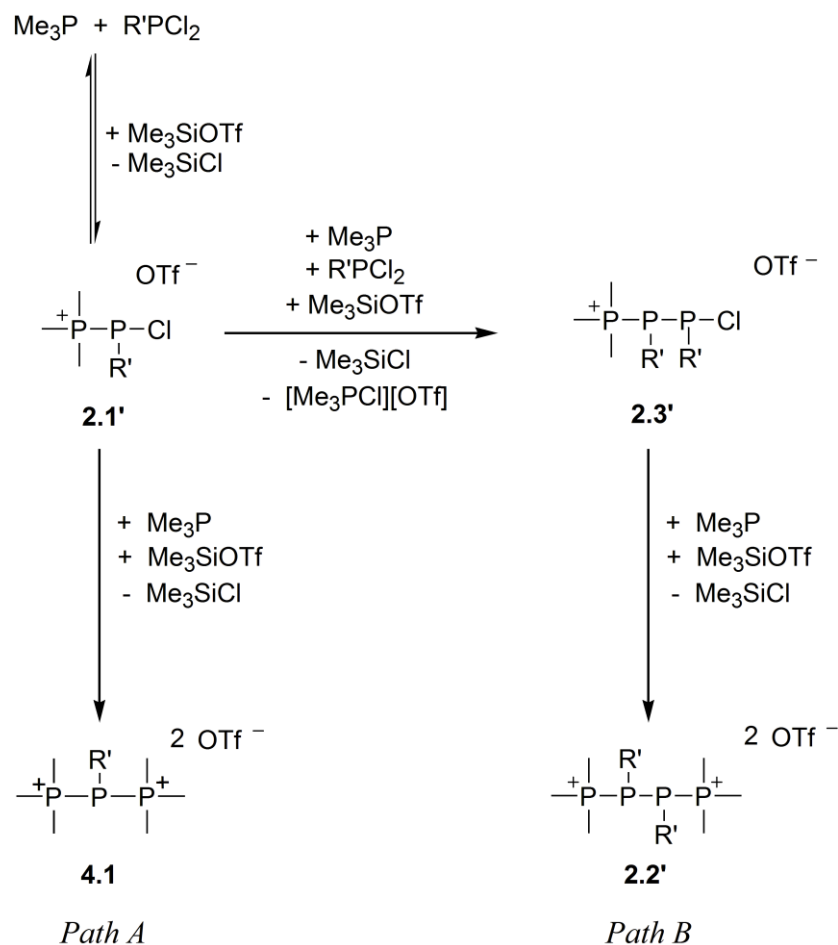
Studies of the phosphinophosphonium species **2.1'** (Chapter 2) suggest that these cations were formed immediately (< 5 min) upon combination of the reagents, implying that they are likely intermediates en route to either end product (Scheme 4.3). Formation of the 4P dication (Path B) requires subsequent reductive coupling to generate the three-membered monocationic intermediate **2.3** (Section 2.3), which necessitates the *in situ* dissociation of **2.1'**. Thus, phosphinophosphonium cations which dissociate more readily in solution favour the generation of the 4P dication.

Table 4.3. $^{31}\text{P}\{^1\text{H}\}$ NMR parameters at 101.3 MHz for previously unreported 2,3-diphosphino-1,4-diphosphonium triflate salts observed in MeCN during the attempted synthesis of 2-phosphino-1,3-diphosphonium species. Chemical shifts (δ) are reported in ppm and coupling constants (J) in Hz.



	R_3P	PR'	δ_A	δ_B	$^1\text{J}_{\text{AA}'}$	$^1\text{J}_{\text{AB}} = ^1\text{J}_{\text{A'B}'}$	$^2\text{J}_{\text{A'B}} = ^2\text{J}_{\text{AB}'}$	$^3\text{J}_{\text{BB}'}$
4.7(Me)	Et_3P	Me	-82	40	-265	-278	59	49
4.7(Cy)		Cy	-56	38	-322	-320	72	48
4.7(Ph)		Ph	-55	39	<i>not determined due to overlapping signals^a</i>			

^a All spectra are AA'BB' spin systems, with coupling constants derived by iterative fitting of experimental data at 298 K where possible. Coupling constants were not determined in cases with substantial overlap with other products.



Scheme 4.3. Possible reaction pathways resulting in the generation of either a three- or four-phosphorus dication.

Observation of $^1J_{\text{PP}}$ coupling in ^{31}P NMR spectra of room temperature solutions of $[\text{AlCl}_4]^-$ and $[\text{GaCl}_4]^-$ derivatives of **2.1** and **2.1'** (Section 2.2) implies minimal dissociation of the P-P bond on an NMR timescale, which, in turn, rationalizes the observation of the 3P derivative as the sole product in Ph_3P reactions with $\text{R}'\text{PCl}_2$ and AlCl_3 (Path A).⁶³ Triflate derivatives of **2.1** show no ^{31}P - ^{31}P coupling at room temperature, making them viable candidates for solution dissociation and subsequent reduction. With respect to the intermediate **2.1' (Ph)**, the poor Lewis acidity of $[\text{PPhCl}]^+$ (demonstrated experimentally in phosphonium exchange studies, Section 2.2.1) would

lead to higher solution dissociation, thereby provide validation for the observation of mixtures of both 3P and 4P products. Finally, the empirically observed reduced solubility of Me₃P derivatives of both 2P and 3P frameworks may also contribute to the isolation of strictly **4.1** as a product, as precipitation of this product from the solution prevents its re-dissociation and availability for reductive coupling.

4.5 Summary

A series of new acyclic 2-phosphino-1,3-diphosphonium triflates have been isolated and characterized by X-ray crystallography. Additional derivatives of this framework were compared with respect to their ³¹P NMR parameters, which have been interpreted in the context of the geometry at the phosphine site. The influence of donor strength, halide abstractor, and central substituent have been assessed in terms of their impact on the competition between reactions yielding three-membered or four-membered acyclic dications from chlorophosphinophosphonium cations.

Chapter 5. Electrochemistry of Phosphinophosphonium Cations

5.1 Introduction

Whereas synthetic methods are often more practical for the large-scale isolation of new compounds, electrochemical techniques offer investigative avenues in electron-transfer reactions that might not be readily available through the use of chemical redox agents. In particular, electrochemical synthesis offers a wide range of precisely controlled potentials for the oxidation or reduction of chemical compounds, whereas chemical redox agents each only offer a single fixed potential.¹⁵⁹ More relevant to this thesis, however, electrochemical studies offer unparalleled opportunities for investigation into the mechanisms of electron transfer reactions.¹⁵⁹⁻¹⁶²

The known electrochemistry of phosphorus-containing species is primarily limited to monophosphines and phosphonium salts. Triphenylphosphine is perhaps the most thoroughly studied of these, although the literature regarding its electrochemical behaviour is not without controversy.¹⁶³ The present consensus, however, seems to state that Ph_3P undergoes a single irreversible oxidation in MeCN, followed by rapid chemical reaction of the resulting radical cation $[\text{Ph}_3\text{P}]^{\bullet+}$.¹⁶⁴⁻¹⁶⁷ In solutions with trace amounts of water, the oxidation products have been assigned to either $[\text{Ph}_3\text{PH}]^+$ or $\text{Ph}_3\text{P}=\text{O}$ using cyclic voltammetry.^{164,166} In contrast, the oxidation of sterically hindered triarylphosphines using pulse voltammetry has permitted the characterization of comparatively long-lived radical cations, observable by ESR.¹⁶⁷ The authors of this work were likewise able to relate the anodic peak potentials of isosteric triarylphosphines to the Hammett substituent parameters (σ^+),¹⁶⁷ extending previous work that correlated the

oxidation potentials of diphosphines with electronic substituent effects, as represented by Taft's polar substituent constant (σ^*).¹⁶⁵

The electroreduction of triphenylphosphine is also well-known, and is seemingly less controversial. Santhanam and Bard reported that Ph_3P undergoes a reversible one-electron reduction in DMF ($E_{1/2} = -2.7 \text{ V vs. SCE}$) for sweep rates down to 67 mV/s, but only an irreversible reduction in MeCN.¹⁶⁸ As the product of the reduction was insufficiently long-lived to observe using ESR, the authors proposed that the initial electroreduction product was the unstable anion radical $[\text{Ph}_3\text{P}]^{\bullet-}$. Immediate solution decomposition was proposed via loss of a phenyl radical, which was subsequently observed in the form of a stable biphenyl byproduct of the reaction. Saveant and Binh additionally proposed that the anion radical reacts with the supporting electrolyte $[\text{nBu}_4\text{N}]\text{I}$ or $[\text{nBu}_4\text{N}][\text{BF}_4]$ to catalytically generate tributylamine, among other products.¹⁶⁹ Similarly, the chlorophosphines Ph_2PCl and PhPCl_2 have been reduced by loss of chloride to their corresponding radicals at -3.4 V and -2.8 V vs. Ag/Ag^+ , respectively.¹⁷⁰ However, the lifetime of these radicals was estimated at less than 10 ms, prior to hydrogen abstraction from the solvent medium (glyme), and only Ph_2PH and PhPH_2 were obtained nearly quantitatively from the controlled potential electrolysis.¹⁷⁰

Very little is known about the electrochemistry of other polyphosphines. Various researchers have recently investigated the cyclic voltammetry of diphosphenes $\text{RP}=\text{PR}$, demonstrating that these species undergo a single reversible reduction,¹⁷¹⁻¹⁷³ which in the presence of sufficient steric bulk (*i.e.* $\text{R} = \text{Tbt} = 2,6\text{-}[(\text{Me}_3\text{Si})_2\text{CH}]_2\text{C}_6\text{H}_3$) permitted the first isolation of a diphosphene anion radical.¹⁷⁴ Much earlier work by Dupont and Mills on the electroreduction of *cyclo*-(PhP)_n and other cyclopolyphosphines suggests that the

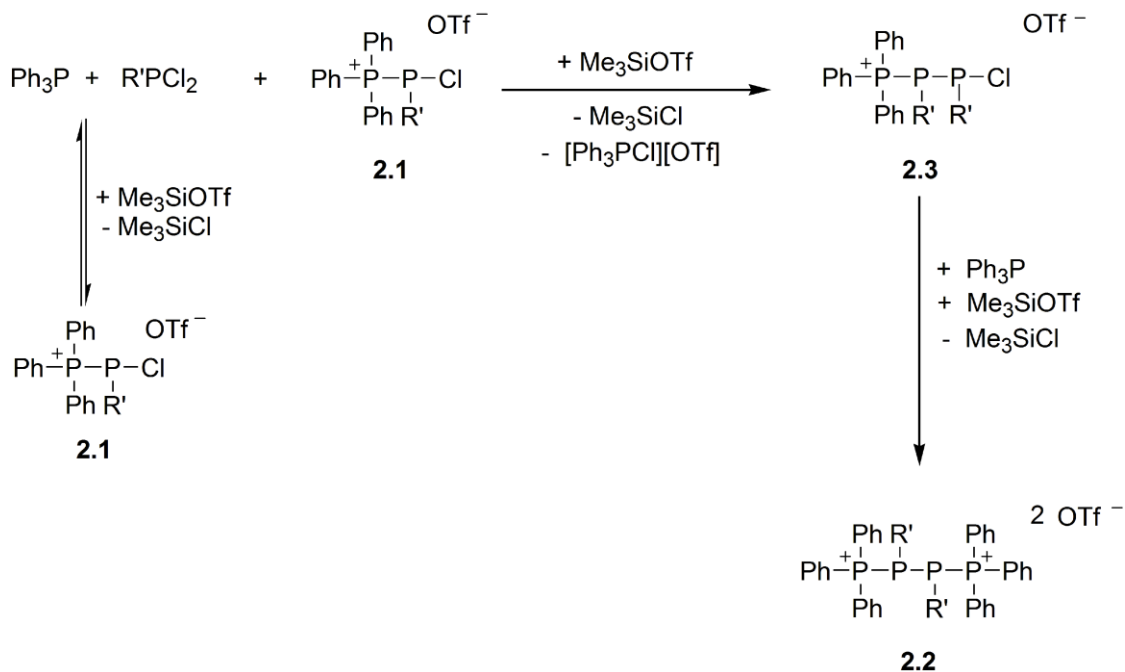
predominant product of these reductions was the linear trimeric dianion $[(\text{PhP})_3]^{2-}$, $1.8(\text{Ph})_{n=1}$, although the monomeric dianion $[\text{PhP}]^{2-}$ was also proposed as a short-lived intermediate.^{175,176} This work was the first to propose that the product of the potassium metal reduction of *cyclo*-(PhP)₅ was a linear anion, rather than the cyclic trimer previously suggested.¹⁷⁷ Later support for this linear structure in the analysis of well-resolved ³¹P NMR spectra offers an indication of the substantial information that electrochemical methods can provide on intermediates and poorly defined or unisolable species in solution.¹⁷⁸ Furthermore, comparisons between various cyclopolyphosphines demonstrated that substituent effects (represented by Taft constants, σ^*) play a more significant role in the determination of reduction potentials than does the ring size of the polyphosphine in question.^{176,179}

Available literature regarding the electrochemical behaviour of cationic phosphorus is limited almost entirely to studies of monophosphonium salts with a variety of substituents, predominantly in aqueous media. In the majority of cases, electrochemical reduction of $[\text{R}_4\text{P}]^+$ was irreversible, as the neutral radicals rapidly undergo P-C bond fission and substituent-loss to generate stable phosphines R_3P . In aprotic media, however, several phosphonium centres with more substantial conjugation of the phosphorus centre into the carbon π -system (*e.g.* 1,4-(R_3P) C_6H_4) yield stable intermediate observable by EPR spectroscopy.¹⁸⁰ The majority of phosphonium salts showed multiple peaks upon reduction, and although proposals have been made in the literature, the identity of these peaks remains unclear.¹⁸¹ Despite this challenge, however, correlation between substituent effects and the reduction potentials of methyltriarylphosphonium salts has been made, in line with similar observations in neutral phosphines (*vide supra*).¹⁸²

While the primary utility of electrochemical analysis lies in its unique capacity to obtain mechanistic information, electrochemical synthesis in phosphorus chemistry is nonetheless an active discipline. As described earlier, the oxidation of triphenylphosphine is expected to generate the cation radical $[\text{Ph}_3\text{P}]^{\bullet+}$; in the absence of water, this reactive species has been shown to act as an effective electrophile in a variety of organic syntheses, including insertion into alkenes, reaction with allylic silanes, and even addition to enol ethers to yield precursors to new Wittig reagents.¹⁸³⁻¹⁸⁵ More interestingly, with the scrupulous exclusion of other potential nucleophiles from the solution medium, the radical cation $[\text{R}_3\text{P}]^{\bullet+}$ (R = alkyl, amido) was found to react with the neutral phosphine itself and undergo a second electrochemical oxidation to the first known diphosphonium dications $[\text{R}_3\text{P-PR}_3]^{2+}$ **1.33**.^{186,187} While chemical alkylation is now known as an alternative route to this framework,⁶⁰ it should be noted that preparative electrochemistry yielded a diverse selection of diphosphonium dications in >80% yields more than ten years earlier.^{186,187} Most recently, electrochemical activation of white phosphorus P_4 has been investigated as a mild, high-yielding route to P-O, P-C and P-N functionalized phosphorus acids.¹⁸⁸

In the context of this work, however, the focus lies primarily in assessing the electrochemistry of the *catena*-phosphorus cations described earlier in this thesis. In particular, since chemical reduction pathways to catenated species have been studied herein (Chapters 2 and 3), it was of interest to determine if electrochemical reduction would yield similar products or provide mechanistic insight into the shorter lived intermediates of the reduction. To this end, the primary target for electrochemical study was the chlorophosphinophosphonium salt $[\text{Ph}_3\text{P-PPhCl}][\text{OTf}]$, [**2.1(Ph)**][OTf], as its

chemical reductive coupling (Scheme 5.1) behaviour was straightforward and readily reproducible under diverse conditions.



Scheme 5.1. Proposed mechanism for the reductive coupling of [2.1][OTf] to [2.2][OTf]₂. Intermediate [2.3][OTf]₂ has been observed by ³¹P{¹H} NMR spectroscopy for sterically encumbered derivatives (R' = ^tPr, Cy, ^tBu). See also, Chapter 2.

5.2 Electrochemistry of [Ph₃P-PPhCl][OTf], [2.1(Ph)][OTf]

Initial experiments using cyclic voltammetry suggested that the electrochemical behaviour of [2.1(Ph)][OTf] is significantly different from the chemical reductive coupling reaction previously described (Scheme 5.1). The features of a typical cyclic voltammogram of a 2.00 mM solution of [2.1(Ph)][OTf] are indicated in Figure 5.1, along with the corresponding peak labels which will be used throughout the discussion. Two irreversible cathodic peaks (I, II) were observed, along with a partially-reversible wave (III) at -2.16 V ($\Delta E_p \approx 100$ mV at 100 mV/s). Notably, the anodic peak (IV) was observed regardless of the direction of potential sweep, but it displayed significantly

higher peak current when the oxidation was performed on the reverse sweep, after both peaks I and II were traced ($\Delta i_p \approx 1 \mu\text{A}$). Based on this observation, and on reported literature potentials,¹⁶⁴⁻¹⁶⁷ peak IV is tentatively assigned to the oxidation of Ph_3P . A more detailed analysis of this anodic peak follows (Section 5.3).

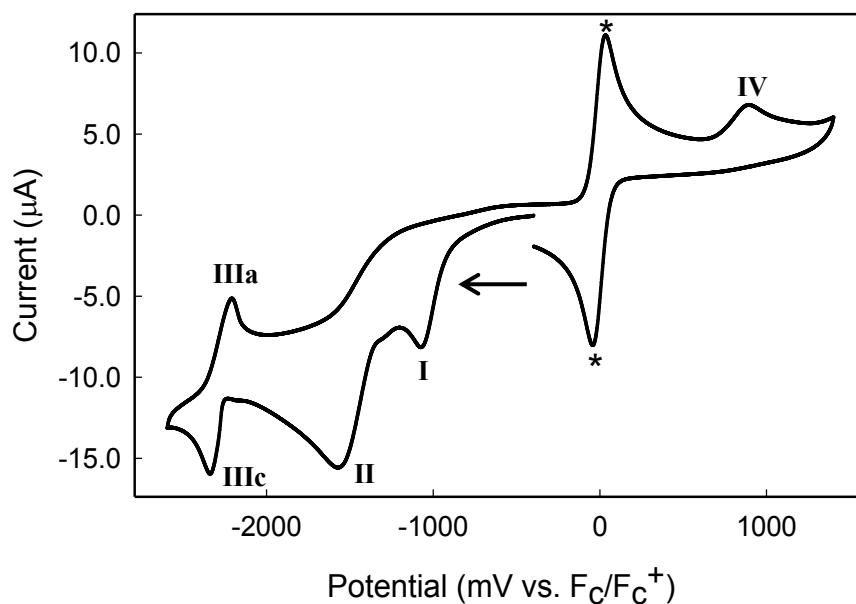


Figure 5.1. Cyclic voltammogram of a 2.00 mM solution of $[\text{Ph}_3\text{P-PPhCl}][\text{OTf}]$, $[\mathbf{2.1}(\text{Ph})][\text{OTf}]$, in 0.1 M $\text{TBAPF}_6/\text{MeCN}$ ($v = 100 \text{ mV/s}$). Potentials are reported relative to the ferrocene redox couple F_c/F_c^+ , marked with an asterisk.

5.2.1 Selection of the Working Electrode

As the primary interest of this project was to investigate the electrochemical reduction of polyphosphorus cations such as $[\mathbf{2.1}(\text{Ph})][\text{OTf}]$, the selection of a working electrode material with a wide reduction window was critical. Of the commonly used working electrode materials for voltammetry, gold was therefore eliminated, having a substantially lower cathodic potential limit in typical organic solvents.¹⁶¹ Previous voltammetric

studies of neutral phosphorus and phosphonium species have generally made use of either Pt or glassy carbon electrodes, so both of these materials were compared with respect to their performance under typical experimental conditions expected for samples in this section (*ca.* 1-2 mM analyte in 0.1 M tetra-*n*-butylammonium hexafluorophosphate (TBAPF₆) in MeCN). Representative voltammograms for Pt and glassy carbon (GC) disc working electrodes are given in Figure 5.1. For solutions of ferrocene (F_c), which was used as an internal standard in most analyses, both working electrodes gave results in good agreement with literature precedent, with a single reversible wave at $E_{1/2} = 90$ mV vs. Ag/Ag⁺ ($\Delta E_p \approx 70$ mV) corresponding to the F_c/F_c⁺ redox couple (Figure 5.1a and b). However, the GC electrode voltammogram was limited to a smaller viable potential window (± 500 mV for both reduction and oxidation) and displayed substantially greater capacitive current. Both of these features proved disadvantageous for the analysis of the desired phosphinophosphonium salt [**2.1(Ph)**][OTf] (Figure 5.1c and d). The smaller potential window of the GC electrode prevented the observation of the partially-reversible redox couple at -2.2 V (peaks **IIIc/IIIa**) and visibly cut off the tail end of the anodic peak at $\sim +0.9$ V. Furthermore, the increased charging current makes the precise measurement of small currents more challenging, and in this case, may entirely obscure the first cathodic wave observed at -1.1 V on the Pt working electrode.

Some concerns have been previously raised in the literature^{166,189} regarding the adsorption of Ph₃P at a Pt electrode in either aqueous HClO₄ and 0.1 M LiClO₄/MeCN. However, as the majority of relevant work in the field of phosphorus electrochemistry has been likewise performed at Pt or glassy carbon surfaces with reasonable success, Pt remains the best electrode for comparison in these preliminary studies. Additionally,

calibration plots of Ph_3P concentration vs. peak current or peak area for concentrations ranging from 0.2 mM to 10 mM were linear.

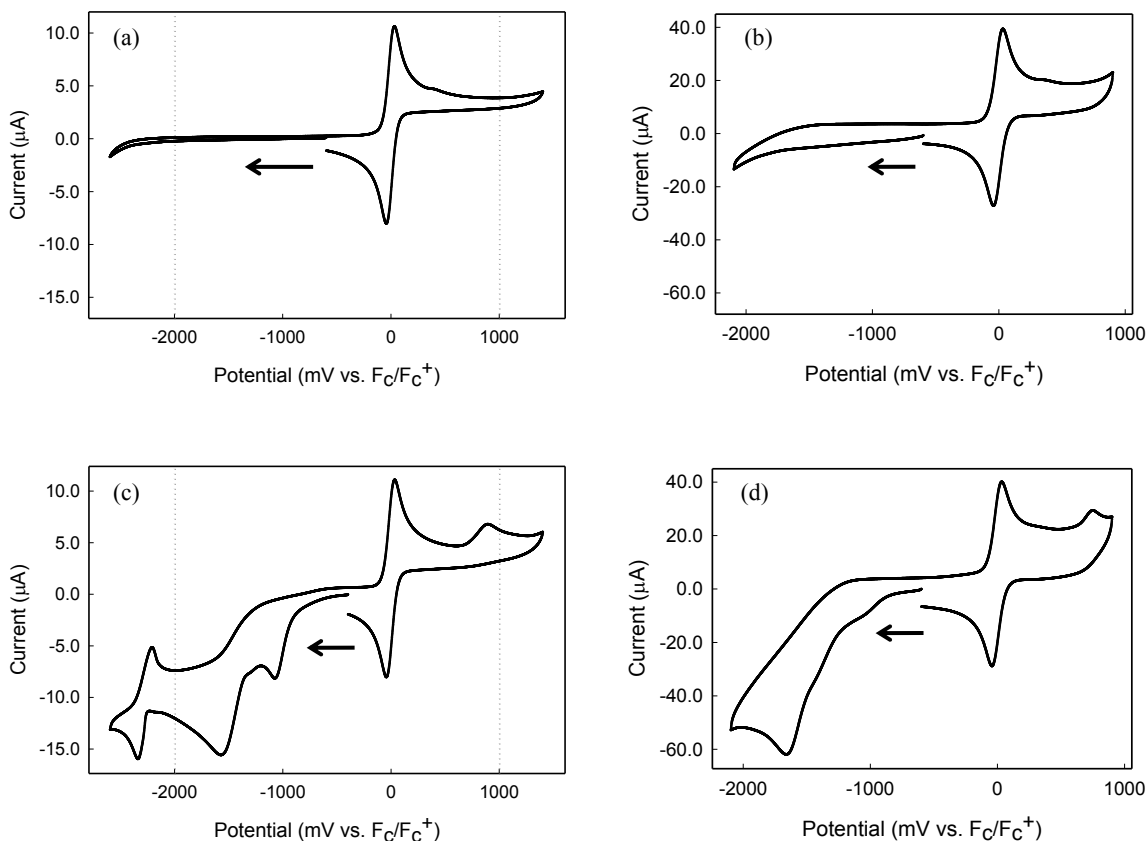


Figure 5.2. Behaviour of platinum disc (Pt, $r = 0.8$ mm) vs. glassy carbon disc (GC, $r = 1.6$ mm) working electrodes. Solutions tested were 1.00 mM Fc on (a) Pt and (b) GC, and 2.00 mM $[\mathbf{2.1}(\text{Ph})][\text{OTf}]/1.00$ mM Fc on (c) Pt and (d) GC. Dotted lines on (a) and (c) indicate the upper and lower redox limits for the glassy-carbon working electrode for comparison.

5.2.2 Sweep Rate Studies

The voltammetric behaviour of a solution of $[\mathbf{2.1}(\text{Ph})][\text{OTf}]$ over a range of sweep rates is shown in Figure 5.3. In contrast to the ideally reversible behaviour of the internal Fc standard (*), all three cathodic waves of $[\mathbf{2.1}(\text{Ph})][\text{OTf}]$ demonstrated substantial shifts to more negative potential with increasing sweep rate. Additionally, at increased sweep

rates, a small peak or shoulder became noticeable at slightly more positive potentials than peak I. Even at sweep rates up to 2 V/s, no reverse peak was observed corresponding to I/II, suggesting perhaps a rapid chemical reaction occurring after the electrochemical reduction. Likewise, no corresponding reduction peak was observed for peak IV. Of the most interest, however, was the behaviour of the partially-reversible coupled peaks IIIc/IIIa at differing sweep rates.

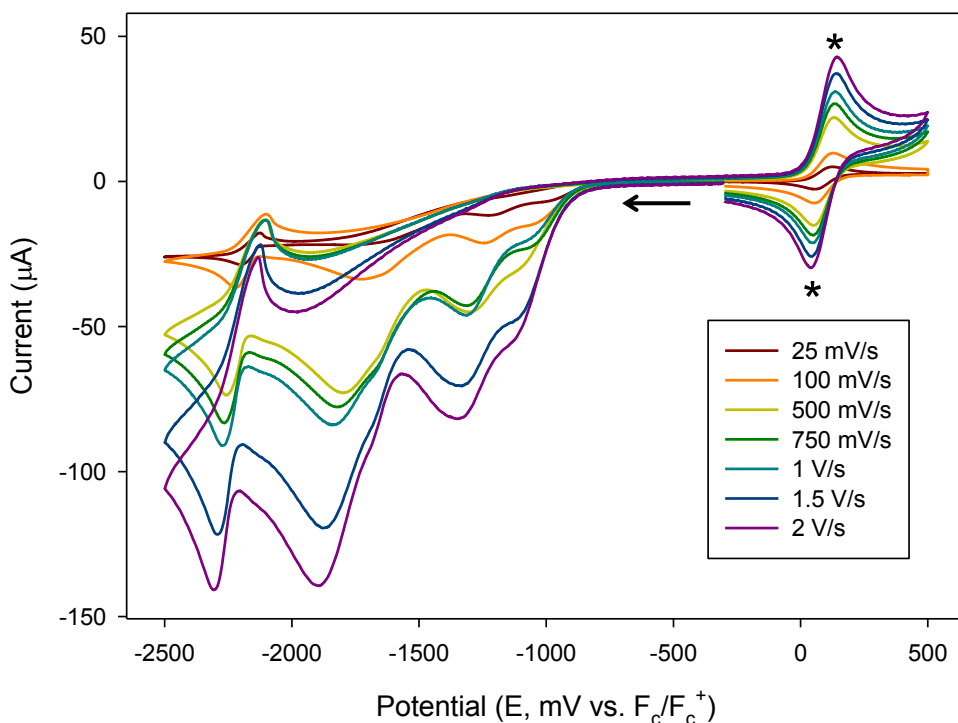


Figure 5.3. Cyclic voltammograms of a 5 mM solution of **[2.1(Ph)]**[OTf] in 0.1 M TBAPF₆/MeCN at varying sweep rates (v). Peaks corresponding to the internal standard (1 mM F_c) are marked with asterisks.

The change in peak potential versus sweep rate for IIIc/IIIa are plotted in Figure 5.4a, indicating increasing peak separation at higher sweep rates. While the peak separations are consistently larger than should be observed for an ideally reversible Nernstian process

(59 mV), the peak may still be considered partially-reversible for sweep rates of up to 100 mV/s, suggesting predominantly diffusion-controlled behaviour.[§] While simple mechanisms involving electron transfer (E) either preceding or following chemical reactions (C) should be straightforward to model according to the kinetic parameters outlined by Nicholson and Shain,¹⁹⁰ the plot of normalized current ($i_{pa}/v^{1/2}$) vs. sweep rate does not match any of the simple CE or EC type mechanisms they describe (Figure 5.4b). However, the partial reversibility of the IIIc/IIIa redox couple, along with the substantial negative shift of the cathodic peak suggests that at least one preceding chemical reaction is involved.

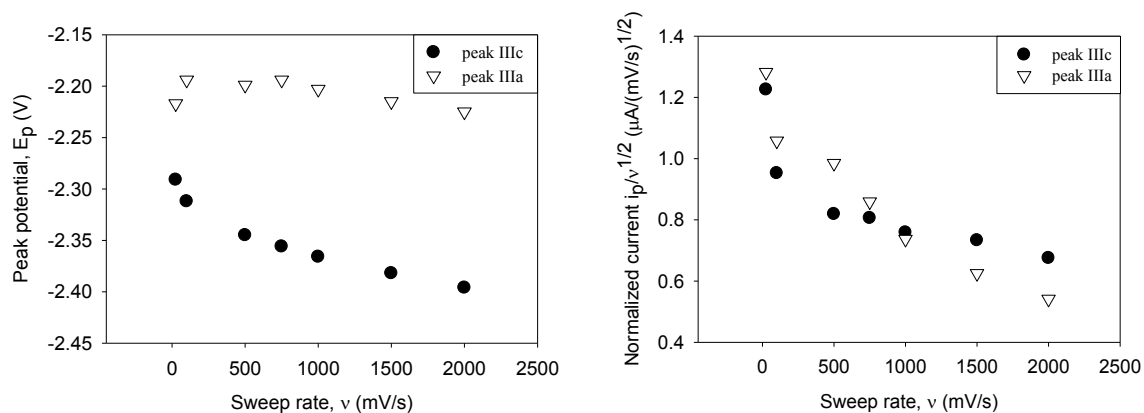
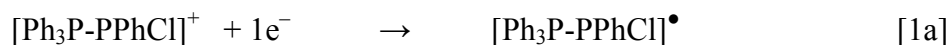


Figure 5.4. Peak potentials (vs. F_c/F_c^+) and normalized current of the partially-reversible voltammetric peaks **IIIc/IIIa** over a range of sweep rates (v) for a 5.00 mM solution of [**2.1(Ph)**][OTf] in 0.1 M TBAPF₆/MeCN.

[§] Notably, the idealized peak separation of 59 mV does not account for uncompensated solution resistance, R_s , which is expected to increase the peak separation (ΔE_p) by a factor of $2 iR_s$. Comparison of ΔE_p for peaks IIIa/c to that of the reversible internal standard, ferrocene, is instructive in this regard. For the F_c/F_c^+ redox couple, ΔE_p ranges from 70 mV (at $v = 25$ mV/s) to 100 mV (at $v = 2$ V/s). The IIIa/c redox couple is, by this standard, reversible at 25 mV/s ($\Delta E_p = 74$ mV) and partially reversible at 100 mV/s ($\Delta E_p = 118$ mV/s), but displays relatively poor reversibility above this sweep rate ($\Delta E_p = 146$ -171 mV).

5.2.3 Proposed Mechanism for Electroreduction

Without substantially greater investigation of the reduction products, any proposed mechanism for the electroreduction of **[2.1(Ph)][OTf]** must be considered speculative. However, based on substantial existing precedents in the reduction of phosphonium cations and chlorophosphines, the following mechanism is proposed.



In an analogous fashion to the one electron reduction of phosphonium, the reduction of **[2.1(Ph)][OTf]** is expected to proceed initially via reduction to the radical (step 1a). Whereas rapid loss of a substituent is expected for tetraarylphosphonium cations,¹⁸⁰⁻¹⁸² the inherently weaker P-P bond in the phosphinophosphonium cation suggests that loss of the phospheniumyl radical $[\text{PPhCl}]^\bullet$ would proceed more rapidly (step 2a).

The second reduction wave (II) was assigned to the one electron reduction of the phosphenium radical (step 3a) and subsequent loss of chloride to yield the transient phosphinidene (step 4a), based on the reduction pathway previously proposed for PhPCl_2 .¹⁷⁰ Notably, this mechanism implies that reduction of $[\text{PPhCl}]^\bullet$ is substantially easier (~ -1.7 V vs. 10 mM Ag/Ag⁺) than the reduction of its PhPCl_2 precursor (-2.5 V vs. 1 mM Ag/Ag⁺).



Following the first two reduction waves, however, the mechanism is more obscure, and four possible pathways [5a-d] are proposed. The observation of a partially-reversible couple IIIc/IIIa allows for the immediate elimination of several possible chemical pathways following the second reduction peak, (II). Hydrogen abstraction from the solvent (path [5a]) seems unlikely, as previous work¹⁷⁰ on the reduction of PhPCl₂ reported no reversible redox chemistry for the resulting PhPH₂. However, it should be noted that the partially-reversible couple IIIc/IIIa consumed significantly less current than the preceding reduction waves I or II, suggesting that the concentration of the redox active species in III was substantially lower than that of the previous steps. This decrease in concentration is more substantial than can be accounted for by diffusion alone, therefore implying oligomerization of the unstable phosphinidene [PPh] generated in step 4, or partial consumption of this species to redox-inactive products, as in [5a].

Oligomerization of the phosphinidene fragment to the most stable *cyclo*-polyphosphine (PPh)₅ seems the most chemically viable option; however, the known irreversibility of electrochemical reduction *cyclo*-(PPh)₅ renders path [5d] unlikely as the reduction of (PhP)₅ in THF has been previously observed to be irreversible.¹⁷⁵

Conversely, neither diphenylphosphene nor the phospho-Wittig type complex $[\text{Ph}_3\text{P}=\text{PPh}]$ proposed in [5b] and [5c] are known to be stable species, as diphosphenes^{171,173,191,192} and phosphine-stabilized phosphinidenes^{122,193,194} generally require substantial steric bulk for their isolation. Cyclic voltammetry of diphosphenes generally shows a reversible reduction between *ca.* -1.7 to -2.0 V *vs.* SCE,¹⁷¹⁻¹⁷⁴ which is compatible with the observed partially-reversible couple IIIc/IIIa. Indeed, the 110 mV peak separation observed in for the reduction of TbtP=PTbt closely mimics the partially-reversible character of the IIIc/IIIa redox couple. However, the absence of any existing evidence for even transient diphosphenes in the absence of steric-protection, as well as the significantly less negative oxidation potential previously reported for the proposed $(\text{PPh})_2^{n-}$ dimer (-1.0 V *vs.* 0.1 M Ag/Ag⁺) tends to disfavour the selection of path [5c].

While it could not be isolated, the sterically-unhindered phosphine-stabilized phosphinidene species $\text{Me}_3\text{P}=\text{P}(\text{CF}_3)$ has been observed in solution.^{195,196} Variable-temperature NMR studies of this species further suggest that the observed solution dynamics may result from coordination of a second equivalent of Me_3P to transiently generate the bis-stabilized phosphinidene adduct $(\text{Me}_3\text{P})_2\text{-P}(\text{CF}_3)$.¹⁹⁷ These observations suggest that sterically unhindered phosphine-phosphinidene species such as proposed in [5b] could exist in solution, even if they are not stable enough to permit isolation.

Electrochemical studies of phospho-Wittig type complexes $\text{R}_3\text{P-PR}'$ are unknown; however, the NHC-adduct of $[\text{PPh}]$ has been characterized and shown to exhibit only an irreversible one electron oxidation in MeCN on Pt (at -0.08 V *vs.* SCE).¹⁹⁸ However, based on both the P-C bond length and the formation of 2:1 BH_3 adducts for NHC-PPh, the bonding in this complex has been previously described as a coordinative (single-

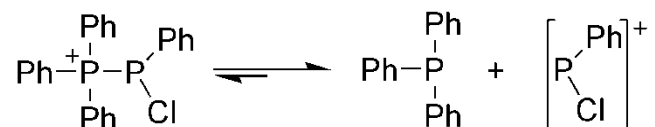
bond) interaction.¹⁹⁸ In contrast, the phospho-Wittig complex Me₃P=PDmp forms only 1:1 adducts with borane, and exhibits a substantially shortened P-P bond in the solid state, in line with a description invoking π -bonding contribution to the bond.¹²² Although no electrochemical data was reported for Me₃P=PDmp, it is structurally more similar to the aforementioned diphosphenes than to the carbene, and might be therefore expected to display similar redox potentials. Therefore, path [5b] is tentatively suggested to be the most viable reaction to precede the IIIc/IIIa redox wave. The product of [5b] might also be generated by an initial two-electron reduction (I) and concomitant loss of Cl⁻, as described in Equations 1b and 2b, leaving peak II to be assigned to the irreversible reduction of this phospho-Wittig type species.



In either case, considerably more work, including preparative scale electrolysis and ³¹P NMR of the resulting products, would be required to substantiate these mechanistic hypotheses.

5.3 Dissociation of [Ph₃P-PPhCl][OTf], [2.1(Ph)][OTf]

As described in the previous section, peak IV, tentatively assigned to free Ph₃P, was observed even before any reduction was attempted on [2.1(Ph)][OTf]. ³¹P NMR spectra of [2.1(Ph)][OTf] (Section 2.2) as well as the previously described mechanism for reductive coupling of [2.1(Ph)][OTf] (Scheme 5.1) suggest that a dissociative equilibrium may exist for phosphinophosponium triflates in solution (Scheme 5.2).



Scheme 5.2. Dissociative equilibrium proposed for **[2.1(Ph)][OTf]** resulting in low concentrations of free Ph_3P in solution.

^{31}P NMR spectra of the reaction of a 0.2 mmol Ph_3P , PhPCl_2 and Me_3SiOTf in 1 mL of 0.1M $\text{TBAPF}_6/\text{MeCN}$ showed slightly broadened peaks for **[2.1(Ph)][OTf]**, relative to the ^{31}P NMR spectra collected in the absence of supporting electrolyte, suggesting that P-P bond dissociation was promoted in a more ionic medium. Attempts to quantify this dissociation were hampered by the difficulty in recording ^{31}P NMR spectra with a sufficiently high molar ratio of TBAPF_6 to **[2.1(Ph)][OTf]** to reflect the electrochemical experimental conditions. Furthermore, substantial ionic strength effects on the local magnetic field experienced in samples with substantial amounts of supporting electrolyte made direct comparison of peak broadening between NMR spectra solely qualitative.

As organic molecules with aryl substituents are well-known to adsorb on Pt electrode, it was proposed that the dissociation of **[2.1(Ph)][OTf]** in the electrochemical cell might be artificially increased. To assess the effect that adsorption of **[2.1(Ph)][OTf]** on Pt might have on its dissociation, the oxidation current for solutions of this analyte were compared with a Pt disc working electrode ($r = 0.8$ mm) versus a Pt wire working electrode (length *ca.* 5 mm). The proportional increase in anodic current and charge as a result of the larger Pt-wire surface area was the same (*ca.* 3.5-3.7 times) for both the internal F_c standard and **[2.1(Ph)][OTf]**. This suggests that despite any potential surface adsorption of either Ph_3P or the phosphinophonium cation, the Pt surface was not responsible for catalyzing the dissociation of the P-P bond.

To quantify the dissociation of Ph₃P from [2.1(Ph)][OTf], calibration curves of current (i_{pa}) and charge (q_{pa}) versus Ph₃P concentration were plotted for both high (0.5 to 10 mM) and low (0.2 to 0.5 mM) concentration ranges.

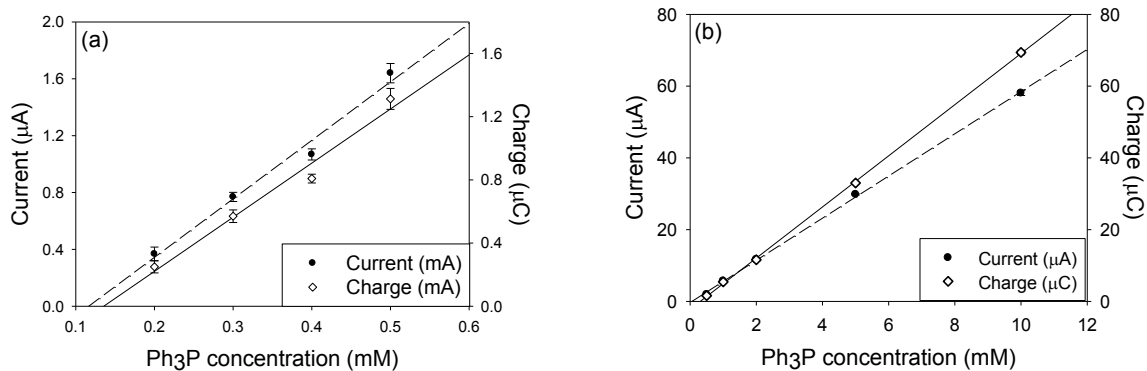


Figure 5.5. Calibration curves for (a) current and (b) charge vs. Ph₃P concentration for a series of Ph₃P standard solutions. Error bars are too small to be plotted in (b).

Linear regression was performed separately on the low and high concentration plots, as the data acquisition parameters were different between the two datasets. The following calibration curves for low concentration samples (Equations L1 and L2) and high concentration samples (Equations H1 and H2) were calculated based on a simple linear regression model:

$$i_{pa} = 4.116 \cdot C_{Ph_3P} - 0.479 \quad [L1]$$

$$q_{pa} = 3.428 \cdot C_{Ph_3P} - 0.465 \quad [L2]$$

$$i_{pa} = 5.879 \cdot C_{Ph_3P} - 0.321 \quad [H1]$$

$$q_{pa} = 7.129 \cdot C_{Ph_3P} - 2.176 \quad [H2]$$

Based on the low concentration calibration curve, the concentration of Ph₃P in a 2 mM solution of [2.1(Ph)][OTf] in 0.1M TBAPF₆/MeCN was 0.280 mM (based on i_{pa}) or 0.322 mM (based on q_{pa}). However, upon an increase of the concentration of [2.1(Ph)][OTf] to 4 mM, an observed decrease in the peak current for IV was noted, and at a [2.1(Ph)][OTf] concentration of 8 mM, the amplitude of peak IV was negligible. These observations run counter to the expected linear increase in Ph₃P concentration that should be observed if the dissociation of [2.1(Ph)][OTf] were governed by a standard equilibrium constant, K_{eq} .

5.3.1 Effect of TBAPF₆ as a Supporting Electrolyte

One of the variables unique to electrochemical experiments that is not relevant in chemical synthesis is the presence of a vast excess of an organic salt, which acts as a supporting electrolyte to reduce overall solution resistance to current and prevent concentration gradients of the analyte resulting from migration of the species of interest. Generally, a 50-fold molar excess of supporting electrolyte is used, and the non-innocence of these species has been observed to be at times problematic.^{169,199,200} As such, it was of interest in this case to investigate whether the concentration of TBAPF₆ was influencing the observed anodic peak current i_{pa} for Ph₃P. To minimize resistive effects, measurements were conducted in a small diameter electrochemical cell, thereby minimizing the path length for current to traverse between electrodes. Comparative measurements on samples of [2.1(Ph)][OTf] in the small cell and large cell were not significantly different.

Cyclic voltammograms of 2 mM, 4 mM and 8 mM solutions of [2.1(Ph)][OTf] with 25-100 mM concentrations of TBAPF₆ were compared (Figure 5.6). Resistive effects appeared qualitatively minimal for all concentrations except 25 mM TBAPF₆, for which notable linearity of the peak currents were observed. For all concentrations of [2.1(Ph)][OTf], the peak oxidation current increased in the presence of a higher concentration of supporting electrolyte. For all concentrations of TBAPF₆, the highest anodic peak current was observed in the most dilute solution of [2.1(Ph)][OTf].

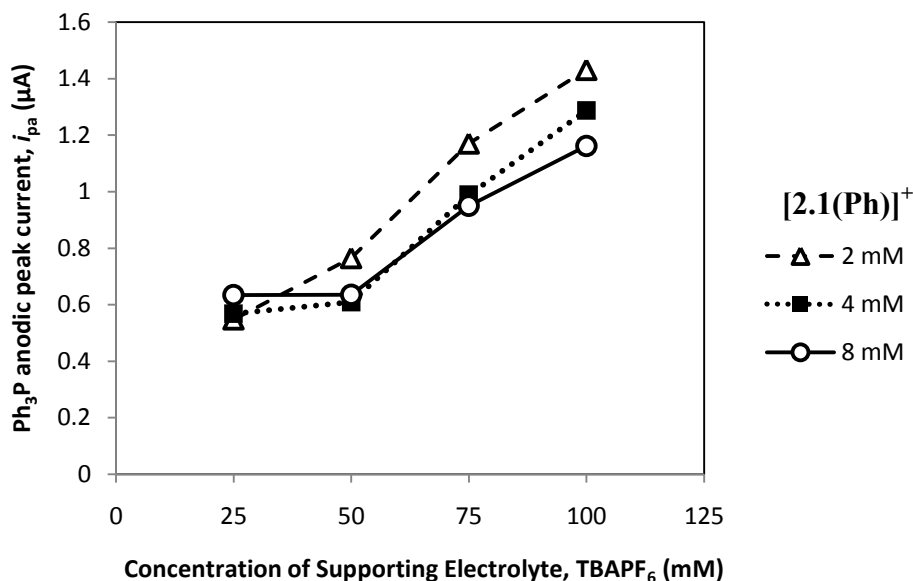


Figure 5.6. Anodic peak current vs. TBAPF₆ concentration for various concentrations of [2.1(Ph)][OTf].

Effectively, however, it is the molar excess and not the molarity of the supporting electrolyte which is relevant. If the data is therefore re-plotted in terms of the molar ratio of supporting electrolyte vs. analyte, and the anodic current scaled according to the analyte concentration, it is clear that all of the data reflects a single trend (Figure 5.7).

That is, the anodic current per mole of **[2.1(Ph)][OTf]** increases nearly linearly with increasing molar excess of TBAPF₆.

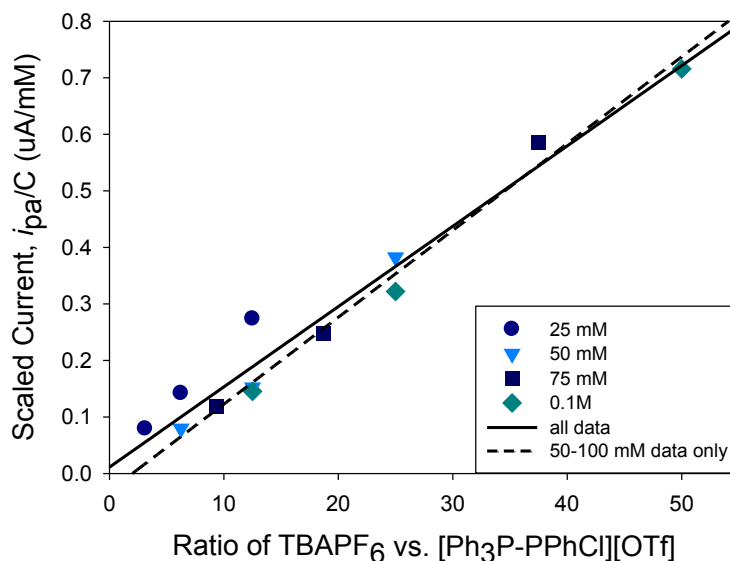


Figure 5.7. Scaled current function ($i_{pa} \cdot C^{-1}$) vs. the molar ratio of supporting electrolyte to analyte for **[2.1(Ph)][OTf]**. Regression lines are plotted for all data and excluding data at 25 mM TBAPF₆, to compare the possible effect of solution resistance.

Notably, when the effect of TBAPF₆ concentration on a 2 mM solution of Ph₃P was investigated, the opposite trend was observed, and the effect was of considerably smaller magnitude. Additionally, cyclic voltammograms of reaction mixtures, rather than isolated samples, of **[2.1(Ph)][OTf]** did not demonstrate an inverse relationship between anodic peak current and analyte concentration (Figure 5.8). However, the anodic peak currents observed in both of these cases were substantially larger (*ca.* 4-20 μ A) than those observed in solutions of redissolved **[2.1(Ph)][OTf]** (0.6-0.8 μ A). In previous work with Ph₃P oxidation, Caram and Vasini noted likewise that i_p/C (peak current divided by concentration) decreased with increasing Ph₃P concentration, and they ascribed this effect

to Ph_3P adsorption on Pt electrodes in both DMF and MeCN.¹⁶⁶ When organic molecules are undergoing weak adsorption on a surface, they are in equilibrium with solution molecules and consequently not undergoing electron transfer. As such, adsorption is itself characterized by null current, typically until the species are oxidatively desorbed at higher potentials.^{160,189} To minimize the influence of adsorption on the observed current of Ph_3P , sufficiently high concentrations of analyte and sufficiently low sweep rates are required.¹⁶⁶ Thus, at the higher concentrations of Ph_3P evident in both the Ph_3P standard and the reaction mixtures, adsorption effects were negligible.

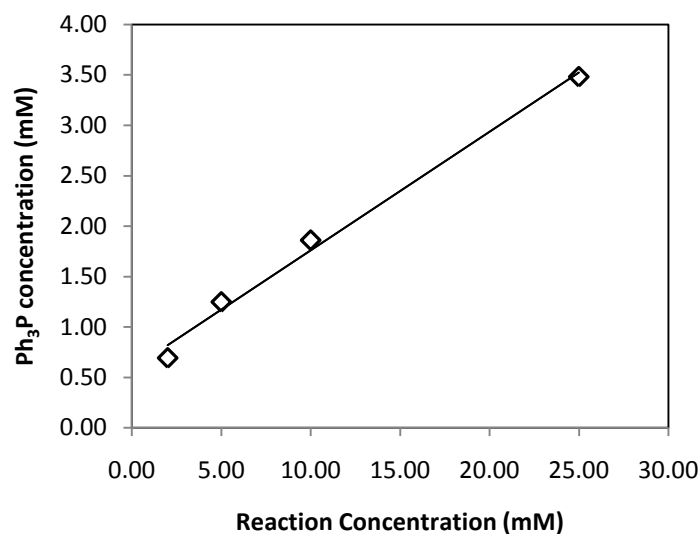


Figure 5.8. Calculated concentration of Ph_3P vs. reaction based on anodic peak currents observed in cyclic voltammograms of reaction mixtures of Ph_3P , PhPCl_2 and Me_3SiOTf in 0.1 M $\text{TBAPF}_6/\text{MeCN}$. Ph_3P concentrations calculated based on calibration curve H3.

To rationalize the dependence of the anodic current on the concentration of TBAPF_6 , it is sufficient to note that the thermodynamics of adsorption are highly dependent on the characteristics of the electrolyte. For adsorption of an organic molecule to occur, solvent-molecule interactions must be broken, and any existing surface coverage by the solvent or

electrolyte must be displaced from the electrode.¹⁶⁰ To this end, the relatively non-polar nature of Ph₃P (compared to the other ions in solution) would make adsorption increasingly favourable in solutions of high ionic strength, where surface interaction would be favoured over ion-Ph₃P interactions.

Since [2.1(Ph)][OTf] was synthesized as a triflate salt, TBAOTf was considered as an alternative supporting electrolyte which might minimize the observed Ph₃P adsorption. However, as evidenced in Figure 5.9a, no peak current was observed for Ph₃P over a range of [2.1(Ph)][OTf] concentrations (2 to 8 mM in 0.1 M TBAOTf/MeCN). This was not, however, a result of Ph₃P inhibition by the supporting electrolyte, as the Ph₃P peak was clearly visible following an initial cathodic sweep (Figure 5.9b). This suggests that the high concentration of triflate anions in solution may inhibit the dissociation of [2.1(Ph)][OTf] altogether. In the absence of a Ph₃P oxidation peak, adsorption effects are difficult to assess.

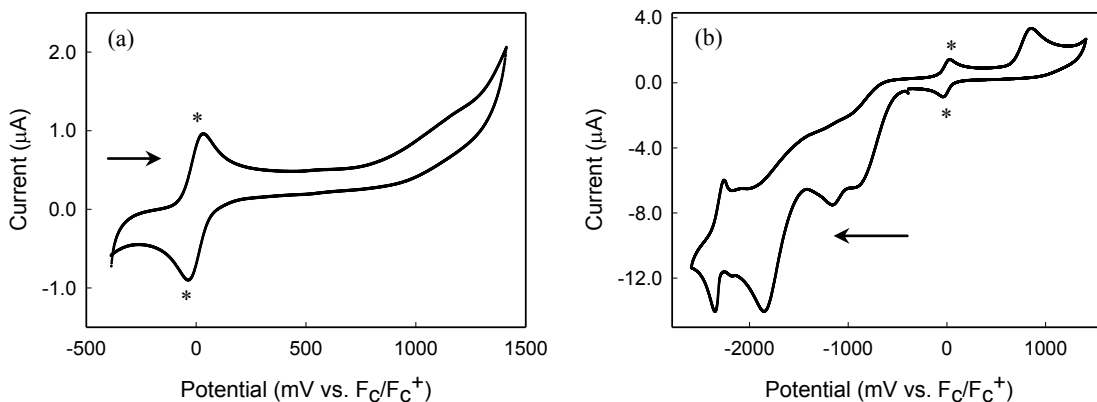


Figure 5.9. Cyclic voltammograms of a 2.00 mM solution of [2.1(Ph)][OTf] in 0.1 M TBAOTf/MeCN, with potentials referenced to 1 mM F_c/F_c⁺ (*). Arrows indicate the direction of the initial sweep.

5.4 Electrochemistry of Other *Catena*-phosphorus Cations

In addition to the more extensive cyclic voltammetric studies of $[\text{Ph}_3\text{P-PPhCl}][\text{OTf}]$, $[\mathbf{2.1}(\text{Ph})][\text{OTf}]$, preliminary investigations into the electrochemistry of several other *catena*-phosphorus cations were conducted.

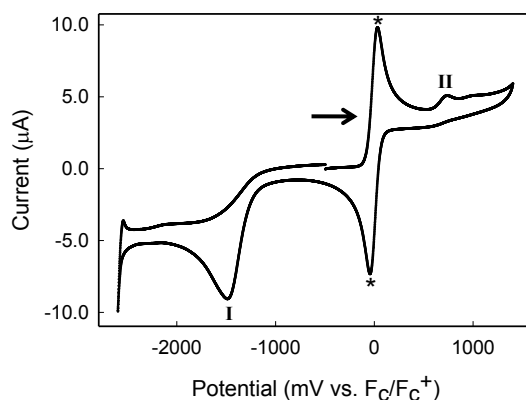


Figure 5.10. Cyclic voltammogram of a 2 mM solution of $[\text{Ph}_3\text{P-PPh}_2][\text{OTf}]$, $\mathbf{1.24}[\text{OTf}]$ at 100 mV/s in 0.1 M TBAPF₆/MeCN, with an initial potential sweep in the anodic direction.

The homoleptic phosphinophosphonium cation $[\text{Ph}_3\text{P-PPh}_2][\text{OTf}]$, $\mathbf{1.24}(\text{Ph})$, was investigated as a direct comparison to $[\mathbf{2.1}(\text{Ph})][\text{OTf}]$. As expected based on the mechanism proposed in Section 5.2.3, cyclic voltammograms of $\mathbf{1.24}(\text{Ph})$ exhibit only a single reduction wave (I) at -1.5 V vs. Fc/Fc^+ (Figure 5.10), likely corresponding to one electron reduction and subsequent P-P bond cleavage to Ph_3P and the neutral radical $[\text{Ph}_2\text{P}]^\bullet$. Again, the oxidation wave (II) was observed regardless of the initial sweep direction, although an increase in current was observed following reduction. This was therefore assigned to Ph_3P , resulting from *in situ* dissociation of $\mathbf{1.24}(\text{Ph})$. Notably, using the Ph_3P concentration vs. current or charge relationships developed in Section 5.3, the concentration of Ph_3P in a 2 mM solution of $\mathbf{1.24}(\text{Ph})$ was calculated to be only 0.04

mM less than the analogous concentration in a solution of **[2.1(Ph)][OTf]**. Although this difference was smaller than might be expected based on the near quantitative phosphonium exchange observed in Section 2.2.1, it is nonetheless statistically significant ($\sigma = 0.2 \mu\text{M}$). The apparent similarity in the dissociation constants of these two species by electrochemical methods might therefore be attributed instead to ionic strength effects not observed in the electrolyte free phosphonium exchange reactions previously described.

Cyclic voltammograms of the closely related salts **2.1(Me)[OTf]** and its chemical reductive coupling product **2.2(Me)[OTf]₂** likewise showed a single irreversible reduction peak (at -1.1 V and -1.4 V, respectively), although a small shoulder was also visible at -1.7 V in the reduction of **2.2(Me)**. In addition, a small anodic peak was observed near 1.1 V, regardless of initial sweep direction, likely resulting from the oxidation of Ph_3P .

Unfortunately, analysis of the polychlorinated phosphinophosphonium derivatives described in Chapter 3 was not possible, owing to the overlapping potential window of the tetrachlorogallate anion.²⁰¹

5.5 Summary

The electrochemical behaviour of $[\text{Ph}_3\text{P-PPhCl}][\text{OTf}]$, **[2.1(Ph)][OTf]**, and several other *catena*-phosphorus cations have been investigated by cyclic voltammetry. One possible mechanism for the electroreduction of **[2.1(Ph)][OTf]** was proposed, based on literature precedents for the electrochemistry of other phosphorus species, and the dissociation of **[2.1(Ph)][OTf]** was analyzed. Conclusions regarding the dissociative behaviour of

[2.1(Ph)][OTf] were unfortunately hampered by substantial adsorption effects within the concentration regime studied. Although considerably more time will be needed to provide a concrete understanding of the electrochemical behaviour of these and other cationic polyphosphorus compound, this chapter nonetheless provides framework studies from which this area can be further explored.

Chapter 6. Stibinophosphonium Cations

6.1 Background

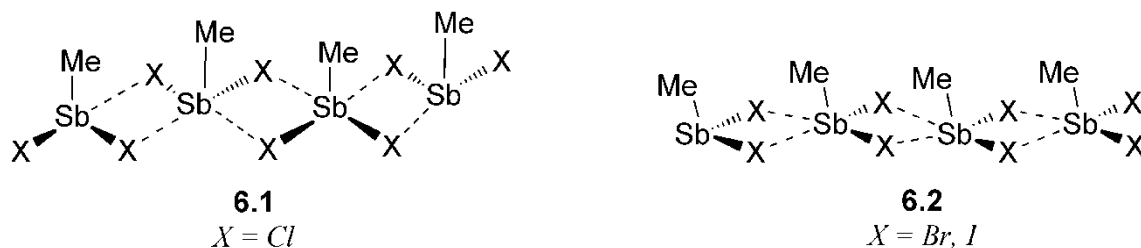
Antimony, like its lighter congener phosphorus, possesses rich acceptor chemistry. In fact, the larger atomic radius of antimony (Table 6.1) allows for a larger coordination sphere, and many neutral Sb(III) species display extended structures owing to weak donor-acceptor interactions.

Table 6.1. Comparison of selected properties of phosphorus vs. antimony. References are from Emsley⁹ unless otherwise indicated.

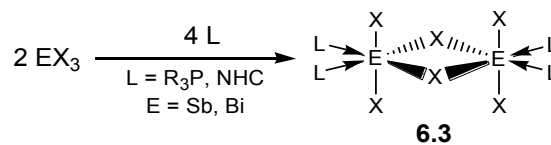
	P	Sb
Electronegativity, (Pauling, χ^P)	2.19	2.05
Single-bond covalent radius, r_{cov} (Å)	1.11 ¹⁰	1.40 ¹⁰
van der Waals radius, r_{vdw} (Å)	1.90	2.20
E-E bond length (Å)	2.21	2.90
E-E bond strength (kJ/mol)	201	121 ¹⁴⁹
E-C bond strength (kJ/mol)	264	215

Organoantimony(III) dihalides, for example **6.1** and **6.2**, crystallize in infinite-chain network structures, where each Sb centre has two short (covalent) Sb-X bonds and two long Sb-X interactions ($<\Sigma r_{\text{vdw}}$), resulting in a pseudo square-pyramidal geometry at antimony when the overall coordination sphere is considered.²⁰²⁻²⁰⁴ These intermolecular interactions can be disrupted with the addition of substantial steric bulk, as evidenced by the dimeric structure of DmpSbCl₂ and monomeric structure of DmpSbBr₂ and (2,6,-Trip₂C₆H₃)SbCl₂ in the solid state (Dmp = 2,6-dimethylphenyl and Trip = 2,4,6-

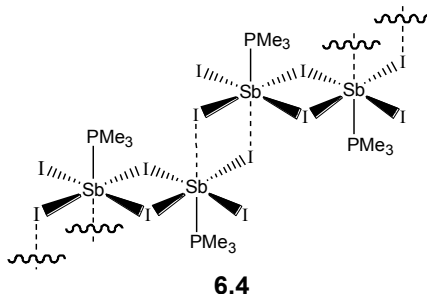
triisopropylphenyl).^{205,206} Alternately, monomeric species have also been achieved by the introduction of strong donor ligands, as in the case of the 1:1 adducts of 2,2'-bipyridine and MeSbCl₂ or PhSbCl₂.^{207,208}



Similarly, reaction of Sb or Bi trihalides with phosphines or other donors consistently yields neutral dimeric 1:1 or 2:1 donor-acceptor adducts (Scheme 6.1), where additional stabilization of the complex is provided by a weak covalent interaction with the bridging halide atom.^{105,209,210} In the case of the 1:1 adduct Me₃P-SbI₃ **6.4**, this stabilization is further bolstered by weak interactions between dimeric units.²¹⁰



Scheme 6.1. Reaction of Sb or Bi trihalides with phosphine or N-heterocyclic carbene donor ligands to yield 2:1 adducts



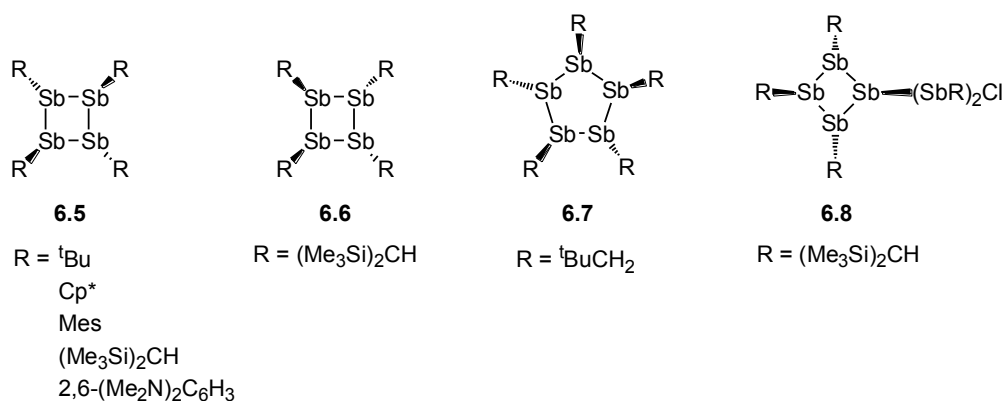
6.1.1 *Catena*-antimony Compounds

Owing to the increasingly weak E-E and E-C bonds of the heavier elements (Table 6.1), the number and types of stable *catena*-antimony systems is limited in comparison to that of phosphorus. Although in the solid state, acyclic neutral polystibines with small substituents are proposed to exist as long chain oligomers

(e.g. $\text{Me}_2\text{Sb}-(\text{SbMe})_{11}-\text{SbMe}_2$),²⁰² these undergo solution disproportionation to a mixture of cyclic species and distibines, in a fashion identical to long chain polyphosphines (Scheme 1.3).¹⁴⁹ Unlike polyphosphines, however, comparatively few short chain polystibines have been comprehensively characterized, as the majority are only stable in the presence of an excess of distibine.^{149,211} Bulky terminal organo-substituents have been used to stabilize short chain stibines by disfavoured the formation of the corresponding distibine, allowing the NMR spectroscopic characterization of ${}^t\text{Bu}_2\text{Sb}-(\text{SbMe})_n-\text{Sb}{}^t\text{Bu}_2$ and $\text{Me}_2\text{Sb}-(\text{SbPh})_n-\text{SbMe}_2$, as mixtures of tri- and tetra-stibines ($n = 1, 2$).²¹² The only acyclic polystibine which exists as a single chain length in solution is the tristibine $\text{Dmp}_2\text{Sb}-\text{SbMe}-\text{SbDmp}_2$.²⁰⁵ Additionally, two anionic *catena*-antimony frameworks are known, $[\text{R}_2\text{Sb}-\text{Sb}-\text{SbR}_2]^-$ ($\text{R} = \text{Ph}, {}^t\text{Bu}$) and $[{}^t\text{Bu}_2\text{Sb}-\text{Sb}{}^t\text{Bu}]^-$, formed by the alkali metal reduction of $({}^t\text{BuSb})_4$ or Ph_3Sb .^{213,214}

Ring-size redistribution, previously described for monocyclic polyphosphines (Section 1.2.2), is also known for cyclic polystibines, although again few cyclic polystibines have been isolated without the aid of sterically encumbering substituents.¹⁴⁹ Whereas cyclohexyl and *tert*-butyl offer sufficient steric bulk to favour the synthesis of *cyclo*-(PR)₃, *cyclo*-[(Me₃Si)₂CHSb]₃ is presently the only three-membered ring known for antimony in the solid state.²¹⁵ Use of bulky substituents (*i.e.* ${}^t\text{Bu}$,²¹⁶ Me_5C_5 ,²¹⁷

(Me₃Si)₂CH,²¹⁸ 2,6-(Me₂N)₂C₆H₃,²¹⁹ Mes²²⁰) has allowed for the solution and solid state characterization of *all-trans* four-membered rings **6.5**, whereas smaller R-groups (*i.e.* Et, ⁿPr, Ph, Tol, (Me₃Si)CH₂) yielded only inseparable equilibrium mixtures of (RSb)₄ and (RSb)₅, and gradual decomposition to amorphous oligomeric material.¹⁴⁹ In addition, solid-state structures are known for one *cis-trans* isomer, [(Me₃Si)₂CHSb]₄ **6.6**,²²¹ one five-membered ring, *cyclo*-(^tBuCH₂Sb)₅ **6.7**,²²² one branched ring, *cyclo*-R₃Sb₄-Sb₂R₂Cl [R = (Me₃Si)₂CH] **6.8**,²²³ and a series of aryl substituted six-membered rings (ArSb)₆ (Ar = Ph, *o*-Tol, *m*-Tol, *p*-Tol),^{224,225} which redistribute in solution to a mixture of four- and five-membered rings. In addition, a limited number neutral of polycyclic species have been characterized, predominantly consisting of sterically protected Sb-cages,^{219,221} and one bridged bicyclic system[(RSb)₄]₂.²²¹



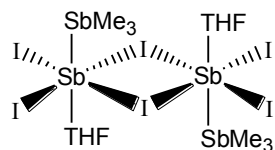
The syntheses of polystibines and related species are not as generalizable as the corresponding methods for polyphosphines, although the majority of the derivatives described herein result from Mg-reduction of RSbCl₂.¹⁴⁹ Other methods, including H₂ elimination,²²¹ photochemical ring contraction,^{149,221} and oxidative loss of (Me₃Si)₂O^{224,225} are possible, but do not generalize beyond a single set of substituents in each case. Moreover, while many synthetic routes to polyphosphines offer excellent

yields (75-90%, Section 1.2.2) most syntheses of polystibines are at present low yielding pathways (5-20%), owing to the multitude of Sb-redistribution reactions which occur in solution.¹⁴⁹

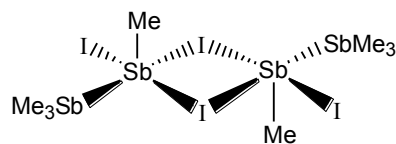
In particular, while scrambling reactions in polyphosphorus systems are typically restricted to cleavage of the P-P bond, substituent migration (requiring cleavage of E-C bonds) is well-known for antimony compounds. For example, the literature synthesis of Ph_2SbCl and PhSbCl_2 is a reported substituent redistribution between Ph_3Sb and SbCl_3 in the absence of solvent.¹⁴⁸ Additionally, equilibrium mixtures of acyclic tri- and tetra-stibines (*vide supra*), decompose by migration of the organo substituents.¹⁴⁹

6.1.2 *Catena*-antimony Coordination Complexes

The substantial coordination sphere of antimony suggests that *catena*-antimony coordination complexes must also be accessible, but the low donor strength of antimony renders their isolation comparatively challenging. Like the neutral adducts **6.3** described at the start of this chapter, neutral adducts containing dative Sb-Sb bonds are dimeric, requiring stabilization from bridging halides, but the only known neutral *catena*-antimony coordination complexes $\text{Me}_3\text{Sb-SbI}_3 \cdot \text{THF}$ (**6.9**) and $\text{Me}_3\text{Sb-SbMe}_2$ (**6.10**) are unstable except in the solid state.²⁰³ Notably, the Sb-Sb bonds in crystalline **6.9** and **6.10** [2.8430(10) Å and 2.859(1) Å, respectively]^{203,226} are not appreciably longer than a typical Sb-Sb bond (*cf.* 2.838(1) Å in $\text{Me}_2\text{Sb-SbMe}_2$),²¹⁴ their relative instability in solution can again be attributed to the inherently weaker E-E bond in the heavier pnictogens (Table 6.1).²⁰³

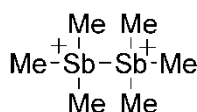


6.9

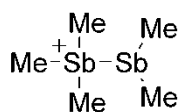


6.10

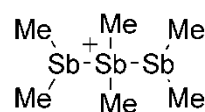
Presently, only three examples of cationic *catena*-antimony systems are known, and, as such, unlike *catena*-phosphorus cations, no generalizable synthetic methods are yet available. The hexamethyldistibonium cation **6.11**[SbF₆] \cdot SO₂, was isolated as a decomposition product of [Me₃SbH][AsF₆] in SO₂.²²⁷ The cation possesses a significantly shorter Sb-Sb bond length (2.7624(11) or 2.7867(12) Å) in the solid state than a typical neutral Sb-Sb bond length (2.83-2.86 Å).[ref] Both Sb-centres are, however, stabilized by weak interactions with the F-atoms of the anion (Sb-F = 2.98-3.13 Å < $\Sigma_{\text{vdw}}=3.67$ Å⁹).²²⁷ Moreover, the surreptitious synthetic pathway provides little insight into the further development of catenated cationic Sb systems.



6.11



6.12



6.13

The pentamethylstibinostibonium cation **6.12**[MeSbBr₃] was isolated in 80% yield from the melt crystallization of Me₂SbBr, presumably by the initial scrambling of substituents to yield a mixture of MeSbBr₂, Me₃Sb and starting material.²²⁸ Subsequent halide abstraction by MeSbBr₂ to yield both the stibonium cation [SbMe₂]⁺ and the hypervalent phosphorane-analogue [MeSbBr₃]⁻ anion provides the product. It is notable that halide abstraction is presumed to be an equilibrium process due to the observed formation of the three neutral species when crystals of the cation are redissolved.²²⁸ In the solid state, the Sb-Sb bond length is no different than typical neutral Sb-Sb species. However, significant

changes in geometry are observed at the Me_3Sb centre, and the authors attribute the wider of the C-Sb-C angles to increased hybridization upon quaternization, despite the typical claim that Sb(III) is reluctant to hybridize.²²⁹ The counteranion displays the expected dimeric square pyramidal structure shown in analogous $[\text{PhSbCl}_3]^-$ anions, but, notably, the extended structure shows Br^- linearly disposed with respect to the Sb-Sb bond. Thus, the proposed solution equilibrium can be envisaged as the transfer of this atom between the cationic and anionic Sb-centres.

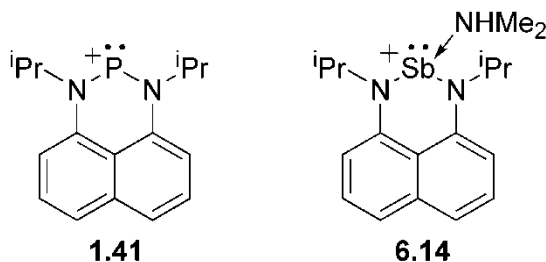
The 1,3-distibinostibonium cation **6.13** $[\text{Me}_2\text{SbBr}_2]$ is formed by the reaction of Me_2SbBr with excess $\text{Me}_2\text{Sb-SbMe}_2$.²³⁰ Again, this can be regarded as the redistribution of two equivalents of Me_2SbBr to yield the distibine-stabilized stibenium cation $[\text{SbMe}_2]^+$ and the expected disphenoidal anion $[\text{Me}_2\text{SbBr}_2]^-$. As electrophilic attack on the Sb-Sb bond is strongly favoured, both the synthesis and storage of **6.13** requires an excess of the distibine reagent.²³⁰

Given the observed limitations of synthesizing cationic *catena*-antimony complexes, it is useful to investigate other means of stabilizing cationic Sb-centres.

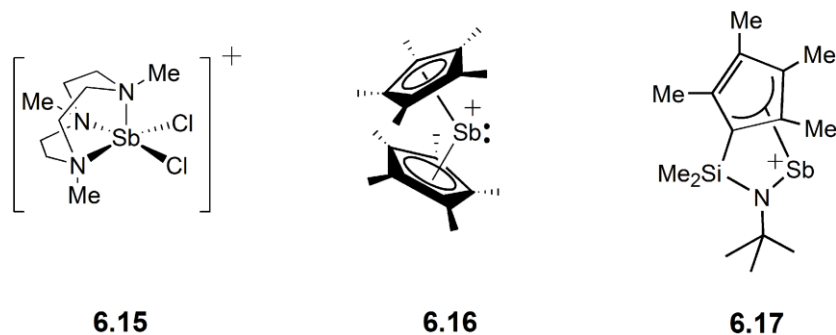
6.1.3 Stibenium Cations, $[\text{SbR}_2]^+$

Whereas stabilized phosphonium cations have been known since the 1970s (Section 1.3.2), examples of stibenium cations are comparatively rare. The isolation of heavier analogues of these two-coordinate cationic species is hindered by their higher energy LUMO, and consequent poorer accepting capability. This is well-demonstrated by the ease of isolation observed for the diamidonaphthalene-supported phosphonium cation,

1.41, versus its stibonium analogue **6.14**, which required additional stabilization from HNMe₂ to permit its isolation.²³¹



Similarly, halide abstraction by Me₃SiOTf from the sterically protected but otherwise unstabilized chlorostibine (2,4,6-(CF₃)₃C₆H₂)₂SbCl results in an Sb-O covalent interaction rather than the desired cation-anion pair; instead, the weakly basic triflate anion serves to stabilize the empty *p*-orbital at Sb.²³² Coordination of secondary donors has been prevented only through the use of tridentate or greater chelating ligands, such as in structurally-characterized oxacrown²³³ and azamacrocyle²³⁴ complexes (e.g. **6.15**) of [SbCl₂]⁺. Cationic antimony species have also been observed in the presences of sterically-hindering cyclopentadienyl-type ligands, **6.16**²³⁵ and **6.17**²³⁶, but the η⁵- and η³-coordination of these species excludes them from a discussion of more traditional two-coordinate stibonium cations.



While ligand-stabilized stibonium cations should be considerably more accessible, phosphine-stabilized stibonium cations nonetheless eluded structural characterization

until only five years ago.²³⁷ Much like the neutral adduct **6.4**, the first phosphinostibonium cations **6.18** [(Me₃P-SbPh₂)₄X][PF₆]₃ (X = Cl, Br) were found to be additionally stabilized by Sb-X interactions, in this case by arrangement into supramolecular square-planar halide complexes (Figure 6.1).²³⁷

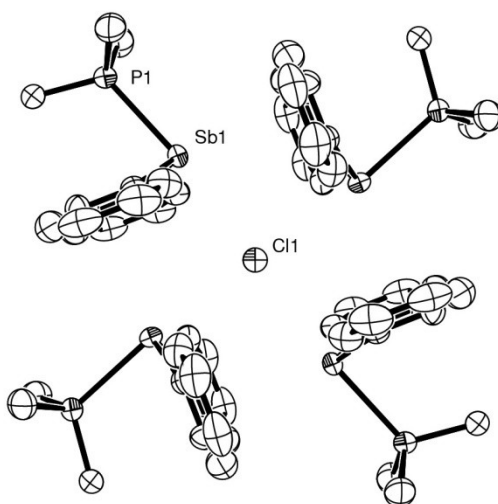
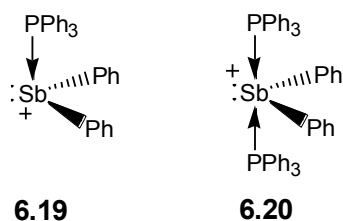


Figure 6.1. ORTEP representation of the crystal structure of [(Me₃P-SbPh₂)₄Cl]³⁺, **6.18**[PF₆]₃. Thermal ellipsoids are shown at 30% probability, and hydrogen atoms have been omitted for clarity (adapted from published CIF).²³⁷

In the absence of residual halide anions, monomeric formulations have been characterized, specifically the Ph₃P-stabilized adduct **6.19** [Ph₃P-SbPh₂][PF₆].²³⁸ Just as the P-P bond distance in polyphosphorus compounds appears to be independent of molecular charge, the P-Sb distance in **6.19** [2.5950(12) Å] falls within the range observed in both neutral and anionic complexes with both covalent and coordinate P-Sb interactions [2.489(3)-2.662(3) Å, excluding disordered atoms and one poorly refined²⁰⁹ structure].^{210,239-245}

Unlike for phosphonium cations, the bis-stabilized adducts $[(\text{Ph}_3\text{P})_2\text{SbPh}_2][\text{PF}_6]$ (**6.20**) is also known, and displays geometric parameters similar to the phosphoranides (Section 1.3.1), featuring a distorted disphenoidal geometry with $86\text{-}87^\circ$ between the equatorial phenyl substituents and 170° between the axial donor Ph_3P groups.²³⁸ In both **6.19** and **6.20**, solution state ^{31}P NMR spectra were indicative of a dissociative equilibrium for the donating groups, supporting a coordinate model for the P-Sb bond, and corresponding theoretical studies describe the bonding in **6.20** as primarily dative covalent, rather than ionic.²³⁸ The solid-state structural data, however, suggest a comparatively weak interaction in **6.20** vs. **6.19**, with significantly longer P-Sb distances observed in the bis-adduct $[2.8694(8) \text{ \AA}]$.²³⁸



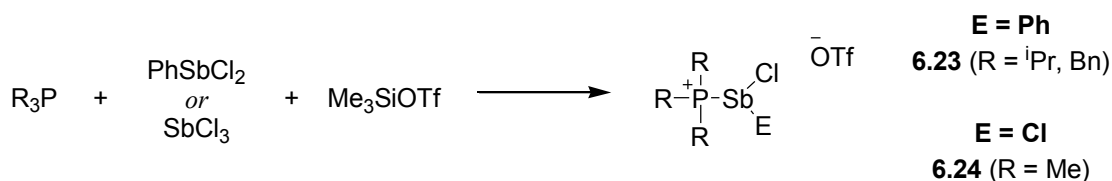
Most recently, *cyclo*-(PCy)₄ has been used to stabilize both stibenium and distibenium cations, as in $[(\text{PCy})_4\text{SbCl}_2][\text{AlCl}_4]$, **6.21**, and $[(\text{PCy})_4\text{SbCl}]_2[\text{AlCl}_4]_2$, **6.22**.²⁴⁶ The isolation of **6.21** serves to again highlight the divergent reactivity of phosphorus and antimony cations, as insertion chemistry predominates over coordination chemistry for reactions of phosphonium cations with neutral $(\text{RP})_n$ rings. Presumably, the larger coordination sphere and poorer oxidative capacity of Sb contribute substantially to this divergence. Nonetheless, the isolation of **6.22** demonstrates that reductive coupling, described for the synthesis of stabilized diphosphenium cations in Chapter 2, is also viable as a synthetic method for antimony cations.

6.1.4 Background Summary

Given the diversity of phosphine-stabilized chlorophosphenium cations, or phosphinophosponium cations, described in section 2.2, the next challenge is the extension of this type of reactivity to heavier group 15 pnictogenium cations. Towards this end, the functionalization of the stibinophosponium framework is described herein.

6.2 Synthesis of Functionalized Stibinophosponium Cations

In a manner analogous to the synthesis of chlorophosphinophosponium cations described in Section 2.2, equimolar reaction of a chlorostibine with a halide abstractor in the presence of a supporting donor trialkylphosphine resulted in rapid conversion to the corresponding chlorostibinophosponium cation.



Scheme 6.2. Synthesis of stibinophosponium cations by halide abstraction.

Crystallization of the resulting reaction solutions by slow evaporation yielded X-ray quality crystals of the triflate salts of cations $[\text{Pr}_3\text{P}-\text{SbPhCl}]^+$ **6.23**(ⁱPr) and $[\text{Bn}_3\text{P}-\text{SbPhCl}]^+$ **6.23**(ⁱPr). Substitution of PhSbCl₂ with SbCl₃ was also viable in the presence of Me₃P as a donor, and $[\text{Me}_3\text{P}-\text{SbCl}_2][\text{OTf}]$, **6.24**(Me)[OTf], was isolated from the reaction as a CH₂Cl₂-insoluble white powder, which was readily recrystallized from MeCN-solution by vapour diffusion of either Et₂O or CH₂Cl₂. In all cases, ¹⁹F NMR of the reaction mixture supported the presence of the triflate anion and complete consumption of covalently bound Me₃SiOTf.

The observed ^{31}P NMR chemical shift for all three compounds (10-36 ppm) were shifted appreciably downfield of the previously known phosphine-stabilized $[\text{SbPh}_2]^+$ salts $[\{\text{Me}_3\text{P}(\text{SbPh}_2)\}_4\text{X}][\text{PF}_6]_3$ (**6.18**): -30 ppm in CDCl_3 ,²³⁷ and $[\text{Ph}_3\text{P}-\text{SbPh}_2][\text{PF}_6]$ (**6.19**): -4.2 ppm in CD_2Cl_2)²³⁸ in spite of the comparable solid state geometry about the phosphonium centre. This trend is readily rationalized by comparison with phosphinophosphonium cations, wherein replacement of a phenyl-substituent by a chloro-substituent at the acceptor site resulted in a 10 ppm increase in the chemical shift of otherwise identical phosphonium centres (Table 2.1). The more substantial divergence in the case of **6.18**, however, emphasizes the weak $\text{Sb}\cdots\text{X}$ interactions present its extended structure,²³⁷ which may permit more ready dissociation of the phosphine centre and, correspondingly, a more upfield ^{31}P NMR chemical shift resembling that of free Me_3P (-62 ppm).²⁴⁷

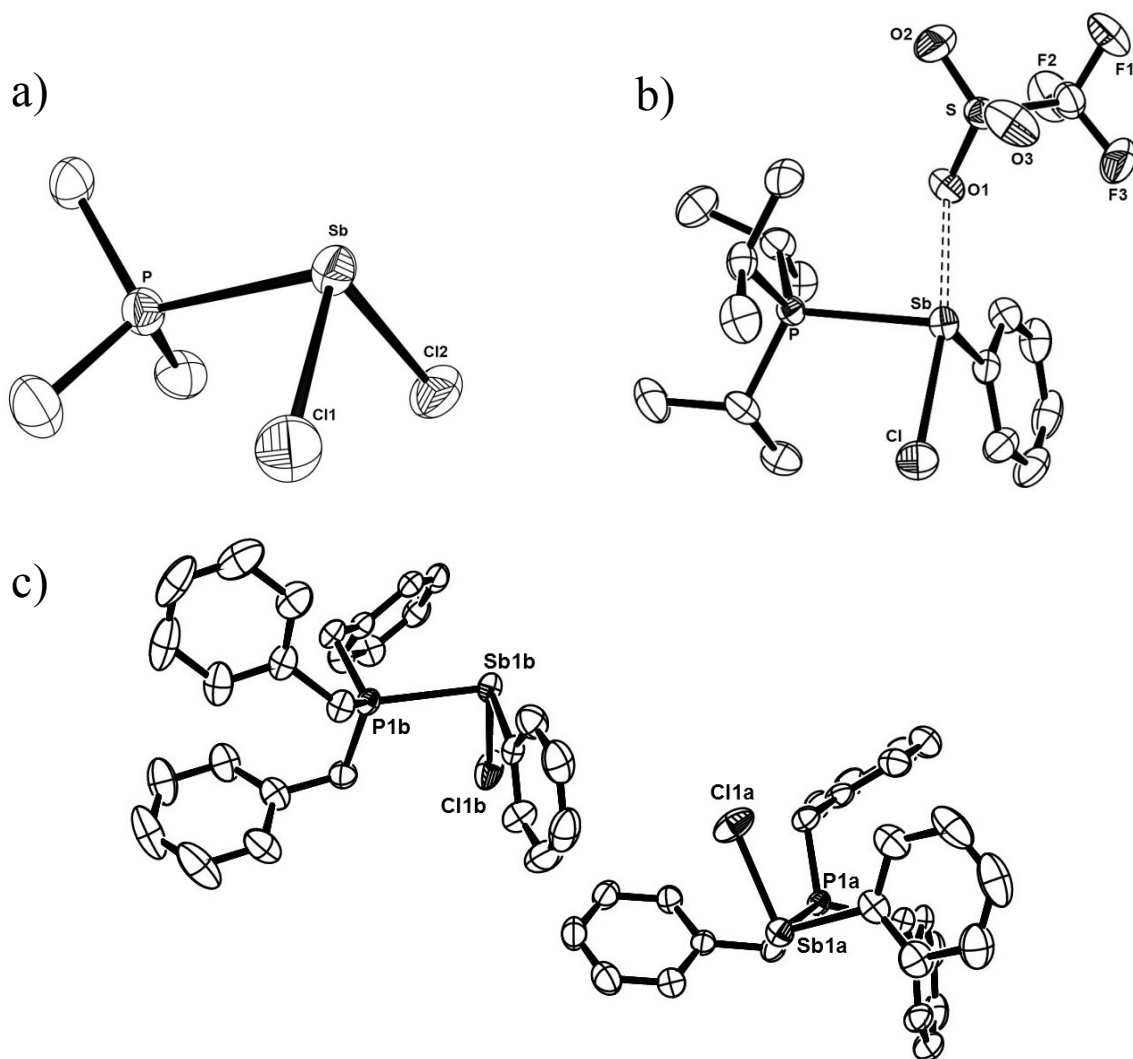


Figure 6.2. ORTEP representations of the solid-state structure of (a) **6.24(Me)**[OTf], (b) **6.23(ⁱPr)**[OTf], and (c) **6.23(Bn)**[OTf]. Thermal ellipsoids are shown at 50% probability, and hydrogen atoms have been omitted for clarity. The triflate counterion is shown in (b) as an example to indicate the geometry about Sb when the weak cation-anion contact is considered.

Table 6.2. Selected structural parameters for stibinophosphonium cations.

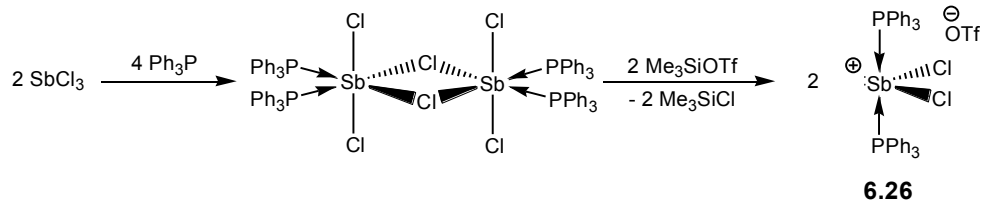
		[ⁱ Pr ₃ P-SbPhCl][OTf] 6.23(Pr)	[Bn ₃ P-SbPhCl][OTf] 6.23(Bn) <i>2 crystallographically independent molecules</i>		[Me ₃ PSbCl ₂][OTf] 6.24
Bond lengths (Å)	Sb-P	2.6150(5)	2.6126(8)	2.5819(8)	2.6043(9)
	Sb-Cl	2.4233(6)	2.3734(9)	2.3997(9)	2.3926(8) 2.3719(9)
	Sb-C	2.165(2)	2.157(3)	2.164(3)	--
	Sb-O	2.5667(17)	2.713(2) 2.877(3)	2.583(2)	2.705(2) 2.755(2) 2.986(2)
Bond Angles (°)	P-Sb-Cl	89.20(2)	93.13(8)	89.00(3)	90.71(3) 90.62(3)
	P-Sb-C	99.74(5)	88.31(3)	93.65(8)	--
	E-Sb-Cl (<i>E</i> = C, Cl)	94.22(6)	95.76(10)	95.29(9)	92.78(3)
	Σ at Sb	283	277	278	274
	C-P-C	106.75(11) 113.87(11) 107.32(11)	108.30(14) 107.85(15) 107.96(14)	108.05(16) 109.29(16) 110.43(14)	107.44(16) 107.11(15) 107.65(17)

In the solid state, all three stibinophosphonium cations **6.23-6.24** display Sb-P distances [2.5819(8)-2.6150(5) Å] comparable to those of the analogous previously reported stibinophosphonium species **6.18** [2.591 Å]²³⁷ and **6.19** [2.5950(12) Å],²³⁸ and within the range of Sb-P distances reported for both neutral and anionic Sb(III)-phosphine complexes in the solid state [2.489(3)-2.662(3) Å].^{210,239-245} The Sb-P bonds of **6.23-6.24** are, however, consistently longer than the analogous bonds [2.503(3)-2.5387(5) Å] in known diphosphenodistibonium complexes [Ph₃Sb-PR-PR-SbPh₃][AlCl₄]₂,

6.25[AlCl₄]₂.¹³³ This is counterintuitive, as the longer bonds would normally be expected in the case involving the weaker Ph₃Sb donors; this suggests, therefore, that the acceptor strength of the diphosphenium core exerts substantially more influence on the corresponding bond strength.

The Sb-Cl distances in the triflate salts of **6.23-6.24** are comparable to the sum of the covalent radii (2.39 Å),¹⁰ and thus, markedly distinct from the extended network structure found in **6.18** [Sb··Cl 3.1362(3) Å vs. Σr_{vdw} 4.01 Å]. The substituents at Sb are all nearly orthogonal, as is expected for an unhybridized (*p*³) configuration, while the geometry at phosphorus is pseudo-tetrahedral. The only substantial geometry change between these new cations **6.23-6.24** and the previously reported **6.19**[PF₆] are the existence of smaller E-Sb-E angles between the substituents at antimony [**6.23-6.24**: 93-96° vs. **6.19**: 100.14(18)°],²³⁸ which emphasizes the reduced steric requirements of the Cl-substituent(s). In addition, stabilizing cation-anion contacts are observed with the more coordinating triflate counterions in **6.23-6.24** (*cf.* [PF₆]⁻), resulting in non-covalent Sb-O (Σr_{cov} = 2.00 Å)¹⁰ interactions that lie well within the sum of the van der Waals radii (3.60 Å).⁹

In contrast to the reactions observed for trialkylphosphines (Scheme 6.2) with SbCl₃, the use of the comparatively weak donor phosphine, Ph₃P, yielded the bis-phosphine adduct of the resulting stibonium cation **6.26**[OTf] upon halide abstraction. Complex **6.26** can be readily envisaged as the product of halide abstraction from an initially formed dimeric donor-acceptor complex (Scheme 6.3), formed upon addition of two equivalents of a Lewis base to SbX₃ (X = Cl, Br).¹⁰⁵



Scheme 6.3. Proposed halide abstraction from dimeric $(\text{Ph}_3\text{P})_2\text{SbCl}_3$ complexes.

The broad resonance at -5 ppm observed in ^{31}P NMR spectra reaction mixtures and redissolved crystalline samples of **6.26**[OTf] suggest comparatively dynamic behaviour in solution relative to the mono-phosphine stabilized stibonium analogues **6.23-6.24**, which exhibit relatively sharp ^{31}P NMR signals. Additionally, the ^{31}P chemical shift closely approximates that of free triphenylphosphine (-5 to -8 ppm)²⁴⁷⁻²⁴⁹ further supporting the idea of a weak solution interaction. Notably, the ^{31}P NMR spectrum of the reaction solution and characterized crystalline material consistently identify the product produced as **6.26**[OTf] regardless of the stoichiometry of the reaction, suggesting that stabilization by a single Ph_3P donor is insufficient to allow formation of the stibonium cation. In contrast, the ^{31}P NMR spectrum of both **6.19** and **6.20** were reported as -4.4 (± 0.2) ppm, although, again the resonance of bis-adduct **6.20** was broad compared to the mono-adduct.²³⁸

The bonding in bis-phosphine stabilized stibonium complexes can be described using a standard Lewis convention (**6.26''**) or by a fully coordinate bonding description (**6.26**, Figure 6.3); however the dynamic behaviour observed in solution, and rapid decomposition of this salt tend support a weakly coordinative bonding description (**6.26**).

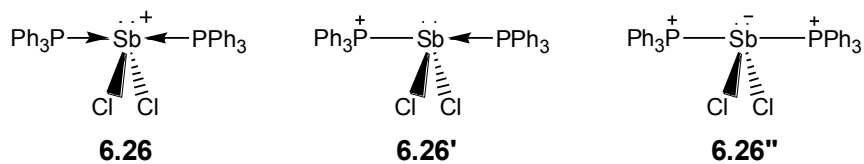


Figure 6.3. Possible bonding models to describe the bonding in **6.26**[OTf].

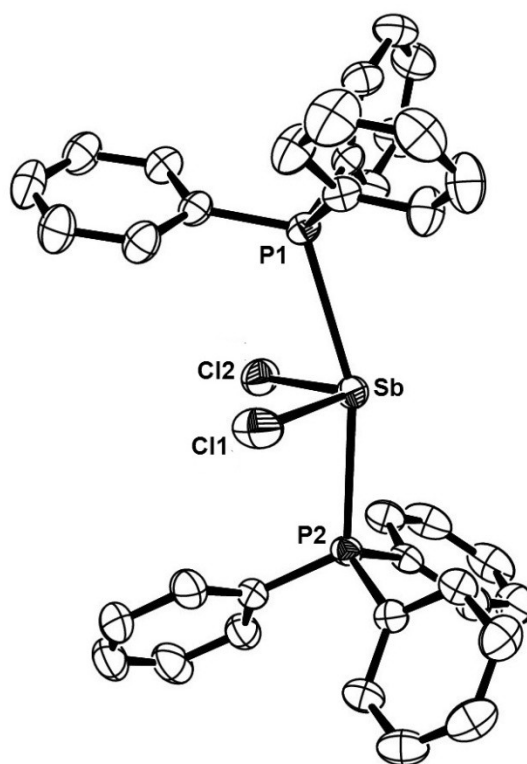


Figure 6.4. ORTEP representation of the solid-state structure of **6.26**. Thermal ellipsoids are shown at 50% probability. Carbon atoms have been left unlabelled and hydrogen atoms omitted for clarity. Relevant angles are as follows: Cl1-Sb-P: 81.519(18)° / 82.142(18)°; Cl2-Sb-P: 84.404(19)° / 88.230(19)°.

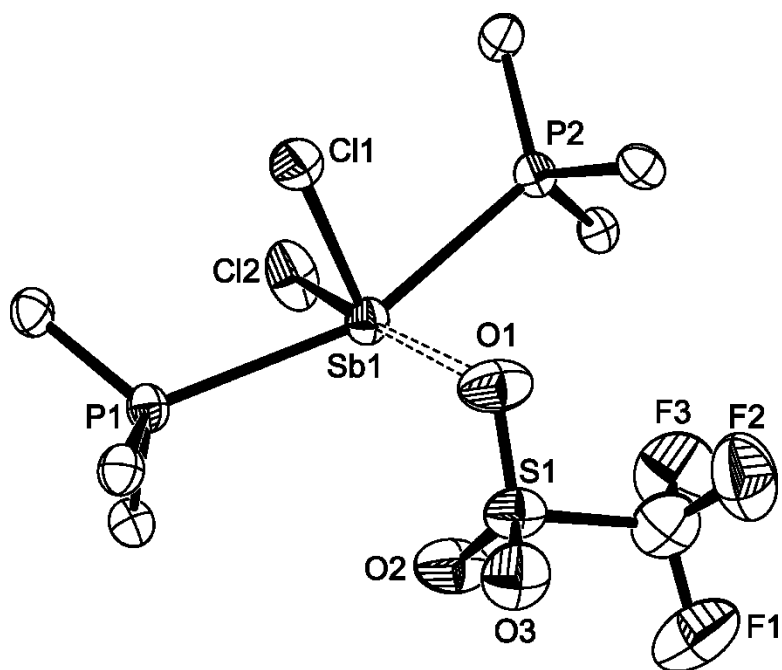


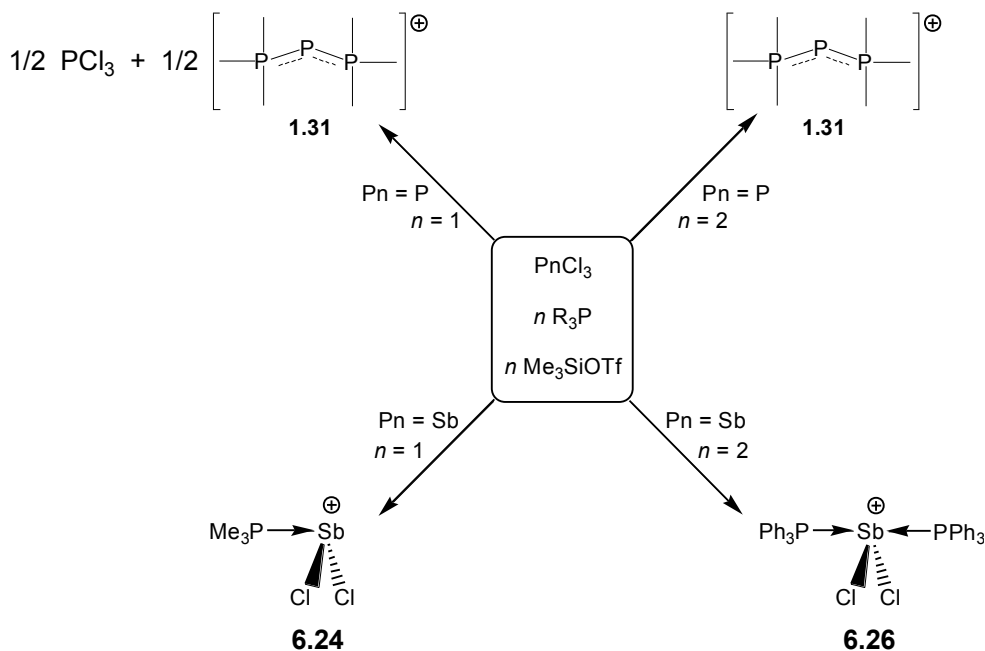
Figure 6.5. Alternative view of **6.26**[OTf] showing the close cation-anion contact (Sb-O: 2.6793(17) Å). Only the ipso carbons of the phenyl substituents are shown (unlabelled atoms). Thermal ellipsoids are shown at 50% probability, and hydrogen atoms have been omitted for clarity. Other relevant bond angles are as follows: Cl1-Sb-O: 88.45(4)°; Cl2-Sb-O: 170.49(5)°; P1-Sb-O: 103.33(4)°; P2-Sb-O: 86.02(4)°.

The geometry about the Sb-centre in **6.26**[OTf] is approximately disphenoidal: the P-Sb-P angle of 160.901(17)° and a Cl-Sb-Cl angle of 98.27(3)°, closely resemble the analogous diphenylstibenium species [(Ph₃P)₂SbPh₂][PF₆] (**6.20**) isolated by Wild and co-workers.³² This distorted geometry is highlighted in Figure 6.4, which also lists selected bond angles. The Cl-Sb-Cl angle of 98.27(3)° that defines the equatorial plane is smaller than the corresponding C-Sb-C angle (102.46(11)°) in **6.20**[PF₆],²³⁸ but this can be attributed primarily to steric repulsion between the phenyl rings of the [SbPh₂]⁺ unit. Likewise, the considerably smaller P-Sb-P angle (*cf.* **6.20**, 170.49(2)°)²³⁸ is by the reduced steric interaction of the Cl-substituents with the Ph₃P donors. The Sb-P bond lengths of 2.8621(5) Å (Sb-P1) and 2.8042(5) Å (Sb-P2) are comparable to those in **6.20**

(2.84-2.86 Å), and, as such, appreciably longer than the corresponding bonds in chloro-stibinophosphonium cations (**6.23**[OTf]-**6.24**[OTf]: 2.58-2.61 Å) or other typical Sb-P single bonds [max. 2.662(3) Å, *vide supra*].^{210,239-245} This suggests that the presence of two donors at a single cationic centre allows for weaker interactions between each phosphine donor and the stibonium acceptor. Different bond lengths are observed between Sb and each phosphine donor ($\Delta = 0.0201(5)$ Å), potentially supporting the bonding description **6.26'** in the solid state; however, both bond lengths are within normal deviation, so the difference between them is by no means conclusive. The mixed covalent-coordinate model **6.26'** is not without precedent, though, as phosphoranides [PR₄]⁻ are commonly depicted with this convention (Section 1.3.1).

Willey and coworkers have previously attributed observed Sb-Cl bond contraction to an increase in positive charge at Sb in a series of oxacrown stabilized SbCl_{*n*} (*n* = 1-3) complexes, as well as in cationic and neutral amino/amido-substituted [SbCl₂] species.²³⁴ Without a neutral analogue for direct comparison, however, the same conclusions cannot be drawn for **6.26**[OTf], where the Sb-Cl bond lengths [2.3643(6)-2.4083(6) Å] are comparable to both the cations cited by Willey *et al.* (2.365-2.466 Å)²³⁴ and to simple neutral antimony(III) dihalides [*e.g.* MeSbCl₂, **6.1**, 2.392(3)-2.430(3) Å].²⁰² The significant shortening of the Sb-Cl₁ bond length in **6.26** [2.3643(6) Å], compared to the Sb-Cl₂ distance [2.4083(6) Å], has been described as characteristic for the substituent *trans* to the lone pair,²³⁴ despite the fact that the lone pair of the heavy pnictines occupies an essentially pure *s*-orbital and should be stereochemically inactive.²¹ For **6.26**[OTf], it is therefore more reasonable to suggest that close coordination of the triflate anion *trans* to Cl₂ [Sb-O: 2.6793(17) Å vs. Σr_{vdw} : 3.72 Å]⁹ contributes electron density into the σ^* -

orbital of the Sb-Cl₂ bond, resulting in the observed increase in bond length. This is likewise the rationale for the lengthened Sb-Cl₂ bond [2.3926(8) Å vs. 2.3719(9) for Sb-Cl₁] observed in the solid-state structure of **6.24**[OTf], where the triflate anion is again coordinated *trans* to Cl₂. These Sb-O bonds are non-covalent in nature, as nearly equal S-O bond lengths in the triflate moiety (*e.g.* 1.4258(17) Å to 1.4596(17) Å in **6.26**[OTf]) are typical of anionic triflates.²³²



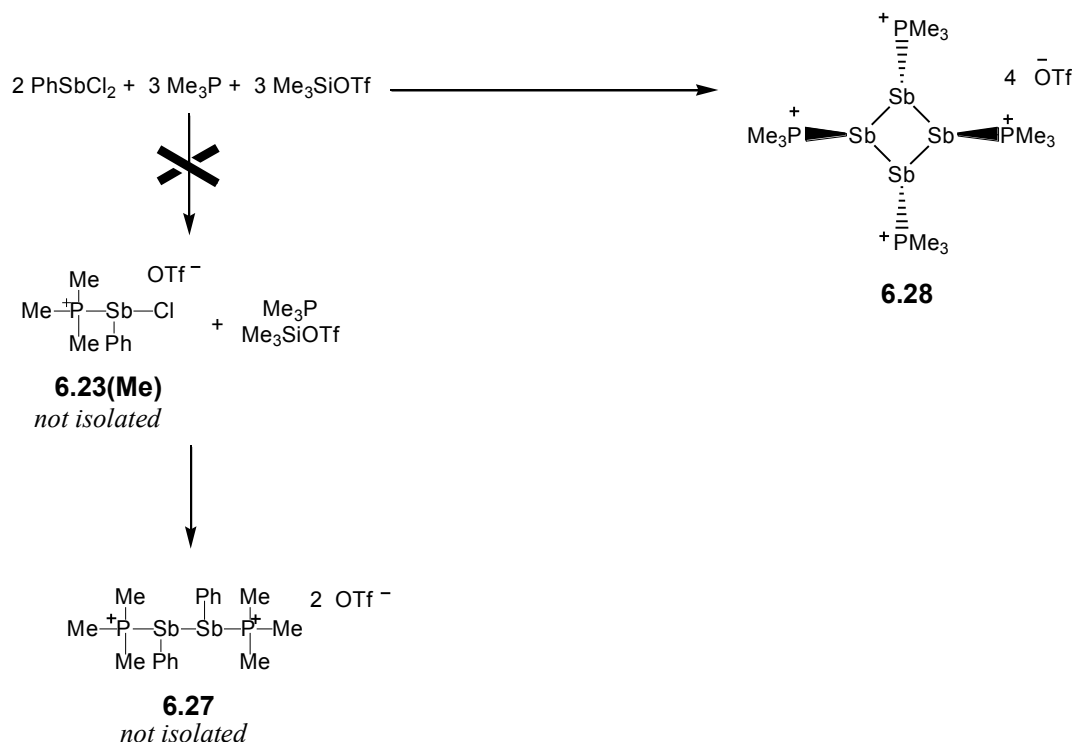
Scheme 6.4. The differing reactivity of P and Sb with 1-2 equivalents of phosphine.

The observation of this bisphosphine-stabilized stibonium centre along with the mono-stabilized stibonium species present a valuable opportunity for comparison between the chemistry of SbCl₃ and its lighter congener PCl₃. In spite of a comparatively strong P-Cl bond, reaction of the latter with Me₃P or Ph₃P and various halide abstractors (Me₃SiOTf or AlCl₃) yields only the corresponding triphosphenium cation [Me₃P-P-PMe₃]⁺ (**1.31**), even in the presence of a molar excess of PCl₃ (Scheme 6.4). In contrast, the reaction of

SbCl₃ with a phosphine donor and halide abstractor yields either [R₃P-SbCl₂]⁺ **6.24** (1:1) or [(R₃P)₂SbCl₂]⁺ **6.26** (1:2), depending primarily on the relative donor strength of the phosphine. This can be rationalized by considering not only the larger coordination sphere available on Sb, but also its tendency to favour the +3 oxidation state over the Pn(I) centre required for the formation of [R₃P-Sb-PR₃]⁺.¹⁰⁵ Moreover, as pπ-pπ overlap is poor for heavier atoms, additional π-donation from the donor phosphines is not present to stabilize Sb(I), where it offers substantial stabilization in the catena-phosphorus framework.²⁵⁰ Thus, the isolation of the a bis-phosphine stabilized [SbCl₂]⁺ centre re-emphasizes the characteristic differences between phosphorus and the heavier pnictogen elements.

6.3 Redistribution and Reductive Coupling: *Cyclo*-[{(Me₃P)Sb}₄]⁴⁺

As described in Chapter 2, reductive coupling of chlorophosphinophosphonium cations **2.1**[OTf] [Ph₃P-PRCl][OTf] has been demonstrated to be a generalizable, high yield method to acyclic dication **2.2**[OTf]₂ [Ph₃P-PR-PR-PPh₃][OTf]₂. Extension of this synthetic method to the chloro-functionalized stibinophosphonium analogues **6.23**[OTf] was therefore targeted as the next step in expanding the scope of this reaction. The one-pot reaction of PhSbCl₂, Me₃P and Me₃SiOTf (Scheme 6.5) in CH₂Cl₂ was expected to generate an intermediate chlorostibinophosphonium cation **6.23(Me)** and subsequently reductively couple two cations to generate the distibinodiphosphonium dication **6.27**.



Scheme 6.5. Attempted reductive coupling of PhSbCl₂ yielding the tetracation **6.28**[OTf]₄.

After 20 h at room temperature, no definitive assignment could be made for the major CH₂Cl₂-soluble product observed in the supernatant (³¹P NMR: -7.1 ppm). However, isolation and MeCN-dissolution of the white precipitate from the reaction yielded a ³¹P{¹H} NMR spectrum showing one broad singlet at -1.9 ppm. After an additional two weeks left standing at room temperature, slow evaporation of the MeCN-solution yielded several needle-like yellow crystals, identified by single-crystal X-ray diffraction as the unexpected cyclic tetracation, *cyclo*-[{(Me₃P)Sb}₄][OTf]₄·MeCN (**6.28**[OTf]₄·MeCN, Figure 6.6). The crystals were stable at room temperature and could be washed with CH₂Cl₂ with no change in appearance. However, once redissolved in MeCN, the complex reacted rapidly with trace amounts of CH₂Cl₂, resulting in precipitation of all phosphorus containing materials as an insoluble dark orange solid.

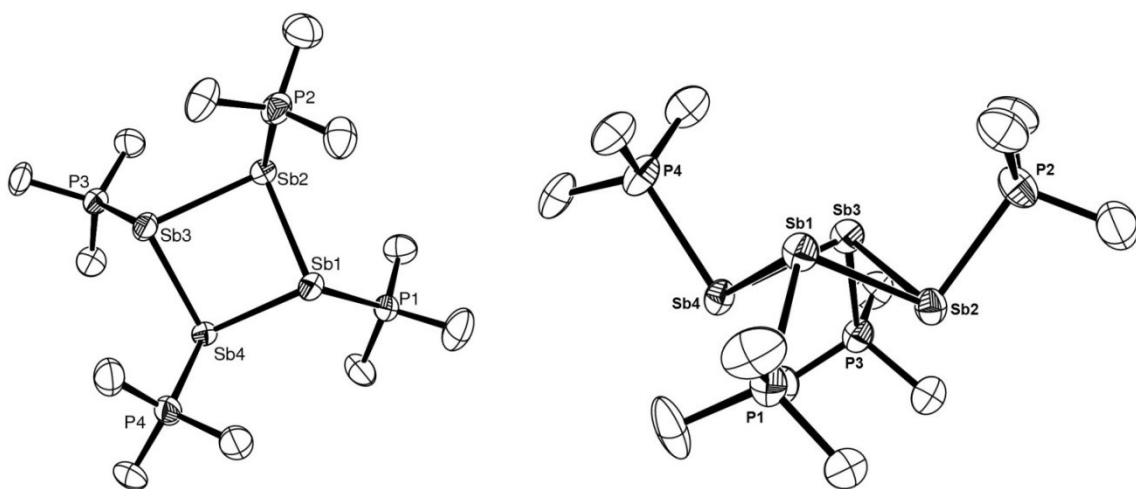


Figure 6.6. ORTEP representations of the solid-state structure of the cation in **6.28**[OTf]₄·MeCN from above and alongside the Sb₄-ring. Thermal ellipsoids are shown at 50% probability, and hydrogen atoms have been omitted for clarity. Unlabelled ellipsoids represent carbon atoms.

Structurally, the cation in **6.28**[OTf]₄ can be compared to the all-*trans*-substituted four-membered neutral stibine ring (^tBuSb)₄, presuming that the quaternized Me₃P centre [C-P-C: 104.9(6)^o-109.8(6)^o] possesses comparable steric bulk to a ^tBu-substituent (Table 6.3). The Sb-Sb distances are appreciably longer than those in the neutral ring²¹⁶ and lie at the upper end of the known range for Sb-Sb single bonds [2.843(1) Å in **6.9** (Me₃Sb-SbI₃·THF) and 2.859(1) Å in **6.10** (Me₃Sb-SbMeI₂)].²¹¹ The Sb-P distances [avg. 2.559(3) Å] are shorter than those found in the stibinophosphonium cations discussed in Section 6.2 [*cf.* 2.6043(9) Å in **6.24**], but still lie within the known range for covalent Sb-P bonds (Section 6.1.3). The exocyclic angles between the ring and phosphine donors are slightly smaller than the exocyclic angles in (^tBuSb)₄,²¹⁶ but the range of angles overlap sufficiently to be considered similar. While the E-Sb-Sb-E torsional angle (E = C, P) indicates comparable *trans*-substitution of both compounds, the remaining angles indicate a higher degree of folding in the tetracation relative to the

neutral species. This is best summarized in the calculated¹³¹ Cremer-Pople puckering parameter Q_2 , which describes the amplitude of the displacement of two atoms from a reference plane. The larger magnitude Q_2 amplitude of the tetracation is indicative of a more puckered or bent ring conformation in the solid state.

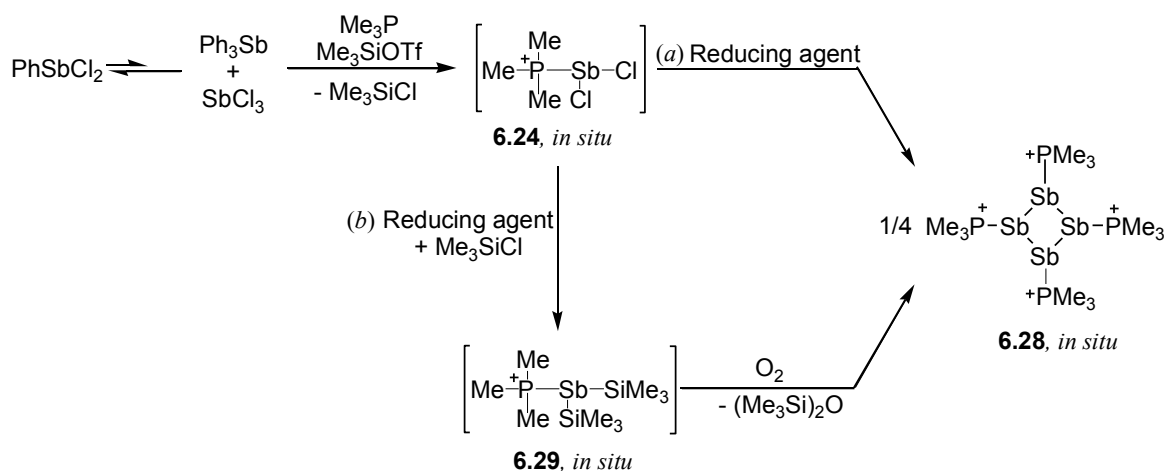
Table 6.3. Comparison of selected structural parameters in *cyclo*-[$\{(Me_3P)Sb\}_4\]^{4+}$ (**6.28**) vs. *cyclo*-(^tBuSb)₄. Single value parameters indicate the average.

	<i>cyclo</i> -[$\{(Me_3P)Sb\}_4\]^{4+}$ (E = P)	<i>cyclo</i> -(^t BuSb) ₄ (E = C)
Sb-Sb (Å)	2.8403(10)-2.8708(10)	2.814(2)-2.821(2)
Sb-E (Å)	2.551(3)-2.567(3)	<i>not relevant</i>
E-Sb-Sb (°)	94.16(7)-99.38(7)	97.7(5)-100.9(5)
Sb-Sb-Sb (°)	82.14(3)-83.30(3)	84.77(7)-85.18(6)
E-Sb-Sb-E (°)	127.14(10)-132.34(10)	130.7
Sb-Sb-Sb-E (°)	133.06(8)-136.52(7)	131.1
Sb-Sb-Sb-Sb (°)	39.12(3)-39.32(3)	32.9
Cremer-Pople puckering parameter, Q_2 (Å)	-1.0174(8)	-0.8330(16) ^a

^a Calculated using PLATON¹³¹ from coordinates reported in the original reference.²¹⁶

Tetracation **6.28** can be formally considered an Sb(I) species, which is relatively rare for Sb and entirely unknown for cationic or neutral Sb.¹⁰⁵ Only one previous report of a cyclic Sb(I) derivative exists in the literature, namely a Na-bridged dimer of the five-membered anion $[Sb(PCy)_4]^-$.²⁴¹ However, it should be noted that neutral cyclopolystibines are best considered Sb(III) species, despite their formal oxidation state

[Sb(I)]. This assignment is based on the premise that the number of available lone pairs at an atom better represents the chemistry, and therefore the oxidation state, of that atom.¹⁰⁵ Analogously, then, the tetracation in **6.28**[OTf]₄ is best structurally and chemically related to the phosphine-stabilized stibonium cations described earlier (Section 6.2), and therefore best assigned as Sb(III).



Scheme 6.6. Possible reaction pathways for the formation of **6.28**[OTf]₄, both of which involve substituent redistribution and reductive coupling.

The pathway for formation of **6.28**[OTf]₄ has not yet been determined, but the known substituent redistribution behaviour¹⁴⁸ of Ph₃Sb/SbCl₃ mixtures in the synthesis of PhSbCl₂ suggests that the reverse reaction might occur herein, even if only to a minimal degree (Scheme 6.6). SbCl₃ resulting from this disproportionation would be expected to undergo halide abstraction to yield **6.24**[OTf] *in situ*. Notably, the ³¹P NMR signal observed for the MeCN-soluble fraction of the reaction (-2 ppm) was substantially downfield of the resonance expected for **6.24** (16 ppm), suggesting perhaps that [Me₃P-SbPhCl]⁺ was formed *in situ* as originally expected, and the requisite Ph/Cl-substituent exchange occurred on the resulting cation to yield trace amounts of

6.24 over a two week period. Reduction of **6.24** to **6.28** might then occur directly, with Me_3P or SbPh_3 acting as reducing agents [Scheme 6.6(a)]. Conversely, in the presence of Me_3SiCl (produced by formation of the cation), reductive Si-Sb coupling might also occur, forming cation **6.29** [Scheme 6.6(b)]. This behaviour is known for neutral ArSbCl_2 in the presence of Me_3SiCl and Mg metal, in which case the presence of adventitious oxygen prompts the elimination of trimethylsilylether and formation of six-membered neutral rings $(\text{ArSb})_6$ in the solid state.^{224,225} Therefore, the formation of several crystals of **6.28** may be proposed to result from trace oxygen over a two week period. Finally, Li reduction of Ph_3Sb has been previously demonstrated to produce anionic $[\text{Ph}_2\text{Sb}]^-$ or $[\text{Ph}_2\text{Sb-Sb-SbPh}_2]^-$ by Ph-abstraction rather than the more traditional reduction of chlorostibines.^{214,251} Thus, direct reduction of the $[\text{Me}_3\text{P-SbPhCl}]^+$ intermediate by Me_3P or Ph_3Sb might also be envisioned. The comparatively weak reducing strength of these reagents does, however, render this path less likely.

The irreproducibility of the synthesis of crystalline **6.28** suggests that the mechanistic pathway is either strongly kinetically disfavoured relative to other possible products or may involve adventitious reagents, such as trace SbCl_3 in the sample of PhSbCl_2 or trace O_2 in the glovebox. Attempts to systematically synthesize **6.28** from either isolated or in situ **6.24** by reduction with Ph_3P , Me_3P , Cp_2Co , $\text{Li}[\text{Ph}_2\text{Sb}]$,²⁵¹ SbPh_3 , or SbBu_3 were unsuccessful, yielding only **6.24** or unidentifiable insoluble black precipitates, potentially corresponding to a mixture of oligomeric $(\text{RSb})_n$ compounds¹⁴⁹ or to metallic antimony.

Nonetheless, the isolation of **6.28** $[\text{OTf}]_4$, even as a minor byproduct of this reaction, provides preliminary evidence for the potential utility of reductive coupling in the synthesis of novel cationic *catena*-antimony species.

6.4 Summary

A series of mono- and bis-phosphine stabilized chlorostibonium cations have been isolated and characterized in the solution and solid state. These functionalized cations provide an entry point for the development of increasingly catenated Sb-cations.

Fortuitous isolation of a phosphine-stabilized tetracationic tetra-antimony ring **6.28**[OTf]₄ provides lends support to the possibility of extending reductive coupling methodologies from the *catena*-phosphorus domain (established in Chapter 2 and Chapter 3) to heavier antimony analogues.

Chapter 7. Conclusions

7.1 Summary

The development of synthetic methods in cationic polyphosphorus chemistry has only begun to explore generalizable, logical routes to new frameworks within the past ten or so years, so enormous capacity for expansion in this realm is yet possible. Specifically, present methods towards cationic *catena*-phosphorus species rely heavily on existing neutral polyphosphorus starting materials which, besides requiring additional synthetic steps, bias the synthesis of new cationic frameworks towards architectures that originate in neutral phosphorus chemistry.

In an effort to develop new routes to *catena*-phosphorus cations that might avoid the need for neutral polyphosphines, this thesis focused on the reactivity of chloro-functionalized phosphinophosponium cations as building blocks towards novel cationic motifs. Of primary utility was the reductive coupling of mono-, di- and tri-chloro derivatives of the phosphinophosponium framework, which was used to access a diverse array of acyclic and monocyclic cations. Significantly, a number of these frameworks were chloro-functionalized themselves, opening the door to future reactivity at these sites, particularly with the use of SbPh_3 and SbBu_3 , which have been demonstrated herein as very effective reductants for cationic polyphosphorus systems. Conversely, the first electrochemical studies of phosphinophosponium cations have been conducted, suggesting significant mechanistic differences between electroreduction and chemical reduction processes.

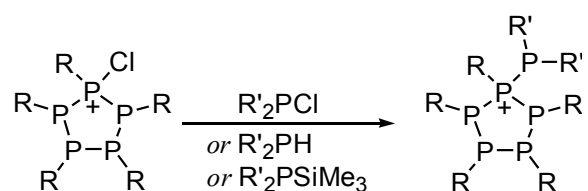
The systematic study of the reactivity of these chlorophosphinophosponium cations also presented an opportunity to compare the competitive synthesis of acyclic dicationic 3P

vs. 4P frameworks, as well as *cis* vs. *trans* isomers of five-membered cyclic dications, with the first reported *cis*-substituted frameworks being reported herein. The solution dynamics of [¹Pr₇P₅][OTf] presented here additionally represent an important link in the understanding of the steric requirements in these dications, and presents a new example of a potentially low inversion barrier for a *catena*-phosphorus system.

Finally, the synthesis and isolation several chloro-functionalized stibinophosphonium cations and the adventitious observation of the reductive coupling to yield the tetracation salt [Me₃PSb]₄[OTf]₄ opens the door to possible extension of this work towards systematic synthetic methods in *catena*-antimony chemistry.

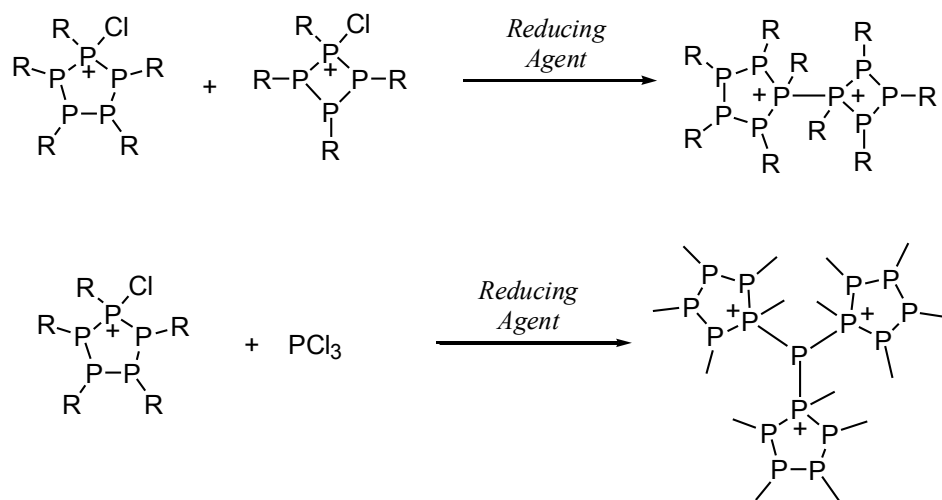
7.2 Future Work

The opportunities to expand on the chemistry of functionalized phosphinophosphonium cations are extensive, owing to the simple fact that so few functionalized frameworks are known among cationic polyphosphorus frameworks, so the area remains relatively unexplored in terms of its potential synthetic utility. As a simple example, the larger chloro-functionalized frameworks developed in Chapter 3 provide diverse new cationic starting materials for the synthesis of branched polyphosphorus cations, which are as yet unknown (*e.g.* Scheme 7.1).



Scheme 7.1. Synthesis of branched *cyclo*-polyphosphorus cations from chloro-functionalized cations.

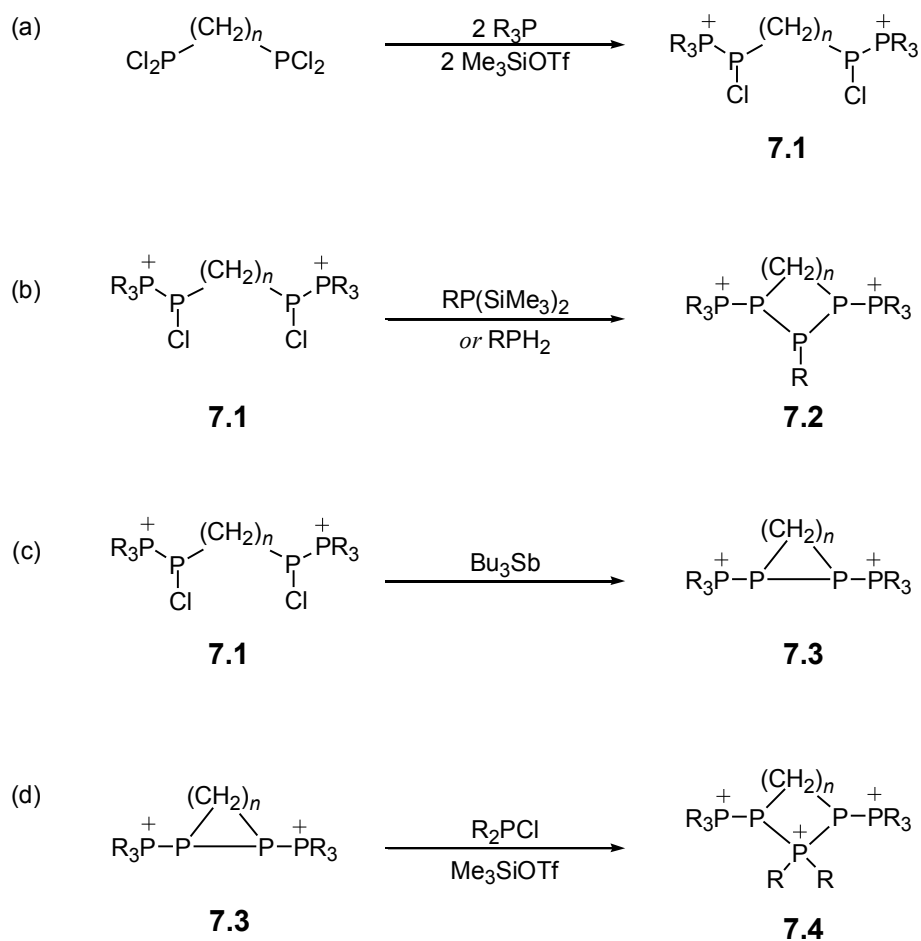
Additionally, chloro-functionalized cationic frameworks can be regarded as potential starting materials for the synthesis of polycyclic phosphorus cations, of which only three examples are presently known.⁷⁰ Promise of the potential utility of chloro-functionalized phosphinophosphonium cations in the synthesis of larger polycycles was evidenced by the proposed P₉ dication **3.11**, formed by the *in situ* reductive coupling of two smaller monocyclic chloro-functionalized cations. Whereas the synthesis of neutral polycyclic polyphosphines, typically by reductive coupling of R₂PCl₂ or *cyclo*-(PR)_n and PCl₃ with Mg, relies solely on the thermodynamic or kinetic stability of the products to determine the arrangement of atoms in the product, synthesis of polycycles from cationic rings and chains with specifically positioned Cl-functionalities may be used to favour the generation of specific architectures (e.g. Scheme 7.2).



Scheme 7.2. Systematic generation of polycyclic polycations from chloro-functionalized cationic phosphorus rings.

Ligand exchange on the 2,3-diphosphino-1,4-diphosphonium framework **2.2** with carbon-bridged diphosphines (Section 2.4.3) highlights the potential utility of ring strain and the well-known pentagonal stability⁵⁰ of *cyclo*-polyphosphorus frameworks as mechanisms

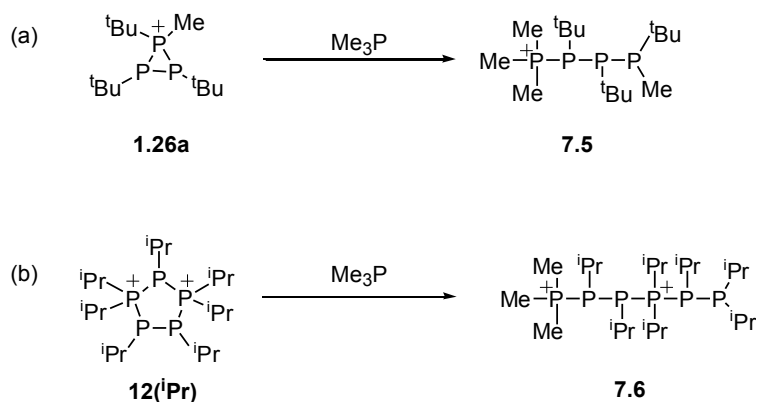
to target new cyclic cations. As an alternative to using diphosphines as the donor (phosphonium) sites in cationic frameworks, it would be of significant interest to investigate the use of chloro-functionalized diphosphines of the type $\text{Cl}_2\text{P}-(\text{CH}_2)_n-\text{PCl}_2$, including the ethane, methane, and more rigid benzene linkers. Reaction of these diphosphines with two equivalents of a donor phosphine and a halide abstractor should readily generate the bis(phosphinophosphonium) dication **7.1** (Scheme 7.3a). Addition of bifunctional phosphines could potentially result in $[x+1]$ cycloaddition behaviour, generating mixed carbon-phosphorus ring systems **7.2** (Scheme 7.3b), which would represent examples of a dicationic five-membered acyclic P-framework $[\text{R}_3\text{P-PR-PR-PR-PR}_3]^{2+}$, the first example of which is described in this thesis (Section 2.4.3). Alternately, addition of a reducing agent such as SbBu_3 to **7.1** could potentially result in ring closure and synthesis of the strained three- and four-membered heterocycles **7.3** (Scheme 7.3c). One example of a diphosphinodiphosphonium framework possessing this architecture (**2.0a**, $n = 1$) is known in the literature,²⁵² but no further work has been done to investigate its synthetic utility. The substantial ring strain in **7.3** may allow for phosphonium insertion into the endocyclic P-P bond, resulting in the first example of a tricationic polyphosphorus framework not originating from the P_4 tetrahedron (**7.4**, Scheme 7.3d).



Scheme 7.3. Proposed synthesis and potential reactions of bridged bis(phosphinophosphonium) dications.

Besides expanding the chemistry of functionalized phosphinophosphonium cations, it would also be valuable to investigate the chemistry and electrochemistry of the now diverse examples acyclic and cyclic cationic frameworks described herein. As an example, ring-opening of the strained three-membered ring **1.26a** is at present the only known route to terminal acyclic monocations **7.5** $[\text{R}_3\text{P-PR-PR-PR}_2]^+$ (Scheme 7.4a).⁶⁵ With sufficient steric bulk, other cationic ring systems may likewise be vulnerable to nucleophilic ring-opening reactions. For example, the dication $[\text{}^i\text{Pr}_7\text{P}_5]^{2+}$ was shown

herein to undergo chloride-induced ring-opening under mild conditions (Section 3.4), so introduction of a stoichiometric amount of stronger nucleophile may provide an alternative ring-opening product (Scheme 7.4b). While **7.6** may itself be subject to subsequent rearrangement or decomposition, the steric bulk of the isopropyl substituents may offer sufficient kinetic stabilization for the NMR observation and isolation of **7.6** or any of its potential acyclic decomposition products.



Scheme 7.4. Ring-opening of cationic *catena*-phosphorus rings by attack of strong nucleophiles.

Finally, both the reactivity of chlorostibinophosphonium cations and the electrochemistry of both cationic *catena*-phosphorus and *catena*-antimony derivatives should be considered very much in their infancy. Extensive possibilities exist for the potential reductive coupling of antimony systems, but as it is prone to reduction to metallic-Sb, electrochemical studies may provide substantial insight into the precise redox potentials to favour cationic products. In addition to further cyclic voltammetric work, coulometry and controlled potential electrolysis should be investigated to provide a complete picture of the complex reactivity of these cationic small molecule building blocks.

Chapter 8. Experimental

8.1 General

Unless otherwise specified, reactions were carried out in a glove box under an inert N₂ atmosphere. Small amounts (< 0.2 mL) of liquid reagents were measured using an Ependorff pipettor (10-100 μL) unless otherwise specified. Solvents were dried on an MBraun solvent purification system and stored over 4 Å molecular sieves unless otherwise specified. MeCN was purchased anhydrous from Aldrich and used as received, Et₂O was dried by heating at reflux temperature over Na/benzophenone and distilled before use, and CHCl₃ was degassed by three freeze-pump-thaw cycles and stored over molecular sieves for 24 h before use. For electrochemical analyses, acetonitrile was purchased anhydrous from Aldrich (99.8% purity or 99.93% purity, biotechnical grade), sparged with Ar for a minimum of 1 h, and stored over 3 Å molecular sieves for a minimum of 24 h before use. Deuterated solvents were purchased from Aldrich or Cambridge Isotope Laboratories, and used as received (CD₃CN, CD₃NO₂ in ampoules), or stored over molecular sieves for 24 hours prior to use (CDCl₃).

Me₂PCl and MePCl₂ were purchased from Strem and used as received. Ph₃P, ¹Pr₂PCl, ¹PrPCl₂, ¹BuPCl₂, Et₃P, SbPh₃ and Me₃P (neat and 1.0 M solution in toluene) were purchased from Aldrich and used as received. Ph₂PCl, PhPCl₂, EtPCl₂, and Me₃SiOTf were purchased from Aldrich and purified by vacuum distillation prior to use. GaCl₃ was purchased from Strem and sublimed under static vacuum prior to use. SbCl₃ and FeCp₂ were purchased from Aldrich and sublimed under static vacuum prior to use.

Tetra-*n*-butylammonium hexafluorophosphate (TBAPF₆) was purchased from Aldrich

and dried under vacuum between 60-80°C for 24 h before use. Tetra-*n*-butylammonium triflate (TBAOTf) was purchased from Aldrich and dried under vacuum at 60°C for 48 h. Me₃SiCl was purchased from Aldrich, degassed by three freeze-pump-thaw cycles, distilled under static vacuum, and stored over 3Å sieves for 18-24 h before use. Ph₃P (99%) was purchased from Aldrich and used as received. SbⁿBu₃ was used as received (supplier unknown). AgNO₃ was used as received from BASi analytical.

CyPCl₂ was prepared according to literature methods.²⁵³ The synthesis of (¹Pr₂N)PCl₂ was adapted from the literature, but performed instead at -78°C in CH₂Cl₂.²⁵⁴ The solvent was then removed *in vacuo*, and the product extracted from the residues with hexanes. Removal of hexanes *in vacuo* yielded the desired product, which was used without further purification. [Ph₃P-PPh₂][OTf],^{83,88} **1.24(Ph)**, [R₂(Cl)P-PR₂][GaCl₄],^{84,116} **1.34(Ph)** and **1.34(Me)**, [Ph₃P-PRCl][OTf],^{80,81} **2.1(Ph)** and **2.1(Me)**, [Ph₃P-PR-PR-PPh₃][OTf]₂,⁸⁰ **2.2(Ph)** and **2.2(Me)**, [Me₃P-PR-PR-PMe₃][OTf]₂, **2.2'(Ph)** and **2.2'(Me)**, PhSbCl₂,^{148,255} were prepared according to literature methods.^{84,116}

8.2 NMR Spectroscopy

Solution ¹H, ¹³C, and ³¹P NMR spectra were collected at room temperature on Bruker AC-250 (5.9 T) and Bruker Avance 500 (11.7 T) NMR spectrometers. Chemical shifts are reported in ppm relative to trace protonated solvent (¹H), to perdeuterated solvent (¹³C), or to an external reference standard (³¹P, 85% H₃PO₄ and ¹⁹F, 0.5% CF₃C₆H₅ in CDCl₃ at -63.72 ppm).** NMR spectra of reaction mixtures were obtained by transferring

** The ¹⁹F NMR chemical shift of a free triflate ion is expected to lie approximately within the range -77 to -79 ppm.²⁵⁶

an aliquot of the bulk solution to a 5 mm NMR tube, which was then capped and sealed with Parafilm. All reported $^{31}\text{P}\{^1\text{H}\}$ NMR parameters for second-order spin systems (except [**3.9**(**iPr**)] $[\text{GaCl}_4]_2$, **4.1**[OTf], **4.2**[OTf] and **4.7**[OTf] $_2$) were derived by iterative simulation of experimental data obtained at both fields (^{31}P Larmor frequencies of 101.3 MHz and 202.6 MHz) using gNMR, version 4.0 or 5.0.6.0.^{257,258} Typically, the higher field experimental spectrum was used to find the spin system parameters, and the lower field data was subsequently used to ensure the parameters were valid at both fields. For [**3.9**(**iPr**)] $[\text{GaCl}_4]_2$ (188 K), **4.1**[OTf], **4.2**[OTf] and **4.7**[OTf] $_2$, only data acquired at 101.3 MHz was used for iterative fitting and determination of $^{31}\text{P}\{^1\text{H}\}$ NMR parameters. For [**3.8**(**Ph**)] $[\text{GaCl}_4]$, data acquired at 298 K and 202.6 MHz showed line broadening that prevented a viable simulation, so the sample was cooled to 280 K. Difference calculations between simulated and experimental spectra were produced with Bruker Topspin, version 2.0,²⁵⁹ using data at 202.6 MHz. The signs of the P–P coupling constants have been established by assigning the $^1J_{\text{PP}}$ coupling constants as negative.^{128,151} Product distributions for *in situ* reaction mixtures were assessed by integration of assigned signals in the ^{31}P NMR spectra. ^{31}P NMR integrations are approximate, but are estimated to be accurate to within $\pm 10\%$ for identical coordination numbers, or $\pm 20\%$ otherwise.²⁶⁰ Letter designations for the phosphorus spin systems have been assigned by calculating the ratio $|\Delta\nu/J|$, where $\Delta\nu$ is the difference in ^{31}P chemical shifts in Hz, and using a value of 10 at the lower field as the threshold between a first and second order letter designation.

8.2.1.1 Dynamic NMR Analysis of **3.9(iPr)**

Temperatures reported above 298 K for $^{31}\text{P}\{^1\text{H}\}$ NMR spectra of **[3.9(ⁱPr)][GaCl₄]₂** were calibrated against a neat ethylene glycol standard according to equations reported by Ammann *et al.*²⁶¹ Temperatures below 298 K are reported based on a linear plot of observed temperatures vs. temperatures calculated²⁶¹ from ^1H NMR measurements of a neat MeOH standard over the range 188-309 K. Errors in temperature calibration are assumed to be negligibly small relative to the error in k . This assumption is reasonable in view of the fact that temperature calibration by exchange of the sample tube for a neat MeOH standard at each temperature is expected to have an accuracy of $\pm 1^\circ\text{C}$.²⁶² To account for variations due to the exchange of the MeOH and sample NMR sample tubes, temperatures were calibrated across the range of 188 K to 294 K and plotted against observed temperatures. The resulting curve was linear, with a calculated standard deviation of $\pm 2^\circ\text{C}$. The error in $1/T$ is therefore $\sigma_{1/T} = \sigma_T/T^2 = 2/T^2$ (see Appendix A1), which was calculated to be less than 1% in all cases.

Rate constants k (Table 8.1) for the solution dynamics of **[3.9(ⁱPr)][GaCl₄]₂** in EtCN (*ca.* 0.04 M) were calculated by line-shape analysis using dynamic NMR as implemented in gNMR version 5.0.6.0,²⁵⁸ assuming a two site exchange between P1/P3 and P4/P5. Data from temperatures above 292 K were omitted owing to observed thermal decomposition of **3.9(ⁱPr)** to **3.5(ⁱPr)**. Data from temperatures below 246 K were omitted as the small magnitude rate constants resulted in estimated errors in k on the same order of magnitude as k itself. Weighted linear regression and error analysis of the Eyring plot data $[\ln(k/T) \text{ versus } 1/T]$ ²⁶² was performed using Octave²⁶³ and plotted using

Sigmaplot.²⁶⁴ Details of the regression and error analysis for ΔH^\ddagger , ΔS^\ddagger and ΔG^\ddagger can be found in the Appendix A1.

Table 8.1. Rate constants determined by lineshape analysis of $^{31}\text{P}\{^1\text{H}\}$ NMR spectra of $[\mathbf{3.9}(\text{iPr})][\text{GaCl}_4]_2$ in EtCN.

Temperature (K)	$\log_{10}k$	error in $\log_{10}k$	k (Hz)
246	1.6693	0.1989	46.7
255	2.1434	0.0617	139.1
264	2.5266	0.0528	336.2
273	2.8237	0.1472	666.3
282	3.1104	0.1093	1289.4
291	3.4544	0.1166	2847.1

8.3 Miscellaneous Instrumental Analyses

Infrared spectra were collected on samples prepared as nujol mulls between CsI plates using a Bruker Vector FT-IR spectrometer. Peaks are reported in wavenumbers (cm^{-1}) with either ranked intensities or relative intensities (strong, medium, weak) in parentheses. For ranked intensities, a value of one corresponds to the most intense peak in the spectrum. Melting points were obtained using an Electrothermal apparatus, on samples flame-sealed in glass capillaries under dry nitrogen. Electrospray ionization mass spectrometric (ESI-MS) analyses were performed on a Bruker Daltonics microTOF instrument in both positive and negative ion modes. Instrument parameters were set as follows: spray voltage 4500 V (positive) or 3300 V (negative); nebulizer gas (N_2) 1 bar; dry gas (N_2) 4 L/min; dry temperature 180°C; exit voltage of the heated capillary 130 V (positive) or 90 V (negative); and sample flow rate 2 $\mu\text{L}/\text{min}$. Observed peaks with intensities $\geq 2\%$ relative to the base peak are reported. Only glass syringes were used in

the preparation of samples, to avoid cross-contamination by trace impurities found on typical polypropylene or polyethylene syringes.

8.4 X-ray Crystallography

Unless otherwise stated, crystals for single crystal X-ray diffraction studies were obtained by vapor diffusion at room temperature. Samples were dissolved in a minimal amount (1-2 mL) of a polar solvent in a 5 mL vial placed within a capped 20 mL vial containing ~ 5 mL of a less polar solvent (solvents are indicated in the text as polar/non-polar pairs). After deposition of crystals, the solvent was carefully removed using a pipette and the crystals were coated with Paratone oil. Single crystal X-ray diffraction data from the University of New Brunswick were collected using a Bruker AXS P4/SMART 1000 diffractometer. All measurements were made with graphite monochromated Mo-K α radiation. The data were reduced (SAINT)²⁶⁵ and corrected for absorption (SADABS)²⁶⁶ and were corrected for Lorentz and polarization effects. The structures were solved using direct methods and expanded using Fourier techniques. Full matrix least squares refinement was carried out on F^2 data using the program SHELX97.²⁶⁷ Non-hydrogen atoms were refined anisotropically.

Single crystal X-ray diffraction data from the University of Alberta were collected on a Bruker D8/APEX II CCD diffractometer at 173 K using ω scans with a width of 0.3° and 15 s exposures. All measurements were made with graphite monochromated Mo K α radiation (0.71073 Å). The data were corrected for absorption through Gaussian integration from indexing of the crystal faces. The structures were solved using direct methods (SHELXS-97)²⁶⁸ and refined by full-matrix least squares on F^2 (SHELXL-97)²⁶⁸.

All non-hydrogen atoms were refined anisotropically while hydrogen atoms were assigned positions based on the sp^2 or sp^3 hybridization geometries of their attached carbons, and were given thermal parameters 20% greater than those of their parent atoms.

Crystallographic experimental details are summarized in Section 8.9.

8.4.1 Synthesis and Characterization of Compounds in Chapter 2

8.4.1.1 $[\text{Ph}_3\text{P-PPh}(\text{Cl})][\text{GaCl}_4]$, **[2.1(Ph)][GaCl₄]**

PhPCl_2 (27.1 μL , 0.20 mmol) was added to a stirred solution of Ph_3P (52 mg, 0.20 mmol) and GaCl_3 (39 mg, 0.22 mmol) in CH_2Cl_2 (1 mL). After 15 min, the $^{31}\text{P}\{^1\text{H}\}$ NMR spectrum of the reaction showed near quantitative formation of **[2.1(Ph)][GaCl₄]** (94%) along with $\text{PhPCl}_2\text{-GaCl}_3$ (156 ppm). Attempted isolation by addition of Et_2O yielded an oil.

8.4.1.2 $[\text{Me}_3\text{P-PPh}(\text{Cl})][\text{OTf}]$, **[2.1'(Ph)][OTf]**

Me_3P (1.0 M in toluene, 2 x 100.0 μL , 0.20 mmol) was added to a stirred solution of PhPCl_2 (27.1 μL , 0.20 mmol) and Me_3SiOTf (39.8 μL , 0.22 mmol) in CH_2Cl_2 (0.80 mL). After 1.5 h, the $^{31}\text{P}\{^1\text{H}\}$ NMR spectrum of this reaction mixture showed quantitative formation of **[2.1'(Ph)][OTf]**.

8.4.1.3 General procedure for $[\text{Ph}_3\text{P-PR}'(\text{Cl})][\text{OTf}]$, **2.1[OTf]**

$\text{R}'\text{PCl}_2$ (0.20 mmol, $\text{R}' = \text{Me, Et, } ^i\text{Pr, Cy}$) was added to a stirring solution of Ph_3P (52 mg, 0.20 mmol) in CH_2Cl_2 (0.5-1 mL) followed immediately by the addition of Me_3SiOTf

(39.8 μL , 0.22 mmol). Attempted isolation of **[2.1][OTf]** by addition or vapour diffusion of Et_2O yielded an oil when $\text{R}' = \text{Et}$, ${}^i\text{Pr}$, or Cy .

$[\text{Ph}_3\text{P-PMe}(\text{Cl})][\text{OTf}]$, **[2.1(Me)][OTf]**: After 1 hour, the ${}^{31}\text{P}\{^1\text{H}\}$ NMR spectrum of the reaction showed quantitative formation of **[2.1(Me)][OTf]**. Vapour diffusion of Et_2O into this solution overnight at room temperature afforded colorless needle-like crystals that were washed with Et_2O (2 x 1 mL) and dried *in vacuo*.

Yield (crystalline): 63 mg (64%);

m.p. 117-119.5°C;

FT-IR: 3063 (19), 1586 (10), 1443 (5), 1260 (1), 1189 (20), 1144 (13), 1106 (15), 1029 (7), 996 (16), 891 (18), 873 (8), 751 (6), 725 (14), 690 (4), 637 (2), 573 (11), 545 (9), 506 (3), 460 (17), 301 (12);

Crystal Data: Table 8.2.

$[\text{Ph}_3\text{P-PEt}(\text{Cl})][\text{OTf}]$, **[2.1(Et)][OTf]**: Quantitative formation of **[2.1(Et)][OTf]** was observed after 10 min by ${}^{31}\text{P}\{^1\text{H}\}$ NMR.

$[\text{Ph}_3\text{P-Pr}(\text{Cl})][\text{OTf}]$, **[2.1(Pr)][OTf]**: **[2.1(Pr)][OTf]** was observed as broad resonances (82 ppm and 16 ppm) at 298 K in the ${}^{31}\text{P}\{^1\text{H}\}$ NMR spectrum of the solution after 1 h, together with ${}^i\text{PrPCl}_2$ (*ca.* 15%). Quantitative formation of **[2.1(Pr)][OTf]** was observed at 213 K.

$[\text{Ph}_3\text{P-PCy}(\text{Cl})][\text{OTf}]$, **[2.1(Cy)][OTf]**: **[2.1(Cy)][OTf]** was observed as broad resonances (76 ppm and 18 ppm) at 298 K in the ${}^{31}\text{P}$ NMR spectrum of the reaction mixture after 1 h,

together with CyPCl₂ (*ca.* 23%). Quantitative formation of **[2.1(Cy)][OTf]** was observed at 202 K.

8.4.1.4 [Me₃P-PCy(Cl)][OTf], **[2.1'(Cy)][OTf]**

Me₃P (1.0 M in toluene, 3 x 73.4 μL, 0.22 mmol) was added to a stirred solution of CyPCl₂ (41.4 mg, 0.22 mmol) in CH₂Cl₂ (1 mL) yielding a white precipitate. Upon addition of Me₃SiOTf (43.8 μL, 0.24 mmol), this solid re-dissolved and a white precipitate was formed after a further 5 minutes of stirring. The ³¹P{¹H} NMR spectrum of this reaction mixture after 1 h showed the presence of only **[1'e][OTf]**.

8.4.1.5 [Ph₃P-P^tBu(Cl)][OTf], **[2.1(^tBu)][OTf]**

A solution of Ph₃P (105 mg, 0.40 mmol) in CH₂Cl₂ was added to a stirred solution of ^tBuPCl₂ (64 mg, 0.40 mmol) in CH₂Cl₂ (total volume *ca.* 1 mL), followed immediately by the addition of Me₃SiOTf (79.6 μL, 0.44 mmol). The ³¹P{¹H} NMR spectrum (213 K) of the reaction mixture after 2 h was interpreted as a mixture of **[2.1(^tBu)][OTf]** and ^tBuPCl₂ (200.0 ppm). The ³¹P{¹H} NMR spectrum (213 K) of the reaction mixture after 48 h indicated the presence of small amounts of [Ph₃PCl][OTf] and **[2.3(^tBu)][OTf]** ([Ph₃P_M-P_A^tBu-P_X^tBu(Cl)][OTf] – AMX spin system δ_A = -2 (t), δ_M = 24 (dd), δ_X = 112 ppm (dd); ¹J_{AM} = 345, ¹J_{AX} = 338, ²J_{MX} = 86 Hz.

8.4.1.6 [Ph₃P-P^tBuCl][GaCl₄], **[2.1(^tBu)][GaCl₄]**

A mixture of Ph₃P (52 mg, 0.20 mmol), ^tBuPCl₂ (32 mg, 0.20 mmol) and GaCl₃ (39 mg, 0.22 mmol) in CH₂Cl₂ (1 mL) was stirred for 1 h at room temperature, and the ³¹P{¹H}

NMR spectrum at 298 K was interpreted as a mixture of ^tBuPCl₂-GaCl₃ (184 ppm, 98%,) and [2.1(^tBu)][GaCl₄] (2%).

8.4.1.7 [Me₃P-P^tBu(Cl)][OTf], [2.1'(^tBu)][OTf]

Me₃P (1.0 M in toluene, 2 x 100 μL, 0.20 mmol) was added to a stirred solution of ^tBuPCl₂ (32 mg, 0.20 mmol) in CH₂Cl₂ (0.5-1 mL), followed immediately by the addition of Me₃SiOTf (39.8 μL, 0.22 mmol) and the ³¹P{¹H} NMR spectra of this solution showed nearly quantitative formation of [2.1'(^tBu)][OTf].

8.4.1.8 [Me₃P-P^tBu(Cl)][GaCl₄], [2.1'(^tBu)][GaCl₄]:

Me₃P (1.0 M in toluene, 220 μL, 0.22 mmol) was added to a stirred solution of ^tBuPCl₂ (32 mg, 0.20 mmol) in CH₂Cl₂ (0.5 mL), followed immediately by the addition of GaCl₃ (79.6 μL, 0.44 mmol) in CH₂Cl₂ (0.5 mL). After 1 h, the ³¹P{¹H} NMR spectrum showed essentially quantitative formation of [2.1'(^tBu)][GaCl₄].

8.4.1.9 Phosphenium exchange studies

[PPh₂]⁺/[PhPCl]⁺ exchange

Formation of [Ph₃P-PPh₂][OTf], [1.24(Ph)][OTf], from [Ph₃P-PPh(Cl)][OTf], [2.1(Ph)][OTf]: Addition of Ph₂PCl (26.9 μL, 0.15 mmol) to a stirred solution of [2.1(Ph)][OTf], (83 mg, 0.15 mmol) in CH₂Cl₂ afforded partial conversion to [1.24(Ph)][OTf] and PhPCl₂ (162 ppm) after 30 min (5:1 ratio of 1.24:2.1, as observed by ³¹P{¹H} NMR spectroscopy). No further reaction was observed after 18 h at room temperature. Addition of 0.2 equivalents of Me₃SiOTf at the start of the reaction afforded the same product distribution, but the ³¹P{¹H} NMR signals for both

phosphinophosphonium salts were resolved into doublets at room temperature. Addition of 1.1 equivalents of Me₃SiOTf at the start of the reaction afforded greater conversion to [Ph₃P-PPh₂][OTf] (9:1 after 30 min and 12:1 after 18 h). In contrast, addition of PhPCl₂ (27.1 μL, 0.20 mmol) to a stirred solution of [Ph₃P-PPh₂][OTf] (119 mg, 0.20 mmol) afforded predominantly (> 90% by ³¹P NMR integration) starting materials

[PMe₂]⁺/[PPh₂]⁺ exchange

Me₂PCl (11.9 μL, 0.15 mmol) was added to a stirred solution of [Ph₃P-PPh₂][OTf] (88 mg, 0.15 mmol) in CH₂Cl₂ and allowed to stir for 30 min. The ³¹P{¹H} NMR spectrum of the reaction mixture after 30 min showed extremely broad singlets centered at 82 ppm, 19 ppm, -10 ppm, and -57 ppm. This spectrum was ascribed to a mixture of Ph₂PCl (82 ppm), [Ph₃P-PPh₂][OTf] (15 ppm, -10 ppm) and [Ph₃P-PMe₂][OTf] (15 ppm, -58 ppm), all undergoing rapid exchange in solution. No obvious preference for either phosphinophosphonium species was observed.

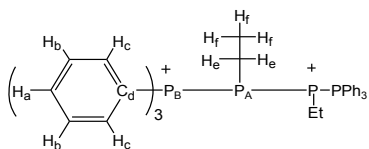
8.4.1.10 [Ph₃P-PEt-PEt-PPh₃][OTf]₂, [**2.2(Et)**][OTf]₂

[**2.1(Et)**][OTf] (1.0 mmol) was prepared *in situ* in a 50 mL 1-necked bulb containing 5 mL CHCl₃. Me₃SiOTf (100.0 μL, 0.55 mmol) and Ph₃P (132 mg, 0.50 mmol, in *ca.* 2 mL CHCl₃) were added, and the solution was degassed by three freeze-pump-thaw cycles and sealed at reduced pressure. This solution was heated at reflux temperature (~55°C) in the closed system for 48 h. The supernatant was decanted from the resulting white precipitate, which was then washed with cold CH₂Cl₂ (-40°C, 2 x 0.5 mL) and Et₂O (2 x 1 mL). Addition of Et₂O (~4 mL) to the supernatant gave a white precipitate, which was

isolated by decantation and washed with cold CH₂Cl₂. Colourless needle-like crystals were obtained by vapour diffusion from MeCN/Et₂O.

Yield (powder): 0.249 g (53% based on EtPCL₂);

m.p. 201-203°C;



¹H NMR (500.1 MHz, CD₃CN, 298 K): δ = 7.91 (vt, 6H, H_a), 7.85 (vq, 12H, H_b), 7.74 (vt, 12H, H_c), 1.93 (m, 3H, H_e), 0.55 ppm (m, 6H, H_f);

¹³C NMR (125.8 MHz, DEPTQ135, CD₃CN, 298 K): δ = 136.91 (s, +, C_{a/b}), 135.07 (s, +, C_{a/b}), 132.06 (t, +, C_c), 119.07 (t, -, C_d), 14.26 (t, -, C_e), 12.42 ppm (m, +, C_f);

FT-IR (nujol, cm⁻¹, ranked intensities): 1584 (15), 1439 (6), 1270 (1), 1224 (7), 1147 (4), 1101 (5), 1031 (2), 996 (11), 754 (10), 721 (12), 690 (8), 637 (3), 572 (14), 542 (9), 509 (13);

Crystal Data: Table 8.2.

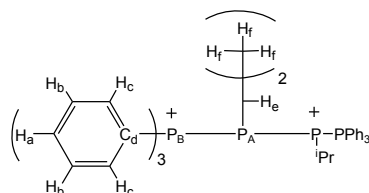
8.4.1.11 [Ph₃P-PiPr-PiPr-PPh₃][OTf]₂, [2.2(iPr)][OTf]₂

ⁱPrPCL₂ (36.0 μL, 0.29 mmol) and Me₃SiOTf (58.1 μL, 0.32 mmol) were added to a solution of Ph₃P (77 mg, 0.29 mmol) in CH₂Cl₂ (0.60 mL). After stirring for 1 h at room temperature, this solution was transferred to a vial containing Ph₃P (39 mg, 0.15 mmol), followed by subsequent addition of Me₃SiOTf (29.1 uL, 0.16 mmol) with stirring. This

solution was stirred for 5 days at room temperature, resulting in the precipitation of a white powder. This solid was isolated by filtration and washed with cold CH_2Cl_2 (-40°C , $2 \times 1 \text{ mL}$). Dissolution of this sparingly soluble powder in MeCN and removal of the solvent *in vacuo* provided $[\mathbf{2.2}(\text{iPr})][\text{OTf}]_2$ (45 mg). The supernatant was analyzed using $^{31}\text{P}\{^1\text{H}\}$ NMR spectroscopy and showed a mixture of $[\mathbf{2.1}(\text{iPr})][\text{OTf}]$, $[\text{Ph}_3\text{PCl}][\text{OTf}]$ and a new AMX spin system ($\delta\text{A} = -35.7 \text{ ppm}$, $\delta\text{M} = 23.0 \text{ ppm}$, $\delta\text{X} = 96.5 \text{ ppm}$, $^1J_{\text{AM}} = -309 \text{ Hz}$, $^1J_{\text{AX}} = -305 \text{ Hz}$, $^2J_{\text{MX}} = 59 \text{ Hz}$), tentatively assigned to $[\text{Ph}_3\text{P}-\text{P}^{\text{iPr}}\text{Pr}-\text{P}^{\text{iPr}}\text{PrCl}][\text{OTf}]$, $[\mathbf{2.3}(\text{iPr})][\text{OTf}]$. Slow evaporation of the supernatant over 2 days yielded an additional 18 mg of $[\mathbf{2.2}(\text{iPr})][\text{OTf}]_2$ as a semi-crystalline material. In contrast, $^{31}\text{P}\{^1\text{H}\}$ NMR spectra of reactions performed in more dilute solutions ($< 0.50 \text{ M}$) showed no evidence of $\mathbf{2.2}(\text{iPr})$. Instead, a mixture resembling the supernatant in more concentrated reactions was observed, with a 1:2 ratio of $[\text{Ph}_3\text{PCl}][\text{OTf}]$ to $[\mathbf{2.3}(\text{iPr})][\text{OTf}]$. ^1H NMR spectra of a dilute reaction mixture (0.25 M in $^{\text{iPr}}\text{P}(\text{Cl})_2$) show overlapping septets assigned as the methine resonances in $\mathbf{2.1}(\text{iPr})$ (2.42 ppm) and $\mathbf{2.3}(\text{iPr})$ (2.50 ppm and 2.56 ppm). The remaining ^1H NMR signals could not be assigned.

Yield ($[\mathbf{2.2}(\text{iPr})][\text{OTf}]_2$): 63 mg (45%);

M.p. 170-171.5 $^\circ\text{C}$;



^1H NMR (500.1 MHz, CD_3NO_2 , 298 K): $\delta = 7.87$ (vt, 6H, H_A), 7.68 (m, 24H, $\text{H}_{\text{B/C}}$), 3.26 (m, 2H, H_E), 0.93 ppm (m, 12H, H_F);

^{13}C NMR (125.8 MHz, DEPTQ135, CD_3CN , 298 K): $\delta = 136.60$ (s, +, $\text{C}_{\text{A/B}}$), 135.83 (s, +, $\text{C}_{\text{A/B}}$), 131.68 (t, +, C_{C}), 118.86 (t, -, C_{D}), 28.11 (t, +, C_{E}), 23.13 ppm (broad s, +, C_{F});

FT-IR (nujol, cm^{-1} , ranked intensities): 1439 (6), 1266 (1), 1225 (7), 1150 (4), 1098 (5), 1032 (2), 996 (11), 757 (10), 720 (13), 690 (9), 638 (3), 539 (8), 500 (12).

8.4.1.12 $[\text{Ph}_3\text{P-PCy-PCy-PPh}_3][\text{OTf}]_2$, **[2.2(Cy)][OTf]₂**

The synthesis of **[2.2(Cy)][OTf]₂** was attempted following the procedure for **[2.2(Pr)][OTf]₂** (*vide supra*) but with an additional equivalent of both Ph_3P and Me_3SiOTf and stirring for 40 h to maximize the yield of **2.2(Cy)** as observed by $^{31}\text{P}\{^1\text{H}\}$ NMR spectroscopy of the reaction mixture, which contained **[2.1(Cy)][OTf]**, **[2.2(Cy)][OTf]₂**, **[Ph₃PCl][OTf]**, and **[2.3(Cy)][OTf]** (**[Ph₃P-PCy-PCyCl][OTf]**, AMX spin system, not simulated, approximate shifts -44 ppm (t), 22.5 ppm (dd), and 93 ppm (dd)).

8.4.1.13 General Ligand Exchange on $[\text{Ph}_3\text{P-PPh-PPh-PPh}_3][\text{OTf}]_2$, **[2.2(Ph)][OTf]₂**

To a solution of **[2.2(Ph)][OTf]** (104 mg, 0.1 mmol) in *ca.* 0.5-1 mL CH_2Cl_2 was added a solution of dppm or dmpm (15.8 μL , 0.1 mmol) in CH_2Cl_2 (0.5-1 mL). ^{31}P NMR spectra were acquired after 1-2 h to assess the conversion to products, and then the reaction solution was layered with Et_2O until a slight cloudiness was observed to persist. The sample was then gently transferred to the freezer to allow for crystallization. On one occasion, this procedure, with dppm as a ligand, yielded a crop of fine needle-like colourless crystals, several of which were identified using X-ray diffraction as **2.7[OTf]₂**. It was not determined if the bulk crystalline material consisted solely of **2.7[OTf]₂**. Re-

dissolution of the bulk material in CH₂Cl₂ gave ³¹P NMR spectroscopic features that can be attributed to an approximately 1:1 mixture of the five- and six- membered rings **2.6** and **2.7**. Crystallization of the same reaction solution at room temperature yielded instead small cubic crystals, identified by ³¹P NMR as **2.6**[OTf]₂.

³¹P{¹H} NMR (101.3 MHz, CH₂Cl₂, 298K): **2.7**[OTf]₂:AMM'XX' spin system –

δ_A = -66.9, δ_M = -51.5, δ_X = 19.4 ppm; ¹J_{AM} = -108, ¹J_{MX} = -324, ¹J_{AM'} = -110, ²J_{AX} = 44, ²J_{AX'} = 45, ²J_{MM'} = 185, ³J_{MX'} = -4, ²J_{XX'} = -1 Hz.

8.4.2 Computational Methods Used in Chapter 2

Density functional theory calculations were performed using the Gaussian 03W software package.¹³² Initial geometry optimizations were performed using B3LYP/3-21G(d), then further optimized to find SCF and zero-point energies with a 6-31+G(d) basis set. Initial geometry optimizations were performed on both diastereomers of [H₃P-PR'-PR'-PH₃]²⁺ (R' = Me, Ph, ⁱPr), where the initial C-P-P-C torsion angles (τ_{R'}) were set at 0°, 60°, or 180°. Calculations on the [Me₃P-PR'-PR'-PMe₃]²⁺ derivatives (**2.2'**) were performed using the optimized PH₃ structural analogues as starting geometries. Frequency calculations were performed on all optimized structures to identify each as a local minimum on the potential energy surface. Although a recent study²⁶⁹ of the conformational preferences in neutral diphosphines favoured the use of the B3PW91 functional for reproducing qualitative trends, experimental observations for 2,3-diphosphino-1,4-diphosphonium cations are consistent with the results provided by B3LYP.

8.5 Synthetic Methods Used in Chapter 3

8.5.1 Sample Preparation for Derivatives of $[R_2(Cl)P-PR'Cl][GaCl_4]$, **3.1** $[GaCl_4]$

Addition of $R'PCl_2$ (0.20 mmol) and then R_2PCl (0.20 mmol) to a stirring solution of $GaCl_3$ (35 mg, 0.20 mmol) in CH_2Cl_2 (1 mL) afforded a pale yellow solution, with virtually quantitative formation of **3.1** $[GaCl_4]$ (> 99% as observed using ^{31}P NMR spectroscopy) after 1 h at room temperature. Solvent removal *in vacuo* or addition of Et_2O or pentane yielded an oil.

8.5.2 Sample Preparation for Derivatives of $[R(Cl)_2P-PRCl][GaCl_4]$, **3.2** $[GaCl_4]$

$RPCl_2$ (0.40 mmol) was added to a stirring solution of $GaCl_3$ (35 mg, 0.20 mmol) in CH_2Cl_2 (1 mL). Formation of **3.2** $[GaCl_4]$ was quantitative (> 99% as observed using ^{31}P NMR spectroscopy) after 30-60 min at room temperature. Removal of solvent *in vacuo* or addition of Et_2O or pentane yielded an oil.

8.5.3 Generalized Procedure for Reductive Coupling Reactions

Phosphinophosponium salts **1.34**, **3.1**, and **3.2** $[GaCl_4]$ (0.2-0.3 mmol) were synthesized *in situ* and allowed to stir for 30 min to 1 hour in 0.7-1 mL CH_2Cl_2 (unless otherwise noted) before the addition of either tri-*n*-butylstibine or triphenylstibine. For reactions involving 1 equivalent of $SbPh_3$ or less, phosphinophosponium salts were initially synthesized in 0.5 mL CH_2Cl_2 , and $SbPh_3$ was dissolved in another 0.5 mL CH_2Cl_2 to be added by pipette. Otherwise, the solution of phosphinophosponium gallate was

transferred directly onto solid SbPh₃ by pipette. SbBu₃ was added directly to the stirring solution by micropipette. For reactions involving additional equivalent(s) of GaCl₃, these were weighed out and added to the initial solution of the phosphinophosphonium gallate, before the addition of any reducing agent. Solutions were allowed to stir at room temperature for 1 h and 18-24 h before NMR spectra were collected. Reactions resulting in precipitation of solids were filtered through a pipette filter, and the solid washed with CH₂Cl₂ prior to dissolution in MeCN.

8.5.3.1 NMR Observation of [Et₂(Cl)P_X-P_AEt-P_AEt-P_X(Cl)Et₂][GaCl₄]₂, [**3.4'(Et)**][GaCl₄]₂ and Cyclo-[Et₇P₅][GaCl₄]₂, [**3.9(Et)**][GaCl₄]₂

Following the generalized procedure for reductive coupling, [**3.1(Et)**][GaCl₄] was synthesized *in situ* (0.3 mmol) and reacted in the ratio of 1:1:2 equivalents of **3.1(Et)**:GaCl₃:SbPh₃. ³¹P {¹H} NMR spectra (101.3 MHz, 298 K, CH₂Cl₂) collected after 1 h indicated nearly quantitative conversion to a single product with an AA'BB' spin system, assigned as **3.4'(Et)** [$\delta_A = 111$, $\delta_X = -38$, $^1J_{AA'} = -271$ Hz, $^1J_{AX} = ^1J_{AX'} = -374$ Hz, $^2J_{AX'} = ^2J_{A'X} = 86$ Hz, $^3J_{XX'} = 84$ Hz]. Attempted crystallization by vapour diffusion of pentane into the reaction mixture yielded a viscous oil, which, upon standing for six months, gave rise to a colourless semi-crystalline material coated in yellow oil. ³¹P {¹H} NMR spectra of the inseparable redissolved material showed effectively complete conversion to [**3.9(Et)**][GaCl₄]₂. ¹H NMR spectra indicated that the mixture was predominantly composed of [**3.9(Et)**][GaCl₄]₂ and the oxidized antimony byproduct [Ph₃SbCl][GaCl₄] or Ph₃SbCl₂.

8.5.3.2 NMR Observation of Cyclo-[(MeP)₃(PPh₂)₂][GaCl₄]₂, [**3.9**(Ph₂/Me)][GaCl₄]₂

Following the generalized procedure for reductive coupling, [**3.1**(Ph₂/Me)][GaCl₄] was synthesized *in situ* (0.3 mmol) and reacted with 0, 1, or 2 equivalents of GaCl₃ and either 1 equivalent of SbBu₃ or 1-2 equivalents of SbPh₃. ³¹P{¹H} NMR spectra collected after 18 h indicated **3.9**(Ph₂/Me) and **1.34**(Ph) as the major products, along with 3-20% of **3.10**(Ph₂/Me). In all cases, the ratio of the *trans*:*cis* isomers of **3.9** was approximately 2:1 as assessed by the relative areas of the ³¹P{¹H} NMR resonances. ³¹P{¹H} NMR of [**3.9**(Ph₂/Me)][GaCl₄]₂ (101.3 MHz, 298 K, CH₂Cl₂): *trans*-isomer – AGHMX spin system, see Table 3.4; *cis*-isomer – ABB'XX' spin system: δ_A = -63.3, δ_B = -34.4, δ_X = 52.8, ¹J_{AX} = ¹J_{AX'} = -314 Hz, ¹J_{BX} = ¹J_{B'X'} = -350 Hz, ¹J_{BB'} = -323 Hz, ²J_{BX'} = ²J_{B'X} = 17 Hz, ²J_{AB} = 10 Hz, ²J_{AB'} = 2 Hz, ²J_{XX'} = 21 Hz.

8.5.3.3 Synthesis of Cyclo-[ⁱPr₇P₅][GaCl₄]₂, [**3.9**(ⁱPr)][GaCl₄]₂

[ⁱPr₂(Cl)P-ⁱPrCl][GaCl₄], [**3.1**(ⁱPr)][GaCl₄] (0.3 mmol) was synthesized *in situ* in 0.7 mL CH₂Cl₂ according to the generalized procedure (*vide supra*) and allowed to stir for 1 hour at room temperature prior to the addition of SbBu₃ (73.8 uL, 0.3 mmol). No readily identifiable products could be distinguished from the reaction solution by ³¹P{¹H} NMR spectroscopy after 1.5 h. Upon standing for 20-24h in an NMR sample tube, colourless crystals suitable for X-ray diffraction precipitated from the reaction solution. The solution was decanted and the crystals were washed with 2 x 1 mL CH₂Cl₂ and dried. Elemental analysis was not performed owing to the observed decomposition at elevated temperatures. Low temperature resolution of ¹H/¹³C NMR peaks could not be achieved.

Yield: 26 mg (0.030 mmol, 30%);

D.p. 178-182°C;

FT-IR (nujol mull, cm^{-1} , [intensity]): 1275 [m], 1222 [s], 1024 [s], 935 [w], 901 [m], 884 [m], 739, [w], 705 [m], 538 [m], 419 [s];

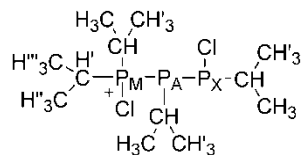
ESI-MS (10^{-5} M in MeCN): *positive ion mode* [m/z (relative intensity, assignment)] – 223.1 (4, [$^i\text{Pr}_3\text{P}_3 + \text{H}$] $^+$), 242.3 (3, unassigned), 265.1 (100, [$^i\text{Pr}_4\text{P}_3$] $^+$), 299.1 (4, unassigned), 306.2 (6, [$^i\text{Pr}_4\text{P}_3 + \text{MeCN}$] $^+$), 339.2 (51, [$^i\text{Pr}_5\text{P}_4$] $^+$), 413.3 (7, [$^i\text{Pr}_6\text{P}_5$] $^+$), 429.2 (6, [$^i\text{Pr}_4\text{P}_3 + 4\text{MeCN}$] $^+$), 445.1 (3, unassigned); *negative ion mode* – [GaCl_4] $^-$ supported by isotope pattern analysis (base peak: 210.8).

Crystal data: Table 8.3.

8.5.3.4 Synthesis of [$^i\text{Pr}_2(\text{Cl})\text{P}-\text{P}^i\text{Pr}-\text{P}^i\text{PrCl}$][GaCl_4], [**3.5**(^iPr)] [GaCl_4]

A sample of [**3.9**(^iPr)] [GaCl_4] $_2$ (26 mg, 0.029 mmol) in EtCN was heated in an NMR tube at 60°C for 1 h under Ar, after which time complete conversion to **3.5**(^iPr) was indicated by $^{31}\text{P}\{^1\text{H}\}$ spectroscopy. Removal of solvent *in vacuo* yielded an oil.

Yield: 18.4 mg (0.034 mmol);



$^{31}\text{P}\{^1\text{H}\}$ NMR (EtCN, 101.3 MHz, 294 K): *AMX spin system* $\delta_{\text{A}} = -79$, $\delta_{\text{M}} = 96$, $\delta_{\text{X}} = 132$ ppm; $^1\text{J}_{\text{AM}} = -375$ Hz, $^1\text{J}_{\text{AM}} = -224$ Hz, $^2\text{J}_{\text{MX}} = 29$ Hz;

$^1\text{H}\{^{31}\text{P}\}$ NMR (CD_2Cl_2 , 500.1 MHz, 298K): $\delta = 1.22$ (broad s, 3H, $-\text{P}_\text{A}\text{CHC}\underline{\text{H}}_3$), 1.27 (d, 3H, $-\text{P}_\text{X}\text{CHC}\underline{\text{H}}_3$), 1.31 (d, $-\text{P}_\text{A}\text{CHC}\underline{\text{H}}'_3$) and 1.33 (broad s, $-\text{P}_\text{M}\text{CH}'\text{C}\underline{\text{H}}''_3$) [6H together], 1.37 (broad s, 3H, $-\text{P}_\text{M}\text{CHC}\underline{\text{H}}_3$), 1.42 (broad s, 3H, $-\text{P}_\text{M}\text{CHC}\underline{\text{H}}'_3$), 1.48 (d, 3H, $-\text{P}_\text{X}\text{CHC}\underline{\text{H}}'_3$), 1.63 (d, 3H, $-\text{P}_\text{M}\text{CH}'\text{C}\underline{\text{H}}''_3$), 2.45 (sept, 1H, $-\text{P}_\text{A}\text{C}\underline{\text{H}}$), 2.63 (sept, 1H, $-\text{P}_\text{M}\text{C}\underline{\text{H}}$), 2.95 (sept, 1H, $-\text{P}_\text{M}\text{C}\underline{\text{H}}'$), 3.17 ppm (sept, 2H, $-\text{P}_\text{X}\text{C}\underline{\text{H}}$);

^{13}C NMR ($\text{d}_3\text{-MeCN}$, 125.8 MHz, 298K): 17.6-18.96 (overlapping signals in HSQC, $-\text{CH}_3$), 21.4 (m, $-\text{P}_\text{M}\text{C}\underline{\text{H}}$), 23.2 (m, $-\text{P}_\text{X}\text{C}\underline{\text{H}}$), 24.0 (m, $-\text{P}_\text{M}\text{C}\underline{\text{H}}'$), 31.2 ppm (m, $-\text{P}_\text{A}\text{C}\underline{\text{H}}$);

ESI-MS (10^{-5} M in MeCN): *positive ion mode* [m/z (relative intensity, assignment)] – 223.2 (4, [$^1\text{Pr}_3\text{P}_3 + \text{H}$] $^+$), 265.1 (100, [$^1\text{Pr}_4\text{P}_3$] $^+$), 320.2 (3, [$^1\text{Pr}_4\text{P}_3 + \text{EtCN}$] $^+$), 339.2 (2, [$^1\text{Pr}_3\text{P}_4$] $^+$); *negative ion mode* – [GaCl_4] $^-$ supported by isotope pattern analysis (base peak: 210.8).

8.6 Synthetic Methods Used in Chapter 4

8.6.1 Synthesis and Isolation of $[\text{Me}_3\text{P-P}^t\text{Bu-PMe}_3][\text{OTf}]_2$, **[4.1(^tBu)][OTf] $_2$**

A solution of $^t\text{BuPCl}_2$ (32 mg, 0.2 mmol) and Me_3SiOTf (79.6 μL , 0.44 mmol) in 0.5 mL MeCN was stirred for 5 min in a vial sealed with a rubber septum. A solution of 4.0 M Me_3P in hexanes (2 x 55.0 μL , 0.44 mmol) in 0.5 mL MeCN was added to the stirring solution by syringe. Once the reaction ceased to visibly fume (*ca.* 5 min), the septum was removed, and the reaction capped and stirred for 1 h at room temperature. Vapour diffusion of Et_2O or CH_2Cl_2 into the reaction solution at room temperature yielded long, needle-like colourless crystals suitable for X-ray diffraction after 24-48 h.

$^1\text{H}\{^{31}\text{P}\}$ NMR (500.1 MHz, d_3 -MeCN, 298K): $\delta = 1.59$ (s, 9H, $-\text{C}(\text{CH}_3)_3$),
2.32 ppm (s, 18H, $-\text{P}(\text{CH}_3)_3$);

^1H NMR (500.1 MHz, d_3 -MeCN, 298K): $\delta = 1.59$ (dt [$^3J_{\text{PH}} = 17$ Hz, $^4J_{\text{PH}} = 10$ Hz]),
9H, $-\text{C}(\text{CH}_3)_3$, 2.30-2.34 ppm (m, 18H, $-\text{P}(\text{CH}_3)_3$);

^{13}C NMR (125.8 MHz, DEPTQ135, d_3 -MeCN, 298 K): $\delta = 13.7$ -14.3 (m, +, $-\text{C}(\underline{\text{C}}\text{H}_3)_3$),
32.2 (dt [$^2J_{\text{CP}} = 14$ Hz, $^3J_{\text{CP}} = 5$ Hz], +, $-\text{P}(\text{CH}_3)_3$), 41.5 ppm (dt [$^1J_{\text{CP}} = 33$ Hz, $^2J_{\text{CP}} = \text{too broad to determine}$], -, $-\underline{\text{C}}(\text{CH}_3)_3$);

Crystal Data: Table 8.4.

8.6.2 Synthesis and Isolation of $[\text{Me}_3\text{P-PR-PMe}_3][\text{OTf}]_2$, **4.1** $[\text{OTf}]_2$, R = NiPr_2 , Cy

To 1.6 mL of CH_2Cl_2 in a vial was added sequentially, with stirring, Me_3SiOTf (2 x 72.4 μL , 0.8 mmol), RPCl_2 (0.4 mmol), and Me_3P (82.4 μL , 0.8 mmol), resulting in fuming and immediate generation of a white precipitate. After stirring for 1 h, the solvent was removed *in vacuo*. Isolated solids were redissolved in MeCN and crystallized by vapour diffusion of a secondary solvent over a period of 12 h. Crystals grown by this method were suitable for analysis by X-ray diffraction. The solution was decanted from the remaining crystals, which were subsequently dried *in vacuo* and washed with 5 mL hexanes, 6 x 1 mL THF and 6 x 1 mL CH_2Cl_2 for further analyses.

8.6.2.1 $[\text{Me}_3\text{P-P}(\text{NiPr}_2)\text{-PMe}_3][\text{OTf}]_2$, **4.1**(NiPr_2) $[\text{OTf}]_2$

Crystallization solvents: MeCN/ CH_2Cl_2 (*note: crystals not submitted for X-ray analysis were stored under hexanes to prevent decomposition*)

Yield: 156 mg (0.27 mmol, 67%);

D.p. 189-190°C;

$^1\text{H}\{^{31}\text{P}\}$ NMR (500.1 MHz, d_3 -MeCN, 298K): δ = 1.24 (d, slightly broad, 6H, -N[CH(CH₃)₂]₂) and 1.28 (d, 6H, -N[CH(CH₃)₂]₂), *restricted rotation*, 2.22 (s, 18H, -P(CH₃)₃), 3.49 ppm (septet, 1H, -N[CH(CH₃)₂]₂);

^{13}C NMR (125.8 MHz, DEPTQ135, d_3 -MeCN, 298 K): δ = 25.9 and 26.0 (s, +, -N[CH(CH₃)₂]₂), 48.3 (d [$^1J_{\text{CP}}$ = 30 Hz], +, -P(CH₃)₃), 61.6 ppm (d [$^2J_{\text{CP}}$ = 11 Hz], +, -N[CH(CH₃)₂]₂);

FT-IR (nujol mull, cm^{-1} , [relative intensities]): 2288 [w], 1457 [bs], 1376 [m], 1351 [m], 1263 [bs], 1161 [bs], 1031 [s], 955 [m], 875 [m], 765 [w], 755 [m], 671 [m], 637 [m], 573 [m], 518 [m];

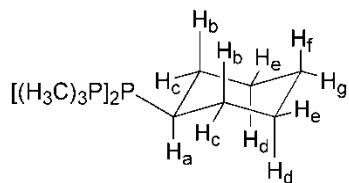
Crystal Data: Table 8.4.

8.6.2.2 [Me₃P-PCy-PMe₃][OTf]₂, [4.1(Cy)][OTf]₂

Crystallization solvents: MeCN/hexanes;

Yield: 168 mg (0.298 mmol, 75%);

D.p. 224-226°C;



$^1\text{H}\{^{31}\text{P}\}$ NMR (500.1 MHz, d_3 -MeCN, 298K): δ = 1.34 (qt, 1H, H_f), 1.49 (qt, 2H, H_d), 1.67 (qd/td, 2H, H_b), 1.71 (broad d, 1H, H_g), 1.85 (dt, 2H, H_e), 2.06 (broad d, 2H, H_c), 2.27 (s, 18H, -P[CH₃]₃), 2.82 ppm (tt, 1H, H_a);

^{13}C NMR (125.8 MHz, DEPTQ135, d_3 -MeCN, 298 K): δ = 13.0-13.5 (m, +, -P[CH₃]₃), 25.4 (s, -, CH_{2(f/g)}), 27.8 (d [$^3J_{\text{CP}} = 13$ Hz], -, CH_{2(d/e)}), 34.0-34.2 (m, -, CH_{2(b/c)}), 35.6 ppm (d [$^1J_{\text{CP}} = 29$ Hz], +, CH_a);

FT-IR (nujol mull, cm⁻¹, [relative intensities]): 1457 [bs], 1309 [w], 1260 [bs], 1226 [s], 1159 [s], 1028 [s], 954 [m], 757 [w], 634 [m], 572 [w], 517 [w];

Crystal Data: Table 8.4.

8.6.3 Reaction Mixtures and ^{31}P NMR Observation of Other Derivatives

8.6.3.1 [Me₃P-PR-PMe₃][OTf]₂, **4.1**[OTf]₂, R = Me, ⁱPr

The same preparative procedure was used for these derivatives as for **4.1**(^tBu)[OTf]₂ (Section 8.6.1), except that crystalline material could not be isolated. Instead, $^{31}\text{P}\{^1\text{H}\}$ NMR spectra were collected on the reaction solution after 1 h reaction time. For **4.1**(Me), the observation of broad NMR features prompted an attempt crystallize by vapour diffusion of Et₂O into the reaction solution – an oil resulted after 12-18 h, which subsequently solidified into a white powder, coated with trace droplets of oil, after an additional 5-6 days. The supernatant was decanted, and the solids washed with 3 x 1 mL Et₂O to remove all traces of the oily product. $^{31}\text{P}\{^1\text{H}\}$ analysis of the solids redissolved in EtCN provided spectra with sharp signals corresponding solely to the desired product.

8.6.3.2 $[\text{Me}_3\text{P-PR-PMe}_3][\text{OTf}]_2$, **4.1** $[\text{OTf}]_2$, R = Ph, and Attempted Syntheses of $[\text{Et}_3\text{P-PR-PEt}_3][\text{OTf}]_2$, **4.2** $[\text{OTf}]_2$,

The same preparative procedure was used for these derivatives as for **4.1(Cy)** and **4.1(NⁱPr₂)**, except that crystalline material could not be isolated via vapour diffusion of hexanes, pentane, or CH_2Cl_2 into the MeCN-solution of the isolated powder from the reaction. Instead, $^{31}\text{P}\{^1\text{H}\}$ NMR spectra were collected on the dissolved material isolated after 1 h reaction time, or on the reaction solution in the attempted syntheses of **4.2(Ph)** and **4.2(NⁱPr₂)**.

8.7 Electrochemical Methods

8.7.1 Reagents and Preparation of Analytes for Electrochemistry

Syntheses and preparation of reaction mixtures were performed in a glovebox under an N_2 atmosphere. The synthesis of $[\text{Ph}_3\text{P-PPhCl}][\text{OTf}]$, **2.1(Ph)** $[\text{OTf}]$, was adapted from references 80 and 81, but with shortened reaction times (15 min) to avoid the formation of $[\text{Ph}_3\text{P-PPh-PPh-PPh}_3][\text{OTf}]_2$ at the desired scale (0.5 mmol per 1.5 mL CH_2Cl_2).

Addition of Et_2O to precipitate the product as a white powder required stirring times of 1-2 h to avoid formation of an oily residue. The purity of the resulting powder was assessed by $^{31}\text{P}\{^1\text{H}\}$ NMR spectroscopy of a solution of a sample of re-dissolved solid. All powder samples of analytes were placed under vacuum for 1 h before transfer into an Ar atmosphere glovebox for electrochemical experiments.

8.7.2 Solution Preparation

All solution preparations and dilutions described herein were performed using standard volumetric glassware, unless otherwise specified. All analyte solutions were made up to

the specified volume using a stock solution of 0.1 M TBAPF₆/MeCN, prepared by the dissolution of 3.8743 g of TBAPF₆ into 100.00 mL of MeCN. The reference electrode solution (0.01 M AgNO₃/0.1 M TBAPF₆/MeCN, unless otherwise noted) was prepared dissolving 17.0 mg AgNO₃ in 10.00 mL of this stock supporting electrolyte solution. Analyte solutions, unless otherwise noted, were prepared by dissolution of a weighed amount of the solid of interest in 1.00 mL of 0.01 M F_c/0.1 M TBAPF₆ stock solution (18.6 mg in 10.00 mL 0.1M TBAPF₆/MeCN), and subsequent dilution to 10.00 mL with 0.1 M TBAPF₆/MeCN. Solutions containing [2.1(Ph)][OTf] were analyzed immediately to prevent any possible formation of [Ph₃P-PPh-PPh-PPh₃][OTf]₂ *in situ*. Solutions using other supporting electrolytes were prepared in the same way, beginning with a 50.00 mL stock solution of the selected electrolyte.

8.7.2.1 Solutions for the Calibration of Ph₃P Concentration

All solutions in this section were made with 0.1 M TBAPF₆/MeCN. The 10.0 ± 0.2 mM Ph₃P solution for analysis was prepared by addition of 1.00 mL of 10 mM F_c solution and subsequent dilution to 10.00 mL. Aliquots of a stock 10.0 ± 0.2 mM solution of Ph₃P were each combined with 1.00 mL of 10 mM F_c solution and diluted to 10.00 mL to yield solutions of Ph₃P with the following concentrations: 4.99 ± 0.08 mM (5.00 mL stock solution), 2.00 ± 0.03 mM (2.00 mL stock solution), 1.00 ± 0.02 mM (1.00 mL stock solution). Solutions of Ph₃P at lower concentrations (0.200 ± 0.04, 0.30 ± 0.01, 0.40 ± 0.01 and 0.50 ± 0.01 mM) were prepared by combining aliquots (2.00 mL, 3.00 mL, 2 x 2.00 mL or 5.00 mL, respectively) of a 1.00 mM Ph₃P solution (10 x dilution of the 10.00 mM solution prepared above) with 1.00 mL of 1 mM F_c solution (1.00 mL of 10 mM F_c stock solution diluted to 10.00 mL) and diluting to 10.00 mL. The

lower concentration of F_c was required to ensure adequate decay of the anodic current response from the internal standard before oxidation of Ph_3P occurred. The 0.50 mM Ph_3P solution was alternately prepared using 1.00 mL of 10 mM F_c solution for comparison.

8.7.2.2 Solutions Related to the Effects of Varied $TBAPF_6$ Concentration

Reference electrode solutions with reduced concentrations of supporting electrolyte (25.0 ± 0.2 mM, 50 ± 0.3 mM, 75.0 ± 0.4 mM) were prepared by dissolving weighed amounts of $TBAPF_6$ in 5.00 mL of 0.01 M $AgNO_3$ stock solution (42.4 mg of $AgNO_3$ in 25.00 mL MeCN). Baseline solutions of $FeCp_2$ were prepared at each concentration of $TBAPF_6$ by the addition of 1.00 mL of 0.01 M $FeCp_2$ stock solution (18.6 mg $FeCp_2$ diluted to 10.00 mL with MeCN) to weighed amounts of $TBAPF_6$. Resulting solutions were made up to 10.00 mL by addition of MeCN. Solutions of **[2.1(Ph)][OTf]** (2.00 ± 0.02 mM and 4.00 ± 0.04 mM) were prepared by serial dilution of an initial 8.00 ± 0.08 mM solution (44.4 mg **[2.1(Ph)][OTf]** in 10.00 mL $TBAPF_6/MeCN$ stock solution). In each case, a 5.00 mL aliquot of the concentration solution was diluted to 10.00 mL, while the remaining solution was analyzed by cyclic voltammetry. The four required stock solutions of $TBAPF_6/MeCN$ (25.00 ± 0.05 mM, 50.00 ± 0.07 mM, 75.0 ± 0.1 mM and 100.0 ± 0.1 mM) were prepared by dissolution of a weighed amount of $TBAPF_6$ in MeCN in a 25.00 mL volumetric flask. A 2.00 mM solution of Ph_3P was also prepared at all four concentrations of $TBAPF_6$ by dilution from a 4.00 mM solution of Ph_3P using each of the $TBAPF_6$ stock solutions described above.

8.7.2.3 Solutions Related to the Effect of Me₃SiCl

In situ reaction mixtures of [2.1(Ph)][OTf] for electrochemical analysis were prepared in a glovebox under N₂ atmosphere at with 0.5 mmol of all reagents in 3 mL of 0.1 M TBAPF₆/MeCN. The reaction was stirred for 50 min, then quantitatively transferred to a 25 mL bulb by rinsing the original reaction vessel with 3 x *ca.* 0.75 mL 0.1 M TBAPF₆/MeCN. The solution was then degassed by three freeze-pump-thaw cycles for transfer to the Ar glovebox. ³¹P NMR of the reaction solution after transfer and degassing supported quantitative conversion to the desired product with no visible interaction or coordination of the [PF₆]⁻ anion *in situ*.

Electrochemical measurements were conducted on solutions of varying concentration (25.0 ± 0.2, 10.00 ± 0.07, 5.00 ± 0.04, 2.00 ± 0.02, and 1.000 ± 0.008 mM) prepared by serial dilution from a stock solution of the reaction mixture diluted to 10 mL in a volumetric flask. To each analyte solution, 1 mL of 0.01 M F_c solution (in 0.1 M TBAPF₆/MeCN) was added prior to dilution to the desired volume.

For the addition of Me₃SiCl to solutions of isolated [2.1(Ph)][OTf], a 0.39 ± 0.02 M stock solution of Me₃SiCl in 0.1 M TBAPF₆/1 mM F_c/MeCN was prepared by the addition of 2 x 250 μL of Me₃SiCl using a 500 μL syringe. A background cyclic voltammogram of Me₃SiCl was performed on a 2 mM solution of Me₃SiCl in 0.1 M TBAPF₆/1 mM F_c/MeCN, which was prepared by serial dilution, first of a 1.00 mL aliquot of the stock solution to 2.00 mL, and then two successive dilutions of 1.00 mL aliquots of the resulting solutions to 10.00 mL. The solution of [2.1(Ph)][OTf] in 0.1 M

TBAPF₆/1 mM F_c/MeCN was prepared by addition of 1 mL 0.01 M F_c/MeCN to 111.0 mg of [2.1(Ph)][OTf] and dilution to 10.00 mL.

8.7.3 Cyclic Voltammetry

All electrochemical experiments were performed using an Epsilon EC potentiostat and C3 cell stand from Bioanalytical Systems Inc. (BASi). The standard glass cell (base diameter: 25 mm; minimum practical volume: 7 mL) was used for experiments with solutions containing a minimum 0.1 M concentration of supporting electrolyte, unless otherwise noted. Experiments involving lower concentrations of supporting electrolyte were conducted in a narrower base glass cell (base diameter: 16 mm; minimum practical volume: 4 mL), referred to in this text as the “small volume cell”. The cell stand and accompanying electrodes were located in a glovebox under an inert Ar atmosphere at a temperature between 30-33°C. The working electrode was a 0.8 mm radius platinum disc, unless otherwise specified in the text, cleaned electrochemically by repeatedly sweeping the potential to -3.2 V and +3.2 V in a solution of 0.1 M TBAPF₆/MeCN until a baseline cyclic voltammogram showed no extraneous peaks. The counter electrode was a 4 cm long platinum wire, and the reference electrode was Ag/0.01 M AgNO₃ in MeCN with supporting electrolyte at the same concentration as in the analyte, separated from the solution by a vycor junction. All potentials are reported relative to ferrocene (F_c, 1.00 ± 0.02 mM) as an internal standard, unless otherwise specified,^{270,271} which displayed an average E^{o'} of +91 mV vs. the Ag/Ag⁺ reference electrode. For reference, literature values for the F_c/F_c⁺ couple have been reported as E^{o'} = 0.40 V vs. SCE in 0.1 M TBAPF₆/MeCN,¹⁵⁹ or E^o = 0.400 V vs. NHE in water.²⁷¹ Cyclic voltammograms

of **[2.1(Ph)][OTf]** in the presence or absence of F_c were not substantially different, so F_c/F_c^+ were assumed to be innocent in the redox chemistry of the studied species.

The usable window for electrolysis with TBAPF₆ as a supporting electrolyte was determined to range from -2.5 V to +1.5 V, relative to Ag/Ag⁺. Each day, before analysis of any other samples was conducted, an initial baseline cyclic voltammogram of 1 mM F_c in 0.1 M TBAPF₆/MeCN was performed on this potential window. For quantitative analyses conducted on a smaller potential window, at least one cyclic voltammogram was conducted on the full window to determine qualitative features and eliminate variation between samples. All cyclic voltammograms were performed at a sweep rate (v) of 100 mV/s and full scale current limit of 10 μ A, unless otherwise noted.

In any series of solutions where concentration was varied, solutions were analyzed in order of increasing concentration of analyte. In between solutions, electrodes were rinsed with the new solution of interest, while the cell was rinsed with MeCN and dried.

Statistical rigor for all quantitative data was obtained through collection of repeated cyclic voltammograms (5 cycles with a 60 s delay time between cycles, unless otherwise specified). If the concentration of supporting electrolyte in the cell was varied between experiments, the reference electrode compartment was emptied and rinsed with the new solution of 0.01 M AgNO₃ before being refilled. When the identity of the supporting electrolyte was changed, the rinsed reference electrode was soaked overnight in MeCN to eliminate any residual salts, then soaked in the desired supporting electrolyte solution for a minimum of 1 h.

8.7.4 Uncertainty Calculations

8.7.4.1 Random Errors

Uncertainties in the concentrations of solutions mentioned herein were estimated using standard equations for the mathematical propagation of random errors. That is, for the measured quantities a, b, c, the uncertainty (σ_y) resulting from addition/subtraction ($y = k + k_a a + k_b b + k_c c$, where k are constants) is given by Equation [8.1], and from multiplication/division ($y = kab/cd$) by Equation [8.2].

$$\sigma_y = \sqrt{(k_a \sigma_a)^2 + (k_b \sigma_b)^2 + (k_c \sigma_c)^2} \quad [8.1]$$

$$\sigma_y = y \sqrt{\left(\frac{\sigma_a}{a}\right)^2 + \left(\frac{\sigma_b}{b}\right)^2 + \left(\frac{\sigma_c}{c}\right)^2} \quad [8.2]$$

The uncertainties for the applicable volumetric glassware used are as follows: volumetric flasks (± 0.03 mL for 10 mL, 25 mL; ± 0.02 mL for 1 mL, 2mL, 5 mL) and volumetric pipettes (± 0.006 mL for 1 mL, 2 mL; ± 0.01 mL for 3mL, 5 mL). Small volume syringes (Hamilton) used in the preparation and addition of Me_3SiCl stock solutions have uncertainties of 1% of the nominal volume of the syringe. Of these, the 25 μL syringe was pre-calibrated to account for the dead volume in the needle, while measurements using the 250 μL and 500 μL syringes were made by differences. The addition of reagents for the analysis of in situ reaction solutions was made using a 10-100 μL variable volume Eppendorf pipettor, which has reported precisions of $\leq 0.3\%$ for volumes greater than 50 μL (as used herein). Error in the reported density of the reagents was assumed to be negligible in comparison to other uncertainties. Mass measurements were made by difference, with a reported uncertainty in any given mass reading of 0.1 mg

(minimum mass: 10 mg). However, empirical observation of the performance of the analytical balance in the glovebox has suggested that an uncertainty of 0.3 mg is a more reasonable estimate under these conditions. In the case of all measurements made by differences, the overall uncertainty for a reported value must be derived according to Equation [8.3]:

$$\sigma_{\text{diff}} = \sqrt{(\sigma_{\text{reading}})^2 + (\sigma_{\text{reading}})^2} = \sqrt{2}\sigma_{\text{reading}} \quad [8.3]$$

It has been assumed that the uncertainties in the molar masses were negligible compared to all other sources of error.

8.7.4.2 Linear Regression and Calibration Errors

Statistical treatment of data and procedures for linear regression and error analysis from calibration curves were performed in accordance with standard methods outlined in Appendix A1. Unweighted regression was performed if the uncertainty in all points was similar, whereas weighted regression was performed otherwise.

8.8 Synthesis and Characterization of Compounds in Chapter 6

8.8.1 $[\text{}^i\text{Pr}_3\text{P-SbPhCl}][\text{OTf}]$, **[6.23(^iPr)][\text{OTf}]**,

Addition of $^i\text{Pr}_3\text{P}$ (38.2 μL , 0.20 mmol) to a CH_2Cl_2 solution of PhSbCl_2 (54 mg, 0.20 mmol) afforded a slightly cloudy, colourless mixture which was allowed to stir for 30 min (^{31}P NMR spectrum of the reaction mixture shows >90% conversion to a singlet at 29.7 ppm). Addition of Me_3SiOTf (36.2 μL , 0.20 mmol) resulted in a clear, pale yellow solution which was stirred for 1.5 h at room temperature. Slow evaporation of this

solution in a CH₂Cl₂/pentane vapour diffusion setup afforded colourless, rectangular prism-like crystals suitable for X-ray diffraction after 1 day. Crystals not submitted for X-ray analysis were washed with 2 x 0.5 mL pentane and 2 x 0.5 mL Et₂O, and dried *in vacuo*.

Yield (crystalline): 78 mg (0.14 mmol, 72 %)

D.p. 110-113°C (dark brown crystalline material)

³¹P{¹H} NMR (101.3 MHz, CH₂Cl₂, 298 K): 36.1 ppm (s);

¹⁹F NMR (235.4 MHz, CH₂Cl₂, 298 K): -80.4 ppm (s, OSO₂CF₃);

¹H NMR (500.1 MHz, CDCl₃, 298 K): 8.33 (d, 2H, *o*-Ph), 7.54 (t, 2H, *m*-Ph), 7.45 (t, H, -Ph), 3.11 (m, 3H, P[CH(CH₃)₂]₃), 1.44 ppm (dd, 18H, P[CH(CH₃)₂]₃);

¹³C NMR (125.8 MHz, DEPTQ135, CDCl₃, 298 K): 136.2 (s, +), 131.2 (s, +), 129.9 (s, +), 24.3 (d, +), 18.8 ppm (d, +), *quaternary C (SbPh) not observed – possibly due to broadening associated with the Sb-quadrupole*;

FT-IR (nujol mull, cm⁻¹, [relative intensities]): 1260 [bs], 1225 [w], 1199 [w], 1151 [m], 1063 [w], 1030 [m], 1009 [w], 886 [bw], 732 [bw], 693 [w], 637 [m], 574 [w], 517 [w];

Crystal Data: Table 8.5.

8.8.2 [Bn₃P-SbPhCl][OTf], [**6.23(Bn)**][OTf]

Addition of Bn₃P (60 mg, 0.20 mmol) in CH₂Cl₂ (0.5 mL) to a CH₂Cl₂ solution of PhSbCl₂ (54 mg, 0.20 mmol in 0.5 mL) resulted in a cloudy white suspension.

Subsequent addition of Me₃SiOTf (36.2 μL, 0.20 mmol) afforded a clear, colourless

solution, which was stirred for 1.5 h. Slow evaporation of the reaction solution by vapour diffusion of CH₂Cl₂ into pentane afforded colourless crystals suitable for X-ray diffraction. Crystals not submitted for X-ray analysis were washed with pentane and dried *in vacuo*. Storage of the crystalline material at room temperature resulted in slow degradation to an amorphous CH₂Cl₂-insoluble black solid over a period of weeks.

Yield (crystalline): 113 mg (0.17 mmol, 83%)

D.p. 121-133°C (xtals turn dark brown, liquefies from 131-133°C)

³¹P{¹H} NMR (101.3 MHz, CH₂Cl₂, 298 K): 10.4 ppm (s);

¹⁹F NMR (235.4 MHz, MeCN, 298 K): -80.0 ppm (s, OSO₂CF₃);

¹H NMR (500.1 MHz, CDCl₃, 298 K): 3.43 (d, 6H, CH₂), 6.96 (d, 6H, *o*-Bn), 7.28-7.34 (m, 9H, *m*-Bn and *p*-Bn), 7.50 (t, 1H, *p*-PhSb), 7.58 (t, 2H, *m*-PhSb), 8.11 ppm (d, 2H, *o*-PhSb);

¹³C NMR (125.8 MHz, DEPTQ135, CDCl₃, 298 K): 27.0 (d [¹J_{CP} = 18 Hz], -, CH₂), 128.6 (d [^{4/5}J_{CP} = 3 Hz], +, *m*-Bn and *p*-Bn), 129.4 (d [²J_{CP} = 9 Hz], -, quaternary C-Bn), 129.6 (d [^{4/5}J_{CP} = 3 Hz], +, *m*-Bn and *p*-Bn), 130.1 (s, +, *m*-PhSb), 130.2 (d [³J_{CP} = 5 Hz], +, *o*-Bn), 131.2 (s, +, *p*-PhSb), 135.3 ppm (broad s, +, *o*-PhSb), *quaternary C (SbPh) not observed – possibly due to broadening associated with the Sb-quadrupole*;

Crystal Data: Table 8.5.

8.8.3 [Me₃P-SbCl₂][OTf], **6.24**[OTf]

Me₃P (1.0 M in toluene, 3 x 63.4 μL, 0.20 mmol) was added in three portions to a stirring solution of SbCl₃ (46 mg, 0.20 mmol) in CH₂Cl₂ (1 mL). A small amount of white precipitate was formed upon addition of the second portion of Me₃P (0.66 equiv.), the majority of which redissolved after 30 s of stirring. Addition of the third portion of Me₃P yielded substantial quantities of a heavy white precipitate, and subsequent reaction with Me₃SiOTf ((36.2 μL, 0.20 mmol) yielded a clear solution and an insoluble colourless oil. After an additional 5 minutes of stirring, a white solid precipitated from this mixture, and the resulting slurry was stirred for 1.5 h at room temperature. The ³¹P{¹H} NMR spectrum of the CH₂Cl₂ supernatant of the reaction displayed two singlets (-3.8 ppm [unassigned] and 15.6 ppm), while the precipitate displayed a singlet at 15.6 ppm when dissolved in MeCN (¹⁹F: -80.0 ppm). Colourless, needle-like crystals suitable for X-ray diffraction were isolated by slow evaporation of the CH₂Cl₂-supernatant, assisted by vapour diffusion of the CH₂Cl₂ into pentane. Alternately, removal of solvent *in vacuo* and washing with CH₂Cl₂ afforded a white powder possessing the same ³¹P NMR chemical shift and melting point as the crystals.

Yield: 43 mg (0.10 mmol, 50%);

m.p.: 108-111°C;

³¹P{¹H} NMR (101.3 MHz, MeCN, 298 K): 15.6 ppm (s);

¹⁹F NMR (235.4 MHz, MeCN, 298 K): -80.0 ppm (s, OSO₂CF₃);

Crystal Data: Table 8.5.

8.8.4 [(Ph₃P)₂SbCl₂][OTf], **6.26**[OTf]

A CH₂Cl₂ solution of Ph₃P (105 mg, 0.40 mmol in 0.8 mL) was added to a CH₂Cl₂ solution of SbCl₃ (91 mg, 0.40 mmol in 0.8 mL), affording a bright yellow solution. Addition of Me₃SiOTf (72.4 μL, 0.4 mmol) yielded a solution with ³¹P{¹H} NMR singlet peaks at 45 ppm and -5 ppm. Slow evaporation of CH₂Cl₂ from the reaction mixture by vapour diffusion of the solvent into pentane afforded first a bright yellow oil (1 day), and subsequently a mixture of yellow cubic crystals (suitable for X-ray diffraction) and an insoluble amorphous black solid (2 days). The crystals were redissolved in CH₂Cl₂ and the mixture filtered to remove the black solids. Removal of CH₂Cl₂ *in vacuo* yielded a yellow powder with trace amounts of dark brown impurities.

Yield: 49.5 mg (0.06 mmol, 29%)

D.p. 105-110°C (begins to brown); 120-125°C (solid turns dark green, and shrinks in volume); 140-145°C (turns black then liquefies);

³¹P{¹H} NMR (101.3 MHz, CH₂Cl₂, 298 K): -5 ppm (broad s);

¹H NMR (500.1 MHz, CDCl₃, 298 K): 7.46-7.57 ppm (m, Ph);

¹³C NMR (125.8 MHz, DEPTQ135, CDCl₃, 298 K): 128.4 (d [¹J_{CP} = 24 Hz], -, quaternary C), 129.2 (d [³J_{CP} = 10 Hz], +, *m*-Ph, ³J_{CP} = 6 Hz), 131.3 (s, +, *p*-Ph), 134.0 ppm (d [²J_{CP} = 13 Hz], +, *o*-Ph, ²J_{CP} = 13 Hz);

FT-IR (nujol mull, cm⁻¹, [relative intensities]): 1450 [m], 1436 [s], 1419 [w], 1395 [w], 1298 [bm], 1226 [m], 1212 [bm], 1165 [bm], 1095 [w], 1028 [w], 1017 [s], 998 [w],

747 [bm], 725 [w], 711 [w], 691 [s], 634 [s], 619 [w], 570 [w], 516 [m], 498 [m],
493 [m], 419 [w], 398 [w], 375 [w], 354 [w], 335 [w], 328 [w], 324 [w], 304 [s];

Crystal Data: *see* Table 8.6.

8.8.5 Observation of *cyclo*-[(Me₃P)Sb]₄[OTf]₄, **6.28**[OTf]₄

Addition of Me₃P (1.0 M in toluene, 350 μL, 0.35 mmol) and then Me₃SiOTf (59.7 μL, 0.33 mmol) to a stirred solution of PhSbCl₂ (54 mg, 0.20 mmol) in CH₂Cl₂ resulted in the immediate formation of a white precipitate. The ³¹P{¹H} NMR spectrum of the supernatant showed singlet peaks at 82.5 ppm (minor) and -5.4 ppm (major) after 2 h, with an upfield shift of the latter peak to -7.1 ppm (96%) after an addition 20 h at room temperature. The mixture was allowed to stir for total of 22 h at room temperature before the white precipitate was isolated and washed with cold CH₂Cl₂. This solid was dissolved in MeCN (³¹P NMR: -1.9 ppm) and allowed to stand for two weeks at room temperature, yielding several needle-like yellow crystals suitable for X-ray diffraction. These crystals decomposed upon dissolution in a mixture of CH₂Cl₂ and MeCN to a virtually insoluble orange-brown precipitate, so no NMR data for the crystals is available.

³¹P{¹H} NMR (101.3 MHz, MeCN-reaction mixture, 298 K): -1.9 ppm (broad s);

Crystal Data: Table 8.6

8.9 Crystallographic Experimental Details

Table 8.2. Selected crystallographic data and collection parameters for compounds in Chapter 2. Data collected and refined at the University of New Brunswick.

	[Ph ₃ P-PMe(Cl)][OTf] [2.1(Me)][OTf]	[Ph ₃ P-PEt-PEt-PPh ₃][OTf] ₂ [2.2(Et)][OTf]₂	<i>cyclo</i> -[(dppm)(PPh ₃)] ₂ [OTf] ₂ 2.7[OTf]₂^d
CCDC #	694816	694390	n/a
formula	C ₂₀ H ₁₈ ClF ₃ O ₃ P ₂ S	C ₄₂ H ₄₀ F ₆ O ₆ P ₄ S ₂	C ₄₅ H ₃₇ F ₆ O ₆ P ₅ S ₂
molecular weight (g/mol)	492.79	942.74	1006.72
crystal system	triclinic	monoclinic	triclinic
Space group	$\bar{P}1$	C2/c	$\bar{P}1$
colour, habit	colourless plate	colourless rod	colourless plate
<i>a</i> / Å	8.3728(10)	15.5968(16)	10.182(3)
<i>b</i> / Å	11.0797(13)	14.5043(16)	13.566(4)
<i>c</i> / Å	12.4662(15)	19.895(2)	18.299(6)
<i>α</i> / °	83.4150(10)	90	98.178(5)
<i>β</i> / °	72.798(2)	102.483(2)	93.391(5)
<i>γ</i> / °	85.040(2)	90	99.033(5)
<i>V</i> / Å ³	1095.8(2)	4394.3(8)	2462.3(14)
T / K	198(1)	173(1)	173(1)
<i>Z</i>	2	4	2
crystal size / mm ³	0.50 x 0.30 x 0.10	0.50 x 0.20 x 0.20	0.50 x 0.10 x 0.03
<i>μ</i> / mm ⁻¹	0.461	0.338	0.338
2θ _{max} / °	54.98	55.00	55.00
reflections collected	7617	15089	16713
independent reflections	4767	4932	10563
R _{int}	0.0177	0.0263	0.0280
parameters	358	272	693
<i>R</i> _I ^a (I > 2σ(I))	0.0347	0.0461	0.0561
<i>wR</i> ₂ ^b (all data)	0.0972	0.1282	0.1555
GOF ^c	1.065	1.069	1.060
Δρ max and min / e Å ⁻³	0.382, -0.228	0.820, -0.579	1.249, -0.378

^a $R_I = \sum ||F_o| - |F_c|| / \sum |F_o|$ ^b $wR_2 = (\sum [w(F_o^2 - F_c^2)^2] / \sum [w(F_o^4)])^{1/2}$.

^c GOF = $[\sum w(|F_o| - |F_c|)^2 / (n - p)]^{1/2}$, where *n* = number of reflections, and *p* = number of parameters

^d Disorder in one of the phenyl groups (C14 – C19) resulted in large thermal parameters and high bond length uncertainties (2-3 times larger than those for the remaining phenyl groups). A disorder model was employed that worked reasonably well as long as bond length restraints (SADI) and an isotropic model was used. Anisotropic refinement failed and no convergence was achieved. Restraints (SIMU, SADI) as well as constraints (EADP) lead to non positive definite thermal parameters (i.e. peanut shaped) and had to be abandoned.

Table 8.3. Selected crystallographic data and collection parameters for **[3.9(ⁱPr)]**[OTf]₂, *cyclo*-[ⁱPr₇P₅][GaCl₄]₂ (Chapter 3). Data collected and refined at the University of Alberta.

4.1(Cy)[OTf]₂	
Formula	C ₂₁ H ₄₉ Cl ₈ Ga ₂ P ₅ ·CH ₂ Cl ₂
molecular weight (g/mol)	964.42
crystal system	monoclinic
Space group	<i>P2₁/n</i>
Colour, habit	colourless, blocks
<i>a</i> / Å	11.6226 (11)
<i>b</i> / Å	22.014 (2)
<i>c</i> / Å	16.9005 (15)
<i>α</i> / °	90
<i>β</i> / °	98.2769 (11)
<i>γ</i> / °	90
<i>V</i> / Å ³	4279.0 (7)
<i>T</i> /K	193
<i>Z</i>	2
crystal size / mm ³	0.58 x 0.41 x 0.34
<i>μ</i> / mm ⁻¹	2.086
2θ _{max} / °	54.92
reflections collected	37146
independent reflections	9779
<i>R</i> _{int}	0.0235
parameters	380
<i>R</i> _i ^a [F _o ² ≥ 2σ(F _o ²)]	0.0399
<i>wR</i> ₂ ^b (all data)	0.1136
GoF ^c	1.025
Δρ max and min /e Å ⁻³	1.041, -0.777

$$^a R_1 = \frac{\sum ||F_o| - |F_c||}{\sum |F_o|}$$

$$^b wR_2 = [\sum w(F_o^2 - F_c^2)^2 / \sum w(F_o^4)]^{1/2}$$

$$^c \text{GoF} = [\sum w(F_o^2 - F_c^2)^2 / (n - p)]^{1/2} \quad (n = \text{number of data}; p = \text{number of parameters varied})$$

Table 8.4. Selected crystallographic data and collection parameters for derivatives of **4.1(R)**][OTf]₂, [Me₃P-PR-PMe₃][OTf]₂ (Chapter 4). Data collected and refined at the University of Alberta.

	4.1(Cy)][OTf] ₂	4.1(^tBu)][OTf] ₂	4.1(NⁱPr₂)][OTf] ₂
Formula	C ₁₄ H ₂₉ F ₆ O ₆ P ₃ S ₂	C ₁₂ H ₂₇ F ₆ O ₆ P ₃ S ₂	C ₁₄ H ₃₂ F ₆ NO ₆ P ₃ S ₂
molecular weight (g/mol)	564.40	538.37	581.44
crystal system	orthorhombic	monoclinic	monoclinic
Space group	<i>Pba2</i>	<i>P2₁/c</i>	<i>P2₁</i>
Colour, habit	colourless, blocks	colourless, needles	colourless, blocks
<i>a</i> / Å	16.7757 (19)	6.581 (4)	11.9037 (6)
<i>b</i> / Å	22.426 (3)	21.895 (12)	13.9854 (7)
<i>c</i> / Å	6.3922 (7)	16.904 (9)	24.2752 (11)
<i>α</i> / °	90	90	90
<i>β</i> / °	90	91.650 (8)	104.1515 (5)
<i>γ</i> / °	90	90	90
<i>V</i> / Å ³	2404.8 (5)	2435 (2)	3918.6 (3)
<i>T</i> / K	193	193	193
<i>Z</i>	4	4	6
crystal size / mm ³	0.60 x 0.57 x 0.27	0.78 x 0.31 x 0.08	0.39 x 0.36 x 0.22
<i>μ</i> / mm ⁻¹	0.495	0.485	0.459
2θ _{max} / °	54.98	53.20	55.02
reflections collected	47736	18399	35259
independent reflections	5523	5045	17964
<i>R</i> _{int}	0.0235	0.0779	0.0151
parameters	286	262	884
<i>R</i> _{<i>I</i>} ^a [F _o ² ≥ 2σ(F _o ²)]	0.0234	0.0524	0.0312
<i>wR</i> ₂ ^b (all data)	0.0619	0.1061	0.0837
GoF ^c	1.047	1.093	1.012
Δρ max and min / e Å ⁻³	0.362, -0.198	0.471, -0.424	1.439, -0.414

^a $R_1 = \sum ||F_o| - |F_c|| / \sum |F_o|$

^b $wR_2 = [\sum w(F_o^2 - F_c^2)^2 / \sum w(F_o^4)]^{1/2}$

^c $GoF = [\sum w(F_o^2 - F_c^2)^2 / (n - p)]^{1/2}$ (*n* = number of data; *p* = number of parameters varied)

Table 8.5. Selected crystallographic data and collection parameters for stibinophosphonium cations in Chapter 6. Data collected and refined at the University of Alberta.

	[(Me₃P)SbCl₂][OTf] 6.16[OTf]	[(ⁱPr₃P)SbPhCl][OTf] 6.17[OTf]	[(Bn₃P)SbClPh][OTf]^d 6.18[OTf]
Formula	C ₄ H ₉ Cl ₂ F ₃ O ₃ PSSb	C ₁₆ H ₂₆ ClF ₃ O ₃ PSSb	C ₂₈ H ₂₆ ClF ₃ O ₃ PSSb
molecular weight (g/mol)	417.79	543.60	687.72
crystal system	monoclinic	triclinic	monoclinic
Space group	P2 ₁ /c	<i>P</i> $\bar{1}$	P2 ₁ /n
colour, habit	colourless rod	colourless plate	colourless
<i>a</i> / Å	10.798(2)	8.8175(5)	10.8024(8)
<i>b</i> / Å	11.059(2)	10.8696(7)	18.4899(13)
<i>c</i> / Å	12.214(3)	12.8560(8)	29.029(2)
α / °	90	74.2811(8)	90
β / °	114.382(2)	84.7562(8)	92.7140(10)
γ / °	90	66.4137(7)	90
<i>V</i> / Å ³	1328.5(5)	1086.79(12)	5791.6(7)
<i>T</i> / K	193	193	193
<i>Z</i>	4	2	8
crystal size / mm ³	0.59 x 0.22 x 0.18	0.37 x 0.21 x 0.06	0.52 x 0.17 x 0.07
μ / mm ⁻¹	2.777	1.600	1.220
2 θ _{max} / °	55.24	55.02	55.00
reflections collected	11005	9225	48285
independent reflections	3069	4912	13229
<i>R</i> _{int}	0.0485	0.0192	0.0457
parameters	136	235	685
<i>R</i> _{<i>i</i>} ^a (<i>I</i> > 2 σ (<i>I</i>), all data)	0.0313	0.0258	0.0373
<i>wR</i> ₂ ^b (<i>I</i> > 2 σ (<i>I</i>), all data)	0.0810	0.0657	0.0940
GoF ^c	1.081	1.068	1.019
$\Delta\rho$ max and min / e Å ⁻³	2.082, -0.761	0.952, -0.264	1.498, -0.509

$$^a R_1 = \frac{\sum ||F_o| - |F_c||}{\sum |F_o|}$$

$$^b wR_2 = [\sum w(F_o^2 - F_c^2)^2 / \sum w(F_o^4)]^{1/2}$$

$$^c \text{GoF} = [\sum w(F_o^2 - F_c^2)^2 / (n - p)]^{1/2} \quad (n = \text{number of data}; p = \text{number of parameters varied})$$

^d asymmetric unit contains two crystallographically independent molecules of the compound

Table 8.6. Selected crystallographic data and collection parameters for miscellaneous phosphine-stabilized stibonium cations (Chapter 6).

	[(Ph₃P)₂SbCl₂][OTf] 6.19[OTf]	<i>cyclo</i>-[(Me₃P)Sb]₄[OTf]₄·MeCN^a 6.20[OTf]₄·MeCN
Data collected and refined at	University of Alberta	University of New Brunswick
Formula	C ₃₇ H ₃₀ Cl ₂ F ₃ O ₃ P ₂ SSb	C ₁₈ H ₃₉ F ₁₂ N O ₁₂ P ₄ S ₄ Sb ₄
molecular weight (g/mol)	866.26	1428.62
crystal system	Triclinic	monoclinic
Space group	<i>P</i> 1	<i>P</i> 2 ₁ / <i>n</i>
colour, habit	yellow blocks	pale yellow rod
<i>a</i> / Å	9.5641 (7)	12.4072(17)
<i>b</i> / Å	12.0248 (8)	21.596(3)
<i>c</i> / Å	17.5876 (12)	18.649(3)
<i>α</i> / °	94.0493 (9)	90
<i>β</i> / °	96.8668 (10)	98.350(2)
<i>γ</i> / °	110.3615 (9)	90
<i>V</i> / Å ³	1869.0 (2)	4943.8(11)
<i>T</i> / K	193	198(1)
<i>Z</i>	2	4
crystal size / mm ³	0.31 x 0.26 x 0.12	0.40 x 0.10 x 0.05
<i>μ</i> / mm ⁻¹	1.073	2.549
2θ _{max} / °	54.94	55.00
reflections collected	16455	33100
independent reflections	8482	10998
<i>R</i> _{int}	0.0207	0.0680
parameters	442	563
<i>R</i> _{<i>I</i>} ^a (<i>I</i> > 2σ(<i>I</i>), all data)	0.0289	0.1349
<i>wR</i> ₂ ^b (<i>I</i> > 2σ(<i>I</i>), all data)	0.0719	0.1601
GoF ^c	1.062	1.099
Δρ max and min / e Å ⁻³	0.755, -0.348	1.343, -0.842

^a This structure possesses one highly disordered triflate anion. In addition, the structure contains 4 x 100 Å³ voids per unit cell, each large enough to fit a small solvent molecule, i.e. an additional MeCN. However, the electron count for each site comes to 8, while MeCN requires 22. Consequently, refinement with diffuse electron distribution (SQUEEZE in PLATON) was omitted.

Appendix A1. Statistical Treatment of Data

A1.2. Dynamic NMR Lineshape Analysis and Regression (Section 3.4)

While unweighted linear regression from the data in Table 8.1 yielded a reasonable value for ΔG^\ddagger (Table A1.1), the comparatively large error margin for the determination of k at 246 K relative to all other temperatures demands more stringent uncertainty estimates. The linear regression was therefore weighted according to the error in $\ln(k/T)$ at each temperature. These weights s_y were calculated according to standard propagation of error (Eqn. 1) from the error in $\log_{10}k$ as calculated by the least-squares residual of the lineshape fit in gNMR (s_g).

$$S_y^2 = \left(\frac{\partial y}{\partial g}\right)^2 \cdot S_g^2 \quad [1]$$

Since $g = \log_{10}k$, then $y = \ln\left(\frac{k}{T}\right) = \ln\left(\frac{10^g}{T}\right) = \ln\left(\frac{e^{\ln 10 \cdot g}}{T}\right) = \ln 10 \cdot g - \ln T$

$$\therefore S_y^2 = (\ln 10)^2 \cdot S_g^2$$

$$S_y = 2.303 S_g \quad [2]$$

The squared errors for each temperature, s_{yn}^2 , are compiled to produce the diagonal weight matrix, Σ :

$$\Sigma = \begin{bmatrix} s_{y1}^2 & 0 & \cdots & 0 \\ 0 & s_{y2}^2 & \cdots & 0 \\ \vdots & \vdots & \ddots & \vdots \\ 0 & 0 & 0 & s_{yn}^2 \end{bmatrix} \quad [3]$$

The slope (m) and intercept (b) of the weighted regression line for the Eyring plot were calculated according to Eqn. 4,

$$\hat{\beta} = \begin{bmatrix} b \\ m \end{bmatrix} = (X^T \Sigma^{-1} X)^{-1} X^T \Sigma^{-1} y \quad [4]$$

where X and y are the matrices defined in Eqn. 5, and X^T is the transpose of X :

$$X = \begin{bmatrix} 1 & 1/T_1 \\ 1 & 1/T_2 \\ \vdots & \vdots \\ 1 & 1/T_n \end{bmatrix} \text{ and } y = \begin{bmatrix} \ln\left(\frac{k_1}{T_1}\right) \\ \ln\left(\frac{k_2}{T_2}\right) \\ \vdots \\ \ln\left(\frac{k_n}{T_n}\right) \end{bmatrix} \quad [5]$$

From these calculated regression parameters, the activation parameters were calculated according to the Eyring equation (Eqn. 6):

$$\ln\left(\frac{k}{T}\right) = -\frac{\Delta H^\ddagger}{R} + \frac{\Delta S^\ddagger}{R} + \ln\left(\frac{k_b}{h}\right)$$

$$\text{slope} = m = -\frac{\Delta H^\ddagger}{R} \qquad \text{intercept} = b = \frac{\Delta S^\ddagger}{R} + \ln\left(\frac{k_b}{h}\right)$$

$$\Delta H^\ddagger = -mR \quad [7] \qquad \Delta S^\ddagger = bR - R \ln\left(\frac{k_b}{h}\right) \cong bR - 23.76 \quad [8]$$

Here, R is the ideal gas constant, h is Planck's constant, and k_b is Boltzmann's constant.

The free energy of activation can then be calculated according to Eqn. 9:

$$\Delta G^\ddagger = \Delta H^\ddagger - T\Delta S^\ddagger \quad [9]$$

By propagation of error (Eqn. 1), the standard error in ΔH^\ddagger and ΔS^\ddagger are as follows:

$$\sigma_{\Delta H^\ddagger} = R \cdot \sigma_m \quad \text{and} \quad \sigma_{\Delta S^\ddagger} = R \cdot \sigma_b \quad [10]$$

However, as ΔG^\ddagger depends on both regression parameters (b, m), the error in ΔG^\ddagger must take into account the covariance (σ_{mb}) between these parameters.

$$\begin{aligned} \sigma_{\Delta G^\ddagger}^2 &= \left(\frac{\partial \Delta G^\ddagger}{\partial m}\right)^2 \sigma_m^2 + \left(\frac{\partial \Delta G^\ddagger}{\partial b}\right)^2 \sigma_b^2 + 2 \left(\frac{\partial \Delta G^\ddagger}{\partial m}\right) \left(\frac{\partial \Delta G^\ddagger}{\partial b}\right) \sigma_{mb} \\ \sigma_{\Delta G^\ddagger}^2 &= R^2 \cdot \sigma_m^2 + (RT)^2 \cdot \sigma_m^2 + 2(R)(RT) \sigma_{mb} \end{aligned} \quad [11]$$

The requisite parameters for this equation were calculated for the weighted regression as follows:

$$\text{var}(\beta) = \begin{bmatrix} \sigma_m^2 & \sigma_{mb} \\ \sigma_{mb} & \sigma_m^2 \end{bmatrix} = (X^T \Sigma^{-1} X)^{-1} \quad [12]$$

The results of these calculations vs. simple regression results are summarized in Table A1.1 and Figure A1.1.

Table A1.1. Comparative results of simple and weighted linear regression analysis of Eyring plot data for $[3.9^i\text{Pr}][\text{GaCl}_4]_2$ in EtCN. Error limits indicated for ΔH^\ddagger and ΔS^\ddagger are standard deviations, while error in ΔG^\ddagger is reported at the 95% confidence level. Standard error in the simple regression was calculated based on the sum of the squared residuals.

	ΔH^\ddagger (kJ·mol ⁻¹)	ΔS^\ddagger (J·mol ⁻¹ ·K ⁻¹)	ΔG^\ddagger (kJ·mol ⁻¹)
simple regression	50 ± 1.5	-7 ± 6	52.1 ± 0.5
weighted regression	48 ± 4	-12 ± 16	52.1 ± 1.5

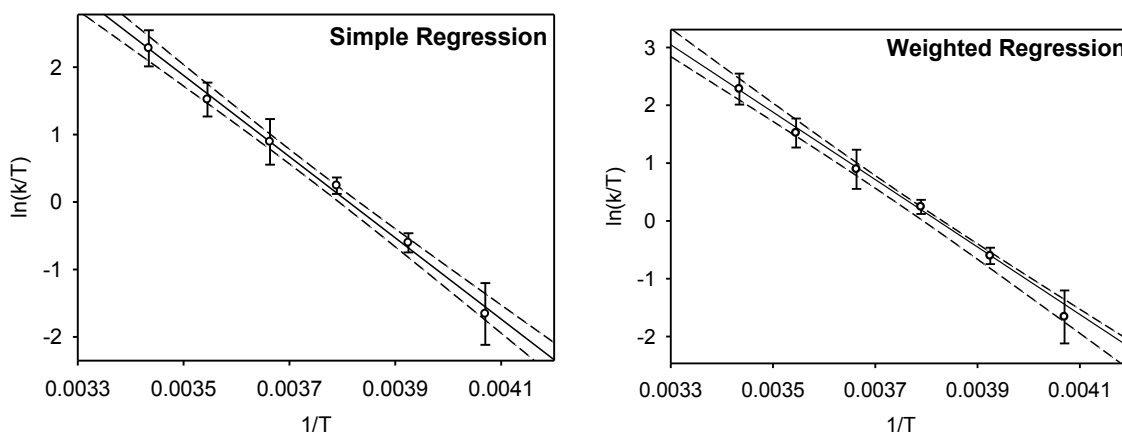


Figure A1.1. Comparison between the results of simple (unweighted) linear regression (left) and weighted regression (right) for the Eyring plot of the solution dynamics of $[3.9^i\text{Pr}][\text{GaCl}_4]_2$ in EtCN. Note that the weighted regression line falls within the 95% confidence interval for the simple regression (dotted lines on both plots).

Similar linear regression methods were used in the analysis of electrochemical data, where regression lines were instead weighted against standard deviations in each parameter as required.

Appendix A2. Cremer-Pople Puckering Coordinates

The full array of possible conformations of five-membered rings has already been depicted in terms of the Cremer-Pople puckering angle (φ) in Section 3.4, but a detailed treatise of six-membered rings is warranted with respect to the single example ($2.7[\text{OTf}]_2$) in Section 2.4.3.

According to Cremer and Pople, six-membered ring conformations can be precisely described in terms of three parameters: the puckering amplitude (Q), and a set of polar coordinates, the puckering angles (θ, φ).^{130,272} These define the extent of puckering of different atoms away from a well-defined average or mean plane. With five-membered rings, for a given puckering amplitude Q , the different conformations can be understood by pseudorotational changes that interconvert between various conformers outlined on a circle (Figure 3.4), with φ indicating where on this circle a specific conformer lies. As six-membered rings are described by two angles, they can be understood to define a spherical surface of possible conformations (Figure A2.1).

The angle θ describes a latitudinal coordinate on this surface corresponding to the interconversion between chair ($C, \theta = 0^\circ$ or 180°) and boat ($B, \theta = 90^\circ$) conformations. Intermediate between these at $\theta = 45^\circ$ are the half-boat or envelope conformer (E), and the half-chair conformer (H). The angle φ describes the longitudinal coordinates of the surface corresponding to the interconversion between boat ($B, \varphi = 60n^\circ$) and twist-boat ($T, \varphi = [30 + 60n]^\circ$) configurations.

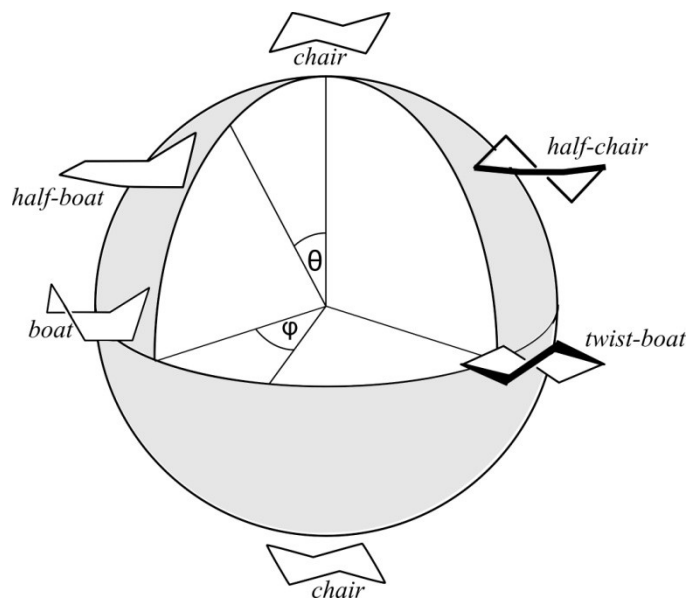


Figure A2.1. Cremer-Pople puckering angles (θ , φ) of six-membered rings.

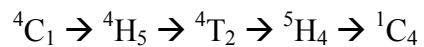
To clarify, envision a series of pseudorotations that might be mapped along the equator of this sphere ($\theta = 90^\circ$). As in Chapter 3, conventional shorthand notation will be used wherein superscript numerals indicate atoms above the plane of the ring and subscript numerals indicate atoms below the plane. Starting from $\varphi = 0^\circ$ and proceeding towards increasing values of φ , a six-membered ring of interest will traverse the following conformations, in sequence:



Similarly, traversing a longitudinal path at the meridian ($\varphi = 0^\circ$), from the North to South poles of this model sphere, demonstrates the interconversion between opposing chair conformations via an envelope:



Conversely, traversing a longitudinal path along $\varphi = 30^\circ$, offers the same net interconversion, via a half-chair pathway:



Thus, Cremer-Pople puckering angles specify not only the conformation of the ring as a whole, but also the specific atoms that are out-of-plane. Therefore, direct comparison of Cremer-Pople parameters between two rings, particularly if the rings are asymmetrically substituted, requires knowledge of the enumeration system used in the calculation.

References

- [1] Tanino, T.; Ichikawa, S.; Shiro, M.; Matsuda, A. *J. Org. Chem.* **2010**, *75*, 1366-1377.
- [2] Smith, M. B.; March, J. *Advanced Organic Chemistry*. Wiley: New York, 2001.
- [3] Gross, R. A.; Kalra, B. *Science*. **2002**, *297*, 803-807.
- [4] Dechy-Cabaret, O.; Martin-Vaca, B.; Bourissou, D. *Chem. Rev.* **2004**, *104*, 6147-6176.
- [5] Kim, H. J.; Jeong, Y. H.; Lee, E.; Lee, M. *J. Am. Chem. Soc.* **2009**, *131*, 17371-17375.
- [6] Dillon, K. B.; Mathey, F.; Nixon, J. F. *Phosphorus: The Carbon Copy*. John Wiley & Sons: New York, 1998.
- [7] Bates, J. I.; Dugal-Tessier, J.; Gates, D. P. *Dalton Trans.* **2010**, *39*, 3151-3159.
- [8] Washington, M. P.; Gudimetla, V. B.; Laughlin, F. L.; Deligonul, N.; He, S.; Payton, J. L.; Simpson, M. C.; Protasiewicz, J. D. *J. Am. Chem. Soc.* **2010**, *132*, 4566-4567.
- [9] Emsley, J. *The Elements*. Oxford University Press: Oxford, 1998.
- [10] Pyykkö, P.; Atsumi, M. *Chem. Eur. J.* **2009**, *15*, 186-197.
- [11] Corbridge, D. E. C.; Lowe, E. J. *Nature*. **1952**, *170*, 629.
- [12] Östmark, H.; Wallin, S.; Hore, N.; Launila, O. *J. Chem. Phys.* **2003**, *119*, 5918-5922.
- [13] Pfitzner, A. *Angew. Chem. Int. Ed.* **2006**, *45*, 699-700.
- [14] Brown, A.; Rundqvist, S. *Acta Crystallogr.* **1965**, *19*, 684-685.
- [15] Lange, S.; Schmidt, P.; Nilges, T. *Inorg. Chem.* **2007**, *46*, 4028-4035.
- [16] Corbridge, D. E. C. *The Structural Chemistry of Phosphorus*. Elsevier: New York, 1974.
- [17] Thurn, H.; Krebs, H. *Acta Crystallogr. Sect. B.* **1969**, *25*, 125-135.
- [18] Pfitzner, A.; Bräu, M. F.; Zweck, J.; Brunklaus, G.; Eckert, H. *Angew. Chem. Int. Ed.* **2004**, *43*, 4228-4231.
- [19] Winchester, R. A. L.; Whitby, M.; Shaffer, M. S. P. *Angew. Chem. Int. Ed.* **2009**, *48*, 3616-3621.
- [20] Cotton, F. A.; Wilkinson, G. *Advanced Inorganic Chemistry, Fifth Edition*. John Wiley & Sons: New York, 1988.
- [21] Kutzelnigg, W. *Angew. Chem. Int. Ed.* **1984**, *23*, 272-295.
- [22] Baudler, M.; Glinka, K. *Chem. Rev.* **1993**, *93*, 1623-1667.
- [23] Baudler, M. *Angew. Chem. Int. Ed.* **1982**, *21*, 492-512.

- [24] von Schnering, H. G.; Manriquez, V.; Höhle, W. *Angew. Chem. Int. Ed.* **1981**, *20*, 594-595.
- [25] Baudler, M.; Düster, D.; Langerbeins, K.; Germeshausen, J. *Angew. Chem. Int. Ed.* **1984**, *23*, 317-318.
- [26] Scherer, O. J. *Acc. Chem. Res.* **1999**, *32*, 751-762.
- [27] Cossairt, B. M.; Piro, N. A.; Cummins, C. C. *Chem. Rev.* **2010**, *110*, 4164-4177.
- [28] Dielmann, F.; Sierka, M.; Virovets, A. V.; Scheer, M. *Angew. Chem. Int. Ed.* **2010**, *49*, 6860-6864.
- [29] Abicht, H.-P.; Höhle, W.; von Schnering, H. G. *Z. Anorg. Allg. Chem.* **1984**, *519*, 7-23.
- [30] Schmettow, W.; Lipka, A.; von Schnering, H. G. *Angew. Chem. Int. Ed.* **1974**, *13*, 345.
- [31] von Schnering, H. G.; Meyer, T.; Höhle, W.; Schmettow, W.; Hinze, U.; Bauhofer, W.; Kliche, G. *Z. Anorg. Allg. Chem.* **1987**, *553*, 261-279.
- [32] Kraus, F.; Hanauer, T.; Korber, N. *Angew. Chem. Int. Ed.* **2005**, *44*, 7200-7204.
- [33] Kraus, F.; Korber, N. *Chem. Eur. J.* **2005**, *11*, 5945-5959.
- [34] Kraus, F.; Aschenbrenner, J.; Korber, N. *Angew. Chem. Int. Ed.* **2003**, *42*, 4030-4033.
- [35] Baudler, M. *Angew. Chem. Int. Ed.* **1987**, *26*, 419-441.
- [36] Stein, D.; Dransfeld, A.; Flock, M.; Ruegger, H.; Grutzmacher, H. *Eur. J. Inorg. Chem.* **2006**, 4157-4167.
- [37] Wolf, R.; Hey-Hawkins, E. *Z. Anorg. Allg. Chem.* **2006**, *632*, 727-734.
- [38] Geier, J.; Harmer, J.; Grutzmacher, H. *Angew. Chem. Int. Ed.* **2004**, *43*, 4093-4097.
- [39] Geier, J.; Ruegger, H.; Worle, M.; Grutzmacher, H. *Angew. Chem. Int. Ed.* **2003**, *42*, 3951-3954.
- [40] Schisler, A.; Lonnecke, P.; Huniar, U.; Ahlrichs, R.; Hey-Hawkins, E. *Angew. Chem. Int. Ed.* **2001**, *40*, 4217-4219.
- [41] Wolf, R.; Schisler, A.; Lonnecke, P.; Jones, C.; Hey-Hawkins, E. *Eur. J. Inorg. Chem.* **2004**, 3277-3286.
- [42] Herrero, R.; Gómez-Ruiz, S.; Dávalos, J. Z.; Hey-Hawkins, E. *C. R. Chim.* **2010**, *13*, 1185-1190.
- [43] Wang, Y.; Xie, Y.; Wei, P.; King, R. B.; Schaefer, I. I. I.; Schleyer, P.; Robinson, G. H. *J. Am. Chem. Soc.* **2008**, *130*, 14970-14971.
- [44] Masuda, J. D.; Schoeller, W. W.; Donnadiou, B.; Bertrand, G. *J. Am. Chem. Soc.* **2007**, *129*, 14180-14181.

- [45] Masuda, J. D.; Schoeller, W. W.; Donnadiou, B.; Bertrand, G. *Angew. Chem. Int. Ed.* **2007**, *46*, 7052-7055.
- [46] Baudler, M.; Glinka, K. *Chem. Rev.* **1994**, *94*, 1273-1297.
- [47] Lambert, J. B.; Jackson III, G. F.; Mueller, D. C. *J. Am. Chem. Soc.* **1970**, *92*, 3093-3097.
- [48] Baechler, R. D.; Mislou, K. *J. Am. Chem. Soc.* **1970**, *92*, 3090-3093.
- [49] Breen, T. L.; Stephan, D. W. *Organometallics*. **1997**, *16*, 365-369.
- [50] Ma, J.; Hozaki, A.; Inagaki, S. *Inorg. Chem.* **2002**, *41*, 1876-1882.
- [51] Baudler, M.; Makowka, B. *Z. Anorg. Allg. Chem.* **1985**, *528*, 7-21.
- [52] Fritz, G.; Vaahs, T.; Hönle, W.; von Schnering, H. G. *Z. Anorg. Allg. Chem.* **1987**, *552*, 34-49.
- [53] Baudler, M.; Aktalay, Y.; Arndt, V.; Tebbe, K.-F.; Fehér, M. *Angew. Chem. Int. Ed. Engl.* **1983**, *22*, 1002-1003.
- [54] Baudler, M.; Koll, B.; Adamek, C.; Gleiter, R. *Angew. Chem. Int. Ed.* **1987**, *26*, 347-348.
- [55] Brownridge, S.; Crawford, M. J.; Du, H.; Harcourt, R. D.; Knapp, C.; Laitinen, R. S.; Passmore, J.; Rautiainen, J. M.; Suontamo, R. J.; Valkonen, J. *Inorg. Chem.* **2007**, *46*, 681-699.
- [56] Schmidt, M. W.; Truong, P. N.; Gordon, M. S. *J. Am. Chem. Soc.* **1987**, *109*, 5217-5227.
- [57] Burford, N.; Dyker, C. A.; Lumsden, M. D.; Decken, A. *Angew. Chem. Int. Ed.* **2005**, *44*, 6196-6199.
- [58] Riegel, S. D. *Catena-Phosphinophosphonium and Phosphinodiphosphonium Cations*. M.Sc. Thesis, Dalhousie University, Halifax, NS, July 2007.
- [59] Dyker, C. A.; Riegel, S. D.; Burford, N.; Lumsden, M. D.; Decken, A. *J. Am. Chem. Soc.* **2007**, *129*, 7464-7474.
- [60] Weigand, J. J.; Riegel, S. D.; Burford, N.; Decken, A. *J. Am. Chem. Soc.* **2007**, *129*, 7969-7976.
- [61] Riegel, S. D.; Burford, N.; Lumsden, M. D.; Decken, A. *Chem. Commun.* **2007**, 4668-4670.
- [62] Weigand, J. J.; Burford, N.; Davidson, R. J.; Cameron, T. S.; Seelheim, P. *J. Am. Chem. Soc.* **2009**, *131*, 17943-17953.
- [63] Schmidpeter, A.; Lochschmidt, S.; Karaghiosoff, K.; Sheldrick, W. S. *Chem. Commun.* **1985**, 1447-1448.
- [64] Dyker, C. A.; Burford, N. *Chem. Asian J.* **2008**, *3*, 28-36.
- [65] Dyker, C. A. *Catena-Phosphorus Cations*. Ph.D. Thesis, Dalhousie University, Halifax, NS, Canada, December 2006.

- [66] Robinson, T.; Whoriskey, M. Unpublished Work.
- [67] Burford, N.; Dyker, C. A.; Decken, A. *Angew. Chem. Int. Ed.* **2005**, *44*, 2364-2367.
- [68] Dyker, C. A.; Burford, N.; Menard, G.; Lumsden, M. D.; Decken, A. *Inorg. Chem.* **2007**, *46*, 4277-4285.
- [69] Weigand, J. J.; Burford, N.; Lumsden, M. D.; Decken, A. *Angew. Chem. Int. Ed.* **2006**, *45*, 6733-6737.
- [70] Weigand, J. J.; Holthausen, M.; Frölich, R. *Angew. Chem. Int. Ed.* **2009**, *48*, 295-298.
- [71] Schmidpeter, A.; Lochschmidt, S. *Inorg. Synth.* **1990**, *27*, 253-258.
- [72] Schmidpeter, A.; Lochschmidt, S.; Sheldrick, W. S. *Angew. Chem. Int. Ed.* **1985**, *24*, 226-227.
- [73] Lochschmidt, S.; Schmidpeter, A. *Z. Naturforsch.* **1985**, *40b*, 765-773.
- [74] Dillon, K. B.; Monks, P. K. *Dalton Trans.* **2007**, 1420-1424.
- [75] Barnham, R. J.; Deng, R. M. K.; Dillon, K. B.; Goeta, A. E.; Howard, J. A. K.; Puschmann, H. *Heteroat. Chem.* **2001**, *12*, 501-510.
- [76] Norton, E. L.; Szekely, K. L. S.; Dube, J. W.; Bomben, P. G.; MacDonald, C. L. B. *Inorg. Chem.* **2008**, *47*, 1196-1203.
- [77] Dillon, K. B.; Monks, P. A.; Olivey, R. J.; Karsch, H. H. *Heteroatom Chem.* **2004**, *15*, 464-467.
- [78] Ellis, B. D.; Carlesimo, M.; Macdonald, C. L. B. *Chem. Commun.* **2003**, 1946-1947.
- [79] Ellis, B. D.; Macdonald, C. L. B. *Inorg. Chem.* **2006**, *45*, 6864-6874.
- [80] Dyker, C. A.; Burford, N.; Lumsden, M. D.; Decken, A. *J. Am. Chem. Soc.* **2006**, *128*, 9632-9633.
- [81] Carpenter, Y.; Dyker, C. A.; Burford, N.; Lumsden, M. D.; Decken, A. *J. Am. Chem. Soc.* **2008**, *130*, 15732-15741.
- [82] Boyall, A. J.; Dillon, K. B.; Howard, J. A. K.; Monks, P. K.; Thompson, A. L. *Dalton Trans.* **2007**, 1374-1376.
- [83] Burford, N.; Ragona, P. J.; McDonald, R.; Ferguson, M. J. *Chem. Commun.* **2003**, 2066-2067.
- [84] Burford, N.; Ragona, P. J.; McDonald, R.; Ferguson, M. J. *J. Am. Chem. Soc.* **2003**, *125*, 14404-14410.
- [85] Burford, N.; Herbert, D. E.; Ragona, P. J.; McDonald, R.; Ferguson, M. J. *J. Am. Chem. Soc.* **2004**, *126*, 17067-17073.
- [86] Pietschnig, R. *J. Organomet. Chem.* **2007**, *692*, 3363-3369.
- [87] Schultz, C. W.; Parry, R. W. *Inorg. Chem.* **1976**, *15*, 3046-3050.

- [88] Burford, N.; Cameron, T. S.; Ragona, P. J.; Ocando-Mavarez, E.; Gee, M.; McDonald, R.; Wasylishen, R. E. *J. Am. Chem. Soc.* **2001**, *123*, 7947-7948.
- [89] Burford, N.; Ragona, P. J. *Dalton Trans.* **2002**, 4307-4315.
- [90] Dillon, K. B. *Chem. Rev.* **1994**, *94*, 1441-1456.
- [91] Sheldrick, W. S.; Schmidpeter, A.; Zwaschka, F.; Dillon, K. B.; Platt, A. W. G.; Waddington, T. C. *Dalton Trans.* **1981**, 413-418.
- [92] Sheldrick, W. S.; Kiefer, J. Z. *Naturforsch.* **1989**, *44b*, 609-611.
- [93] Müller, G.; Matheus, H.-J.; Winkler, M. Z. *Naturforsch.* **2001**, *56b*, 1155-1162.
- [94] Burford, N.; Phillips, A. D.; Spinney, H. A.; Robertson, K. N.; Cameron, T. S.; McDonald, R. *Inorg. Chem.* **2003**, *42*, 4949-4954.
- [95] Burford, N.; Phillips, A. D.; Spinney, H. A.; Lumsden, M. D.; Werner-Zwanziger, U.; Ferguson, M. J.; McDonald, R. *J. Am. Chem. Soc.* **2005**, *127*, 3921-3927.
- [96] Burford, N.; Spinney, H. A.; Ferguson, M. J.; McDonald, R. *Chem. Commun.* **2004**, 2696-2697.
- [97] Weigand, J. J.; Burford, N.; Decken, A.; Schulz, A. *Eur. J. Inorg. Chem.* **2007**, 4868-4872.
- [98] Cowley, A. H.; Kemp, R. A. *Chem. Rev.* **1985**, *85*, 367-382.
- [99] Fleming, S.; Lupton, M. K.; Jekot, K. *Inorg. Chem.* **1972**, *11*, 2534-2540.
- [100] Bourissou, D.; Guerret, O.; Gabbai, F. P.; Bertrand, G. *Chem. Rev.* **2000**, *100*, 39-91.
- [101] Gudat, D. *Coord. Chem. Rev.* **1997**, *163*, 71-106.
- [102] Spinney, H. A.; Yap, G. P. A.; Korobkov, I.; DiLabio, G.; Richeson, D. S. *Organometallics*. **2006**, *25*, 3541-3543.
- [103] Spinney, H. A.; Korobkov, I.; DiLabio, G. A.; Yap, G. P. A.; Richeson, D. S. *Organometallics*. **2007**, *26*, 4972-4982.
- [104] Reeske, G.; Hoberg, C. R.; Hill, N. J.; Cowley, A. H. *J. Am. Chem. Soc.* **2006**, *128*, 2800-2801.
- [105] Ellis, B. D.; Macdonald, C. L. B. *Coord. Chem. Rev.* **2007**, *251*, 936-973.
- [106] Gudat, D.; Haghverdi, A.; Hupfer, H.; Nieger, M. *Chem. Eur. J.* **2000**, *6*, 3414-3425.
- [107] Cowley, A. H.; Cushner, M. C.; Lattman, M.; McKee, M. L.; Szobota, J. S.; Wilburn, J. C. *Pure Appl. Chem.* **1980**, *52*, 789-797.
- [108] Cowley, A. H.; Lattman, M.; Wilburn, J. C. *Inorg. Chem.* **1981**, *20*, 2916-2919.
- [109] du Mont, W. W.; Kroth, H. J.; Schumann, H. *Chem. Ber.* **1976**, *109*, 3017-3024.
- [110] Thomas, M. G.; Schultz, C. W.; Parry, R. W. *Inorg. Chem.* **1977**, *16*, 994-1001.

- [111] Burford, N.; Losier, P.; Sereda, S. V.; Cameron, T. S.; Wu, G. *J. Am. Chem. Soc.* **1994**, *116*, 6474-6475.
- [112] Azouri, M.; Andrieu, J.; Picquet, M.; Cattey, H. *Inorg. Chem.* **2009**, *48*, 1236-1242.
- [113] Lochschmidt, S.; Muller, G.; Huber, B.; Schmidpeter, A. *Z. Naturforsch.* **1986**, *41b*, 444-454.
- [114] Kilian, P.; Slawin, A. M. Z.; Woollins, J. D. *Dalton Trans.* **2006**, 2175-2183.
- [115] Karaghiosoff, K. Heterophosphole. Ph.D. Thesis, Ludwig-Maximilians-Universität, Munich, Germany, 1986.
- [116] Burford, N.; Cameron, T. S.; LeBlanc, D. J.; Losier, P.; Sereda, S.; Wu, G. *Organometallics.* **1997**, *16*, 4712-4717.
- [117] Burck, S.; Gudat, D. *Inorg. Chem.* **2008**, *47*, 315-321.
- [118] Hoffman, P. R.; Caulton, K. G. *Inorg. Chem.* **1975**, *14*, 1997-1999.
- [119] Smith, L. R.; Mills, J. L. *J. Chem. Soc., Chem. Commun.* **1974**, 808-809.
- [120] Beauchamp, P. S.; Marquez, R. *J. Chem. Educ.* **1997**, *74*, 1483-1485.
- [121] Gee, M.; Wasylishen, R. E.; Ragogna, P. J.; Burford, N.; McDonald, R. *Can. J. Chem.* **2002**, *80*, 1488-1500.
- [122] Shah, S.; Yap, G. P. A.; Protasiewicz, J. D. *J. Organomet. Chem.* **2000**, *608*, 12-20.
- [123] Arduengo, A. J.; Calabrese, J. C.; Cowley, A. H.; Dias, H. V. R.; Goerlich, J. R.; Marshall, W. J.; Riegel, B. *Inorg. Chem.* **1997**, *36*, 2151-2158.
- [124] Albrand, J. P.; Gagnaire, D.; Robert, J. B. *J. Am. Chem. Soc.* **1973**, *95*, 6498-6500.
- [125] Albrand, J. P.; Gagnaire, D.; Robert, J. B. *J. Am. Chem. Soc.* **1974**, *96*, 1643.
- [126] Albrand, J. P.; Robert, J. B. *Chem. Commun.* **1974**, 644-645.
- [127] Albrand, J. P.; Faucher, H.; Gagnaire, D.; Robert, J. B. *Chem. Phys. Lett.* **1976**, *38*, 521-523.
- [128] Forgeron, M. A. M.; Gee, M.; Wasylishen, R. E. *J. Phys. Chem.* **2004**, *108*, 4895-4908.
- [129] Slattery, J. M.; Fish, C.; Green, M.; Hooper, T. N.; Jeffery, J. C.; Kilby, R. J.; Lynam, J. M.; McGrady, J. E.; Pantazis, D. A.; Russell, C. A.; Willans, C. E. *Chem. Eur. J.* **2007**, *13*, 6967-6974.
- [130] Cremer, D.; Pople, J. A. *J. Am. Chem. Soc.* **1975**, *97*, 1354-1358.
- [131] Spek, A. L. *J. Appl. Crystallogr.* **2003**, *36*, 7-13.

- [132] Frisch, M. J.; Trucks, G. W.; Schlegel, H. B.; Scuseria, G. E.; Robb, M. A.; Cheeseman, J. R.; Montgomery, J. A. Jr.; Vreven, T.; Kudin, K. N.; Burant, J. C.; Millam, J. M.; Iyengar, S. S.; Tomasi, J.; Barone, V.; Mennucci, B.; Cossi, M.; Scalmani, G.; Rega, N.; Petersson, G. A.; Nakatsuji, H.; Hada, M.; Ehara, M.; Toyota, K.; Fukuda, R.; Hasegawa, J.; Ishida, M.; Nakajima, J.; Honda, Y.; Kitao, O.; Nakai, H.; Klene, M.; Li, X.; Knox, J. E.; Hratchian, H. P.; Cross, J. B.; Adamo, C.; Jaramillo, J.; Gomperts, R.; Stratmann, R. E.; Yazyev, O.; Austin, J.; Cammi, R.; Pomelli, C.; Ochterski, J.; Ayala, P. Y.; Morokuma, K.; Voth, G. A.; Salvador, P.; Dannenberg, J. J.; Zakrzewski, V. G.; Dapprich, S.; Daniels, A. D.; Strain, M. C.; Farkas, O.; Malick, D. K.; Rabuck, A. D.; Raghavachari, K.; Foresman, J. B.; Ortiz, J.; Cui, Q.; Baboul, A. G.; Clifford, S.; Cioslowski, J.; Stefanov, B. B.; Liu, G.; Liashenko, A.; Piskorz, P.; Komaromi, I.; Martin, R. L.; Fox, D. J.; Keith, T.; Al-Laham, M. A.; Peng, C. Y.; Nanayakkara, A.; Challacombe, M.; Gill, P. M. W.; Johnson, B.; Chen, W.; Wong, M. W.; Gonzalez, C.; Pople, J. A. *Gaussian 03*, Revision B.05; Gaussian, Inc.: Pittsburgh, PA, 2003.
- [133] Conrad, E.; Burford, N.; McDonald, R.; Ferguson, M. J. *J. Am. Chem. Soc.* **2009**, *131*, 17000-17008.
- [134] Tarasova, R. I.; Zykova, T. V.; Shagvaleev, F. Sh.; Sitdikova, T. Sh.; Moskva, V. V. *Zh. Obshch. Khim.* **1989**, *60*, 1775-1779; *J. Gen. Chem. U.S.S.R.* **1989**, 1063.
- [135] Tarasova, R. I.; Sitdikova, T. Sh.; Zykova, T. V.; Shagvaleev, F. Sh.; Moskva, V. V.; Kormachev, V. V.; Rusanov, V. M.; Baranov, Yu. I.; Danilov, S. D. Method of producing arylchlorophosphinophosphonium aluminochlorides. U.S.S.R. Patent SU 1449565, July 1, 1989; *Scifinder Scholar*: 1989:497499.
- [136] Shagvaleev, F. Sh.; Zykova, T. V.; Tarasova, R. I.; Sitdikova, T. Sh.; Moskva, V. V. *Zh. Obshch. Khim.* **1990**, *60*, 1775-1779; *J. Gen. Chem. U.S.S.R.* **1991**, 1585-1589.
- [137] Tarasova, R. I.; Zykova, T. V.; Shagvaleev, F. Sh.; Sitdikova, T. Sh.; Moskva, V. V. *Zh. Obshch. Khim.* **1991**, *61*, 2529-2532; *J. Gen. Chem. U.S.S.R.* **1992**, 2346-2349.
- [138] Krossing, I.; Raabe, I. *Angew. Chem. Int. Ed. Engl.* **2001**, *40*, 4406-4409.
- [139] Gonsior, M.; Krossing, I.; Müller, L.; Raabe, I.; Jansen, M.; van Wüllen; L. *Chem. Eur. J.* **2002**, *8*, 4475-4492.
- [140] Krossing, I. *Dalton Trans.* **2002**, 500-512.
- [141] Spencer, C. J.; Simpson, P. G.; Lipscomb, W. N. *Acta Crystallogr.* **1962**, *15*, 509.
- [142] Spencer, C. J.; Lipscomb, W. N. *Acta Crystallogr.* **1961**, *14*, 250-256.
- [143] Lex, J.; Baudler, M. *Z. Anorg. Allg. Chem.* **1977**, *431*, 49-60.
- [144] Wolf, R.; Hey-Hawkins, E. *Chem. Commun.* **2004**, 2626-2627.
- [145] Günther, H. The Influence of Dynamic Effects on ¹H Nuclear Magnetic Resonance Spectra; In *NMR Spectroscopy: Basic Principles, Concepts, and Applications in Chemistry*; Wiley: Chichester, UK, 1992; pp. 335-390.

- [146] Baechler, R. D.; Mislow, K. *J. Am. Chem. Soc.* **1970**, *92*, 4758-4759.
- [147] Rauk, A.; Allen, L. C.; Mitcherling, B. *Angew. Chem. Int. Ed.* **1970**, *9*, 400-414.
- [148] Nunn, M.; Sowerby, D. B.; Wesolek, D. M. *J. Organomet. Chem.* **1983**, *251*, C45-C46.
- [149] Balázs, L.; Breunig, H. J. *Coord. Chem. Rev.* **2004**, *248*, 603-621.
- [150] Dillon, K. B.; Goeta, A. E.; Howard, J. A. K.; Monks, P. K.; Shepherd, H. J.; Thompson, A. L. *Dalton Trans.* **2008**, 1144-1149.
- [151] Finer, E. G.; Harris, R. K. *Prog. Nucl. Magn. Reson. Spectrosc.* **1971**, *6*, 61-118.
- [152] McFarlane, H. C. E.; McFarlane, W. *J. Chem. Soc., Chem. Commun.* **1975**, 582-583.
- [153] McFarlane, H. C. E.; McFarlane, W.; Nash, J. A. *Dalton Trans.* **1980**, 240-244.
- [154] Hansch, C.; Leo, A.; Taft, R. W. *Chem. Rev.* **1991**, *91*, 165-195.
- [155] Mastryukova, T. A.; Kabachnik, M. I. *Russ. Chem. Rev.* **1969**, *38*, 795-811.
- [156] Ellis, B. D.; Macdonald, C. L. B. *Acta Cryst. Sect. E: Struct. Rep. Online.* **2006**, *E62*, m1869-m1870.
- [157] Tolman, C. A. *Chem. Rev.* **1977**, *73*, 313-348.
- [158] Allen, C. W. *Coord. Chem. Rev.* **1994**, *130*, 137-173.
- [159] Connelly, N. G.; Geiger, W. E. *Chem. Rev.* **1996**, *96*, 877-910.
- [160] Bockris, J. O.; Reddy, A. M. K.; Gamboa-Aldeco, M. *Modern Electrochemistry*. Kluwer Academic/Plenum Publishers: New York, 2000.
- [161] *Organic Electrochemistry*. Lund, H.; Hammerich, O., Eds. Marcel Dekker: New York, 2001.
- [162] *Electroanalytical Methods*. Scholz, F., Ed. Springer-Verlag: Berlin, 2002.
- [163] Davies, J. A.; Uma, V. *J. Electroanal. Chem.* **1984**, *179*, 273-276.
- [164] Schiavon, G.; Zecchin, S.; Cogoni, G.; Bontempelli, G. *J. Electroanal. Chem. Interfacial Electrochem.* **1973**, *48*, 425-431.
- [165] Matschiner, H.; Krause, L.; Krech, F. *Z. Anorg. Allg. Chem.* **1970**, *373*, 1-7.
- [166] Caram, J. A.; Vasini, E. *J. Electrochim. Acta.* **1994**, *39*, 2395-2400.
- [167] Culcasi, M.; Berchadsky, Y.; Gronchi, G.; Tordo, P. *J. Org. Chem.* **1991**, *56*, 3537-3542.
- [168] Santhanam, K. S. V.; Bard, A. J. *J. Am. Chem. Soc.* **1968**, *90*, 1118-1122.
- [169] Saveant, J. M.; Binh, S. K. *J. Electroanal. Chem.* **1978**, *88*, 27-41.
- [170] Dessy, R. E.; Chivers, T.; Kitching, W. *J. Am. Chem. Soc.* **1966**, *88*, 467-470.
- [171] Dutan, C.; Shah, S.; Smith, R. C.; Choua, S.; Berclaz, T.; Geoffroy, M.; Protasiewicz, J. D. *Inorg. Chem.* **2003**, *42*, 6241-6251.

- [172] Tsuji, K.; Sasaki, S.; Yoshifuji, M. *Tetrahedron Lett.* **1999**, *40*, 3203-3206.
- [173] Weber, L. *Chem. Rev.* **1992**, *92*, 1839-1906.
- [174] Nagahora, N.; Sasamori, T.; Hosoi, Y.; Furukawa, Y.; Tokitoh, N. *J. Organomet. Chem.* **2008**, *693*, 625-632.
- [175] DuPont, T. J.; Mills, J. L. *Inorg. Chem.* **1973**, *12*, 2487-2489.
- [176] Dupont, T. J. Electrochemical Investigation of Selected Air-Sensitive Compounds. Ph.D. Thesis, Texas Tech University, Lubbock, TX, USA, August 1974.
- [177] Issleib, K.; Fluck, E. *Angew. Chem. Int. Ed.* **1966**, *5*, 587-588.
- [178] Hoffman, P. R.; Caulton, K. G. *J. Am. Chem. Soc.* **1975**, *97*, 6370-6374.
- [179] Dupont, T. J.; Smith, L. R.; Mills, J. L. *J. Chem. Soc., Chem. Commun.* **1974**, 1001-1002.
- [180] White, C. K.; Rieke, R. D. *J. Org. Chem.* **1978**, *43*, 4638-4641.
- [181] Horner, L.; Haufe, J. *J. Electroanal. Chem.* **1969**, *20*, 245-261.
- [182] Bugner, D. E. *J. Org. Chem.* **1989**, *54*, 2580-2586.
- [183] Ohmori, H.; Takanami, T.; Masui, M. *Tetrahedron Lett.* **1985**, *26*, 2199-2200.
- [184] Takanami, T.; Suda, K.; Ohmori, H. *Chem. Lett.* **1987**, 1335-1336.
- [185] Takanami, T.; Abe, A.; Suda, K.; Ohmori, H. *J. Chem. Soc., Chem. Commun.* **1990**, 1310-1311.
- [186] Romakhin, A. S.; Palyutin, F. M.; Ignat'ev, Yu. A.; Nikitin, E. V.; Kargin, Yu. M.; Litvinov, I. A.; Naumov, V. A. *Izv. Akad. Nauk. SSSR, Ser. Khim.* **1990**, *3*, 664-669.
- [187] Nikitin, E. V.; Romakhin, A. S.; Zagumennov, V. A.; Babkin, Yu. A. *Electrochim. Acta.* **1997**, *42*, 2217-2224.
- [188] Kargin, Yu. M.; Budnikova, Yu. H.; Martynov, B. I.; Turygin, V. V.; Tomilov, A. P. *J. Electroanal. Chem.* **2001**, *507*, 157-169.
- [189] Stickney, J. L.; Soriaga, M. P.; Hubbard, A. T.; Anderson, S. E. *J. Electroanal. Chem.* **1981**, *125*, 73-88.
- [190] Nicholson, R. S.; Shain, I. *Anal. Chem.* **1964**, *36*, 706-723.
- [191] Protasiewicz, J. D.; Rheingold, A. L.; Shah, S.; Concolino, T. *Inorg. Chem.* **2000**, *39*, 3860-3867.
- [192] Peng, H. L.; Payton, J. L.; Protasiewicz, J. D.; Simpson, M. C. *The Journal of Physical Chemistry A.* **2009**, *113*, 7054-7063.
- [193] Shah, S.; Protasiewicz, D. *Chem. Commun.* **1998**, 1585-1586.
- [194] Partyka, D. V.; Washington, M. P.; Updegraff, J. B., III; Woloszynek, R. A.; Protasiewicz, J. D. *Angew. Chem. Int. Ed.* **2008**, *47*, 7489-7492.

- [195] Burg, A. B.; Mahler, W. *J. Am. Chem. Soc.* **1961**, *83*, 2388-2389.
- [196] Burg, A. B. *J. Inorg. Nucl. Chem.* **1971**, *33*, 1575-1581.
- [197] Cowley, A. H.; Cushner, M. C. *Inorg. Chem.* **1980**, *19*, 515-518.
- [198] Arduengo, A. J.; Carmalt, C. J.; Clyburne, J. A. C.; Cowley, A. H.; Pyati, R. *Chem. Commun.* **1997**, 981-982.
- [199] LeSuer, R. J.; Buttolph, C.; Geiger, W. E. *Anal. Chem.* **2004**, *76*, 6395-6401.
- [200] Camire, N.; Nafady, A.; Geiger, W. E. *J. Am. Chem. Soc.* **2002**, *124*, 7260-7261.
- [201] Taylor, M. J.; Tuck, D. G. *Inorg. Synth.* **1983**, *22*, 135-142.
- [202] Breunig, H. J.; Denker, M.; Ebert, K. H. *J. Organomet. Chem.* **1994**, *470*, 87-92.
- [203] Breunig, H. J.; Ebert, K. H.; Gülec, S.; Dräger, M.; Sowerby, D. B.; Begley, M. J.; Behrens, U. *J. Organomet. Chem.* **1992**, *427*, 39-48.
- [204] Millington, P. L.; Sowerby, D. B. *J. Organomet. Chem.* **1994**, *480*, 227-234.
- [205] Breunig, H. J.; Lork, E.; Moldovan, O.; Rat, C. I. *J. Organomet. Chem.* **2008**, *693*, 2527-2534.
- [206] Twamley, B.; Sofield, C. D.; Olmstead, M. M.; Power, P. P. *J. Am. Chem. Soc.* **1999**, *121*, 3357-3367.
- [207] Althaus, H.; Breunig, H. J.; Lork, E. *Organometallics*. **2001**, *20*, 586-589.
- [208] Nunn, M.; Begley, M. J.; Sowerby, D. B.; Haiduc, I. *Polyhedron*. **1996**, *15*, 3167-3174.
- [209] Genge, A. R. J.; Hill, N. J.; Levason, W.; Reid, G. *J. Chem. Soc., Dalton Trans.* **2001**, 1007-1012.
- [210] Clegg, W.; Elsegood, M. R. J.; Graham, V.; Norman, N. C.; Pickett, N. L.; Tavakkoli, K. *J. Chem. Soc., Dalton Trans.* **1994**, 1743-1751.
- [211] Breunig, H. J.; Rösler, R. *Coor. Chem. Rev.* **1997**, *163*, 33-53.
- [212] Breunig, H. J.; Ghesner, I.; Ghesner, M. E.; Lork, E. *J. Organomet. Chem.* **2003**, *677*, 15-20.
- [213] Althaus, H.; Breunig, H. J.; Probst, J.; Rösler, R.; Lork, E. *J. Organomet. Chem.* **1999**, *585*, 285-289.
- [214] Bartlett, R. A.; Dias, H. V. R.; Hope, H.; Murray, B. D.; Olmstead, M. M.; Power, P. P. *J. Am. Chem. Soc.* **1986**, *108*, 6921-6926.
- [215] Breunig, H. J.; Rosler, R.; Lork, E. *Organometallics*. **1998**, *17*, 5594-5595.
- [216] Mundt, O.; Becker, G.; Wessely, H. J.; Breunig, H. J.; Kischkel, H. Z. *Anorg. Allg. Chem.* **1982**, *486*, 70-89.
- [217] Kekia, O. M.; Jones, R. L.; Rheingold, A. L. *Organometallics*. **1996**, *15*, 4104-4106.

- [218] Ates, M.; Breunig, H. J.; Ebert, K.; Gülec, S.; Kaller, R.; Dräger, M. *Organometallics*. **1992**, *11*, 145-150.
- [219] Dostál, L.; Jambor, R.; Růžička, A.; Holeček, J. *Organometallics*. **2008**, *27*, 2169-2171.
- [220] Ates, M.; Breunig, H. J.; Gülec, S.; Offermann, W.; Häberle, K.; Dräger, M. *Chem. Ber.* **1989**, *122*, 473-478.
- [221] Balázs, G.; Breunig, H. J.; Lork, E.; Mason, S. *Organometallics*. **2003**, *22*, 576-585.
- [222] Balázs, G.; Balázs, L.; Breunig, H. J.; Lork, E. *Organometallics*. **2003**, *22*, 2919-2924.
- [223] Balázs, G.; Breunig, H. J.; Lork, E. *Z. Anorg. Allg. Chem.* **2003**, *629*, 637-640.
- [224] Breunig, H. J.; Häberle, K.; Dräger, M.; Severengiz, T. *Angew. Chem. Int. Ed.* **1985**, *24*, 72-73.
- [225] Breunig, H. J.; Ebert, K. H.; Gülec, S.; Probst, J. *Chem. Ber.* **1995**, *128*, 599-603.
- [226] Breunig, H. J.; Denker, M.; Ebert, K. H. *J. Chem. Soc., Chem. Commun.* **1994**, 875-876.
- [227] Minkwitz, R.; Hirsch, C. *Z. Anorg. Allg. Chem.* **1999**, *625*, 1674-1682.
- [228] Althaus, H.; Breunig, H. J.; Lork, E. *Chem. Commun.* **1999**, 1971-1972.
- [229] Carmalt, C. J.; Norman, N. C. *Chemistry of Arsenic, Antimony and Bismuth*. Norman, N. C., Ed. Blackie Academic and Professional: New York, 1998.
- [230] Breunig, H. J.; Denker, M.; Lork, E. *Angew. Chem. Int. Ed.* **1996**, *35*, 1005-1006.
- [231] Spinney, H. A.; Korobkov, I.; Richeson, D. S. *Chem. Commun.* **2007**, 1647-1649.
- [232] Burford, N.; Macdonald, C. L. B.; LeBlanc, D. J.; Cameron, T. S. *Organometallics*. **2000**, *19*, 152-155.
- [233] Neuhaus, A.; Frenzen, G.; Pebler, J.; Dehnicke, K. *Z. Anorg. Allg. Chem.* **1992**, *618*, 93-97.
- [234] Willey, G. R.; Spry, M. P.; Drew, M. G. B. *Polyhedron*. **1996**, *15*, 4497-4500.
- [235] Jutzi, P.; Wippermann, T.; Krüger, C.; Kraus, H.-J. *Angew. Chem. Int. Ed.* **1983**, *22*, 250.
- [236] Wiacek, R. J.; Macdonald, C. L. B.; Jones, J. N.; Pietryga, J. M.; Cowley, A. H. *Chem. Commun.* **2003**, 430-431.
- [237] Wielandt, J. W.; Kilah, N. L.; Willis, A. C.; Wild, S. B. *Chem. Commun.* **2006**, 3679-3680.
- [238] Kilah, N. L.; Petrie, S.; Stranger, R.; Wielandt, J. W.; Willis, A. C.; Wild, S. B. *Organometallics*. **2007**, *26*, 6106-6113.
- [239] Clegg, W.; Elsegood, M. R. J.; Norman, N. C.; Pickett, N. L. *J. Chem. Soc., Dalton Trans.* **1994**, 1753-1757.

- [240] Clegg, W.; Elsegood, M. R. J.; Graham, V.; Norman, N. C.; Pickett, N. L. *J. Chem. Soc., Dalton Trans.* **1993**, 997-998.
- [241] Beswick, M. A.; Choi, N.; Hopkins, A. D.; McPartlin, M.; Mosquera, M. E. G.; Raithby, P. R.; Rothenberger, A.; Stalke, D.; Wheatley, A. J.; Wright, D. S. *Chem. Commun.* **1998**, 2485-2486.
- [242] Nikolova, D.; von Hänisch, C. *Eur. J. Inorg. Chem.* **2005**, 378-382.
- [243] Sigwarth, B.; Weber, U.; Zsolnai, L.; Huttner, G. *Chem. Ber.* **1985**, *118*, 3114-3126.
- [244] Kaul, H.-A.; Greissing, D.; Malisch, W.; Klein, H.-P.; Thewalt, U. *Angew. Chem. Int. Ed.* **1983**, *22*, 60-61.
- [245] Bashall, A.; García, F.; Lawson, G. T.; McPartlin, M.; Rothenberger, A.; Woods, A. D.; Wright, D. S. *Can. J. Chem.* **2002**, *80*, 1421-1427.
- [246] Conrad, E.; Burford, N.; Werner-Zwanziger, U.; McDonald, R.; Ferguson, M. J. *Chem. Commun.* **2010**, *46*, 2465-2467.
- [247] Bosque, R.; Sales, J. *J. Chem. Inf. Comput. Sci.* **2000**, *41*, 225-232.
- [248] Grim, S. O.; McFarlane, W. *Nature.* **1965**, *208*, 995-996.
- [249] Karaghiosoff, K. Phosphorus-31 NMR; In *Encyclopedia of Nuclear Magnetic Resonance*; Grant, D. M., Harris, R. K., Eds. 1996; pp. 3612-3619.
- [250] Power, P. P. *Chem. Rev.* **1999**, *99*, 3463-3503.
- [251] Breunig, H. J.; Knobloch, T. P. *Z. Anorg. Allg. Chem.* **1978**, *446*, 119-125.
- [252] Schmidpeter, A.; Lochschmidt, S. *Angew. Chem. Int. Ed.* **1986**, *25*, 253-254.
- [253] Weferling, N. *Z. Anorg. Allg. Chem.* **1987**, *548*, 55-62.
- [254] King, R. B.; Sundaram, P. M. *J. Org. Chem.* **1984**, *49*, 1784-1789.
- [255] Calderazzo, F.; Marchetti, F.; Ungari, F.; Wieber, M. *Gazz. Chim. Ital.* **1991**, *121*, 93-100.
- [256] Leininger, S.; Fan, J.; Schmitz, M.; Stang, P. J. *PNAS.* **2000**, *97*, 1381-1384.
- [257] Budzelaar, P. H. M. *gNMR for Windows*, 4.0; Cherwell Scientific Publishing Limited: The Magdalen Centre, Oxford Science Park, Oxford OX4 4GA, UK, 1997.
- [258] Budzelaar, P. H. M. *gNMR for Windows*, 5.0.6.0; Ivorysoft: Winnipeg, MB, Canada, 2006.
- [259] *Topspin for Windows*, 2.0, patchlevel 5; Bruker Biospin GmbH: Germany, 2006.
- [260] Huynh, K.; Rivard, E.; LeBlanc, W.; Blackstone, V.; Lough, A. J.; Manners, I. *Inorg. Chem.* **2006**, *45*, 7922-7928.
- [261] Ammann, C.; Meier, P.; Merbach, A. E. *J. Magn. Reson.* **1982**, *46*, 319-321.
- [262] Sandström, J. *Dynamic NMR spectroscopy*. Academic Press: London, 1982.

- [263] Eaton, J. W. *Octave*, 3.2.4; University of Wisconsin: Madison, WI, 2010.
- [264] *Sigmaplot for Windows*, 10.0.0.54; Systat Software Inc.: Point Richmond, CA, USA, 2006.
- [265] *SAINTE 7.23A*, Bruker AXS, Inc: Madison, Wisconsin, USA, 2006.
- [266] Sheldrick, G. M. *SADABS*, Bruker AXS, Inc.: Madison, Wisconsin, USA., 2004.
- [267] Sheldrick, G. M. *SHELXL-97, Program for crystal structure determination*, University of Göttingen, Germany, 1997.
- [268] Sheldrick, G. M. *Acta Crystallogr.* **2008**, *A64*, 112-122.
- [269] Katsyuba, S.; Schmutzler, R. *Dalton Trans.* **2008**, 1465-1470.
- [270] Gritzner, G.; Kuta, J. *Pure Appl. Chem.* **1984**, *56*, 461-466.
- [271] Gagné, R. R.; Koval, C. A.; Lisensky, G. C. *Inorg. Chem.* **1980**, *19*, 2854-2855.
- [272] Kooijman, H. Interpretation of Crystal Structure Determination: Course Notes, v.2.3. <http://www.cryst.chem.uu.nl/huub/notesweb.pdf> (accessed 30 Oct 2010).